DOCTORAL THESIS STOCKHOLM, SWEDEN 2018

Convex Optimal Power Flow Based on Second-Order Cone Programming: Models, Algorithms and Applications

Zhao Yuan







Convex Optimal Power Flow Based on Second-Order Cone Programming: Models, Algorithms and Applications

Zhao Yuan

袁钊

Thesis supervisors:

Associate Prof. Mohammad Reza Hesamzadeh, Kungliga Tekniska Högskolan

Prof. Lennart Söder, Kungliga Tekniska Högskolan

Assistant Prof. Sonja Wogrin, Universidad Pontificia Comillas

Members of the Examination Committee:

Prof. Anders Forsgren, Kungliga Tekniska Högskolan, Examiner

Prof. Luis Rouco Rodríguez, Universidad Pontificia Comillas, Examiner

Prof. Zofia Lukszo, Technische Universiteit Delft, Examiner

Prof. Javier Contreras Sanz, Universidad de Castilla-La Mancha, Examiner

Dr. Viktoria Neimane, Vattenfall Distribution Sweden, Examiner

This doctoral research was funded by the European Commission through the Erasmus Mundus Joint Doctorate Program, and also partially supported by the KTH Royal Institute of Technology.

TRITA-EECS-AVL-2018:10

ISBN 978-91-7729-678-2

Copyright © Zhao Yuan, 2018

Printed by: US-AB 2018

Convex Optimal Power Flow Based on Second-Order Cone Programming: Models, Algorithms and Applications

Dissertation

for the purpose of obtaining the degree of doctor
at Delft University of Technology
by the authority of the Rector Magnificus prof.dr.ir. T.H.J.J. van der Hagen
Chair of the Board for Doctorates
to be defended publicly on
Tuesday 29 May 2018 at 9:00 o'clock

by

Zhao YUAN

Master of Electrical Engineering,
Huazhong University of Science and Technology, China
Master de Sciences et Technologies,
ParisTech, France
born in Handan, China

This dissertation has been approved by the promotors.

Composition of the doctoral committee:

Chairman, KTH Royal Institute of Technology

Dr. M. R. Hesamzadeh, KTH Royal Institute of Technology, Sweden, promotor

Prof.dr.ir. P. M. Herder Delft University of Technology, the Netherlands, promotor

Independent members:

Prof. A. Forsgren, KTH Royal Institute of Technology, Sweden

Prof. L. R. Rodríguez, Comillas Pontifical University, Spain

Prof. Z. Lukszo, Delft University of Technology, the Netherlands

Prof. J. C. Sanz, University of Castilla-La Mancha, Spain

Dr. V. Neimane, Vattenfall Distribution, Sweden

The doctoral research has been carried out in the context of an agreement on joint doctoral supervision between Comillas Pontifical University, Madrid, Spain, KTH Royal Institute of Technology, Stockholm, Sweden and Delft University of Technology, the Netherlands.

Keywords: Optimal Power Flow, Distribution Locational Marginal Pricing, Wind Power, Super Grid.

ISBN 978-91-7729-678-2

Copyright © Zhao Yuan, 2018, Stockholm, Sweden. All rights reserved. No part of the material protected by this copyright notice may be reproduced or utilized in any form or by any means, electronic or mechanical, including photocopying, recording or by any information storage and retrieval system, without written permission from the author.

Printed by: US-AB 2018

SETS Joint Doctorate

The Erasmus Mundus Joint Doctorate in **Sustainable Energy Technologies and Strategies**, SETS Joint Doctorate, is an international programme run by six institutions in cooperation:

- Comillas Pontifical University, Madrid, Spain
- Delft University of Technology, Delft, the Netherlands
- Florence School of Regulation, Florence, Italy
- Johns Hopkins University, Baltimore, USA
- KTH Royal Institute of Technology, Stockholm, Sweden
- University Paris-Sud 11, Paris, France

The Doctoral Degrees issued upon completion of the programme are issued by Comillas Pontifical University, Delft University of Technology, and KTH Royal Institute of Technology.

The Degree Certificates are giving reference to the joint programme. The doctoral candidates are jointly supervised, and must pass a joint examination procedure set up by the three institutions issuing the degrees.

This Thesis is a part of the examination for the doctoral degree.

The invested degrees are official in Spain, the Netherlands and Sweden respectively.

SETS Joint Doctorate was awarded the Erasmus Mundus **excellence label** by the European Commission in year 2010, and the European Commission's **Education**, **Audiovisual and Culture Executive Agency**, EACEA, has supported the funding of this programme.

The EACEA is not to be held responsible for contents of the Thesis.







Contents

C	onter	nts	I
\mathbf{A}	bstra	ct in English Language	2
\mathbf{A}	bstra	act in Spanish Language	4
Sa	mma	anfattning (Summary in Swedish)	6
\mathbf{A}	bstra	act in Dutch Language	8
\mathbf{A}	ckno	wledgements	10
\mathbf{Li}	${f st}$ of	Figures	12
Li	${f st}$ of	Tables	1 4
Li	st of	Symbols	16
\mathbf{Li}	st of	Abbreviations	18
1		roduction	20
	1.1	Background and Motivation	20
	1.2	List of Publications and Patents	23
	1.3	Thesis Outline	25
2	Cor	vex Optimal Power Flow Models	26
	2.1	Introduction	26
	2.2	AC Optimal Power Flow	28
		2.2.1 Full AC Optimal Power Flow Model	28
		2.2.2 SOC-ACOPF: Model P	29
		2.2.3 SOC-ACOPF: Model R	30
		2.2.4 SOC-ACOPF: Model T	32
		2.2.5 SOC-ACOPF: Model E	33
	2.3	Feasibility	34
	2.4	Numerical Results	35

		2.4.1	Performance of SOC-ACOPF models	35
		2.4.2	Feasible Solution	37
	2.5	Conclu	usions	42
3	Tig	htness	and Decomposition Algorithms	44
	3.1	Introd	uction	44
	3.2	Seque	ntial Tightness Algorithm	46
	3.3		Network Partitioning	
	3.4		sing M-BDA and the Parallel Computing	
	3.5		rical Results	59
		3.5.1	The Performance of Sequential Tightness Algorithm	
		3.5.2	8	
		3.5.3	Accelerated M-BDA Using GAMS Parallel Computing	
	3.6	Conclu	usions	66
4	Dis		on Locational Marginal Pricing	68
	4.1		uction	
	4.2	The H	ierarchical Economic Dispatch	
		4.2.1	Decomposing the Economic Dispatch	69
		4.2.2		
	4.3		rical Results and Discussions	
		4.3.1	Convergence of Hierarchical Economic Dispatch	
		4.3.2	Distribution Locational Marginal Price	74
		4.3.3	Results of Generalized Bid Function	
	4.4	Conclu	usions	76
5	Inte	egratin	g Wind Power by Stochastic Conic Programming	82
	5.1	Introd	uction	82
	5.2	Hybrid	d AC-DC Network and FACTS Models	
		5.2.1	The AC Network	84
		5.2.2	The VSC-MTDC System	84
		5.2.3	FACTS Devices	87
	5.3	Conve	xification and Approximation	89
		5.3.1	Formulation	89
	5.4	Wind	Power Scenario Generation	90
	5.5		astic SOC-ACOPF Model	94
	5.6		aposition of Stochastic SOC-ACOPF	96
	5.7		rical Results	98
		5.7.1	Solving Stochastic SOC-ACOPF by M-BDA and Parallel Com-	
			putation	98

III CONTENTS

	5.8	Conclusions	103
6	Coc	ordinated Energy Dispatch for Super Grid	104
	6.1	Introduction	104
	6.2	Proposing the Power Synergy Hub	106
	6.3	Mathematical Foundation of PSHub: Modified Benders Decomposition	108
	6.4	Accelerating the Implementation of Modified BD by Parallel Computation	1111
	6.5	Numerical Results	114
		6.5.1 Performance of Energy Dispatch Coordination by PSHub	114
	6.6	Conclusions	
7	Clos	sure	122
	7.1	Concluding Remarks	122
	7.2	Future Work	
Bi	bliog	graphy	124
Co	ompl	ete List of Publications and Patents	136
Cı	ırric	ulum Vitae	138

Abstract in English Language

Author: Zhao Yuan

Affiliation: KTH Royal Institute of Technology

Title: Convex Optimal Power Flow Based on Second-Order Cone Programming: Mod-

els, Algorithms and Applications

Language: English

Keywords: Optimal Power Flow, Second-Order Cone Programming, Distribution Lo-

cational Marginal Pricing, Wind Power, Super Grid

Optimal power flow (OPF) is the fundamental mathematical model to optimally operate the power system. Improving the solution quality of OPF can help the power industry save billions of dollars annually. Past decades have witnessed enormous research efforts on OPF since J. Carpentier proposed the fully formulated alternating current OPF (ACOPF) model which is nonconvex. This thesis proposes three convex OPF models (SOC-ACOPF) based on second-order cone programming (SOCP) and McCormick envelope. The underlying idea of the proposed SOC-ACOPF models is to drop assumptions of the original SOC-ACOPF model by convex relaxation and approximation methods. A heuristic algorithm to recover feasible OPF solution from the relaxed solution of the proposed SOC-ACOPF models is developed. The quality of solutions with respect to global optimum is evaluated using MATPOWER and LINDOGLOBAL. A computational comparison with other SOC-ACOPF models in the literature is also conducted. The numerical results show robust performance of the proposed SOC-ACOPF models and the feasible solution recovery algorithm. We then propose to speed up solving large-scale SOC-ACOPF problem by decomposition and parallelization. We use spectral factorization to partition large power network to multiple subnetworks connected by tie-lines. A modified Benders decomposition algorithm (M-BDA) is proposed to solve the SOC-ACOPF problem iteratively. Taking the total power output of each subnetwork as the complicating variable, we formulate the SOC-ACOPF problem of tie-lines as the master problem and the SOC-ACOPF problems of the subnetworks as the subproblems in the proposed M-BDA. The feasibility of the proposed M-BDA is analytically proved. A GAMS grid computing framework is designed to compute the formulated subproblems in parallel. The numerical results show that the proposed M-BDA can solve large-scale SOC-ACOPF problem efficiently. Accelerated M-BDA by parallel computing converges within few iterations. Finally, various applications of our SOC-ACOPF models and M-BDA including distribution locational marginal pricing (DLMP), wind power integration and ultra-large-scale power network or super grid operation are demonstrated.

Abstract in Spanish Language

Autor: Zhao Yuan

Afiliación: KTH Royal Institute of Technology

Título: Flujo de potencia óptimo convexo basado en programación cónica de segundo

orden: modelos, algoritmos y aplicaciones

Idioma: Inglés

Palabras clave: Flujo óptimo de potencia, Programación cónica de segunda orden,

Distribución de precios marginales locales, Energía eólica, Supergrid

El flujo óptimo de potencia (OPF) es el modelo matemático fundamental para operar óptimamente el sistema eléctrico de potencia. La mejora de la calidad de la solución del OPF puede ayudar al sector eléctrico a ahorrar billones de dólares anualmente. En las pasadas décadas ha habido enormes esfuerzos de investigación sobre OPF desde que J. Carpentier propuso la formulación completa del modelo OPF de corriente alterna (ACOPF) que es no lineal y no convexo. Esta tesis propone tres modelos OPF convexos (SOC-ACOPF) basados en programación cónica de segundo orden (SOCP) y programación no lineal de McCormick. La idea subyacente de los modelos SOC-ACOPF propuestos es sustituir los supuestos del modelo SOC-ACOPF original mediante métodos de relajación convexa y aproximación. Se desarrolla un algoritmo heurístico para recuperar la solución OPF factible a partir de la solución relajada de los modelos SOC-ACOPF propuestos. La calidad de las soluciones con respecto al óptimo global se evalúa utilizando MATPOWER y LINDOGLOBAL. También se realiza una comparación computacional con otros modelos SOC-ACOPF existentes en la literatura científica. Los resultados numéricos obtenidos muestran un comportamiento robusto de los modelos SOC-ACOPF propuestos y del algoritmo de soluciones viables. A continuación, se propone acelerar la resolución de un problema SOC-ACOPF a gran escala por descomposición y paralelización. Se utiliza factorización espectral para dividir una gran red eléctrica en varias subredes conectadas por líneas de enlace. Se propone un algoritmo de descomposición Benders modificado (M-BDA) para resolver el problema SOC-ACOPF de forma iterativa. Tomando la potencia total de cada subred como factor variable, se formula el problema SOC-ACOPF de líneas de enlace como el problema principal y los problemas SOC-ACOPF de las subredes como los subproblemas en el M-BDA propuesto. La factibilidad del M-BDA es probada analíticamente. Se diseñó un entorno de red de cálculo GAMS para calcular los subproblemas formulados en paralelo. Los resultados numéricos muestran que el M-BDA propuesto puede resolver eficientemente el problema SOC-ACOPF a gran escala. El M-BDA acelerado por cálculo paralelo converge en pocas iteraciones. Finalmente, se analizan y demuestran diversas aplicaciones de los modelos SOC-ACOPF y M-BDA incluyendo la distribución de los precios marginales locales (DLMP), la integración de la energía eólica y la red de energía de ultra-gran escala o supergrid.

Sammanfattning

Optimalt strömflöde (OPF) kan anses vara den grundläggande matematiska modellen för att optimalt driva ett elkraftsystem. Förbättring av OPF-lösningens kvalitet kan hjälpa kraftindustrin att spara miljarder dollar årligen. De senaste decennierna har präglats av enorma forskningsinsatser på OPF sedan J. Carpentier föreslog växelströmsmodellen OPF (ACOPF) som är olinjär och icke konvex. Denna avhandling föreslår tre konvexa OPF-modeller sk SOCP (SOC-ACOPF) vilka är baserad på andra ordningens konprogrammering och sk McCormick envelope. Den underliggande idén med de föreslagna SOC-ACOPF-modellerna är att släppa antaganden om den ursprungliga SOC-ACOPF-modellen med konvexa relaxeringar och approximationsmetoder. En heuristisk algoritm för att återfå en möjlig OPF-lösning av de föreslagna SOC-ACOPF-modellerna har utvecklats. Kvaliteten på lösningar med avseende på globalt optimum utvärderas med hjälp av MATPOWER och LINDOGLOBAL. En beräkningsmässig jämförelse med andra SOC-ACOPF-modeller i litteraturen utförs också. De numeriska resultaten visar robust prestanda för de föreslagna SOC-ACOPFmodellerna och tillhörande algoritmer. Vi föreslår sedan att påskynda lösningen av storskaligt SOC-ACOPF-problem genom sönderdelning och parallellisering. använder spektralfaktorisering för att partitionera stora nätverksnätverk till flera delnät kopplade av bindningar. En modifierad Benders nedbrytningsalgoritm (M-BDA) föreslås lösa SOC-ACOPF-problemet iterativt. Med den totala effekten av varje delnät som komplicerad variabel formulerar vi SOC-ACOPF-problemet med bindningar som huvudproblemet och SOC-ACOPF-problemen i delnätverk som delproblem i den föreslagna M-BDA. Genomförandet av det föreslagna M-BDA är analytiskt bevisat. En GAMS grid computing ram är utformad för att beräkna de formulerade delproblemen parallellt. De numeriska resultaten visar att den föreslagna M-BDA effektivt kan lösa storskaligt SOC-ACOPF-problem. Accelererad M-BDA genom parallell databehandling konvergerar inom få iterationer. Slutligen härleddes och demonstrerades olika tillämpningar av våra SOC-ACOPF-modeller och M-BDA, inklusive distribution av lokal marginalprissättning (DLMP), vindkraftintegration och ultra-storskaligt nätverkseller supernätverk.

Abstract in Dutch Language

Auteur: Zhao Yuan

Affiliatie: KTH Royal Institute of Technology

Titel: Convexe Optimale Powerflowberekening Gebaseerd op Tweede-Orde Cone Pro-

grammering: Modellen, Algoritmes en Toepassingen

Taal: Engels

Trefwoorden: Optimale elektriciteitstroom, Tweede-orde Cone Programmeren, Distri-

bution Locational Marginal Pricing, Windenergie, Super Grid

Optimal power flow (OPF) is het fundamenteel- wiskundige model om het elektriciteitsysteem optimaal te opereren. Het verbeteren van de oplossingskwaliteit van OPF kan de energieindustrie jaarlijks miljarden dollars besparen. De afgelopen decennia zijn er grote onderzoeksinspanningen verricht op het gebied van OPF, sinds J. Carpentier een nonconvex model voor wisselstroom OPF (ACOPF) ontwikkelde. Dit proefschrift stelt drie convexe OPF modellen voor (SOC-ACOPF), gebaseerd op tweede-orde cone programmering (SOCP) en McCormick-enveloppen. Het onderliggende idee van de voorgestelde SOC-ACOPF modellen is het loslaten van aannames in het oorspronkelijke SOC-ACOPF model door convexe relaxaties en benaderingsmethoden. Een heuristisch algoritme is ontwikkeld om toegelaten OPFoplossingen te herstellen uit de gerelaxeerde oplossingen van de voorgestelde SOC-ACOPF modellen. De kwaliteit van de oplossingen met betrekking tot het globale optimum is geëvalueerd met behulp van MATPOWER en LINDOGLOBAL. De rekentijd is vergeleken met andere SOC-ACOPF modellen in de literatuur. De numerieke resultaten tonen aan dat de prestaties van de voorgestelde SOC-ACOPF modellen en het algoritme voor het identificeren van toegelaten oplossingen robuust zijn. Vervolgens stellen wij voor om het oplossen van het grootschalig SOC-ACOPF-probleem te versnellen door middel van decompositie en parallelisatie. We gebruiken spectrale factorisatie om een groot stroomnetwerk te verdelen in meerdere subnetwerken die door de verbindingslijnen worden verbonden. Wij stellen een gemodificeerd Benders decompositiealgoritme (M-BDA) voor om het SOC-ACOPF probleem iteratief op te lossen. Met de totale stroomuitvoer van elk subnetwerk als de complicerende variabele formuleren we het SOC-ACOPF-probleem van verbindingen als het hoofdprobleem en de SOC-ACOPF-problemen van de subnetwerken als de subproblemen in de voorgestelde M-BDA. De haalbaarheid van het voorgestelde M-BDA wordt analytisch bewezen. Wij hebben een GAMS grid computing-raamwerk ontwikkeld om de geformuleerde subproblemen parallel te berekenen. De numerieke resultaten tonen aan dat de voorgestelde M-BDA het grootschalige SOC-ACOPF probleem efficiënt kan oplossen. De door parallel rekenen versnelde M-BDA convergeert binnen enkele Tenslotte worden diverse toepassingen van onze SOC-ACOPF-modellen en M-BDA afgeleid en aangetoond, inclusief distribution locational marginal pricing (DLMP), de integratie van windenergie en het beheer van een ultra-grootschalig netwerk of supernetwerk.

Acknowledgements

This research project is supported financially by the SETS Erasmus Mundus Joint Doctorate Fellowship provided by the European Commission. Most research work is carried out at the Department of Electrical Power and Energy Systems at KTH Royal Institute of Technology. The excellent supports from all partner universities of the SETS program are highly appreciated. I am very thankful to the Scholarships for conference travels from Stiftelse E C Ericssons fond, Velanders stiftelse, Knut and Alice Wallenberg Foundation and Malmes stiftelse.

I would like to express great thanks to my main supervisor Dr. Mohammad Reza Hesamzadeh at KTH for giving me this opportunity to pursue the PhD degree, supporting and guiding me during the research. My deep gratitude also goes to Dr. Sonja Wogrin and Dr. Andrés Ramos Galán who supervise me during my visiting research at Comillas Pontifical University. I want to give special thanks to Dr. Cristian Rojas as the internal reviewer of this thesis work at KTH. I am very grateful to Dr. Miguel Ángel Sanz Bobi, Dr. Laurens de Vries, Dr. Karen Aardaland and Dr. Lina Bertling Tjernberg for the excellent efforts to review the abstract of this thesis.

I want to thank my colleagues and friends at KTH, Comillas and TU Delft for the support, help and all the fun moments we are together. Especially, Dr. Lars Nordström, Dr. Lennart Söder, Dr. Mehrdad Ghandhari Alavijh, Dr. Mikael Amelin, Yue Cui, Meng Song, Wei Li, Dr. Yalin Huang, Dr. Lipeng Liu, Brigitt Högberg, Eleni Nylén, Peyman Mazidi, Ehsan Davari Nejad, Lars Herre, Ekaterina Moiseeva, Mahir Sarfati, Anna Grigoryeva, Dina Khastieva, Ezgi Uzuncan, Ilias Dimoulkas, Omar Kotb, Martin Nilsson, Egill Tomasson, Muhammad Taha Ali, Dr. Andrés Ramos Galán, Dr. Tomás Gómez San Román, Dr. Luis Olmos Camacho, Sara Tamarit Guerola, Diego Alejandro Tejada Arango, Alberto Orgaz Gil, Quanyu Zhao, Ángel Rosso Mateo, Celia Mosácula Atienza and João Gorenstein Dedecca.

Above all, I am indebted to my family for the continuous encouragement. This thesis work is impossible without the support from my parents and sister.

List of Figures

2.1	IEEE14-bus objective values and relaxation gaps for various load scenarios	38
2.2	IEEE57-bus objective values and relaxation gaps for various load scenarios	38
2.3	IEEE118-bus objective values and relaxation gaps for various load scenarios	39
2.4	IEEE300-bus objective values and relaxation gaps for various load scenarios	39
2.5	1354pegase objective values and relaxation gaps for various load scenarios .	40
2.6	$2869 \mathrm{pegase}$ objective values and relaxation gaps for various load scenarios .	40
3.1	The conceptual diagram of the proposed sequential tightness algorithm	49
3.2	The proposed parallel computing structure using M-BDA	54
3.3	IEEE14-bus network partitions (two subnetworks) and its master problem	
	representation	61
3.4	IEEE57-bus network partitions (three subnetworks) and its master problem	
	representation	61
3.5	IEEE118-bus network partitions (four subnetworks) and its master problem	
	representation	61
4.1	The conceptual diagram of the proposed HED mechanism	70
4.2	Approximation of a convex cost function by affine functions	71
4.3	The hierarchy of the modified IEEE342-node test system	73
4.4	The GAMS grid computing structure of hierarchical economic dispatch $$. $$	73
4.5	Local low voltage networks	74
4.6	The convergence of the proposed HED mechanism	77
4.7	The nodal prices in local networks	77
4.8	The total payment of consumers in local networks	78
4.9	The total income of DGs in local networks	78
5.1	The equivalent circuit of VSC-MTDC system	84
5.2	The monopole MTDC connection	85
5.3	The bipolar MTDC connection	86
5.4	The equivalent circuit of STATCOM	87
5.5	The equivalent circuit of SVC	88
5.6	Flow chart of the wind power scenario generation methodology	91
5.7	Weibull and Rayleigh distributions of wind speed measurement	92
5.8	Power curves of two wind turbine models	92
5.9	Power output of 81 wind power scenarios	93
5.10	Probability values of 81 wind power scenarios	94
5.11	Solution approaches of the stochastic SOC-ACOPF model	98

5.12	The IEEE30-bus network with two wind farms integrated by VSC-MTDC	
	system	99
5.13	The convergence of M-BDA	101
6.1	Visualizing the European super grid	106
6.2	The conceptual diagram of PSHub	107
6.3	The flow chart of traditional BD	112
6.4	The flow chart of the modified BD	113
6.5	The parallel computation management in PSHub	114
6.6	1354pegase objective value and computation time for various load scenarios	117
6.7	2869pegase objective value and computation time for various load scenarios	118
6.8	9241pegase objective value and computation time for various load scenarios	118

List of Tables

$2.1 \\ 2.2$	Objective value (\$)	36 37
2.3	Objective values of the recovered feasible solution (\$)	41
2.4	Computation time of the feasible solution recovery algorithm (s)	41
3.1	The performance of sequential tightness algorithm: objective solution $\ . \ .$	60
3.2	The performance of sequential tightness algorithm: computation time	60
3.3	Results of power network partitioning	63
3.4	Computation time of power network partitioning	64
3.5	Accelerated M-BDA by GAMS parallel computing	65
4.1	The results of the active power dispatch from HED mechanism, C: Cen-	
	tralized dispatch, H: HED	75
4.2	The results of the active power dispatch from HED mechanism, C: Cen-	
	tralized dispatch, H: HED	76
4.3	The GBFs in base case	79
4.4	The GBFs in case of x10-x11-x12 congestion	79
4.5	The GBFs in case of x13-x14-x15 congestion	80
4.6	The GBFs in case of x16-x17-x18 congestion	81
4.7	The GBFs in case of x21-x22 congestion	81
5.1	Objective value	101
5.2	Computation time	101
5.3	Value of stochastic solution (VSS)	103
6.1	Scale of operating the super grid	107
6.2	Metrics of regional EMS and power networks	
6.3	PSHub coordination results: base case	116
6.4	Iterations, Benders cuts and solution accuracy	117

List of Symbols

Nodes or Buses.

Lines.

Networks. Tie-lines.

Sets:

 $\frac{N}{L}$

K

 τ J

GGraph. PNetwork partition. N_k Nodes or buses located in regional power network k. Lines or branches located in regional power network k. Nodes or buses of the tie-lines. Parameters: Node to line incidence matrix. $A_{nl}^+, A_{nl}^ X_{l}$ Reactance and resistance of line l. R_l Resistance of line *l*. G_n Shunt conductance at bus n. B_n Shunt susceptance at bus n. P_{d_n} Active power demand at bus n. Q_{d_n} Reactive power demand at bus n. Bound of active power loss of line l. K_l V_n^{min} V_n^{max} p_n^{min} p_n^{max} Lower bound of voltage magnitude square. Upper bound of voltage magnitude square. Lower bound of active power generation. Upper bound of active power generation. q_n^{min} Lower bound of reactive power generation. q_n^{max} Upper bound of reactive power generation. Partitioning cost of cutting line l. c_l $I_{\bar{n}}$ Vector with all elements equal to one. CCost matrix of network partition. \bar{k}, \bar{n} Cardinality of set K and set N. X_T Transformer reactance. R_T Transformer resistance. R_{Cse} VSC station serial resistance. VSC station shunt resistance. R_{Csh} Cost parameter of active power generation at node n. α_n β_n Cost parameter of active power generation at node n. Cost parameter of active power generation at node n (added generator). $C_n^{q^+}$ Cost parameter of reactive power generation at node n (added generator).

Iterations (in Chapter 3) or Scenarios (in Chapter 5).

Variables:

Active power generation at bus n. p_n Reactive power generation at bus n. q_n

Active power flow of line l. p_{s_l} Reactive power flow of line l. q_{s_l} Active power loss of line l. p_{o_l} Reactive power loss of line l. q_{o_l} Voltage magnitude at bus n. v_n Sending end voltage of line l. v_{s_l} Receiving end voltage of line l. v_{r_l} V_n Voltage magnitude square at bus n.

 V_{s_l} Sending end voltage square. V_{r_l} Receiving end voltage square.

 θ_l Voltage phase angle difference of line l.

Sending end phase angle of line l. θ_{s_i} Receiving end phase angle of line l. θ_{r_l}

MNetwork partition matrix.

QOrthogonal matrix. DDiagonal matrix. EPermutation matrix. U, RQR-factorization matrix.

Total active power generation of network k. Total reactive power generation of network k.

 $P_{k,j}^{sum}$ $Q_{k,j}^{sum}$ $\Delta P_{d_n}^+$ $\Delta P_{d_n}^-$ Active power increment. Active power decrement. $\Delta Q_{d_n}^+$ Reactive power increment. Reactive power decrement.

 $\Delta Q_{d_n}^ \mu_{k,j}^P, \mu_{k,j}^Q$ Dual variables in Benders decomposition.

Active power generation (wind). $p_{e_{n,j}}$ Reactive power generation (wind). $q_{e_{n,j}}$ Current at the sending end of line l. I_{s_l}

Active power generation at node n (added generator). p_n^+ Reactive power generation at node n (added generator). q_n^+

List of Abbreviations

OPF Optimal Power Flow

ACOPF Alternating Current Optimal Power Flow
DCOPF Direct Current Optimal Power Flow
SOCP Second-Order Cone Programming
SDP Semi-Definite Programming

SOC-ACOPF Second-Order Cone Programming Based ACOPF

DLMP Distribution Locational Marginal Pricing

LRIC Long-Run Incremental Cost

FCP Forward Cost Pricing

DER Distributed Energy Resources

DG Distributed Generation

TSO Transmission System Operator
DSO Distribution System Operator

EU European Union EV Electric Vehicle HV High Voltage

HVDC High Voltage DC Transmission System HVAC High Voltage AC Transmission System

VSC Voltage Source Converter

MTDC Multi-Terminal DC Transmission System

FACTS Flexible AC Transmission System

GHG Green House Gas

p.u. Per Unit

IPM Interior Point Method KKT Karush-Kuhn-Tucker

ADMM Alternating Direction Method of Multipliers

BD Benders Decomposition

M-BDA Modified Benders Decomposition Algorithm SCUC Security Constrained Unit Commitment

TEP Transmission Expansion Planning

GBF Generalized Bid Function

HED Hierarchical Economic Dispatch
TNO Transmission Network Operator
DNO Distribution Network Operator

LNO Local Network Operator

STATCOM Static Synchronous Compensator

SVC Static VAR Compensator

HP Heat Pump

HPC High Performance Computing

LR Lagrange Relaxation

GEOPF Gas-Electric Integrated Optimal Power Flow

OFP Objective Feasibility Pump

MILP Mixed Integer Nonlinear Programming

MISOCP Mixed Integer Second-Order Cone Programming
MAUTS Multi-Area Generation Unit and Tie-Line Scheduling

RO Robust Optimization

AOP Alternating Optimization Procedure

VSS Value of Stochastic Solution

VoLL Value of Lost Load PSHub Power Synergy Hub

EMS Energy Management System

Chapter 1

Introduction

This Chapter gives a overview of the research topics in this thesis. The motivation of our research work is also explained. As a summary of the research results, we list the publications in peer-reviewed journals and conference proceedings. The submitted patents applications for our techniques are also listed.

1.1 Background and Motivation

Optimal power flow (OPF) is an indispensable tool in fairly wide areas of applications and its applications are still expanding [1–6]. The challenges of integrating large amount of renewable energy, increasing multi-terminal high voltage DC (HVDC) connections and growing number of prosumers in distribution grid are now pushing the electricity industry to seek more accurate, reliable and efficient OPF tools. Since the AC power flow constraints are complex, nonlinear and nonconvex in nature, enormous research efforts have been put into developing efficient algorithms to solve OPF during the past decades. References [7] and [8] summarize methods to solve OPF in the early stages ranging from linear, nonlinear and quadratic programming to Newton-based algorithm and interior point method (IPM). Evolutionary- and intelligence-based approaches to solve OPF can be found in [9] and [10]. Traditionally, the direct current OPF (DCOPF) as an estimation of full alternating current OPF (ACOPF) is pervasively employed for large-scale power system calculations [11]. With fast development of smart grids [12], distribution network is now in the unprecedented interest of advanced monitoring and control [13]. Distribution networks have a larger resistance to reactance (R/X) ratio as compared to the transmission network. Accordingly, the DCOPF results of distribution networks need to be carefully used. Besides, the operation points and nodal prices obtained from solving ACOPF in transmission and distribution networks are more accurate [14,15]. Accordingly, accurate and fast methods to solve ACOPF is in demand. However, after five decades of research, ACOPF remains lacking a thorough solution algorithm [1].

Solving OPF in a decentralized way is favourable in many aspects. Power network is either historically, geographically or technically partitioned into several zones or subnetworks to reduce the complexity of operation, control or planning [16, 17]. For example, Nord Pool operates the electricity market of Sweden over four well-defined

bidding areas from the north to the south [18]. Ten regions (California, MISO, New England, New York, Northwest, PJM, Southeast, Southwest, SPP and Texas) of the USA power system are separately operated by the corresponding independent system operators (ISOs) [19]. One fundamental reason of operating the power system by network partitions is that the dimension of the Hessian matrix and Jacobian matrix during the iterations of the optimization is reduced. It is then easier for the solver to address small-scale optimization problems. Another advantage of decentralized operation is that the OPF problems of multiple subnetworks can be solved in a parallel manner. In facing growing penetrations of distributed energy resources (DERs) which may exceed the capability of centralized operation, parallel and decentralized operation could be a feasible solution [20].

One important recent application of OPF is distribution locational marginal pricing (DLMP) which can reflect the value of energy and network in the dimension of both time and location. Smart grid advocates envisage a future in which small customers are responsive to local market conditions with devices that reduce electricity consumption at times of high prices and increase consumption at times of low prices. The increasing penetration of devices capable of responding to market prices is increasing the need for, and the utility of, improved distribution pricing signals. Efficient distribution pricing signals reflect both losses and congestion on the distribution network. Such prices vary across both time and locations and reflect the short-run marginal cost of the transportation of electricity from one point on the distribution network to another. The time-of-use pricing is proposed in [21]. In this mechanism different price level is defined for different time periods of the day. The drawback of time-of-use pricing is that real peak time periods can be deviated from the pre-defined hours in the pricing structure. As an improvement, the critical-peak pricing is discussed in [22]. critical-peak pricing introduces flexible critical price hours during one year combined with time-of-use pricing. The critical time in critical-peak pricing is broadcasted to consumers well before happening. The real-time pricing is also proposed and discussed in literature [23, 24]. In real-time pricing, prices vary with an hourly basis. However, the distribution networks lack proper locational price signals for the growing small prosumers and distributed energy resources [25]. Reference [26] proposes distribution network use-of-system charges to convey locational signals to distribution network users. Authors in [26] justify their distribution network charges based on absence of DLMPs. In [27], long-run incremental cost pricing (LRIC) and forward cost pricing (FCP) are introduced as distribution charging methodologies for Great Britain. These methodologies offer locational messages in their pricing mechanism. In recent years there has been rapidly increasing interest in locational marginal pricing of distribution networks, especially to facilitate integration of distributed energy resources [28]. The benefit of DLMPs for charging management of electric vehicles is discussed in [29]. References [30,31] discuss boosting of demand-side responses using DLMPs. Reference [32] demonstrates how DLMPs can alleviate congestion caused by high penetration of electric vehicles (EVs) and heat pumps (HPs). By using Danish driving pattern, reference [32] show that without DLMP, the low system price at 24:00 motivates all EVs for charging. Also, the peak conventional demand at 18:00 leads to unavailable line capacity for HP demands causing congestion. When DLMP is applied, EV charging demands are spread to 23:00 and 5:00 and HP produce more heat before 18:00 to deal with the forecasted high price at 18:00 (thermal dynamics of the house structure and air help to maintain the room temperature in a short time interval). Reference [33] proposes to integrate DLMPs and optimization in controlling future distribution networks where electronic devices are enabled to receive control signals generated from DLMP. We solve the computation and coordination challenges of implementing DLMP in this thesis.

More efficient OPF models can also be used to integrate renewable energy sources such as wind power. The Voltage Source Converter (VSC) based multi-terminal DC (VSC-MTDC) system and Flexible AC Transmission System (FACTS) are playing important roles in integrating intermittent renewable energy resources [34]. On the one hand, VSC-MTDC and FACTS can be applied to remove congestion in heavily loaded power systems [35]. On the other hand, FACTS devices can be used to enhance transfer capacity [36]. Claus et al. [37] point out that flexible hybrid AC-DC systems are inevitable in the future smart grid. The importance of VSC-MTDC systems and FACTS is further emphasized by [38], which investigates the benefits of FACTS devices in the IEEE 57-Bus test system with high penetration of wind power. After installing FACTS devices, the total savings of the net present value (NPV) over 20 years amount to \$49.45 million. The most relevant literature regarding the optimal operation of power network including VSC-MTDC system and FACTS devices are generally modeled in an ACOPF problem. We use SOC-ACOPF model in this thesis to tackle the challenge of wind power integration in a stochastic programming framework.

Our OPF models and algorithms are applicable for the European ultra-high voltage power grid which is evolving to a super grid with more high voltage AC (HVAC) and high voltage DC (HVDC) interconnections [39]. The major advantage of building a super grid is balancing energy consumption and generation across the continent [40]. Larger transmission capacity between renewable energy abundant areas and load centers means more efficient complementary energy use in dimension of both location and time. It is cost beneficial to fully exploit the renewable energy resources by expanding the power transmission network throughout Europe [41]. In facing the Energy Roadmap 2050 issued by the European Commission, an ambitious 80% reduction of green house gas emissions (GHG) by the year of 2050 compared with 1990 has been set out [39,42]. Since electricity covers around 20% of energy consumption [39], exploiting the huge potential of the electricity sector in achieving the EU2050 target is critical.

The energy dispatch coordination problem of super grid is addressed in this thesis.

1.2 List of Publications and Patents

My PhD research work is summarized by following publications and patents: Peer-Reviewed Journals included in the Journal Citation Report (JCR)

- [J6]. Z. Yuan, M. R. Hesamzadeh. Second-Order Cone AC Optimal Power Flow: Convex Relaxations and Feasible Solutions, Journal of Modern Power Systems and Clean Energy, 2018 (Submitted).
- [J5]. Z. Yuan, M. R. Hesamzadeh, S. Wogrin and M. Baradar. Stochastic Optimal Operation of VSC-MTDC System and FACTS Considering Large-Scale Integration of Wind Power, Computers & Operations Research, 2017 (Submitted).
- [J4]. Z. Yuan, M. R. Hesamzadeh. A Modified Benders Decomposition Algorithm to Solve Second-Order Cone AC Optimal Power Flow, IEEE Transactions on Smart Grid, 2017 (Published).
- [J3]. Z. Yuan, S. Wogrin and M. R. Hesamzadeh. Towards the Power Synergy Hub (PSHub): Coordinating the Energy Dispatch of Super Grid by Modified Benders Decomposition, Applied Energy, Volume 205, 2017, Pages 1419-1434 (Published).
- [J2]. Z. Yuan, M. R. Hesamzadeh. Hierarchical Coordination of TSO-DSO Economic Dispatch Considering Large-Scale Integration of Distributed Energy Resources, Applied Energy, Volume 195, 2017, Pages 600-615 (Published).
- [J1]. Z. Yuan, M. R. Hesamzadeh, D. Biggar. Distribution Locational Marginal Pricing by Convexified ACOPF and Hierarchical Dispatch, IEEE Transactions on Smart Grid, 2016 (Published).

Peer-Reviewed Conference Proceedings

- [C8]. Z. Yuan, M. R. Hesamzadeh. A Max-Affine Approximation Model to Solve Power Flow Problem with Controllable Accuracy, The International Conference on Innovative Smart Grid Technologies Europe, Sarajevo, October 21-25, 2018 (Submitted).
- [C7]. Z. Yuan, M. R. Hesamzadeh. Improving the Accuracy of Second-Order Cone AC Optimal Power Flow by Convex Approximations, The International Conference on Innovative Smart Grid Technologies Asia, Singapore, May 22-25, 2018 (Accepted).

- [C6]. Z. Yuan, M. R. Hesamzadeh. A Distributed Economic Dispatch Mechanism to Implement Distribution Locational Marginal Pricing, Power Systems Computation Conference, Dublin, Ireland, June 11-15, 2018 (Accepted).
- [C5]. Z. Yuan, M. R. Hesamzadeh. Applying Convex Optimal Power Flow to Distribution Locational Marginal Pricing, 21st Conference of the International Federation of Operational Research Societies, Québec City, Canada, July 17 - 21, 2017.
- [C4]. Z. Yuan, M. R. Hesamzadeh, Y. Cui, L. B. Tjernberg. Applying High Performance Computing to Probabilistic Convex Optimal Power Flow, International Conference on Probabilistic Methods Applied to Power Systems, Beijing, China, October 16 20, 2016.
- [C3]. Z. Yuan, M. R. Hesamzadeh. Implementing Zonal Pricing in Distribution Network: the Concept of Pricing Equivalence, IEEE Power and Energy Society General Meeting, Boston, USA, July 17 21, 2016.
- [C2]. Z. Yuan, M. R. Hesamzadeh. A Hierarchical Dispatch Structure for Distribution Network Pricing, 15th International Conference on Environment and Electrical Engineering, Rome, Italy, June 10 - 13, 2015.
- [C1]. M. Nilsson, L. Soder and Z. Yuan. Estimation of Power System Frequency Response based on Measured & Simulated Frequencies, IEEE Power and Energy Society General Meeting, Boston, USA, July 17 - 21, 2016.

Patents

- [P2]. Z. Yuan (Applicant and Co-Inventor), M. R. Hesamzadeh. Sequential Conic Programming Method to Solve Optimal Power Flow Problem, Sweden, 2016 (Submitted and in the Second Round Evaluation by Swedish Patent Office).
- [P1]. Z. Yuan (Applicant and Co-Inventor), M. R. Hesamzadeh. A Decomposition System to Solve AC Optimal Power Flow Problem, Sweden, 2016 (Submitted and in the Second Round Evaluation by Swedish Patent Office).

25

1.3 Thesis Outline

The rest of this thesis is organized as follows:

Chapter 2 proposes the convex OPF models. The numerical performances of the proposed OPF models compared with other models are examined through various IEEE test cases.

Chapter 3 presents the sequential tightness algorithm to improve feasibility of the OPF solutions. The decentralized OPF solution algorithm based on modified Benders decomposition is proposed and explained in detail. All the proposed algorithms are numerically validated.

Chapter 4 demonstrates the application of our convex OPF models in DLMP and coordinating TSO-DSO operations. The concepts of generalized bid function and hierarchical economic dispatch mechanism are proposed to address the computational and coordinational challenges of implementing DLMP.

Chapter 5 deals with the challenge of integrating wind power by stochastic conic programming and high performance computing. A scenario-based decomposition approach is proposed to tackle large number of wind power scenarios.

Chapter 6 sets up the concept of power synergy hub (PSHub) to coordinate the energy dispatch for ultra-large-scale power grid or super grid. We show that the modified Benders decomposition algorithm can serve as an efficient approach to coordinate the energy dispatch of multiple nations or regions across the continent. Fast convergence of the proposed approach is demonstrated for power networks with up to 9241 nodes.

Chapter 2

Convex Optimal Power Flow Models

2.1 Introduction

Recent developments in ACOPF research can be mainly classified into four branches: (1) convexification [43–45], relaxation and approximation [2,46–48]; (2) decentralized or distributed algorithms [49, 50]; (3) addressing uncertainty [51, 52] and (4) global optimality [53]. Convex relaxation techniques can give useful bound of ACOPF objective function. Convexity also guarantees finding global solution by using mature solution algorithms (e.g. IPM). Considering commercially available solvers (such as MOSEK [54]) for solving convex problems, the remaining task is to tighten the relaxations used in the convexification. It is in this sense that mathematical relaxation techniques that can properly convexify ACOPF are important. Though assuming no lower bound for active power generation to exactly convexify mesh networks are not realistic, the proposed branch flow model in [44] as a convex relaxation of ACOPF is very important and useful. Reference [43] gives exact convex relaxations of OPF under some assumptions on network parameters. Based on the branch flow approach, authors in [55] present an ACOPF model using second-order cone programming (SOCP) and it shows accurate solutions for several IEEE test cases when the objective is transmission loss minimization. A cone-programming-based OPF for radial distribution networks is proposed in [56]. Reference [13] points out that power loss minimization objective function for the developed SOCP-based ACOPF is always exact. For other objective functions than power loss minimization, the proposed model in [13] requires developing new solution algorithms. Reference [13] continues to improve its cone relaxation by generating tight cutting planes. For radial networks, sufficient conditions regarding network property and voltage upper bound under which the proposed relaxed ACOPF can give global ACOPF solution are derived in [43]. Reference [57] formulates a twostage stochastic mixed-integer second order cone program (MISOCP) to model the trade-off between investment in AC and MTDC networks.

Another promising convexification approach for ACOPF is to use Semi-Definite Programming (SDP) [58, 59]. The computational limits of SDP are shown in [60]. Efficient algorithms for solving SDP-based ACOPF model remain to be found [58]. Regarding ACOPF in large-scale power networks, SDP-based ACOPF takes much more CPU time than SOCP-based ACOPF. The pioneering work using matrix com-

27

bination and decomposition techniques by authors in [61] to accelerate SDP-based ACOPF show that more than 1000 seconds solver time are required to compute cases with around 3000 buses. Important analysis and results from [62–64] show that SDP relaxations are exact only for limited types of problems. Even for a 2-bus 1-generator power system, SDP-based ACOPF can be infeasible and inexact [65]. In cases where the exactness is not guaranteed, solutions of SDP-based ACOPF rarely have physical meanings.

Results from [48] show that Quadratic Convex (QC) relaxation of ACOPF may produce some improvements in accuracy over SOCP-based ACOPF but with reduced computational efficiency. The feasible region relationship of SOCP, SDP and QC approaches are analyzed in [48]. The SDP and QC approaches give tighter relaxations than the SOCP approach but they are not equivalent to each other. In terms of computational performance, the QC and SOCP approaches are much faster and reliable than the SDP approach [48]. Based on first-order Taylor expansion, a current-voltage formulation for ACOPF is proposed in [2,66]. The advantages of the current-voltage formulation are that the approximated ACOPF problem is linear and much faster to be solved than nonlinear formulations. However, an iterative algorithm is required to check the violations of nonconvex ACOPF constraints and then to construct the inner or outer bounds of the approximations. The network flow (NF) and copper plate (CP) models for ACOPF are proposed in [67]. The NF and CP models bring significant computational advantage at the cost of reduced accuracy. They either require more complex solution algorithms [2,66] or may result in infeasible solutions [67]. Authors in [68] propose three different relaxation methods to improve SOCP-based ACOPF. The arctangent constraints in the rectangular formulation of ACOPF are convexified by McCormick relaxations, polyhedral envelopes and dynamically generated linear inequalities [68]. The results show prominent computational efficiency of the SOCP approach over the SDP approach [68].

Regarding the feasibility of the relaxed solutions, three types of sufficient conditions about power injections, voltage magnitudes and phase angles to guarantee obtaining exact solutions are proposed in [64]. Authors in [68] strengthen the relaxations of SOCP-based ACOPF model by dynamically generating linear valid inequalities to separate solutions of SOCP-based ACOPF from other relaxed constraints. However, it is not guaranteed that feasible solution can be always recovered by this approach. The complementarity conditions in the Karush-Kuhn-Tucker (KKT) system of DCOPF are used in [69] to recover feasible solution of ACOPF.

Accordingly, the main contributions of the current Chapter are:

1. Three SOC-ACOPF models based on second-order cone relaxations, Taylor expansions and McCormick envelops are proposed;

- 2. A heuristic algorithm is proposed to recover a feasible solution of ACOPF from the relaxed solution;
- 3. A computational comparison with other SOCP-based ACOPF formulations in the literature is conducted.

The rest of this Chapter is organized as follows. Section II presents mathematical formulations of the proposed SOC-ACOPF models. Section III proposes the heuristic algorithm to recover feasible solutions. Section IV discusses numerical results for various IEEE test cases under different load scenarios. Section V concludes.

2.2 AC Optimal Power Flow

2.2.1 Full AC Optimal Power Flow Model

It is assumed that the electric networks are three phase and balanced. The full AC OPF model (based on the validated branch flow model [44,55]) is formulated in optimization problem (2.1). Note p_{s_l}, q_{s_l} represent receiving end power flows in [55] which are different in our formulation. So some constraints are accordingly different. The term s in $p_{s_l}, q_{s_l}, v_{s_l}, V_{s_l}$ is not an index but only to imply the meaning of sending end of line l. The term r in v_{r_l}, V_{r_l} is not an index but only to imply the meaning of power demand. Similar reasoning holds for the term o in p_{o_l}, q_{o_l} which is to denote the meaning of power loss.

$$\underset{\Omega}{\text{Minimize}} \quad f(p_n, q_n, p_{o_l}, q_{o_l}) \tag{2.1a}$$

subject to

$$p_n - p_{d_n} = \sum_{l} (A_{nl}^+ p_{s_l} - A_{nl}^- p_{o_l}) + G_n V_n, \ \forall n \in \mathbb{N}$$
 (2.1b)

$$q_n - q_{d_n} = \sum_{l} (A_{nl}^+ q_{s_l} - A_{nl}^- q_{o_l}) - B_n V_n, \ \forall n \in \mathbb{N}$$
 (2.1c)

$$p_{o_l} = \frac{p_{s_l}^2 + q_{s_l}^2}{V_{s_l}} R_l, \ \forall l \in L$$
 (2.1d)

$$q_{o_l} = \frac{p_{s_l}^2 + q_{s_l}^2}{V_{s_l}} X_l, \ \forall l \in L$$
 (2.1e)

$$V_{s_l} - V_{r_l} = 2R_l p_{s_l} + 2X_l q_{s_l} - R_l p_{o_l} - X_l q_{o_l}, \ \forall l \in L$$
 (2.1f)

$$v_{s_l}v_{r_l}\sin\theta_l = X_l p_{s_l} - R_l q_{s_l}, \ \forall l \in L$$
(2.1g)

$$p_{s_l}^2 + q_{s_l}^2 \le K_l, \ \forall l \in L$$
 (2.1h)

$$V_n = v_n^2, \ \forall n \in N \tag{2.1i}$$

$$v_n^{min} \le v_n \le v_n^{max}, \ \forall n \in N$$
 (2.1j)

$$\theta_l^{min} \le \theta_l \le \theta_l^{max}, \ \forall l \in L$$
 (2.1k)

$$p_n^{min} \le p_n \le p_n^{max}, \ \forall n \in N$$
 (2.11)

$$q_n^{min} \le q_n \le q_n^{max}, \ \forall n \in N \tag{2.1m}$$

Where $\Omega = \{p_n, q_n, p_{s_l}, q_{s_l}, p_{o_l}, q_{o_l}, V_n, v_n, \theta_l\} \in \Re$ is the set of decision variables. Depending on the applications, the objective function $f(p_n, q_n, p_{o_l}, q_{o_l})$ can be the economic cost of energy production, network power loss or security margin. In this thesis, we use the quadratic or linear cost function of energy production in MATPOWER [70] directly. Equations (2.1b) and (2.1c) represent the active and reactive power balance. A_{nl}^+ and A_{nl}^- are the incidence matrices of the network with $A_{nl}^+ = 1$, $A_{nl}^- = 0$ if n is the sending end of line l, and $A_{nl}^+ = -1$, $A_{nl}^- = 1$ if n is the receiving end of line l. $V_{s_l} = v_{s_l}^2$ and $V_{r_l} = v_{r_l}^2$ are voltage magnitude squares. Equations (2.1d)-(2.1e) represent active power and reactive power loss. $\theta_l = \theta_{s_l} - \theta_{r_l}$ is the voltage phase angle difference of line l. Equations (2.2d)-(2.1g) are derived by taking the magnitude and phase angle of the voltage drop phasor along line l respectively [44,55]. Constraints (2.1j)-(2.1m) are bounds for voltage magnitude, voltage phase angle difference, active power generation and reactive power generation. This model is nonconvex because of the nonconvex constraints (2.1d), (2.1e), (2.1g) and (2.1i). Current available nonlinear programming solvers are unable to efficiently find the global optimal solution of this nonconvex model.

The objective function f of typical economic dispatch is quadratic:

$$f(p_n) = \sum_{n} \alpha_n p_n^2 + \beta_n p_n \tag{2.1n}$$

Where α_n , β_n are cost parameters of the active power generation. If we can convexify the nonconvex power flow constraints (2.1d), (2.1e), (2.1g) and (2.1i), minimizing quadratic objective function over a convex feasible region is a convex optimization problem.

2.2.2 SOC-ACOPF: Model P

The proposed SOC-ACOPF models are derived using line sending-end power injections and voltage phase angle difference variables. In this way, we can directly obtain voltage

phase angle solutions from the models. Note that in some of the derived models, voltage square variables are included (voltage can be recovered from the model by taking the root of the voltage square solutions). Model P of the SOC-ACOPF is set out in (2.2), [55].

$$\underset{\Omega}{\text{Minimize}} \quad f(p_n, q_n, p_{o_l}, q_{o_l}) \tag{2.2a}$$

subject to

$$(2.1b) - (2.1c), (2.1j) - (2.1m)$$

$$K_l \ge p_{o_l} \ge \frac{p_{s_l}^2 + q_{s_l}^2}{V_{s_l}} R_l, \ \forall l \in L$$
 (2.2b)

$$p_{o_l} X_l = q_{o_l} R_l, \ \forall l \in L \tag{2.2c}$$

$$V_{s_l} - V_{r_l} = 2R_l p_{s_l} + 2X_l q_{s_l} - R_l p_{o_l} - X_l q_{o_l}, \ \forall l \in L$$
 (2.2d)

$$\theta_l = X_l p_{s_l} - R_l q_{s_l}, \ \forall l \in L \tag{2.2e}$$

Constraints (2.2b)-(2.2c) represent active power and reactive power loss. The left side of (2.2b) bounds p_{ol} (which equivalently bounds capacity of line l). Equation (2.2e) is approximated from the nonconvex constraint (2.1g). This approximation is based on following assumptions:

- (a) Voltage magnitude product $v_{s_l}v_{r_l}$ is approximately equal to 1 per-unit in (2.1g);
- (b) Voltage phase angle difference across each line is small enough such that $\sin \theta_l \approx \theta_l$.

2.2.3 SOC-ACOPF: Model R

To drop assumption (a) in Model P, we use the following bilinear transformation:

$$v_{s_l}v_{r_l} = \frac{1}{4}[(v_{s_l} + v_{r_l})^2 - (v_{s_l} - v_{r_l})^2], \ \forall l \in L$$
(2.3a)

If we introduce auxiliary variable v_{m_l} as:

$$v_{m_l} = v_{s_l} v_{r_l}, \ \forall l \in L \tag{2.3b}$$

And repeat transformation (2.3a) then the left side of equation (2.1g) can be replaced by:

$$v_{m_l}\theta_l = \frac{1}{4}[(v_{m_l} + \theta_l)^2 - (v_{m_l} - \theta_l)^2], \ \forall l \in L$$
 (2.3c)

Introducing new variables u_{x_l} , w_{x_l} , u_{v_l} and w_{v_l} as:

$$u_{x_l} = v_{s_l} + v_{r_l}, \ \forall l \in L \tag{2.3d}$$

$$w_{x_l} = v_{s_l} - v_{r_l}, \ \forall l \in L \tag{2.3e}$$

$$u_{v_l} = v_{m_l} + \theta_l, \ \forall l \in L \tag{2.3f}$$

$$w_{v_l} = v_{m_l} - \theta_l, \ \forall l \in L \tag{2.3g}$$

Equations (2.3a) and (2.3c) can be expressed by the new variables u_{x_l} , w_{x_l} , u_{v_l} and w_{v_l} as:

$$v_{s_l}v_{r_l} = \frac{1}{4}(u_{x_l}^2 - w_{x_l}^2), \ \forall l \in L$$
 (2.3h)

$$v_{m_l}\theta_l = \frac{1}{4}(u_{v_l}^2 - w_{v_l}^2), \ \forall l \in L$$
 (2.3i)

The quadratic functions $u_{x_l}^2$, $w_{x_l}^2$, $u_{v_l}^2$ and $w_{v_l}^2$ are relaxed as following convex cones:

$$u_{xa_l} \ge u_{x_l}^2, \ \forall l \in L \tag{2.3j}$$

$$w_{xa_l} \ge w_{x_l}^2, \ \forall l \in L$$
 (2.3k)

$$u_{va_l} \ge u_{v_l}^2, \ \forall l \in L$$
 (2.31)

$$w_{va_l} \ge w_{v_l}^2, \ \forall l \in L$$
 (2.3m)

The upper bounds are expressed linearly:

$$u_{xa_l} \le (\bar{u}_{x_l} + \underline{u}_{x_l})u_{x_l} - \bar{u}_{x_l}\underline{u}_{x_l}, \ \forall l \in L$$
(2.3n)

$$w_{xa_l} \le (\bar{w}_{x_l} + \underline{w}_{x_l})w_{x_l} - \bar{w}_{x_l}\underline{w}_{x_l}, \ \forall l \in L$$
 (2.30)

$$u_{va_l} \le (\bar{u}_{v_l} + \underline{u}_{v_l})u_{v_l} - \bar{u}_{v_l}\underline{u}_{v_l}, \ \forall l \in L$$

$$(2.3p)$$

$$w_{va_l} \le (\bar{w}_{v_l} + \underline{w}_{v_l}) w_{v_l} - \bar{w}_{v_l} \underline{w}_{v_l}, \ \forall l \in L$$
 (2.3q)

Where constraints (2.3j)-(2.3m) are second-order cones and constraints (2.3n)-(2.3q) are McCormick envelopes. $\bar{u}_{x_l}, \bar{w}_{x_l}, \bar{u}_{v_l}$ and \bar{w}_{v_l} are upper bounds of the corresponding variables. $\underline{u}_{x_l}, \underline{w}_{x_l}, \underline{u}_{v_l}$ and \underline{w}_{v_l} are lower bounds of the corresponding variables. The variables v_{s_l} and v_{r_l} are linked to their squares V_{s_l} and V_{r_l} by following convex constraints.

$$V_n \ge v_n^2, \ \forall n \in N$$
 (2.3r)

$$V_n \le (\bar{v}_n + \underline{v}_n)v_n - \bar{v}_n\underline{v}_n, \ \forall n \in N$$
(2.3s)

Where \bar{v}_n and \underline{v}_n are upper and lower bounds of voltage magnitude. Constraint (2.3s) tightens the cone relaxations in (2.3r). In Model R of SOC-ACOPF, we replace constraints (2.2e) of optimization problem (2.2) by constraints (2.3d)-(2.3g), (2.3j)-(2.3m), (2.3n)-(2.3q), (2.3r)-(2.3s) and constraints (2.3h)-(2.3i) where the quadratic functions $u_{x_l}^2$, $w_{x_l}^2$, $u_{v_l}^2$ and $w_{v_l}^2$ are replaced by u_{xa_l} , w_{xa_l} , u_{va_l} and w_{va_l} , the term $v_{s_l}v_{r_l}$ is replaced by v_{m_l} , the term $v_{m_l}\theta_l$ is replaced by $v_{l}^2 = v_{l}^2 + v_{l}^2 +$

2.2.4 SOC-ACOPF: Model T

To drop assumption (b) of Model R, we propose to apply Taylor series expansion to approximate Sine function:

$$\sin \theta_l = \theta_l - \frac{\theta_l^3}{6} + \frac{\theta_l^5}{120} + O(\theta_l^7), \ \forall l \in L$$
 (2.4a)

As a trade off between model complexity and accuracy, fifth-order Taylor series expansion is selected. The approximation error is less than 0.45% for $|\theta_l| < \frac{\pi}{2}$. Repeating the bilinear transformation procedure similar in Model R derived in the previous Section, we have:

$$u_{\theta_l^2} = \theta_l^2; \qquad u_{\theta_l^3} = \theta_l^3; \qquad u_{\theta_l^5} = \theta_l^5, \ \forall l \in L$$
 (2.4b)

$$\theta_l^3 = \frac{1}{4} [(\theta_l + u_{\theta_l^2})^2 - (\theta_l - u_{\theta_l^2})^2], \ \forall l \in L$$
 (2.4c)

$$\theta_l^5 = \frac{1}{4} [(u_{\theta_l^2} + u_{\theta_l^3})^2 - (u_{\theta_l^2} - u_{\theta_l^3})^2], \ \forall l \in L$$
 (2.4d)

We introduce auxiliary variables to formulate relaxations of quadratic equations:

$$h_{x_l} = \theta_l + u_{\theta_l^2}, \ \forall l \in L \tag{2.4e}$$

$$y_{x_l} = \theta_l - u_{\theta_l^2}, \ \forall l \in L \tag{2.4f}$$

$$h_{v_l} = u_{\theta_l^2} + u_{\theta_l^3}, \ \forall l \in L \tag{2.4g}$$

$$y_{v_l} = u_{\theta_i^2} - u_{\theta_i^3}, \ \forall l \in L \tag{2.4h}$$

$$u_{v_l} = v_{m_l} + (\theta_l - \frac{u_{\theta_l^3}}{6} + \frac{u_{\theta_l^5}}{120}), \ \forall l \in L$$
 (2.4i)

$$w_{v_l} = v_{m_l} - (\theta_l - \frac{u_{\theta_l^3}}{6} + \frac{u_{\theta_l^5}}{120}), \ \forall l \in L$$
 (2.4j)

Higher order terms of θ_l can be expressed similarly by introducing new auxiliary variables. Again, as in Model R, using u_{v_l} and w_{v_l} variables, we have:

$$u_{\theta_l^3} = \frac{1}{4} (h_{x_l}^2 - y_{x_l}^2), \ \forall l \in L$$
 (2.4k)

$$u_{\theta_l^5} = \frac{1}{4} (h_{v_l}^2 - y_{v_l}^2), \ \forall l \in L$$
 (2.41)

$$v_{s_l}v_{r_l}\sin\theta_l \approx \frac{1}{4}(u_{v_l}^2 - w_{v_l}^2), \ \forall l \in L$$
 (2.4m)

Similarly, auxiliary variables h_{xa_l} , y_{xa_l} , h_{va_l} and y_{va_l} are proposed:

$$h_{xa_l} \ge h_{x_l}^2, \ \forall l \in L \tag{2.4n}$$

$$y_{xa_l} \ge y_{x_l}^2, \ \forall l \in L \tag{2.40}$$

$$h_{va_l} \ge h_{v_l}^2, \ \forall l \in L$$
 (2.4p)

$$y_{va_l} \ge y_{v_l}^2, \ \forall l \in L$$
 (2.4q)

Quadratic functions are bounded above by:

$$h_{xa_l} \le (\overline{h}_{x_l} + \underline{h}_{x_l}) h_{x_l} - \overline{h}_{x_l} \underline{h}_{x_l}, \ \forall l \in L$$
 (2.4r)

$$y_{xa_l} \le (\overline{y}_{x_l} + \underline{y}_{x_l})y_{x_l} - \overline{y}_{x_l}\underline{y}_{x_l}, \ \forall l \in L$$
 (2.4s)

$$h_{va_l} \le (\overline{h}_{v_l} + \underline{h}_{v_l}) h_{v_l} - \overline{h}_{v_l} \underline{h}_{v_l}, \ \forall l \in L$$
 (2.4t)

$$y_{va_l} \le (\overline{y}_{v_l} + \underline{y}_{v_l})y_{v_l} - \overline{y}_{v_l}\underline{y}_{v_l}, \ \forall l \in L$$
 (2.4u)

Where \overline{h}_{x_l} , \overline{y}_{x_l} , \overline{h}_{v_l} and \overline{y}_{v_l} are upper bounds of the corresponding variables. \underline{h}_{x_l} , \underline{y}_{x_l} , \underline{h}_{v_l} and \underline{y}_{v_l} are lower bounds of the corresponding variables. $u_{\theta_l^2}$ is bounded as follows:

$$u_{\theta_l^2} \ge \theta_l^2, \ \forall l \in L$$
 (2.4v)

$$u_{\theta_l^2} \le \overline{\theta}_l^2, \ \forall l \in L$$
 (2.4w)

Where $\overline{\theta}_{l}^{2}$ is the upper bound of θ_{l}^{2} . In Model T of SOC-ACOPF, we replace constraints (2.2e) of optimization problem (2.2) by constraints (2.3d)-(2.3e), (2.3j)-(2.3m), (2.3n)-(2.3q), (2.3r)-(2.3s), (2.4e)-(2.4j), (2.4n)-(2.4q), (2.4r)-(2.4u), (2.4v)-(2.4w) and constraints (2.3h), (2.4k)-(2.4m) where quadratic functions $u_{x_{l}}^{2}$, $w_{x_{l}}^{2}$, $h_{x_{l}}^{2}$, $y_{x_{l}}^{2}$, $h_{v_{l}}^{2}$, $y_{v_{l}}^{2}$, $u_{v_{l}}^{2}$ and $w_{v_{l}}^{2}$ are replaced by $u_{xa_{l}}$, $w_{xa_{l}}$, $h_{xa_{l}}$, $y_{xa_{l}}$, $h_{va_{l}}$, $y_{va_{l}}$, $u_{va_{l}}$ and $w_{va_{l}}$, the term $v_{s_{l}}v_{r_{l}}\sin\theta_{l}$ is replaced by $X_{l}p_{s_{l}}-R_{l}q_{s_{l}}$.

2.2.5 SOC-ACOPF: Model E

Nonconvex term in the left side of equation (2.1g) can be directly replaced by its convex envelopes described in [71]. Employing (2.3b) and introducing new variables $z_{\theta_l} = \sin \theta_l$ and $z_{hl} = v_s v_r \sin \theta_l$, we have:

$$v_{s_l}v_{r_l}\sin\theta_l = v_{m_l}z_{\theta_l}, \ \forall l \in L$$
 (2.5a)

$$z_{h_l} = X_l p_{s_l} - R_l q_{s_l}, \ \forall l \in L \tag{2.5b}$$

Convex envelopes for $z_{hl} = v_{ml} z_{\theta_l}$ are:

$$z_{h_l} \geqslant \underline{v}_{m_l} z_{\theta_l} + \underline{z}_{\theta_l} v_{m_l} - \underline{v}_{m_l} \underline{z}_{\theta_l}, \ \forall l \in L$$
 (2.5c)

$$z_{h_l} \geqslant \overline{v}_{m_l} z_{\theta_l} + \overline{z}_{\theta_l} v_{m_l} - \overline{v}_{m_l} \overline{z}_{\theta_l}, \ \forall l \in L$$
 (2.5d)

$$z_{h_l} \leqslant \underline{v}_{m_l} z_{\theta_l} + \overline{z}_{\theta_l} v_{m_l} - \underline{v}_{m_l} \overline{z}_{\theta_l}, \ \forall l \in L$$
 (2.5e)

$$z_{h_l} \leqslant \overline{v}_{m_l} z_{\theta_l} + \underline{z}_{\theta_l} v_{m_l} - \overline{v}_{m_l} \underline{z}_{\theta_l}, \ \forall l \in L$$
 (2.5f)

Where \underline{v}_{m_l} , \underline{z}_{θ_l} are lower bounds and \overline{v}_{m_l} , \overline{z}_{θ_l} are upper bounds for their corresponding variables. Convex envelopes for $v_{m_l} = v_{s_l} v_{r_l}$ are:

$$v_{m_l} \geqslant \underline{v}_{s_l} v_{r_l} + \underline{v}_{r_l} v_{s_l} - \underline{v}_{s_l} \underline{v}_{r_l}, \ \forall l \in L$$
 (2.5g)

$$v_{m_l} \geqslant \overline{v}_{s_l} v_{r_l} + \overline{v}_{r_l} v_{s_l} - \overline{v}_{s_l} \overline{v}_{r_l}, \ \forall l \in L$$
 (2.5h)

$$v_{m_l} \leqslant \underline{v}_{s_l} v_{r_l} + \overline{v}_{r_l} v_{s_l} - \underline{v}_{s_l} \overline{v}_{r_l}, \ \forall l \in L$$
 (2.5i)

$$v_{m_l} \leqslant \overline{v}_{s_l} v_{r_l} + \underline{v}_{r_l} v_{s_l} - \overline{v}_{s_l} \underline{v}_{r_l}, \ \forall l \in L$$
 (2.5j)

Where \underline{v}_{s_l} and \underline{v}_{r_l} are lower bounds and \overline{v}_{s_l} and \overline{v}_{r_l} are upper bounds for their corresponding variables. Convex envelopes for z_{θ_l} are:

$$z_{\theta_l} \geqslant cos(\frac{\overline{\theta_l}}{2})(\theta_l + \frac{\overline{\theta_l}}{2}) - sin(\frac{\overline{\theta_l}}{2}), \ \forall l \in L$$
 (2.5k)

$$z_{\theta_l} \leqslant cos(\frac{\overline{\theta_l}}{2})(\theta_l - \frac{\overline{\theta_l}}{2}) + sin(\frac{\overline{\theta_l}}{2}), \ \forall l \in L$$
 (2.51)

Where $\overline{\theta_l}$ is the upper bound of θ_l . Constraints (2.5c) to (2.5l) are linear. Constraints (2.5k)-(2.5l) are valid for $0 < \overline{\theta_l} < \frac{\pi}{2}$. Bounds of the variables can be determined a priori. In Model E of SOC-ACOPF, we replace constraint (2.2e) of optimization problem (2.2) by constraints (2.3r)-(2.3s) and (2.5b)-(2.5l). Accordingly, assumptions (a) and (b) are not required in Model E.

2.3 Feasibility

In case the AC feasibility is violated by the solutions of the derived SOC-ACOPF models, we propose here a heuristic algorithm to recover feasible solutions from the relaxed solutions. The heuristic technique is summarized in Algorithm 1. We use the relaxed solutions of the active power generation p_n^* from the SOC-ACOPF models. If p_n^* solutions are feasible for all the ACOPF constraints, we can confirm that we have found the global optimal solution of ACOPF. Otherwise, we propose to fix $p_n = p_n^*$ for the cheap generators and take the $p_{n'}$ of the marginal generator (the most expensive generator in N^*) as a variable. Where $N^* \subseteq N$ is a dynamic set initiated

as $\forall n \in N^*, p_n^* > 0$. N^* is updated by removing the element n' which is the index of the marginal generator in each iteration. This process is repeated until the ACOPF is feasible in Algorithm 1. c_n is the marginal cost of generator at node n. i^{max} is the maximum number of allowed iterations. We show in Section V that the feasible solution can be recovered by this algorithm normally in few iterations.

```
Algorithm 1: Feasible Solution Recovery Algorithm

Input: Solution of SOC-ACOPF p_n^*;
Output: Feasible Solution of ACOPF p_n^{**};
Initialization;
i=1;
Define N^* \subseteq N such that \forall n \in N^*, p_n^* > 0;
p_n = p_n^*;
do

| if c_{n'} = Max\{c_n\}, \forall n, n' \in N^* then
| Replace p_{n'} = p_{n'}^* by p_{n'}^{min} < p_{n'} < p_{n'}^{max};
| N^* = N^* \setminus n';
| Solve ACOPF;
| i = i + 1;
| while ACOPF is not feasible and i < i^{max};
```

2.4 Numerical Results

All the SOC-ACOPF models are implemented in GAMS and solved by MOSEK. A computer with 2.4GHz CPU and 8GB RAM is deployed for the simulations (except Section V.2). Solutions of ACOPF from MATPOWER [70] and LINDOGLOBAL are set as the benchmarks. The LINDOGLOBAL solver employs branch-and-cut methods to find the global optimal solution. MATPOWER uses MATLAB built-in Interior Point Solver (MIPS) to solve nonconvex ACOPF. If a solution is not found, we denote the corresponding result as 'NA'.

2.4.1 Performance of SOC-ACOPF models

Base case

The SOC-ACOPF objective values are listed in Table 2.1. When LINDOGLOBAL cannot converge, we use the recovered best feasible solutions from Table 2.3 as the

benchmark. The LINDOGLOBAL solver is able to find global solutions for IEEE14bus, IEEE57-bus and IEEE118-bus cases. For larger networks, the number of variables and constraints exceed the limits of LINDOGLOBAL. The results of MATPOWER and LINDOGLOBAL are very close. All proposed SOC-ACOPF models give very close results as compared to MATPOWER and LINDOGLOBAL solutions. Compared to LINDOGLOBAL results, the objective values of IEEE14-bus case from Model T and Model E are bit higher. The reason is that the voltage phase angle constraint $0 < \overline{\theta_l} < \frac{\pi}{2}$ is included in Model E while this is not necessary for the nonconvex ACOPF model in GAMS solved by LINDOGLOBAL (this can also be due to different accuracy tolerances used by different solvers). The computation time results are listed in Table 2.2. Model P requires least computation time while Model T requires the most. This is because model complexity increases as we increase model accuracy. All proposed SOC-ACOPF models are computationally competitive with MATPOWER. The proposed SOC-ACOPF models require much less computation time as compared to MATPOWER for large-scale network cases (1354pegase and 2869pegase cases in Table 2.2). our proposed SOC-ACOPF models are valid for both radial and mesh networks.

To compare the computational performance of different SOCP-based ACOPF formulations, we have also implemented the ACOPF models in [44] and [48]. The results are listed in Table 2.1 and Table 2.2. It is worth to mention that the model in reference [48] takes much longer time than our proposed SOC-ACOPF models to be converted to the executable model format in GAMS (though the solver CPU time is short). In general, the model in reference [44] has the least number of constraints and requires less computational time. However, this model is not valid for mesh networks because there is no voltage phase angle constraint in this model (the reported results of this model are relaxed solutions for mesh networks). For the model in reference [48], MOSEK in GAMS cannot converge for the IEEE57-bus test case.

Test Case	IEEE14	IEEE57	IEEE118	IEEE300	1354pegase	2869pegase
Model P	8078.84	41696.94	129619.50	719381.80	74053.90	133877.00
Model R	8075.22	41711.78	129339.60	718301.60	74096.14	133875.40
Model T	8106.73	41713.25	129625.50	721368.40	74100.85	133931.40
Model E	8092.32	41711.78	129376.00	718546.27	74040.99	133934.70
Model in [44]	8072.42	41673.10	129330.74	718091.78	74006.84	133866.95
Model in [48]	8073.16	NA	129325.68	719451.23	73974.56	133823.28
MATPOWER	8081.53	41737.79	129660.70	719725.11	74069.35	133999.29
LINDOGLOBAL	8081.54	41737.93	129660.54	NA	NA	NA

Table 2.1: Objective value (\$)

Test Case	IEEE14	IEEE57	IEEE118	IEEE300	1354pegase	2869pegase
Model P	0.08	0.09	0.09	0.25	0.76	1.97
Model R	0.06	0.11	0.27	1.29	2.78	10.94
Model T	0.12	0.25	0.54	1.48	3.92	11.47
Model E	0.09	0.17	0.36	0.64	2.50	9.72
Model in [44]	0.08	0.11	0.13	0.25	0.64	1.23
Model in [48]	0.07	NA	0.09	0.22	2.56	6.82
MATPOWER	0.11	0.12	0.30	0.48	8.58	18.66
LINDOGLOBAL	0.20	2.31	27.10	NA	NA	NA

Table 2.2: Computation time (s)

Load scenarios

We evaluate the performance of the proposed SOC-ACOPF models under different load scenarios and compare the results with MATPOWER results. The incremental load scenarios are generated from 10% to 100% of the load (both active and reactive) in the base case. The results are shown in Fig. 2.1, Fig. 2.2, Fig. 2.3, Fig. 2.4, Fig. 2.5 and Fig. 2.6. To demonstrate the relaxation performance, we also plot the maximum value of relaxation gaps Gap_{o_l} in these figures. The maximum relaxation gap Gap_{o_l} is calculated by:

$$Gap_{o_l} = \max_{l} \left\{ p_{o_l} - \frac{p_{s_l}^2 + q_{s_l}^2}{V_{s_l}} R_l \right\}$$
 (2.6)

For IEEE14-bus, 57-bus, 118-bus and 300-bus cases, $Gap_{o_l} < 10^{-6}$ is valid for all the load scenarios. For load scenarios when MATPOWER cannot converge, the MOSEK solver is convergent for our proposed models however with large relaxation gaps (In these cases, large relaxation gap can serve as an indicator for un-convergence of the original ACOPF model). These results show robustness of the proposed SOC-ACOPF models over the load scenarios.

2.4.2 Feasible Solution

The heuristic algorithm in Section IV for recovering feasible solution is validated numerically in this Section. We use the IPOPT solver in GAMS to solve the nonconvex ACOPF model. A desktop with 3.4GHz CPU and 32GB RAM is used to implement Algorithm 1. For all the relaxed solutions of SOC-ACOPF models listed in Table 2.1, the feasible solutions are recovered within a few iterations. The objective function values of the recovered feasible solutions are listed in Table 2.3. The CPU time required

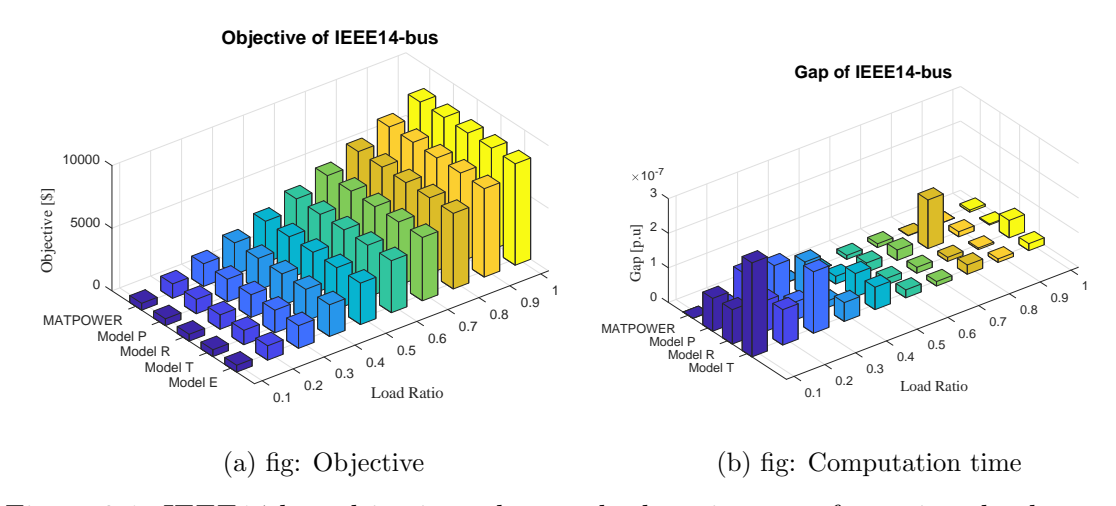


Figure 2.1: IEEE14-bus objective values and relaxation gaps for various load scenarios

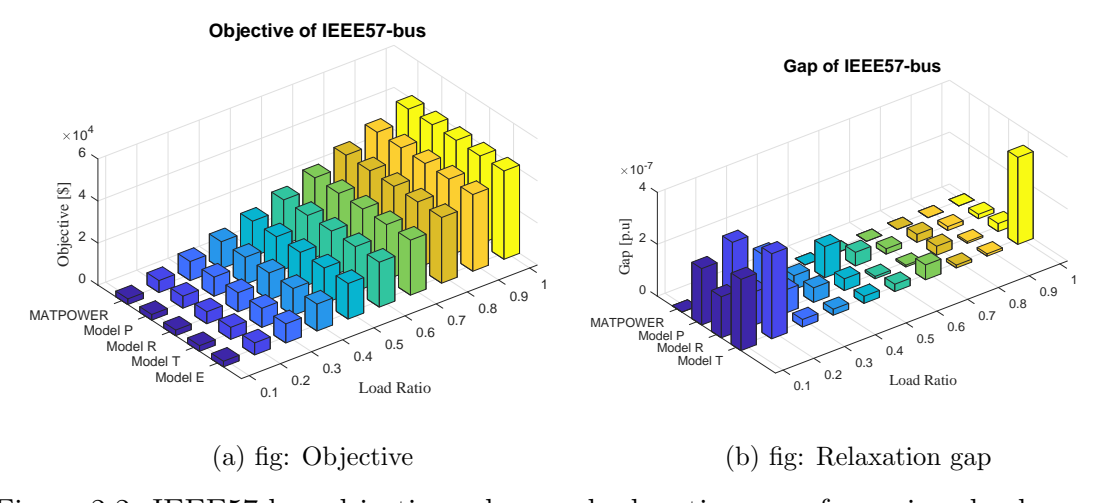


Figure 2.2: IEEE57-bus objective values and relaxation gaps for various load scenarios

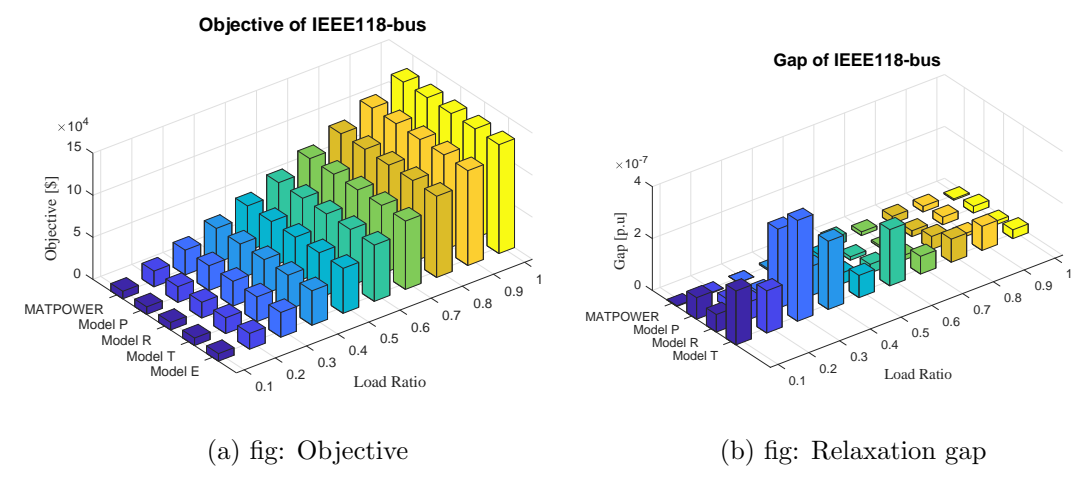


Figure 2.3: IEEE118-bus objective values and relaxation gaps for various load scenarios

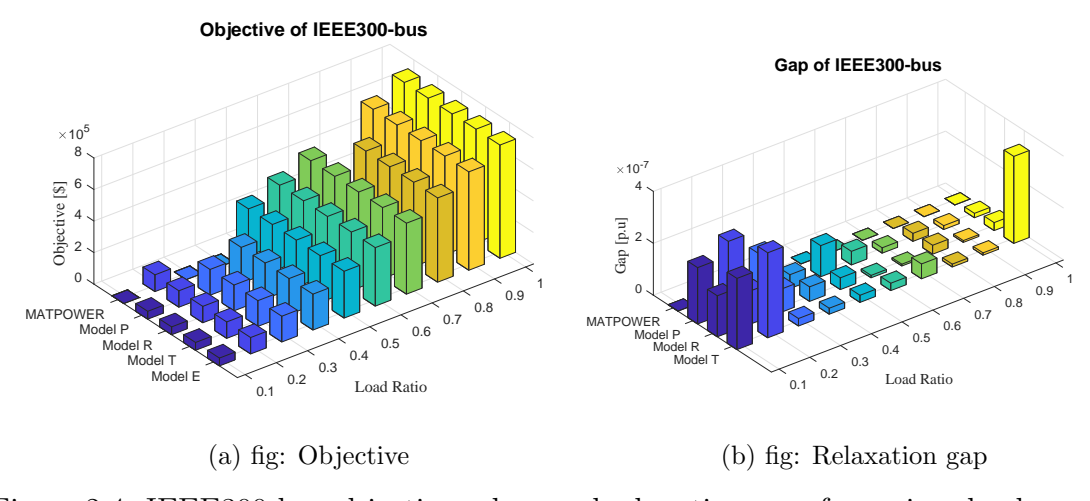


Figure 2.4: IEEE300-bus objective values and relaxation gaps for various load scenarios

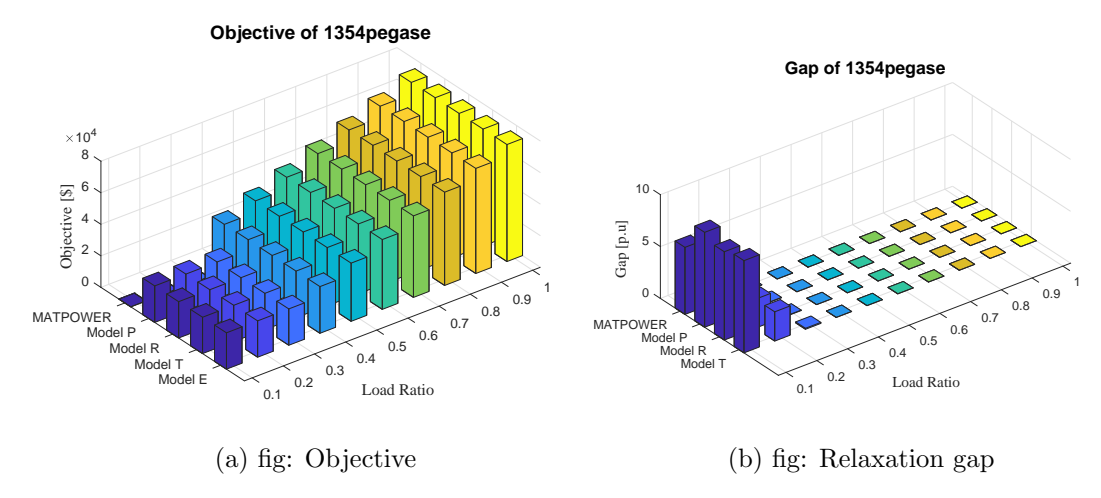


Figure 2.5: 1354pegase objective values and relaxation gaps for various load scenarios

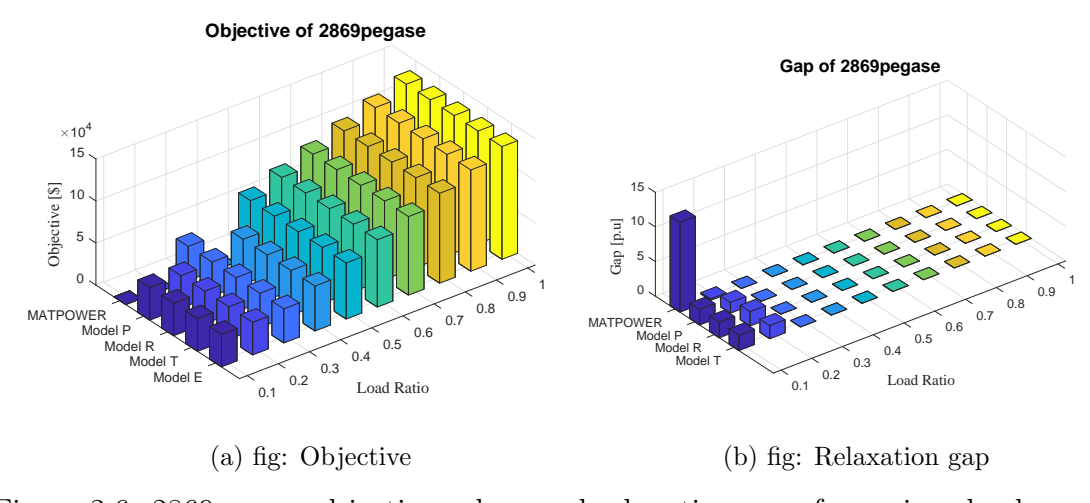


Figure 2.6: 2869pegase objective values and relaxation gaps for various load scenarios

for the computation are reported in Table 2.4. For ease of comparison, the results from MATPOWER and LINDOGLOBAL are listed again in Table 2.3 and Table 2.4. For 1354pegase and 2869pegase, feasible solutions with lower objective function values than the solutions from MATPOWER are recovered. The feasible solutions from the models in [44] and [48] are also recovered and reported. For the most test cases, feasible solutions recovered from our models have lower operation cost as compared to those recovered from models in [44] and [48].

Test Case IEEE14 IEEE57 IEEE118 IEEE300 1354pegase 2869pegase 41738.11 $719900.8\overline{6}$ Model P 8086.61 129660.92 74064.77 133987.76 Model R 8081.63 41738.15 129668.43719536.08 74064.77 133991.67 Model T 8106.73 41738.14 129668329 719516.79 74064.77 133991.67 Model E 41738.158091.10 129667.12 719526.16 74064.77 133991.67 41738.15Model in [44] 8081.63 129668.43 719522.19 74064.77 133991.67 Model in [48] NA 129670.80 720335.29 74064.77 8081.63 133991.67 41737.79 **MATPOWER** 8081.53 129660.70 719725.11 74069.35 133999.29 LINDOGLOBAL 8081.54 41737.93 129660.54 NA NA NA

Table 2.3: Objective values of the recovered feasible solution (\$)

Table 2.4: Computation time of the feasible solution recovery algorithm (s)

Test Case	IEEE14	IEEE57	IEEE118	IEEE300	1354pegase	2869pegase
Model P	0.11	1.05	1.44	14.55	45.90	234.61
Model R	0.18	1.50	2.41	24.56	41.77	769.16
Model T	0.26	1.22	1.37	15.13	69.55	140.58
Model E	0.12	1.17	3.03	131.55	33.91	525.00
Model in [44]	0.22	1.59	4.08	15.28	58.61	203.69
Model in [48]	0.25	NA	3.47	13.42	19.45	127.30
MATPOWER	0.11	0.12	0.30	14.53	8.58	18.66
LINDOGLOBAL	0.20	2.31	27.10	NA	NA	NA

2.5 Conclusions

Three second-order cone models (Model R, Model T and Model E) for ACOPF are proposed using convex relaxation and approximation techniques. Compared with other SOCP-based ACOPF formulations in the literature, our formulations are valid for both mesh and radial power networks. The numerical results show that the proposed SOC-ACOPF models can give accurate results. This accuracy improvement is achieved with similar computation time as compared to MATPOWER. The quality of results with respect to the global solution is also checked using LINDOGLOBAL solver in GAMS. The performance of the proposed SOC-ACOPF models under various power load scenarios is investigated numerically. A computational comparison of different SOCP-based ACOPF formulations shows the strong convergence performance of the proposed SOC-ACOPF models. To recover feasible solutions from the relaxed solutions of the proposed SOC-ACOPF models, we develop a heuristic feasible solution from all the relaxed solutions of the proposed SOC-ACOPF models in the test cases.

Chapter 3

Tightness and Decomposition Algorithms

3.1 Introduction

Decentralized approaches to solve the OPF problem mainly include Lagrangian relaxation [72], Benders decomposition (BD) [73], Dantzig-Wolfe decomposition [74] and Alternating Direction Method of Multipliers (ADMM) [75]. A comprehensive summary of distributed algorithms for optimization and control of power system can be found in [16]. Lagrangian relaxation approach relaxes the coupling constraints between the subnetworks and generally only approximated solutions can be guaranteed [72]. BD and Dantzig-Wolfe decomposition require to firstly formulate the master problem and subproblem and then iterate until the solutions converge [73,74]. BD is widely used to solve the security constrained unit commitment (SCUC) problem and transmission expansion planning (TEP) problem which can be regarded as expanded applications of OPF [76–78]. In SCUC and TEP, mostly the integer variables are taken as the complicating variables to formulate the master problem and subproblem of BD [76–78]. Message exchanges among the subnetworks are required by ADMM [75]. Generally, when more subnetworks are partitioned, more iterations are required for ADMM to converge [75]. Reference [79] investigates three ADMM-based decentralized DCOPF solution algorithm with different communication strategies. It shows numerically that the convergence performance can be improved by enhancing the data exchange with the central controller (or coordinator). The network partitioning approach is also important for the convergence performance [79]. Authors in [80] solve the stochastic SOCP-based ACOPF by ADMM for radial distribution networks. The updates of the variables and multipliers are decomposed by each node and each scenario. As a result, it requires large number of iterations to converge (over 3000 iterations are required for a 50-node test case with 500 scenarios) [80]. Using ADMM, a comprehensive investigation of decomposing nonconvex ACOPF down to the individual node level is conducted by [20]. The results show that convergence speed of ADMM largely depends on test cases. The nonconvexity of ACOPF also requires a suitable selection of the penalty factors of ADMM to guarantee the convergence [20]. Reference [81] proposes a parametric quadratic programming approach to solve the regional correction equation in the proposed fully distributed interior point method (F-DIPM) to solve ACOPF. The power network is partitioned to several regions geographically. Then boundary variables associated with the tie-lines are duplicated for each region. A unidirectional ring communication is employed to transmit the information about boundary variables during each Newton-Raphson iteration. Various test cases show the robust convergence of F-DIPM. However, the network partitioning problem is not systematically addressed in [81].

Graph theory shows that the network-partitioning problem is NP-hard [82, 83]. Accordingly, various heuristic approaches such as geometric approach and flow-based approach have been proposed to solve the network-partitioning problem [82]. Authors in [84] define the electrical distance based on the network admittance parameter as a measure to distinguish strongly connected buses from weakly connected buses. The electrical distance between the buses within each partitioned zone are minimized while the electrical distance between buses of different partitioned zones are maximized in the multi-attribute network partitioning problem [84]. Reference [17] improves the Modularity Index in the community-detection based network-partition algorithm such that both network topology and reactive power capability are taken into account. The goal in [17] is to control the zonal voltage of distribution network in a parallel processing approach. Authors in [85] show promising advantages of solving ACOPF by the optimality condition decomposition based algorithm. The effects of network partitioning on the computation efficiency are also investigated in [85]. However, the proposed intelligent network partitioning method in [85] requires to first solve the ACOPF problem. Considering the complexity of different network-partitioning methods, we use spectral factorization [86] to partition the power networks in this Chapter.

Accordingly, the main contributions of this Chapter are:

- A sequential tightness algorithm to improve AC feasibility of the solutions from our SOC-ACOPF models.
- 2. A modified Benders decomposition algorithm (M-BDA) approach based on network partitions is proposed for solving large-scale SOC-ACOPF problem.
- 3. The feasibility of the proposed M-BDA is analytically proved. Since the proposed M-BDA is modified from the original Benders decomposition, the feasibility proof of M-BDA is necessary.
- 4. Parallel computing is employed to accelerate the computation.

The proposed solution algorithm (based on network partitions, M-BDA and parallel computing) actually provides a feasible framework to speed up large-scale SOC-ACOPF computations. As an important contribution, there is no message exchange

requirement among the subnetworks in the proposed approach. Our decomposition approach also requires few number of iterations and it is robust to the number of partitioned subnetworks. The rest of this Chapter is organized as follows. Section II explains the sequential tightness algorithm. Two theorems are presented in this Sections to show important properties of SOC-ACOPF. Section III explains the network partitioning approach based on spectral factorization. Section IV details the M-BDA. The feasibility of the formulated master problem and subproblem in M-BDA is analytically proved. The parallel computing structure to accelerate the proposed M-BDA is also designed in this Section. Section V discusses numerical results for various IEEE test cases. The power network partitions based on spectral factorization are also plotted. Section VI concludes.

3.2 Sequential Tightness Algorithm

The conic relaxations in (2.2b) are not guaranteed to be tight. To deal with this problem, we propose a sequential algorithm to improve the tightness. This sequential algorithm is based on Theorem 1 and Theorem 2 below:

Theorem 1. Assume that:

- (1). the objective function of nonconvex ACOPF (2.1) and the proposed SOC-ACOPF is convex;
- (2). nonconvex ACOPF (2.1) has exactly one global optimal solution $(p_{s_l}^*, q_{s_l}^*, p_{o_l}^*)$;
- (3). non-exact optimal solution (if exists) of SOC-ACOPF $p'_{o_l} > p^*_{o_l}$. Then, constraint $p_{o_l} \leq p^*_{o_l}$ guarantees the tightness of constraint (2.2b).

Proof. Firstly, we consider the case that SOC-ACOPF is exact (the relaxations are tight). The proof of theorem 1 is based on theorem 3 in reference [43] which proves that second-order conic optimal power flow (SOPF) has at most one optimal solution when SOPF is exact for a radial network. Because our SOC-ACOPF model has one more constraint (2.1g) (to make our model valid for both radial and meshed networks) than the SOPF model described in reference [43], we are actually reducing the feasible region of SOPF in reference [43]. This means that either we keep the unique optimal solution in the feasible region or we exclude the optimal solution. For both cases, the conclusion that there is at most one global optimal solution of SOC-ACOPF when SOC-ACOPF is exact is still valid. Assume the exact optimal solution of SOC-ACOPF is $p_{o_l}^e$. If $p_{o_l}^e \neq p_{o_l}^*$, then $p_{o_l}^e$ must be the global optimal solution of the nonconvex ACOPF since $f^e \leq f^*$. Where f^e and f^* are the value of objective function for SOC-ACOPF and the nonconvex ACOPF respectively. This contradicts our assumption that there is exactly one global optimal solution of the nonconvex ACOPF. So $p_{o_l}^e \neq p_{o_l}^*$ is feasible for SOC-ACOPF when it is exact.

When SOC-ACOPF is not exact, assume $(p'_{s_l}, q'_{s_l}, p'_{o_l}, V'_{s_l})$ is the optimal solution of SOC-ACOPF after we have put the constraint $p_{o_l} \leq p^*_{o_l}$:

$$p_{o_{l}}^{*} \ge p_{o_{l}}^{'} \ge \frac{p_{s_{l}}^{'2} + q_{s_{l}}^{'2}}{V_{s_{l}}^{'}} R_{l}$$

$$(3.1)$$

If $p'_{ol} \neq \frac{p'_{s_l}^2 + q'_{s_l}^2}{V'_{s_l}} R_l$, then:

$$p_{o_{l}}^{'} > p_{o_{l}}^{*}$$
 (3.2)

(3.2) contradicts (3.1). So $p'_{o_l} \neq \frac{p'_{s_l}^2 + q'_{s_l}^2}{V'_{s_l}} R_l$ is not valid. Constraint (2.2b) must be tight.

Theorem 1 shows that as long as we have a good estimation of $p_{o_l}^*$, then we can tighten constraint (2.2b). The problem is that it is difficult to estimate $p_{o_l}^*$ before solving nonconvex ACOPF. We propose the following theorem to design the tightness algorithm.

Theorem 2. If the assumptions in theorem 1 hold and the decreasing sequence $p_{o_l,i-1}$ converges to $p_{o_l}^*$ which is the optimal solution of nonconvex ACOPF, then sequential constraints $p_{o_l} \leq p_{o_l,i}$ guarantee the tightness of constraint (2.2b).

Proof. The proof of theorem 2 is based on theorem 1 and Squeeze Theorem. We denote here the sequential optimization problem constrained by $p_{o_l} \leq p_{o_l,i}$ as SOC-ACOPF-i where i is the index for the sequence. Because SOC-ACOPF is assumed to be feasible for $p_{o_l} \leq p_{o_l}^*$ and $p_{o_l,i} \geq p_{o_l}^*$, SOC-ACOPF-i is always feasible. If the solution of SOC-ACOPF-i is denoted as $(p_{s_l,i}^*, q_{s_l,i}^*, p_{o_l,i}^*, V_{s_l,i}^*)$, we have:

$$p_{o_l,i} \ge p_{o_l,i}^* \ge \frac{p_{s_l,i}^{*2} + q_{s_l,i}^{*2}}{V_{s_l,i}^{*}} R_l \tag{3.3}$$

From Theorem 1, $p_{o_l} \leq p_{o_l}^*$ guarantees the tightness of equation (2.2b):

$$\lim_{i \to +\infty} \frac{p_{s_l,i}^{*2} + q_{s_l,i}^{*2}}{V_{s_l,i}^{*}} R_l = p_{o_l}^*$$
(3.4)

And we have assumed in theorem 2 that sequence $p_{o_l,i} \leq p_{o_l,i-1}$ converges to $p_{o_l}^*$:

$$\lim_{i \to +\infty} p_{o_l,i} = p_{o_l}^* \tag{3.5}$$

According to Squeeze Theorem, (3.3)-(3.5) imply:

$$\lim_{i \to +\infty} p_{o_l,i}^* = p_{o_l}^* \tag{3.6}$$

In other words, the solutions of sequential optimization SOC-ACOPF-i converge to where equation (2.2b) is tight.

Theorem 2 suggests we can find optimal solution of SOC-ACOPF by solving sequential SOC-ACOPF-i. The challenge is how to design or calculate the proper sequence $p_{o_l,i}$ converging to $p_{o_l,i}^*$. Here we propose to begin with a rather rough estimation of $p_{o_l}^*$ and then iteratively improve the estimation quality. The numerical results show that the proposed tightness algorithm can make the relaxation in constraint (2.2b) tight.

Given (2.1h), the initial estimation $K_{o_l,0}$ is simply calculated by (3.7):

$$K_{o_l,0} = \frac{K_l}{V_{s_l}^{min}} R_l \tag{3.7}$$

Where $V_{s_l}^{min}$ is the lower bound of V_{s_l} . The sequential SOC-ACOPF-*i* is then constrained by (3.8):

$$p_{o_l} \le K_{o_l,i}, \ \forall l \in L \tag{3.8}$$

Where $K_{o_l,i}, i \in \{0,1,2,...,i^{max}\}$ is the i^{th} estimation of $p_{o_l}^*$. The tightness algorithm works by iteratively reducing the upper bounds $K_{o_l,i}$ of power loss constraints that violate tightness criterion ε . If $p_{o_l} - \frac{p_{s_l}^2 + q_{s_l}^2}{V_{s_l}} R_l > \varepsilon$, $K_{o_l,i+1} = \alpha_l K_{o_l,i}$, where $0 < \alpha_l < 1$ is the decreasing parameter. The proposed sequential tightness algorithm is summarized in Algorithm 2.

This algorithm is illustrated in Fig. 3.1 where X^* denotes the final solution. i^{max} denotes the maximum number of iterations specified a priori. The original nonconvex feasible region of ACOPF is plotted with solid line in Fig. 3.1. The convex feasible region of proposed SOC-ACOPF is plotted with dashed line in Fig. 3.1. We will show the performance of this algorithm in Section 3 of this Chapter. It is worth to mention that the proposed sequential tightness algorithm can only tighten the relaxation in (2.2b). Because there are additional relaxations we have introduced in (2.5c)-(2.5l), the final solutions of the proposed SOC-ACOPF model are generally not tight for the constraint (2.1g) in ACOPF. Using interior point method to solve the proposed SOC-ACOPF model in polynomial time complexity does not violate the NP-hardness proof [87,88] of ACOPF because the proposed SOC-ACOPF is still a relaxed model of ACOPF.

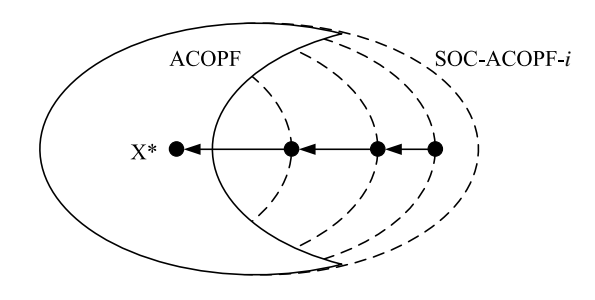


Figure 3.1: The conceptual diagram of the proposed sequential tightness algorithm

3.3 Power Network Partitioning

Power network topology can be always equivalently represented by a graph G=(N,L) with a vertex set N denoting nodes and an edge set L denoting lines or branches. This implies we can use graph-partitioning algorithms to partition a power network. A \bar{k} partition of N defines \bar{k} disjoint subsets of N as $P=\{N_1,N_2,...,N_{\bar{k}}\}$. If the partitioning cost of cutting line l (allocating the ends of the line to two separate subnetworks) is c_l , the total cost of partition P is $C(P) = \sum_{l \in \tau} c_l$ where τ is the set of lines with nodes belonging to different subnetworks i.e. the set of tie-lines. Higher c_l means higher possibility that line l is to be kept in one subnetwork. There can be various strategies to set c_l . If all c_l parameters are equal, the network partitioning algorithm will result in least number of tie-lines. In this Chapter, we set $c_l = 1$ for all lines in order to obtain minimal number of tie-lines after the network partitioning. The network partitioning problem is formulated in (3.7) [86]:

$$\underset{M}{\text{Maximize}} \quad trace \left(M^T C M \right) \tag{3.7a}$$

subject to
$$||M||_F = \sqrt{\bar{n}}$$
 (3.7b)

$$M^T M \le \epsilon I_{\bar{k}\bar{k}} \tag{3.7c}$$

$$M_{nk} \in \{0, 1\}, \quad n = 1, ..., \bar{n}, \quad k = 1, ..., \bar{k}$$
 (3.7d)

where M is $\bar{n} \times \bar{k}$ orthogonal \bar{k} -partition matrix with $M_{nk} = 1$ if $n \in N_k$ and $M_{nk} = 0$ if $n \notin N_k$. $||M||_F = \sqrt{trace\,(M^TM)}$ is Frobenius norm. Constraint (3.7b) is valid because M is a \bar{k} -partition matrix if and only if each row of M is the canonical basic of R^k [86]. C is the $\bar{n} \times \bar{n}$ cost matrix of the network. $C_{in} = c_l$ if i and n are the connecting nodes of line l. $C_{in} = 0$ if i and n are not the connecting nodes of line l. The $I_{\bar{k}\bar{k}}$ is $\bar{k} \times \bar{k}$ unit matrix. Constraint (3.7c) models an ϵ -bounded partition (the maximum number of nodes of all subnetworks is ϵ). C, $I_{\bar{k}\bar{k}}$ and ϵ are parameters of optimization problem (3.7). The objective is to minimize the total cost of partitioning. This is valid because [86]:

$$C(P) = I_{\bar{n}}^T C I_{\bar{n}} - trace \left(M^T C M \right)$$
(3.7e)

where $I_{\bar{n}}$ is \bar{n} -vector with all elements equal to one. Here we use a simple spectral factorization algorithm to solve (3.7). Spectral factorization uses matrix eigenvalue decomposition techniques to solve this \bar{n} -bounded network partitioning problem when C is doubly stochastic (C can be normalized to a doubly stochastic matrix if it is not). According to spectral theorem, real symmetric cost matrix C can always be diagonalized as $QCQ^T = D$, where Q is orthogonal matrix and D is diagonal matrix. Suppose Z = QM, we have:

$$trace\left(M^{T}CM\right) = trace\left(M^{T}Q^{T}DQM\right) = trace\left(Z^{T}DZ\right) \tag{3.7f}$$

Where Q^TZ is a \bar{k} partition matrix, D = I and $Max[trace(M^TCM)] = \bar{n}$. The solution of M is:

$$M^* = \arg\min_{M} \|M - Q^T Z\|_F \tag{3.7g}$$

This is because:

$$\|M - Q^T Z\|_F^2 = \bar{n} + \|Z\|_F - 2\sum_{n=1}^{\bar{n}} \hat{M}_{k'n} M_{nk'}$$
(3.7h)

Where $\hat{M} = Q^T Z$ and $M_{nk'} = 1$. To minimize $\|M - Q^T Z\|_F$, k' should satisfy $\hat{M}_{k'n} = Max[\hat{M}_{kn}]$. This is the projection algorithm proposed in [86] by which the partition matrix M is recovered given matrix Z. $Z = (E_1'Q^T)^{-1}$ is a $\bar{k} \times \bar{k}$ matrix obtained from the clustering algorithm proposed in [86] where QE = UR is a QR-factorization. $E = [E_{n\times k}^{(1)}, E_{n\times (n-k)}^{(2)}]$ is a permutation matrix. It is worth to mention that the graph-partitioning algorithm we used here can solve (3.7) approximately and therefore global optimal solution is not guaranteed to be found. We show in Section V that even by using the approximated solutions of network partitioning problem (3.7), the computation efficiency can still be improved.

3.4 Proposing M-BDA and the Parallel Computing

Model E of SOC-ACOPF derived in Chapter 2 of this thesis is used here to formulate the M-BDA. Other proposed SOC-ACOPF models (Model R and Model T) can also be used. The key contribution is that we decompose SOC-ACOPF by taking the total power generation of each subnetwork as the complicating variable in formulating the proposed M-BDA. This formulation shows very fast convergence performance. We first decompose the large-scale power network to \bar{k} subnetworks using the power network partitioning algorithm described in Section III. The SOC-ACOPF of each subnetwork is taken as a subproblem in the proposed M-BDA. The subproblem k is formulated in (3.8).

$$Cost_{k,j}^{S} = \text{Minimize} \sum_{\forall n \in N_k, l \in L_k} f(p_{g_n}, q_{g_n}, p_{o_l}, q_{o_l})$$
(3.8a)

subject to
$$(2.1b) - (2.1c), (2.1j) - (2.1m), (2.2b) - (2.2d), (2.5b) - (2.5l)$$

 $\forall n \in N_k, l \in L_k$ (3.8b)

$$\sum_{n \in N} p_n = P_{k,j}^{sum} : \mu_{k,j}^P, \, \forall k \in K, j \in J$$
 (3.8c)

$$\sum_{n \in N_k} q_n = Q_{k,j}^{sum} : \mu_{k,j}^Q, \, \forall k \in K, j \in J$$
 (3.8d)

Where (3.8b) refers to the power flow constraints for all lines and nodes located in subnetwork k. N_k and L_k are the sets of nodes and lines located in the subnetwork k. $P_{k,j}^{sum}$ and $Q_{k,j}^{sum}$ are the solutions of subnetwork total power generation from the master problem of the proposed M-BDA in iteration j. $\mu_{k,j}^P$ and $\mu_{k,j}^Q$ are the dual variables for corresponding constraints used for constructing Benders cuts. To guarantee the feasibility of all the subproblems in M-BDA, we allow load increment or decrement for all the nodes in the network. Thus the power balance constraints (2.1b)-(2.1c) in (3.8b) are modified as:

$$p_n - P_{d_n} = \Delta P_{d_n}^+ - \Delta P_{d_n}^- + \sum_{l \in L_k} (A_{nl}^+ p_{s_l} - A_{nl}^- p_{o_l}) + G_n V_n, \, \forall n \in N_k, l \in L_k$$
 (3.8e)

$$q_n - Q_{d_n} = \Delta Q_{d_n}^+ - \Delta Q_{d_n}^- + \sum_{l \in L_k} (A_{nl}^+ q_{s_l} - A_{nl}^- q_{o_l}) - B_n V_n, \, \forall n \in N_k, l \in L_k \quad (3.8f)$$

Where non-negative variables $\Delta P_{d_n}^+$ and $\Delta Q_{d_n}^+$ are the load increments. Non-negative variables $\Delta P_{d_n}^-$ and $\Delta Q_{d_n}^-$ are the load decrements. The load increment and decrement are penalized in the objective function using the penalty parameters $C_{d_n}^{P+}$, $C_{d_n}^{P-}$, $C_{d_n}^{Q+}$, $C_{d_n}^{Q-}$. Note the solutions of tie-line variables are obtained by solving the formulated master problem (3.9) of M-BDA. To force the solutions of tie-line voltage variables to be same as the solutions from the master problem (3.9), we also include penalty terms for the tie-line voltage variables in the objective function of the subproblem. C_n^v , C_n^θ are positive penalty parameters. Minimizing quadratic objective function over a convex feasible region is a convex optimization problem. This is formulated as:

$$Cost_{k,j}^{S} = \text{Minimize} \sum_{\forall n \in N_{k}, l \in L_{k}} f(p_{n}, q_{n}, p_{o_{l}}, q_{o_{l}})$$

$$+ \sum_{n \in N_{k}} (C_{d_{n}}^{P+} \Delta P_{d_{n}}^{+} + C_{d_{n}}^{P-} \Delta P_{d_{n}}^{-} + C_{d_{n}}^{Q+} \Delta Q_{d_{n}}^{+} + C_{d_{n}}^{Q-} \Delta Q_{d_{n}}^{-})$$

$$+ \sum_{n \in N_{k} \cap N_{\tau}, j \in J} [C_{n}^{v} (v_{n} - v_{n,j}^{M})^{2} + C_{n}^{\theta} (\theta_{n} - \theta_{n,j}^{M})^{2}]$$
(3.8g)

Although some load increments or decrements may exist at the beginning of the iterations, the final solution of the proposed M-BDA does not have these increments or decrements. This is because the cost of these increments and decrements are very high and they will iteratively converge to zero. Our simulations show that this method is

more efficient to guarantee the feasibility of the subproblems than using the method of the original feasibility cut approach in Benders decomposition (the MOSEK solver can not converge after several hours when using the original feasibility cut approach).

The master problem of the proposed M-BDA is formulated in (3.9):

Minimize
$$Cost^{M} = \sum_{k \in K} Cost_{k}^{S}$$
 (3.9a)
subject to $(2.1b) - (2.1c), (2.1j) - (2.1m), (2.2b) - (2.2d), (2.5b) - (2.5l) $\forall l \in \tau$ (3.9b)

$$Cost_{k}^{S} \geq Cost_{k,j-1}^{S} + \mu_{k,j-1}^{P} \left(P_{k,j}^{sum} - P_{k,j-1}^{sum} \right) + \mu_{k,j-1}^{Q} \left(Q_{k,j}^{sum} - Q_{k,j-1}^{sum} \right),$$
 $\forall k \in K, j \in J$ (3.9c)$

Where (3.9b) refers to the power flow constraints of all the tie-lines. $P_{k,j-1}^{sum}$ and $Q_{k,j-1}^{sum}$ are the decisions of the previous iteration which are considered as parameters in the current iteration. The decisions of $P_{k,j}^{sum}$ and $Q_{k,j}^{sum}$ are made in the master problem (3.9) by considering the expanding Benders cuts (3.9c) and tie-line constraints (3.9b). We model each subnetwork as a single virtual node in the master problem. This is conceptually illustrated in Fig. 3.3, 3.4 and 3.5 in Section V. Constraints (3.9c) are Benders cuts from subproblems. $\mu_{k,j-1}^P$ and $\mu_{k,j-1}^Q$ are dual variable solutions of equations (3.8c)-(3.8d) in subnetwork k at the previous iteration j-1.

As the iterations proceed, more Benders cuts from the subnetworks are iteratively included into the master problem. After solving the master problem, all the subproblems can be solved in parallel. The proposed parallel computing structure using the M-BDA is illustrated in Fig. 3.2. The master problem is responsible for giving solutions of tie-line power flows and the subproblems are responsible for giving solutions of subnetwork power flows. There is no communication requirement between the subproblems. In each iteration, firstly the master problem is solved and then all the subproblems are solved in parallel. In the network partitioning algorithm, we assign same partition cost c_l to all lines. This minimizes the number of tie-lines which in turn minimizes the size of the master problem. We summarize the parallel computing management algorithm in Algorithm 3.

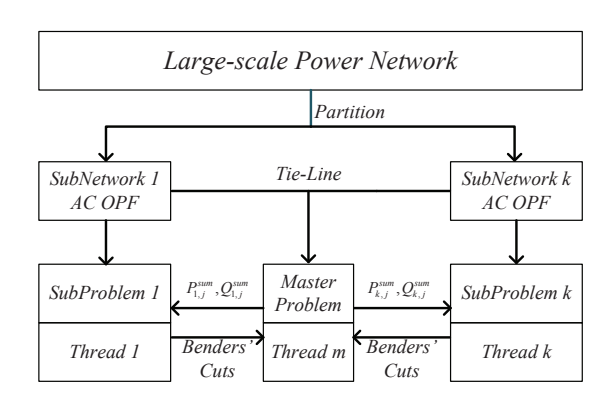


Figure 3.2: The proposed parallel computing structure using M-BDA

```
Algorithm 3: Parallel Computing Management Algorithm
 Initialization: j = 1;
 do
     Generate SOC-ACOPF model (3.9) for the tie-lines:
      SOC-ACOPF-Master;
     Assign SOC-ACOPF-Master to Thread-m;
     Execute Thread-m;
     Broadcast P_{k,j}^{sum} and Q_{k,j}^{sum} to Thread-k for k \in K;
     k = 1;
     do
         Generate SOC-ACOPF model (3.8) for the subnetwork-k:
          SOC-ACOPF-k;
         Assign SOC-ACOPF-k to Thread-k;
         k = k + 1;
     while k < k^{max};
     do
         if thread-k is ready then
             Collect solutions from Thread-k;
            Send Cost_{k,j}^S, \mu_{k,j}^P and \mu_{k,j}^Q to Thread-m; Release Thread-k;
     while SOC-ACOPF thread is nonempty;
     j = j + 1;
 while \frac{\sum_{k \in K} Cost_{k,j}^S - Cost^M}{\sum_{k \in K} Cost_{k,j}^S} > 2\% and j < j^{max};
 Release Thread-m;
```

Theorem 3. If the original SOC-ACOPF model (without decomposition) is feasible, the formulated master problem (3.9) of the proposed M-BDA is feasible.

Proof. We prove theorem 3 by mathematical induction. We prove firstly the formulated master problem (3.9) is feasible at iteration j = 1. Afterwards, we prove for any iteration $j' \in J$, if the formulated master problem (3.9) is feasible for j = j' then it is feasible for the next iteration j = j' + 1.

Step 1: The formulated master problem (3.9) is feasible for j=1. We prove this by constructing one feasible solution for the formulated master problem (3.9) of the proposed M-BDA. Assume $\Omega_0 = \{p_{n,0}, q_{n,0}, p_{s_{l,0}}, q_{s_{l,0}}, p_{o_{l,0}}, q_{o_{l,0}}, v_{n,0}, \theta_{l,0}\} \in \Re$ is one feasible solution of the original SOC-ACOPF model, Ω_0 is also feasible for constraints (3.9b) in the master problem (3.9) of the proposed M-BDA. Note it is not necessarily required that the feasible solution Ω_0 is optimal for the original SOC-ACOPF model.

We construct the feasible solution $P_{k,j,0}^{sum}$, $Q_{k,j,0}^{sum}$, $P_{k,j-1,0}^{sum}$ and $Q_{k,j-1,0}^{sum}$ as:

$$P_{k,j,0}^{sum} = \sum_{n \in N_k} p_{n,0} \tag{3.10a}$$

$$Q_{k,j,0}^{sum} = \sum_{n \in N_k} q_{n,0} \tag{3.10b}$$

$$P_{k,j-1,0}^{sum} = \sum_{n \in N_k} p_{n,0} \tag{3.10c}$$

$$Q_{k,j-1,0}^{sum} = \sum_{n \in N_k} q_{n,0} \tag{3.10d}$$

If we use $\Omega_0, P_{k,j,0}^{sum}, Q_{k,j,0}^{sum}, P_{k,j-1,0}^{sum}$ and $Q_{k,j-1,0}^{sum}$, then constraint (3.9c) becomes:

$$Cost_{k}^{S} \ge Cost_{k,j-1}^{S} + \mu_{k,j-1}^{P} \left(P_{k,j,0}^{sum} - P_{k,j-1}^{sum} \right) + \mu_{k,j-1}^{Q} \left(Q_{k,j,0}^{sum} - Q_{k,j-1}^{sum} \right), \, \forall k \in K$$

$$(3.10e)$$

Which is:

$$Cost_k^S \ge Cost_{k,i-1}^S, \, \forall k \in K$$
 (3.10f)

No matter what values $\mu_{k,j-1}^P$ and $\mu_{k,j-1}^Q$ are chosen at j=1, constraint (3.10f) is always feasible since we do not have upper bound for $Cost_k^S$. The feasible objective solution is:

$$Cost^{M,0} = Min\left[\sum_{k \in K} Cost_k^S\right] = \sum_{k \in K} Cost_{k,j-1}^S$$
(3.10g)

Which is actually the lower bound of the non-negative term $\sum_{k \in K} Cost_{k,j-1}^S$. Thus we successfully construct a feasible solution of the master problem as Ω_0 , $P_{k,j,0}^{sum}$, $Q_{k,j,0}^{sum}$ with objective value of $Cost^{M,0}$. This means the master problem is feasible for j=1.

Step 2: If the formulated master problem (3.9) is feasible for j = j', then it is feasible for j = j' + 1. We prove this step by showing that there is at least one feasible solution for iteration j = j' + 1 which can always be constructed by using the feasible solution for j = j'. Suppose one feasible solution for iteration j = j' is $\Omega_{j'}$, $P_{k,j',0}^{sum}$, $Q_{k,j',0}^{sum}$ with master problem and subproblem objective values as $Cost^{M,j',0}, Cost_k^{S,j',0}$. We construct the feasible solution for j=j'+1 as:

$$P_{k,j'+1,0}^{sum} = P_{k,j',0}^{sum} \tag{3.10h}$$

$$\begin{aligned} P_{k,j'+1,0}^{sum} &= P_{k,j',0}^{sum} \\ Q_{k,j'+1,0}^{sum} &= Q_{k,j',0}^{sum} \end{aligned} \tag{3.10h}$$

The added Benders cuts at iteration j = j' + 1 is:

$$Cost_{k}^{S} \ge Cost_{k,j'}^{S} + \mu_{k,j'}^{P} \left(P_{k,j'+1,0}^{sum} - P_{k,j',0}^{sum} \right) + \mu_{k,j'}^{Q} \left(Q_{k,j'+1,0}^{sum} - Q_{k,j',0}^{sum} \right), \, \forall k \in K$$

$$(3.10j)$$

Or equivalently:

$$Cost_k^S \ge Cost_{k,j'}^S, \forall k \in K$$
 (3.10k)

We show in following that no matter what value $Cost_{k,j'}^S$ takes, we can always construct a feasible solution for the master problem. If there exists:

$$Cost_{k,j'}^S \ge Cost_k^{S,j',0}, \forall k \in K$$
 (3.101)

the feasible solution of $Cost_k^S$ for j = j' + 1 is $Cost_{k,j'}^S$. Accordingly, feasible objective solution is $Cost^{M,j'+1,0} = \sum_{k \in K} Cost^{S}_{k,j'}$.

Otherwise, if there exists $k \in K' \subset K$ such that:

$$Cost_{k,j'}^{S} \le Cost_{k}^{S,j',0}, \forall k \in K' \subset K$$
 (3.10m)

we replace these $Cost_k^S$ by $Cost_k^{S,j',0}$ $(\forall k \in K' \subset K)$. The feasible solution of $Cost_k^S$ is $\left\{Cost_{k,j'}^S, \forall k \notin K' \subset K\right\} \cup \left\{Cost_k^{S,j',0}, \forall k \in K' \subset K\right\}. \text{ Accordingly, feasible objective }$ solution for iteration j = j' + 1 is:

$$Cost^{M,j'+1,0} = \sum_{k \notin K' \subset K} Cost_{k,j'}^{S} + \sum_{k \in K' \subset K} Cost_{k}^{S,j',0}$$
 (3.10n)

Combining Step 1 and Step 2, we have proven that the formulated master problem (3.9) is always feasible as long as the original SOC-ACOPF model is feasible.

Theorem 4. If the original SOC-ACOPF model (without decomposition) is feasible, the necessary and sufficient condition for the feasibility of the formulated subproblem (3.8) of the proposed M-BDA is:

$$\sum_{n \in N_k} p_n^{min} \le P_{k,j}^{sum} \le \sum_{n \in N_k} p_n^{max}, \, \forall k \in K, j \in J$$
(3.11a)

$$\sum_{n \in N_k} q_n^{min} \le Q_{k,j}^{sum} \le \sum_{n \in N_k} q_n^{max}, \, \forall k \in K, j \in J$$
(3.11b)

Proof. We firstly prove (3.11) is necessary for the feasibility of subproblem (3.8) i.e. if subproblem (3.8) is feasible then (3.11) holds. Suppose the feasible solution of subproblem (3.8) at iteration $j \in J$ is $\Omega_j = \{p_{n,j}, q_{n,j}, p_{s_{l,j}}, q_{s_{l,j}}, p_{o_{l,j}}, q_{o_{l,j}}, v_{n,j}, \theta_{l,j}\} \in \Re$, from (3.8c)-(3.8d) of (3.8) we have:

$$\sum_{n \in N_k} p_{n,j} = P_{k,j}^{sum}, \, \forall k \in K, j \in J$$
(3.12a)

$$\sum_{n \in N_k} q_{n,j} = Q_{k,j}^{sum}, \, \forall k \in K, j \in J$$
(3.12b)

 Ω_i is feasible for constraints (3.9b) of (3.9), so:

$$p_n^{min} \le p_{n,j} \le p_n^{max}, \, \forall n \in N_k \tag{3.12c}$$

$$q_n^{min} \le q_{n,j} \le q_n^{max}, \, \forall n \in N_k \tag{3.12d}$$

Obviously,

$$\sum_{n \in N_k} p_n^{min} \le \sum_{n \in N_k} p_{n,j} \le \sum_{n \in N_k} p_n^{max}$$
 (3.12e)

$$\sum_{n \in N_k} q_n^{min} \le \sum_{n \in N_k} p_{n,j} \le \sum_{n \in N_k} q_n^{max}$$
(3.12f)

From (3.12a)-(3.12b) and (3.12e)-(3.12f), the expression (3.11) holds.

Next, we prove (3.11) is sufficient for the feasibility of subproblem (3.8) i.e. if (3.11) holds, subproblem (3.8) is feasible.

Again, we assume $\Omega_0 = \{p_{n,0}, q_{n,0}, p_{s_{l,0}}, q_{s_{l,0}}, p_{o_{l,0}}, q_{o_{l,0}}, V_{n,0}, \theta_{l,0}\} \in \Re$ is one feasible solution of the original SOC-ACOPF model. Obviously, $\{p_{s_{l,0}}, q_{s_{l,0}}, p_{o_{l,0}}, q_{o_{l,0}}, v_{n,0}, \theta_{l,0}\}$ is feasible for constraints (2.1j)-(2.1m), (2.2b)-(2.2d) and (2.5b)-(2.5l) in (3.8b) of (3.8). The remaining constraints are (2.1b)-(2.1c) and (3.8c)-(3.8d). We construct the feasible solution of p_n, q_n at iteration j as $p_{n,j}, q_{n,j}$:

$$p_{n,j} = p_{n,0} + \Delta P_{d_n}^+ - \Delta P_{d_n}^-, \ \forall n \in N_k, l \in L_k$$
 (3.12g)

$$q_{n,j} = q_{n,0} + \Delta Q_{d_n}^+ - \Delta Q_{d_n}^-, \ \forall n \in N_k, l \in L_k$$
 (3.12h)

Substitute (3.12g)-(3.12h) in (2.1b)-(2.1c) (modified as constraints (3.8e)-(3.8f)), we have:

$$p_{n,0} + \Delta P_{d_n}^+ - \Delta P_{d_n}^- - P_{d_n} = \Delta P_{d_n}^+ - \Delta P_{d_n}^- + G_n V_{n,0} + \sum_{l \in L_k} (A_{nl}^+ p_{s_{l,0}} - A_{nl}^- p_{o_{l,0}}), \, \forall n \in N_k, l \in L_k$$
 (3.12i)

$$q_{n,0} + \Delta Q_{d_n}^+ - \Delta Q_{d_n}^- - Q_{d_n} = \Delta Q_{d_n}^+ - \Delta Q_{d_n}^- - B_n V_{n,0} + \sum_{l \in L_k} (A_{nl}^+ q_{s_{l,0}} - A_{nl}^- q_{o_{l,0}}), \, \forall n \in N_k, l \in L_k$$
 (3.12j)

Or equivalently:

$$p_{n,0} - P_{d_n} = \sum_{l} (A_{nl}^+ p_{s_{l,0}} - A_{nl}^- p_{o_{l,0}}) + G_n V_{n,0}, \ \forall n \in N_k, l \in L_k$$
 (3.12k)

$$q_{n,0} - Q_{d_n} = \sum_{l} (A_{nl}^+ q_{s_{l,0}} - A_{nl}^- q_{o_{l,0}}) - B_n V_{n,0}, \ \forall n \in N_k, l \in L_k$$
(3.12l)

Which is feasible since Ω_0 is a feasible solution. To construct the feasible solutions of the load increment or decrement variables, we consider feasibility of the constraints (3.8c)-(3.8d):

$$\sum_{n \in N_k} p_{n,j} = \sum_{n \in N_k} (p_{n,0} + \Delta P_{d_n}^+ - \Delta P_{d_n}^-) = P_{k,j}^{sum}, \, \forall k \in K, j \in J$$
 (3.12m)

$$\sum_{n \in N_k} q_{n,j} = \sum_{n \in N_k} (q_{n,0} + \Delta Q_{d_n}^+ - \Delta Q_{d_n}^-) = Q_{k,j}^{sum}, \, \forall k \in K, j \in J$$
 (3.12n)

Since (3.11) holds, we can express $P_{k,j}^{sum}$ and $Q_{k,j}^{sum}$ as:

$$P_{k,j}^{sum} = \lambda_{k,j} \sum_{n \in N_k} p_n^{max} + (1 - \lambda_{k,j}) \sum_{n \in N_k} p_n^{min}$$
(3.12o)

$$Q_{k,j}^{sum} = \lambda_{k,j} \sum_{n \in N_k} q_n^{max} + (1 - \lambda_{k,j}) \sum_{n \in N_k} q_n^{min}$$
 (3.12p)

Where $0 \le \lambda_{k,j} \le 1$. Similarly, we can express $p_{n,0}, q_{n,0}$ as:

$$p_{n,0} = \lambda_{n,0}^{P} p_n^{max} + (1 - \lambda_{n,0}^{P}) p_n^{min}$$

$$q_{n,0} = \lambda_{n,0}^{Q} q_n^{max} + (1 - \lambda_{n,0}^{Q}) q_n^{min}$$
(3.12q)
$$(3.12r)$$

$$q_{n,0} = \lambda_{n,0}^{Q} q_n^{max} + (1 - \lambda_{n,0}^{Q}) q_n^{min}$$
(3.12r)

Where $0 \le \lambda_{n,0} \le 1$. By which we can construct the feasible solution of $\Delta P_{d_n}^+, \Delta P_{d_n}^-, \Delta Q_{d_n}^+$ and $\Delta Q_{d_n}^-$. If $\lambda_{k,j}^P \ge \lambda_{n,0}^P$ and $\lambda_{k,j}^Q \ge \lambda_{n,0}^Q$, we have:

$$\Delta P_{d_n}^+ = (\lambda_{k,j}^P - \lambda_{n,0}^P)(p_n^{max} - p_n^{min}), \, \forall n \in N_k$$
 (3.12s)

$$\Delta P_{d_n}^- = 0, \, \forall n \in N_k \tag{3.12t}$$

$$\Delta Q_{d_n}^+ = (\lambda_{k,j}^Q - \lambda_{n,0}^Q)(q_n^{max} - q_n^{min}), \ \forall n \in N_k$$
 (3.12u)

$$\Delta Q_{d_n}^- = 0, \, \forall n \in N_k \tag{3.12v}$$

Otherwise If $\lambda_{k,j}^P < \lambda_{n,0}^P$ or $\lambda_{k,j}^Q < \lambda_{n,0}^Q$, then:

$$\Delta P_{d_n}^+ = 0, \, \forall n \in N_k \tag{3.12w}$$

$$\Delta P_{d_n}^- = (\lambda_{n,0}^P - \lambda_{k,j}^P)(p_n^{max} - p_n^{min}), \, \forall n \in N_k$$
 (3.12x)

$$\Delta Q_{d_n}^+ = 0, \, \forall n \in N_k \tag{3.12y}$$

$$\Delta Q_{d_n}^- = (\lambda_{n,0}^Q - \lambda_{k,j}^Q)(q_n^{max} - q_n^{min}), \, \forall n \in N_k$$
 (3.12z)

(3.12s)-(3.12z) guarantee the non-negativity of variables $\Delta P_{d_n}^+$, $\Delta P_{d_n}^-$, $\Delta Q_{d_n}^+$, $\Delta Q_{d_n}^-$, the feasibility of (3.8c)-(3.8d) (equality) as well as the feasibility of $p_{n,j}$ and $q_{n,j}$ (satisfying the constraints (2.1l)-(2.1m)).

3.5 Numerical Results

3.5.1 The Performance of Sequential Tightness Algorithm

The results of SOC-ACOPF with sequential tightness algorithm are reported in Table 3.1 and Table 3.2. Note some constraints (reactive power loss) of the SOC-ACOPF model in this numerical test are different than model E in Chapter 2. So some results are accordingly different in these tables. The relaxation gap of constraints (2.2b) is calculated as:

$$Gp_{o_l} = \max_{l} \left\{ p_{o_l} - \frac{p_{s_l}^2 + q_{s_l}^2}{V_{s_l}} R_l \right\}$$
 (3.13)

The stopping criteria for the SOC-ACOPF iteration is $Gp_{o_l} < 10^{-9}$. In all reported cases, the Gp_{o_l} indicator is less than 10^{-9} . The optimality gap of the proposed SOC-ACOPF is measured in:

$$Gp_f = \frac{f^* - f}{f^*} \times 100\% \tag{3.14}$$

		Objective [\$]			
Case		Gp_{o_l}	Gp_f [%]		
Case	SOC-ACOPF	MATPOWER	Global	$ Gp_{o_l} $	$Op_{f[70]}$
IEEE14	8076.99	8081.53	8078.80	0	0.02
IEEE57	41673.08	41737.79	41698.64	0	0.06
IEEE118	129619.60	129660.70	129626.45	0	0.01
IEEE300	718109.18	719725.11	719459.62	0	0.18

Table 3.1: The performance of sequential tightness algorithm: objective solution

Table 3.2: The performance of sequential tightness algorithm: computation time

Case	CPU time [s]					
Case	SOC-ACOPF	MATPOWER	Global			
IEEE14	0.10	0.11	0.20			
IEEE57	0.19	0.12	2.31			
IEEE118	0.33	0.30	27.1			
IEEE300	3.10	0.40	257.68			

In the calculation of Gp_f , f^* is the global solution of nonconvex ACOPF calculated by LINDOGLOBAL and f is the solution of proposed SOC-ACOPF found by MOSEK solver. As we can see from Table 3.1, the results from SOC-ACOPF is very close to the global solutions obtained by LINDOGLOBAL.

3.5.2 The Power Network Partitioning

The network partitioning algorithm is implemented in MATLAB [86]. We use the power network data from MATPOWER. The GAMS Grid Computing facility [89] is employed for implementing the proposed parallel computing. All simulations are run on a computer with 2.4GHz CPU and 8GB RAM. The results of power network partitioning by spectral factorization are listed in Table 3.3 and Table 3.4. For each test case, we partition the network from two to eight subnetworks. The 'Partition' column in Table 3.3 and Table 3.4 lists the total number of subnetworks which is the parameter used in the network partitioning problem (3.7). Subnetworks are formed such that collection of them constructs the original power network. For small networks, when more subnetworks are partitioned, there can be only one bus for some partitioned subnetworks. Thus, there is no line inside these single-bus subnetworks. The spectral factorization algorithm is capable of partitioning all test cases in reasonable time. Generally, the computation time increases when more subnetworks are partitioned. The CPU time of partitioning large power networks is higher than the

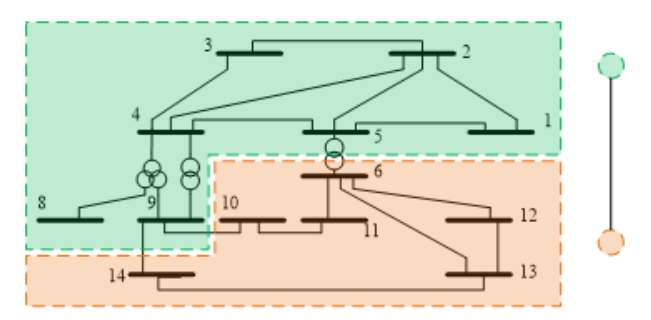


Figure 3.3: IEEE14-bus network partitions (two subnetworks) and its master problem representation ${\bf r}$

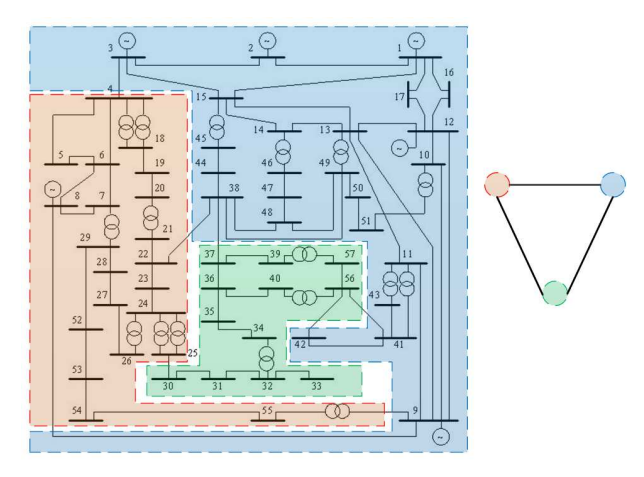


Figure 3.4: IEEE57-bus network partitions (three subnetworks) and its master problem representation $\,$

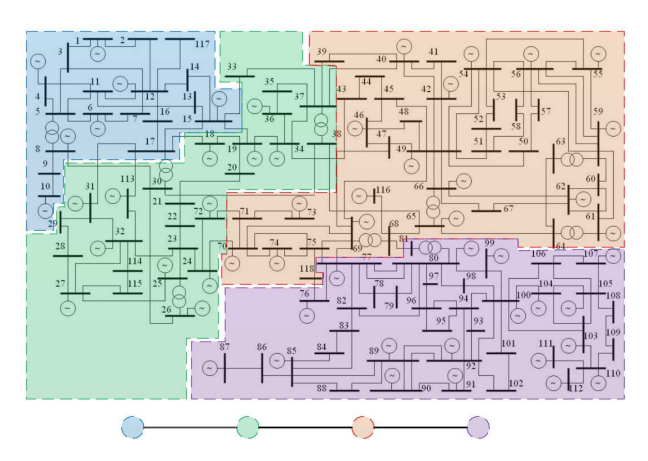


Figure 3.5: IEEE118-bus network partitions (four subnetworks) and its master problem representation ${\bf r}$

one for partitioning small power networks. Fig. 3.3, Fig. 3.4 and Fig. 3.5 are plotted to visualize some representative partitions for IEEE14-bus, IEEE57-bus and IEEE118-bus test cases. We use different colors to distinguish different partitioned subnetworks in these figures. The corresponding master problem of the proposed M-BDA for each partitioned network is also illustrated. We do not plot all the tie-lines in the representative master problems in these figures. Detailed results about the tie-lines are listed in Table 3.4.

3.5.3 Accelerated M-BDA Using GAMS Parallel Computing

The results of accelerated M-BDA using GAMS parallel computing are listed in Table 3.5. The 'Relative Gap' column shows the gap between the upper bound and lower bound of M-BDA. For all these test cases, M-BDA converges to very close solutions to single-stage SOC-ACOPF without decomposition. With the increase of partition depth (more subnetworks and fewer nodes in each subnetwork), the SOC-ACOPF problem complexity is decreasing. All test cases converge within five iterations. Compared with the computation time of single-stage SOC-ACOPF in Chapter 1, the computational efficiency improvement is more prominent in large test cases.

Table 3.3: Results of power network partitioning

Test Case	Partition	No. of Nodes in Subnetworks	No. of Lines in Subnetworks
	2	6, 8	11, 6
	3	3, 5, 6	2, 7, 6
	4	4, 2, 3, 5	4, 1, 2, 7
IEEE14	5	2, 2, 5, 3, 2	1, 1, 7, 2, 1
	6	3, 3, 2, 2, 2, 2	3, 3, 1, 1, 1, 1
	7	2, 1, 3, 2, 2, 1, 3	1, 0, 2, 1, 1, 0, 3
	8	3, 1, 2, 2, 1, 2, 2, 1	3, 0, 1, 1, 0, 0, 1, 0
	2	18, 39	19, 55
	3	12, 21, 24	12, 25, 35
	4	27, 11, 10, 9	38, 13, 10, 9
IEEE57	5	11, 10, 7, 9, 20	11, 12, 6, 9, 29
TEEE91	6	6, 7, 20, 8, 10, 6	6, 8, 29, 7, 12, 5
	7	7, 6, 10, 10, 9, 5, 10	7, 7, 12, 14, 7, 4, 10
	8	6, 9, 5, 7, 9, 4, 6, 11	5, 10, 6, 7, 9, 3, 5, 15
	2	79, 39	121, 60
	3	38, 35, 45	51, 55, 70
	4	25, 38, 37, 18	29, 60, 57, 23
IEEE118	5	22, 16, 27, 19, 34	27, 17, 45, 23, 51
1222110	6	23, 16, 18, 17, 30, 14	29, 23, 25, 21, 48, 18
	7	15, 12, 8, 18, 16, 16, 33	19, 16, 10, 27, 19, 19, 47
	8	21, 15, 6, 16, 15, 12, 16, 17	29, 20, 6, 19, 19, 16, 19, 25
	2	116, 184	159, 246
	3	116, 89, 95	159, 113, 127
	4	35, 87, 98, 80	37, 117, 132, 114
IEEE300	5	80, 105, 45, 33, 37	105, 135, 62, 39, 52
	6	54, 52, 48, 33, 60, 53	74, 59, 65, 39, 84, 69
	7	34, 59, 35, 37, 81, 21, 33	47, 80, 37, 52, 113, 25, 39
	8	34, 33, 53, 35, 35, 21, 35, 54	47, 39, 77, 42, 50, 25, 37, 74
	2	828, 526	1211, 753
	3	585, 428, 341	830, 644, 479
	4	311, 253, 319, 471	481, 352, 443, 659
1354pegase	5	178, 377, 297, 246, 256	253, 536, 460, 337, 355
	6	363, 87, 67, 217, 319, 301	510, 135, 85, 293, 446, 465
	7	120, 255, 72, 288, 152, 225, 242	180, 363, 97, 443, 211, 311, 322
	8	168, 151, 120, 243, 186, 102, 260, 124	242, 210, 180, 331, 274, 138, 354, 193
	2	1899, 970	2929, 1633
	3	600, 903, 1366	1026, 1526, 2010
	4	975, 457, 531, 906	1512, 647, 852, 1532
2869pegase	5	377, 509, 528, 789, 666	536, 818, 849, 1213, 1108
	6	562, 355, 412, 392, 771, 377	944, 585, 644, 621, 1187, 536
	7	354, 312, 579, 322, 508, 580, 214	501, 485, 915, 535, 754, 972, 354
	8	324, 532, 295, 214, 312, 288, 554, 350	544, 791, 491, 354, 485, 464, 876, 494

Table 3.4: Computation time of power network partitioning

Test Case	Partition	No. of Tie-lines	CPU Time [s]
	2	3	0.02
	3	5	0.02
IEEE14	4	6	0.03
	5	8	0.03
	6	10	0.03
	7	12	0.04
	8	14	0.05
	2	6	0.03
	3	8	0.03
	4	10	0.04
IEEE57	5	13	0.04
	6	13	0.04
	7	19	0.05
	8	20	0.05
	2	5	0.03
	3	10	0.04
	4	17	0.04
IEEE118	5	23	0.05
	6	22	0.05
	7	29	0.06
	8	33	0.06
	2	6	0.06
	3	12	0.06
	4	11	0.07
IEEE300	5	18	0.07
	6	21	0.09
	7	18	0.09
	8	20	0.12
	2	27	0.56
	3	38	0.59
	4	56	0.66
1354pegase	5	50	0.65
	6	57	0.67
	7	64	0.72
	8	69	0.92
	2	20	1.20
	3	20	1.25
	4	39	1.43
2869pegase	5	58	1.51
2000 pegase	6	65	1.45
	7	66	1.62
	8	83	2.10

Table 3.5: Accelerated M-BDA by GAMS parallel computing

Test Case	Partition	Upper Bound [\$]	Lower Bound [\$]	Relative Gap	CPU Time [s]
	2	8156.28	8067.17	1.09%	0.16
	3	8115.84	8043.42	0.89%	0.20
	4	8107.18	8043.43	0.79%	0.14
IEEE14	5	8102.82	8057.13	0.56%	0.20
	6	8127.95	8080.57	0.58%	0.28
	7	8099.13	7967.99	1.62%	0.31
	8	8119.83	8073.33	0.57%	0.28
	2	41801.64	41647.12	0.37%	0.30
	3	41871.87	41428.57	1.06%	0.25
	4	41798.99	41624.31	0.42%	0.22
IEEE57	5	41924.35	41675.16	0.59%	0.44
IEEE57	6	41814.77	41445.73	0.88%	0.45
	7	41956.47	41376.34	1.38%	0.25
	8	41848.47	41518.08	0.79%	0.37
	2	130025.49	129261.01	0.59%	0.33
	3	130847.44	128976.06	1.43%	0.76
	4	130066.45	129182.29	0.68%	0.39
IEEE118	5	130201.72	128631.17	1.21%	0.63
	6	131015.94	129089.14	1.47%	0.36
	7	130725.29	128393.25	1.78%	0.39
	8	129620.15	128955.16	0.51%	0.59
	2	722485.13	712303.53	1.41%	0.86
	3	721442.74	709941.27	1.59%	0.55
	4	724036.39	717468.50	0.91%	1.03
IEEE300	5	724084.83	712925.47	1.54%	0.59
	6	724038.39	709888.48	1.95%	0.70
	7	719765.51	716539.87	0.45%	0.52
	8	720591.14	714182.86	0.89%	0.47
	2	74041.62	74041.60	0.00%	3.98
	3	74198.12	74038.80	0.21%	4.17
	4	74040.36	74040.36	0.00%	1.51
1354pegase	5	74040.91	74040.91	0.00%	1.51
	6	74040.42	74040.42	0.00%	1.30
	7	74040.82	74040.82	0.00%	1.61
	8	74041.01	74040.99	0.00%	0.91
	2	133938.47	133886.16	0.04%	11.83
	3	134455.42	133409.29	0.78%	14.26
	4	133940.19	133869.50	0.05%	6.72
2869pegase	5	134122.31	131618.32	1.87%	8.70
~	6	133915.61	133915.57	0.00%	3.42
	7	133928.71	133928.70	0.00%	3.15
	8	135021.76	132710.79	1.71%	5.34

3.6 Conclusions

The tightness of the relaxation from the power loss constraints in the SOC-ACOPF model can be improved by the proposed sequential tightness algorithm. An accelerated M-BDA using parallel computing is proposed to tackle the complexity of large-scale SOC-ACOPF problem. The formulation, feasibility proof and fast convergence of the proposed M-BDA are the main contributions from the current Chapter. The numerical results show that the M-BDA accelerated by GAMS grid computing can reduce SOC-ACOPF problem scale as well as computation time. The advantage of solving SOC-ACOPF in a decomposed way is that we reduce the dimension of Hessian matrix and Jacobian matrix during the iterations of interior point method. This is very useful for large-scale power networks where the number of variables and constraints of the formulated SOC-ACOPF exceed the solver limit. Another advantage of the proposed decomposition is that, by keeping the boundary of different subnetworks or zones for the power system, the data privacy of each operation area can be protected. A coordinator who is solving the master problem of the proposed M-BDA does not need to know the network configuration of the subnetworks. All the required information by the coordinator is communicated through the Benders cuts. We prove analytically the feasibility of M-BDA. The convergence of the proposed approach is guaranteed by the convexity of the SOC-ACOPF model according to [73].

Chapter 4

Distribution Locational Marginal Pricing

4.1 Introduction

Given the very large number of nodes in distribution networks, the complexity involved in calculating DLMPs must be properly addressed. Decentralized dispatch is an attractive solution in smart grids [90–92]. To address the complexity, a decentralized OPF calculated by a Lagrangian-based decomposition procedure is proposed in [93]. Reference [94] reduces high-voltage radial distribution networks to simple networks by feeder reduction techniques. Reference [95] proposes the decentralized economic dispatch for smart grids using the concept of self-organizing dynamic agents. A distributed multi-agent paradigm is proposed in [96] to calculate DLMPs.

Reference [96] reports the DLMPs in a 12-bus distribution network calculated by both DCOPF and ACOPF. The results show that DLMPs from ACOPF are higher than the ones from DCOPF (this is partly because marginal loss costs are included in the ACOPF approach). The DLMP difference between DCOPF and ACOPF is larger in congestion cases (DLMP of bus 1 is 78.33\$/MWh by DCOPF but 149.99\$/MWh by ACOPF). On the other hand, reference [29] calculates DLMPs by DCOPF because of the ACOPF complexity in distribution networks with a large number of nodes.

Limitations on the ability to share network information is another issue in calculating DLMPs. The importance of coordination between the distribution and transmission network layer is discussed in [97] and [98]. This issue is significant for the operation of a power system with large-scale integration of distributed energy resources.

We can distinguish two main challenges in implementing DLMPs: (1) Computational complexity: The DCOPF assumptions are not often valid in distribution grids with high resistance to reactance (R/X) ratio [99]. On the other hand, the ACOPF in distribution networks with a large number of nodes might not be computationally tractable. This demands an OPF formulation which is accurate enough and at the same time which can be solved efficiently for distribution networks with a large number of nodes. (2) Sharing of network information: the correct calculation of DLMPs needs full information of the whole transmission, distribution and local network. Sharing of detailed network information between different network layers might not be feasi-

ble or practical. In this Chapter, these two challenges of implementing DLMPs are addressed.

For the computation complexity challenge, we propose a convexified ACOPF (model E of SOC-ACOPF) based on second-order cone relaxation [43, 44, 55]. The tightness of the employed relaxation is enforced by a sequential tightness algorithm.

To address the issue of sharing information between different network layers, the concept of GBF is proposed. The convexified ACOPF and the GBF are placed in a proposed HED mechanism. We prove that if the GBFs are communicated, the proposed HED achieves results very close to the global economic dispatch. We demonstrate the proposed solutions to implementing DLMP by numerical simulations using a GAMS model. The rest of this Chapter is organized as follows. Section II introduces the concept of HED mechanism and GBF. Section III presents the numerical results and discussions. The convergence of HED mechanism is proved numerically. As the communication requirement between network operators, the capacity of GBF is shown to be small. Section IV concludes the advantages of the proposed SOC-ACOPF approach, HED mechanism and GBF.

4.2 The Hierarchical Economic Dispatch

To define hierarchical economic dispatch (HED), we should firstly explain the traditional centralized economic dispatch (CED). We assume here centralized economic dispatch as one system operator dispatching all generations in transmission, distribution and local networks. To fulfill this dispatch task, the system operator should obtain all network information about his responsible area. Mathematically, CED is to solve ACOPF problem (2.1) or SOC-ACOPF Model E. The CED is a very large scale optimization problem considering the enormous nodes, lines and DERs. To release the complexity of CED, we propose the HED mechanism in this Chapter. HED actually decompose CED by Benders decomposition. We show that Benders cuts in this proposed hierarchical economic dispatch have specific economic meanings in the defined GBF.

4.2.1 Decomposing the Economic Dispatch

We propose a three-level dispatch mechanism with each network operator responsible for its own network. The network layers are connected through tie-lines. At the third level, local network or microgrid operators (LNOs) carry out their own dispatch considering local network constraints. LNOs communicate dispatch results through the proposed GBFs to the second level of hierarchy. At the second level, the distribution network operators (DNOs) run another optimization problem taking into account the

submitted GBFs from all connected LNOs and the second-level network constraints. The results of the second level optimization is packed in the form of GBFs and submitted to the first level of hierarchy. At the first level of hierarchy, transmission network operator (TNO) solves the dispatch problem of transmission network taking into account the submitted GBFs from DNOs. Once the top level of the hierarchy is completed, the dispatch results are determined and the resulting nodal prices can be computed and communicated back down to the hierarchy. This is illustrated in Fig. 4.1.

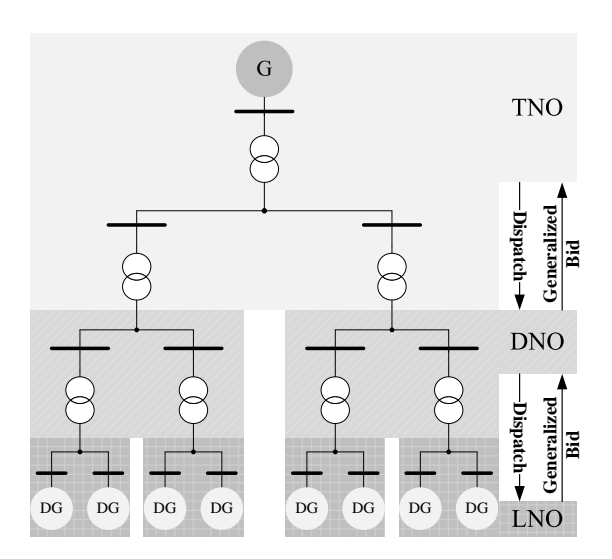


Figure 4.1: The conceptual diagram of the proposed HED mechanism

4.2.2 Generalized Bid Function

The concept of GBF is proposed to avoid communicating detailed network and regional bid information between dispatch levels. The HED problem for LNOs contingent on the total power generation is set out in (4.1).

$$F_{k}(P_{k,j}^{sum}) = \text{Minimize } \sum_{n \in N_{k}} f(p_{n}, q_{n})$$
subject to $(2.1b) - (2.1c), (2.1j) - (2.1m), (2.2b) - (2.2d), (2.5b) - (2.5l)$

$$\sum_{n \in N_{k}} p_{n} = P_{k,j}^{sum} : (\alpha_{k,j})$$

$$(4.1a)$$

Where F_k is the cost of local network dispatch as a function of its total power generation $P_{k,j}^{sum}$. $k \in K$ is the index of the LNO. $f(p_n, q_n)$ is the generation cost of the local DGs. N_k is the set of local nodes. $j \in J_k$ is the index of GBFs. If we use $S(P_{k,j}^{sum})$ to denote the feasible region of (p_n, q_n) as a function of $P_{k,j}^{sum}$. The optimization value function $F_k(P_{k,j}^{sum})$ is convex because: (1). $f(p_n, q_n)$ is jointly convex on $\{(p_n, q_n, P_{k,j}^{sum}) \mid (p_n, q_n) \in S(P_{k,j}^{sum}), P_{k,j}^{sum} \in \Re^+\}$; (2). $S(P_{k,j}^{sum})$ is convex on \Re^+ ; and (3). \Re^+ is convex (see proposition 2.1 in reference [100]). F_k can be approximated from below by a set of affine functions as in (4.2) shown by Fig. 4.2.

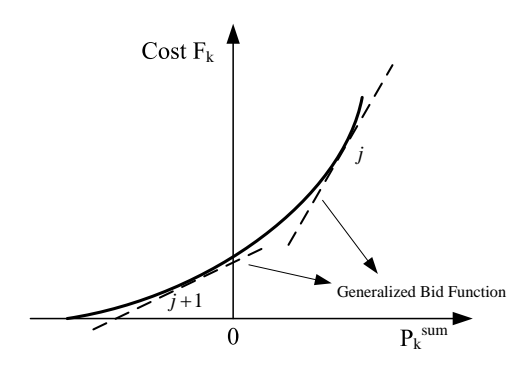


Figure 4.2: Approximation of a convex cost function by affine functions

$$F_k(P_{k,j}^{sum}) \ge \hat{F}_{k,j} + \hat{\alpha}_{k,j} \left(\sum_{n \in N_k} p_n - \hat{P}_{k,j}^{sum} \right), \, \forall j \in J_k, \, \forall k \in K$$
 (4.2)

We define GBF as the set of parameters of the affine approximator (4.2). These parameters are communicated through set $LNO_k = \{(\hat{F}_{k,j}, \hat{\alpha}_{k,j}, \hat{P}_{k,j}^{sum}) : j \in J_k\}$ to the DNO. Once all LNO_k sets are communicated, the DNO solves the following dispatch problem (4.3).

$$G_v(P_{v,j}^{sum}) = \text{Minimize } \sum_{n \in N_v} f(p_n, q_n) + \sum_{k \in K} F_k$$
 (4.3a)

$$subject\ to\ (2.1b)-(2.1c), (2.1j)-(2.1m), (2.2b)-(2.2d), (2.5b)-(2.5l)$$

$$\sum_{n \in N_v} p_n = P_{v,j}^{sum} : (\alpha_{v,j})$$

$$\tag{4.3b}$$

Same as F_k , G_v is also a convex optimization value function based on proposition 2.1 in reference [100]. G_v can be approximated from below by affine functions (4.4b).

 $v \in V$ is the index of the DNO. The parameters of these affine functions are communicated through set $DNO_v = \{(\hat{G}_{v,j}, \hat{\alpha}_{v,j}, \hat{P}^{sum}_{v,j}) : j \in J_v\}$ to TNO. TNO solves the optimization problem (4.4).

Minimize
$$\sum_{n \in N_t} f_t(p_n, q_n) + \sum_{v \in V} G_v$$
 (4.4a)

$$subject\ to\ (2.1b)-(2.1c), (2.1j)-(2.1m), (2.2b)-(2.2d), (2.5b)-(2.5l)$$

$$G_v(P_{v,j}^{sum}) \ge \hat{G}_{v,j} + \hat{\alpha}_{v,j} \left(\sum_{n \in N_v} p_n - P_{v,j}^{sum} \right), \, \forall j \in J_v, \, \forall v \in V$$
 (4.4b)

Once optimization problem (4.4) is solved, TNO finds the nodal prices. It also communicates the total power generation requirement $\hat{P}^{sum}_{v,\hat{j}}$ to DNOs (\hat{j} is the index of final GBF for which the HED converges). Given $\hat{P}^{sum}_{v,\hat{j}}$, DNOs find the nodal prices for their networks. The DNO also communicates $\hat{P}^{sum}_{k,\hat{j}}$ to the connected LNOs. LNOs then calculate the nodal prices for their local networks. The underlying mathematical structure behind the HED mechanism is the Benders decomposition approach. If the problem is convex, it is proved that optimal solution can be found within finite iterations [101].

Algorithm 4: Hierarchical Economic Dispatch Mechanism

Initialization;

TNO solve transmission network dispatch (4.4);

TNO broadcast $\hat{P}_{v,\hat{j}}^{sum}$ to DNOs;

DNOs solve distribution network dispatch (4.3);

DNOs broadcast $\hat{P}_{k,\hat{j}}^{sum}$ to LNOs;

DNOs submit DNO_k to TNO;

LNOs solve local network dispatch (4.2);

LNOs submit LNO_k to DNO;

4.3 Numerical Results and Discussions

Simulations are run on a computer with Intel i7-2760QM 2.4 GHz CPU and 8 GB of RAM.

4.3.1 Convergence of Hierarchical Economic Dispatch

The IEEE342-node network [102] is modified here to illustrate the operation of the proposed HED. This test case has transmission network (nodes P1-P4, P7-P8), distribution network (nodes P5-P6, P9-P390) and local networks (nodes S193-S240 in the eight spot 277/480V networks). The local networks are connected to the distribution network by transformers denoted as X3, X4 to X22 in Fig. 4.5. One 50 MW generator is located in the transmission network. Each 13.2 kV distribution feeder is equipped with one 7.5 MW DG. We distribute 48 DGs among all nodes of the local networks (one 3 MW DG at each node). To simulate congestion in the distribution network and local networks, we increase the load levels in all the local networks by four times and then reduce the tie-line transformer capacity (X10-X18 is reduced to 3 MVA and X21-X22 is reduced to 4 MVA). We assume all generators are dispatchable. To accelerate computation, we design a GAMS grid computing structure to assign the dispatch task of each network to different threads as demonstrated in Fig. 4.4.

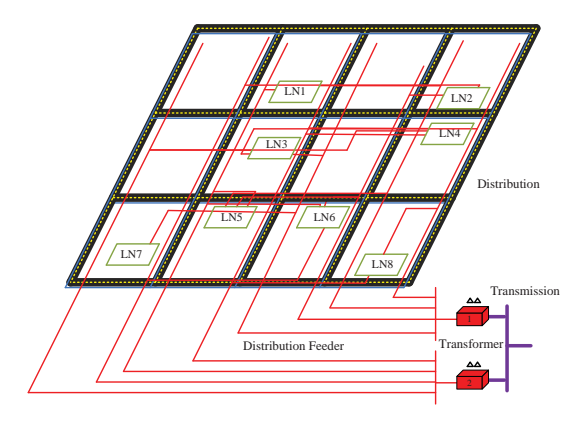


Figure 4.3: The hierarchy of the modified IEEE342-node test system

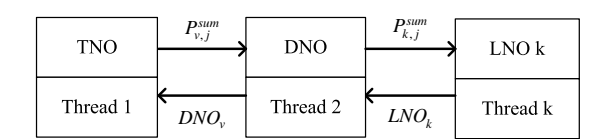


Figure 4.4: The GAMS grid computing structure of hierarchical economic dispatch

The dispatch results of HED are listed in Table 4.1 and Table 4.2. We denote the case of no congestion as the base case in this Chapter. The congestion cases are denoted as the corresponding congested transformers in Table 4.1 and Table 4.2. CED results denoted as 'C' are also listed. The HED results (denoted as 'H') converge

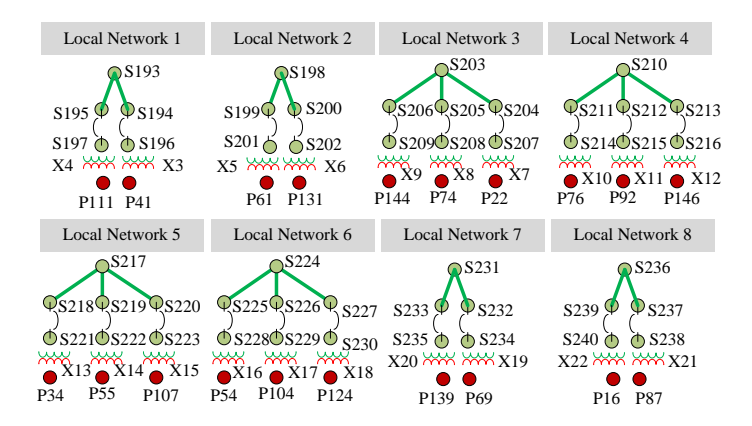


Figure 4.5: Local low voltage networks

to the solution very close to centralized dispatch dispatch cost. All cases converge within three iterations shown in Fig. 4.6. Because of approximations used in HED mechanism, the final cost of HED is a bit different from centralized dispatch (the difference is within 1% after three iterations). The CPU time for computation is within 1.8 second. If the LNOs and DNO submit their GBFs (i.e. parameters of three affine approximators in one package) to the next higher hierarchy, the HED converges in one iteration. It is worth to mention that Benders decomposition is a way to build GBFs in HED. HED does not work in an iterative way.

4.3.2 Distribution Locational Marginal Price

The nodal prices are shown in Fig. 4.7. All nodal prices are very close to each other in the base case. The only differences in the nodal prices are due to the marginal cost of energy loss. This can be clearly observed from the small price spikes at the ending nodes (S193, S198, S203, S210, S217, S224, S231 and S236) of each local network. The congested distribution transformers are indicated in the legend of Fig. 4.7. When congestion happens, the nodes located in the local network have higher prices. The consumers with price-responsive load can response to these higher prices. This can be observed by comparing consumer payment and DG income when congestion happens with the ones in the base case. We plot the total payment of consumers in the local networks in Fig. 4.8. The payment difference as compared to the base-case payments is also shown in Fig. 4.8. The congestion management potential of DLMP can be further demonstrated by the income increase of DGs when congestion happens. This is shown in Fig. 4.9. When congestion happens, the increased nodal prices give local DGs strong incentive to produce more energy.

Table 4.1: The results of the active power dispatch from HED mechanism, C: Centralized dispatch, H: HED

Network	Generator	Base Case [MW]		x10-x11-x12 [MW]		x13-x14-x15 [MW]	
Network	Generator	С	Н	С	Η	С	Н
Transmission	1	50.00	50.00	50.00	50.00	50.00	50.00
	2	7.50	7.50	7.50	7.50	7.50	7.50
	3	7.50	7.50	7.50	7.50	7.50	7.50
	4	7.50	7.50	7.50	7.50	7.50	7.50
Distribution	5	7.50	7.50	7.50	7.50	7.50	7.50
Distribution	6	7.50	7.50	7.50	7.50	7.50	7.50
	7	7.50	7.50	7.50	7.50	7.50	7.50
	8	7.50	7.50	7.50	7.50	7.50	7.50
	9	5.93	5.96	0.99	0.94	0.14	0.15
Local 4	29	0.00	0.00	2.89	3.00	0.00	0.00
Local 4	30	0.00	0.00	1.40	2.07	0.00	0.00
Local 5	36	0.00	0.00	0.00	0.00	2.44	3.00
Local 5	37	0.00	0.00	0.00	0.00	0.17	2.86
	38	0.00	0.00	0.00	0.00	0.18	0.00
	43	0.00	0.00	0.00	0.00	0.00	0.00
Local 6	44	0.00	0.00	0.00	0.00	0.00	0.00
	45	0.00	0.00	0.00	0.00	0.00	0.00
	53	0.00	0.00	0.00	0.00	0.00	0.00
Local 8	54	0.00	0.00	0.00	0.00	0.00	0.00
	55	0.00	0.00	0.00	0.00	0.00	0.00
Total Co	st [€]	731.67	732.25	757.91	755.09	766.93	762.38

4.3.3 Results of Generalized Bid Function

The GBFs are listed in Table 4.3-Table 4.7. We sum the $\hat{F}_{k,j}$ and $\hat{G}_{v,j}$ parameters in the GBFs for all networks and list the accumulated results in the last row of the Table 4.3-Table 4.7. The LNOs submit their calculated GBFs to the DNO. Accordingly, the DNO takes into account submitted GBFs from LNOs and prepares its GBFs to be submitted to the TNO. The TNO calculates the dispatch instructions and nodal prices will be communicated back down to the hierarchy. Note that LNOs only need to submit their GBFs to the DNO. Bids from the 48 local DGs are not required to be submitted to the DNO. In other words, with GBFs, the network layers would not need to share their detailed network information between each others. Table 4.3-Table 4.7 demonstrate the communication burden of HED is small.

Table 4.2: The results of the active power dispatch from HED mechanism, C: Centralized dispatch, H: HED

Network	Commeter	x16-x17	-x18 [MW]	x21-x22	2 [MW]
Network	Generator	С	H	С	Н
Transmission	1	50.00	50.00	50.00	50.00
	2	7.50	7.50	7.50	7.50
	3	7.50	7.50	7.50	7.50
	4	7.50	7.50	7.50	7.50
Distribution	5	7.50	7.50	7.50	7.50
Distribution	6	7.50	7.50	7.50	7.50
	7	7.50	7.50	7.50	7.50
	8	7.50	7.50	7.50	7.50
	9	0.10	0.10	0.05	0.04
Local 4	29	0.00	0.00	0.00	0.00
Local 4	30	0.00	0.00	0.00	0.00
Local 5	36	0.00	0.00	0.00	0.00
Local 5	37	0.00	0.00	0.00	0.00
	38	0.00	0.00	0.00	0.00
	43	2.44	3.00	0.00	0.00
Local 6	44	2.87	2.97	0.00	0.00
	45	0.65	0.00	0.00	0.00
	53	0.00	0.00	2.98	3.00
Local 8	54	0.00	0.00	3.00	3.00
	55	0.00	0.00	0.00	0.13
Total Co	st [€]	769.15	766.96	769.15	776.38

4.4 Conclusions

This Chapter proposes solutions to practical challenges of implementing locational marginal prices in distribution networks. The challenges considered here include (1) the computational complexity of nodal prices in ACOPF and (2) the network information which potentially must be communicated. We propose to apply the SOC-ACOPF model to calculate nodal prices in a distribution network. The proposed SOC-ACOPF model can be solved efficiently to global optimality while it has more accurate results than DCOPF. The issue of network information sharing is addressed through the proposed concept of GBF. The HED mechanism is also proposed to decompose the dispatch task of multiple connected networks. A three-level network is considered. At the third level, LNOs communicate the dispatch cost of their networks through

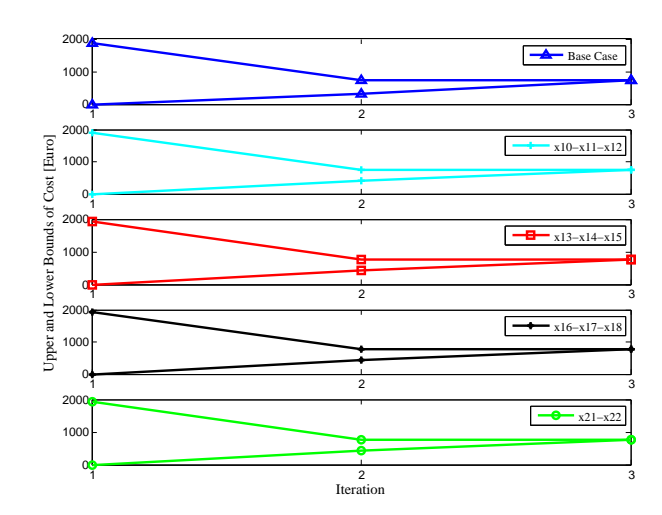


Figure 4.6: The convergence of the proposed HED mechanism

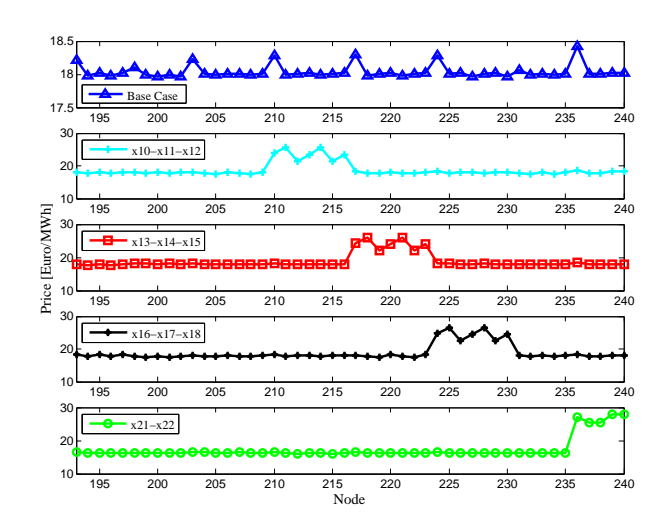


Figure 4.7: The nodal prices in local networks

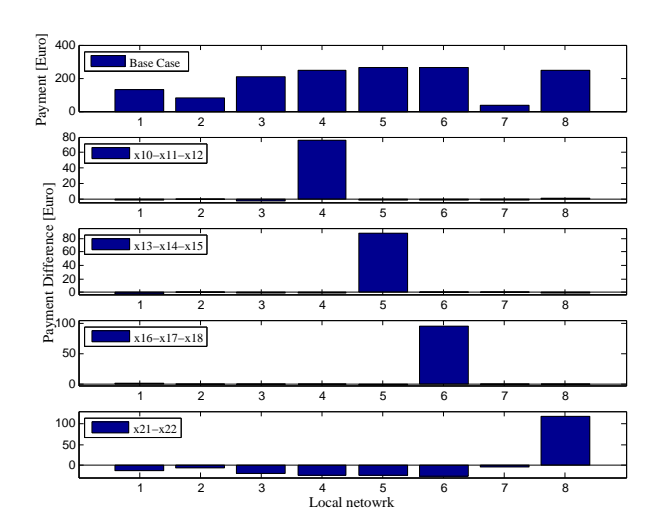


Figure 4.8: The total payment of consumers in local networks

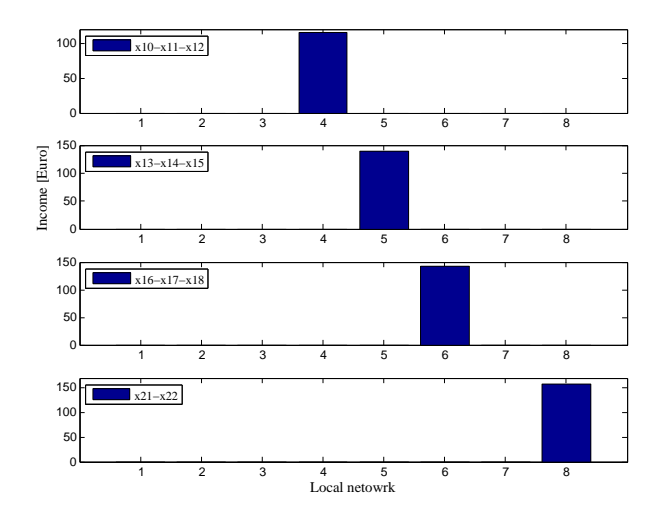


Figure 4.9: The total income of DGs in local networks

Table 4.3: The GBFs in base case $\,$

Network	<i>j</i> =	= 1	<i>j</i> =	j=2		j=3	
Network	P^{sum}	α	P^{sum}	α	P^{sum}	α	
DNO	21.60	8.00	58.46	18.00	58.46	18.00	
LNO1	7.20	24.00	0.00	20.00	0.00	19.98	
LNO2	6.64	24.50	0.00	20.50	0.00	20.48	
LNO3	10.17	26.50	0.00	21.00	0.00	20.98	
LNO4	10.67	27.00	0.00	21.50	0.00	21.47	
LNO5	10.86	27.50	0.00	22.00	0.00	21.98	
LNO6	10.88	28.00	0.00	22.50	0.00	22.48	
LNO7	6.25	27.00	0.00	23.00	0.00	22.95	
LNO8	8.37	27.50	0.00	23.50	0.00	23.45	
Cost [€]	1825.28		632.25		632.25		

Table 4.4: The GBFs in case of x10-x11-x12 congestion

Network	j=1		j=2		j=3		
Network	P^{sum}	α	P^{sum}	α	P^{sum}	α	
DNO	20.32	8.00	53.44	18.00	53.44	18.00	
LNO1	7.10	24.00	0.00	19.98	0.00	20.00	
LNO2	6.55	24.50	0.00	20.48	0.00	20.49	
LNO3	10.00	26.50	0.00	20.98	0.00	20.99	
LNO4	13.77	27.50	5.07	23.50	5.07	23.50	
LNO5	10.69	27.50	0.00	21.98	0.00	21.99	
LNO6	10.71	28.00	0.00	22.48	0.00	22.49	
LNO7	6.16	27.00	0.00	22.98	0.00	22.98	
LNO8	8.28	27.50	0.00	23.48	0.00	23.48	
Cost [€]	1870	6.40	655.09		655	655.09	

Network	j =	= 1	j =	j=2		j=3	
Network	P^{sum}	α	P^{sum}	α	P^{sum}	α	
DNO	20.03	8.00	52.65	18.00	52.65	18.00	
LNO1	7.08	24.00	0.00	20.00	0.00	20.00	
LNO2	6.53	24.50	0.00	20.50	0.00	20.50	
LNO3	9.97	26.50	0.00	21.00	0.00	21.00	
LNO4	10.47	27.00	0.00	21.50	0.00	21.50	
LNO5	14.58	28.00	5.86	24.00	5.86	24.00	
LNO6	10.68	28.00	0.00	22.50	0.00	22.49	
LNO7	6.14	27.00	0.00	23.00	0.00	22.99	
LNO8	8.27	27.50	0.00	23.50	0.00	23.49	
Cost [€]	1888.70		662.38		662.38		

Table 4.5: The GBFs in case of x13-x14-x15 congestion

the proposed GBFs. At the second level, DNO runs another optimization considering its own network conditions and submitted GBFs of the LNOs. The results of this optimization are packed in the form of GBFs and communicated to the first level of hierarchy i.e. TNO. Once the optimization problem of the first level of hierarchy is solved, the dispatch results and nodal prices are communicated back down to the hierarchy. The convergence of HED mechanism is guaranteed by the convexity of the SOC-ACOPF. The simulation results show the utility of proposed mechanism for implementing nodal pricing in distribution and local networks.

Table 4.6: The GBFs in case of x16-x17-x18 congestion

Network	j =	= 1	j =	j=2		j=3	
Network	P^{sum}	α	P^{sum}	α	P^{sum}	α	
DNO	20.03	8.00	52.60	18.00	0.00	18.00	
LNO1	7.08	24.00	0.00	20.00	0.00	20.00	
LNO2	6.53	24.50	0.00	20.50	0.00	20.50	
LNO3	9.97	26.50	0.00	21.00	0.00	21.00	
LNO4	10.47	27.00	0.00	21.50	0.00	21.49	
LNO5	10.66	27.50	0.00	22.00	0.00	21.99	
LNO6	14.66	28.50	5.97	24.50	5.97	24.50	
LNO7	6.14	27.00	0.00	23.00	0.00	22.99	
LNO8	8.27	27.50	0.00	23.50	0.00	23.49	
Cost [€]	1892.15		666.96		666.96		

Table 4.7: The GBFs in case of x21-x22 congestion

Network	j =	= 1	j =	j=2		j=3	
Network	P^{sum}	α	P^{sum}	α	P^{sum}	α	
DNO	20.00	8.00	52.54	18.00	52.54	18.00	
LNO1	7.08	24.00	0.00	19.96	0.00	20.00	
LNO2	6.53	24.50	0.00	20.46	0.00	20.49	
LNO3	9.96	26.50	0.00	20.97	0.00	20.99	
LNO4	10.47	27.00	0.00	21.47	0.00	21.49	
LNO5	10.65	27.50	0.00	21.94	0.00	21.99	
LNO6	10.67	28.00	0.00	22.44	0.00	22.49	
LNO7	6.14	27.00	0.00	22.95	0.00	22.99	
LNO8	12.45	31.50	6.13	27.50	6.13	27.50	
Cost [€]	1900.90		676.38		676	676.38	

Chapter 5

Integrating Wind Power by Stochastic Conic Programming

5.1 Introduction

One severe challenge of operating the power network including VSC-MTDC system and FACTS is the stochastic nature of renewable energy such as wind power. To consider the uncertainty of wind power, authors in [103] propose a scenario generation method that contains wind power forecast errors and fluctuation distribution. The interdependence structure of prediction errors in generating wind scenarios is the focus of [104]. Reference [105] describes a local search algorithm to determine the operation points of two HVDC systems connecting Jeju Island to the Korean Peninsula. The potential of demand responses to deal with the uncertainty of wind power are investigated by [106] using a stochastic programming approach. Reference [107] formulates a stochastic nonconvex multi-period OPF model to integrate wind generation through HVDC system. The HVDC type considered in this work is line-commutated converters HVDC (LCC-HVDC). The power generations of thermal generators are taken as the first-stage variables (fixed for all wind power scenarios) and the second stage-variables (determined according to each wind power scenario) include the wind power generations and HVDC operation points. Although [107] models multiple wind farms, the total number of considered wind power scenarios is limited to twelve. Reference [108] minimizes the wind power spillage by formulating a stochastic non-convex OPF model including FACTS devices. Similarly, the power outputs of thermal (conventional) generators are fixed for all wind power scenarios. The second-stage variables include the wind power outputs and the control variables of FACTS devices. We use the same approach in [107,108] to divide first-stage and second-stage variables in the stochastic programming model of this Chapter.

Considering the uncertainty of wind in the VSC-MTDC system and FACTS leads to a severe computational challenge. For example, if we consider the case of Sweden, there are currently around 38 wind farms [109]. If each wind farm were operated by an individual company, and only two possible scenarios for wind output are taken into account, the total number of scenarios to be analyzed by the transmission system operator (TSO) would be 2^{38} . The scale of the formulated OPF problem grows

exponentially. This large-scale computational challenge is considered in [110], where parallel computation is used to solve a multi-objective security constrained OPF model considering 1000 wind power scenarios. The parallel computation carried out in MAT-LAB takes more than two hours to find the solutions. As an improvement, the maximum number of wind power scenarios addressed in this Chapter is up to 10000. The contributions of this Chapter are:

- 1. We use the SOC-ACOPF model (Model P, based on the work from [111, 112]) which is convex and can be solved efficiently by the interior point method (IPM). Compared with the SOCP-based ACOPF model in [111, 112], we explicitly include voltage phase angle variables in the model and thus these solutions can be obtained directly from our model; Furthermore, we extend the model to include both mono-polar and bi-polar VSC-MTDC system;
- 2. A methodology to generate representative wind power scenarios of multiple wind farms based on wind speed measurements and wind turbine models are proposed;
- 3. Based on the formulated SOC-ACOPF model and wind power scenario generation methodology, the optimal operation of power network including VSC-MTDC system and FACTS devices is formulated in a stochastic SOC-ACOPF model to consider the uncertainties of wind power;
- 4. The large-scale computational challenge up to 10000 wind power scenarios is addressed by the proposed M-BDA and parallel computation approaches; One fundamental reason of the improved performance is, by using M-BDA, we actually reduce the dimension of the Hessian matrix and Jacobian matrix during the iteration of the deployed IPM-based solver (MOSEK). The efficient design of the parallel computation structure in GAMS platform is another reason of the improved performance.

The rest of this Chapter is organized as follows. Section II formulates the exact nonlinear model of the hybrid AC-DC power network including FACTS devices. Section III proposes the convexification and approximation methods of the SOC-ACOPF model. Section IV introduces the wind power scenario generation methodology. Section V presents the stochastic SOC-ACOPF model. Section VI describes the parallel computation structure in GAMS platform based on the proposed M-BDA of the stochastic SOC-ACOPF model. Section VII presents the numerical results and discusses the efficiency of the proposed approaches. Finally, Section VIII concludes this Chapter. The modelling approach in Section 5.2 and Section 5.3 of this Chapter is based on the work from [112].

5.2 Hybrid AC-DC Network and FACTS Models

In this Section we model the AC network, the VSC-MTDC system and FACTS devices.

5.2.1 The AC Network

We use the constraints of SOC-ACOPF (Model P [(2.1b)-(2.1c), (2.1j)-(2.1m),(2.2b)-(2.2e)]) to model the AC network. To distinguish AC network from the DC network, we have specified the sets n_{AC} , l_{AC} (to replace the sets N, L) for all the indexes at the end of the corresponding constraints.

5.2.2 The VSC-MTDC System

The DC Side

The equivalent circuit in Fig. 5.1 is used to derive the constraints for the AC-DC grid and the VSC stations. In Fig. 5.1, PCC is short for point of common coupling. PC is the AC bus coupling with the DC bus of VSC. The VSC is connected with PCC through a coupling transformer. R_{Cse} , R_{Csh} are resistors to model the ohmic losses of VSC. We define n_{DC} to represent the set of DC buses, and l_{DC} to represent the set

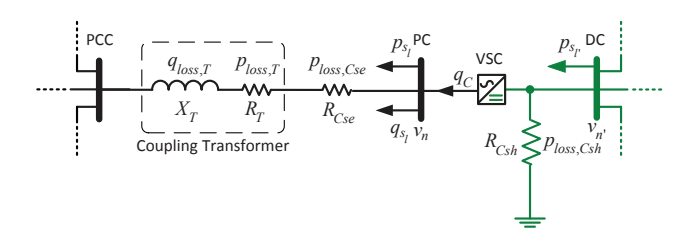


Figure 5.1: The equivalent circuit of VSC-MTDC system

of DC lines connected to the VSC. In order to distinguish from the AC network, we have specified the sets n_{DC} , l_{DC} for all the indexes at the end of each constraint. The active power balance equation at each DC bus can be written as:

$$p_n = \sum_{l \in l_{DC}} (A_{nl}^+ p_{s_l} - A_{nl}^- p_{loss_l}) + G_n v_n^2, \ \forall n \in n_{DC}$$
 (5.1a)

where p_n is the injected active power at DC bus n. For mono-polar DC connections shown in Fig. 5.2, we define $l_{DCmono} \in l_{DC}$ as the set of monopole DC link. The power

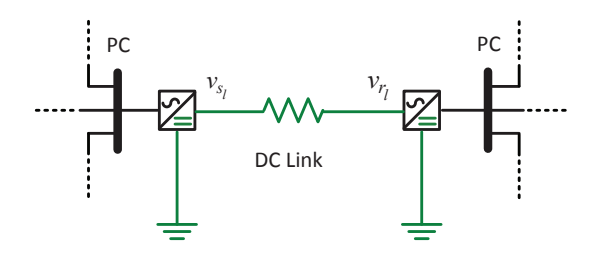


Figure 5.2: The monopole MTDC connection

loss of each monopole DC line is formulated as:

$$p_{loss_l} = \frac{p_{s_l}^2}{v_{s_l}^2} R_l, \ \forall l \in l_{DCmono}$$

$$(5.1b)$$

The voltage square drop across each monopole DC link is:

$$v_{s_{l}}^{2} - v_{r_{l}}^{2} = v_{s_{l}}^{2} - (v_{s_{l}} - \Delta v_{l})^{2}$$

$$= v_{s_{l}}^{2} - v_{s_{l}}^{2} - \Delta v_{l}^{2} + 2v_{s_{l}}\Delta v_{l}$$

$$= 2v_{s_{l}}I_{s_{l}}R_{l} - (I_{s_{l}}R_{l})^{2}$$

$$= 2p_{s_{l}}R_{l} - p_{loss_{l}}R_{l}, \ \forall l \in l_{DCmono}$$
(5.1c)

Where $\Delta v_l = v_{s_l} - v_{r_l}$ is the voltage drop of the DC link. I_{s_l} is the current of the DC link. We make use of $p_{s_l} = v_{s_l}I_{s_l}$ and $p_{loss_l} = I_{s_l}^2R_l$ in the derivations of (5.1c). It is worth to mention that although we use Δv_l , I_{s_l} to derive (5.1c), these variables are not included in our proposed SOC-ACOPF model. The solutions of these variables can be recovered by the solutions of p_{s_l} , v_{s_l} , v_{r_l} . For bipolar DC connections shown in Fig. 5.3, we define $l_{DCbi} \in l_{DC}$ as the set of bi-polar DC line. The power loss of each bipolar DC line is formulated as (Note here R_l is the total resistance of the bi-polar DC link):

$$p_{loss_l} = \frac{p_{s_l}^2}{4v_{s_l}^2} R_l, \ \forall l \in l_{DCbi}$$

$$(5.1d)$$

Similarly, the voltage drop across each bi-polar DC link is:

$$v_{s_l}^2 - v_{r_l}^2 = p_{s_l} R_l - p_{loss_l} R_l, \ \forall l \in l_{DCbi}$$
 (5.1e)

Equations (5.1d)-(5.1e) are valid because $p_{s_l} = 2v_{s_l}I_{s_l}$ for bipolar DC link. The relationship between AC and DC sides are represented using voltage and power couplings.

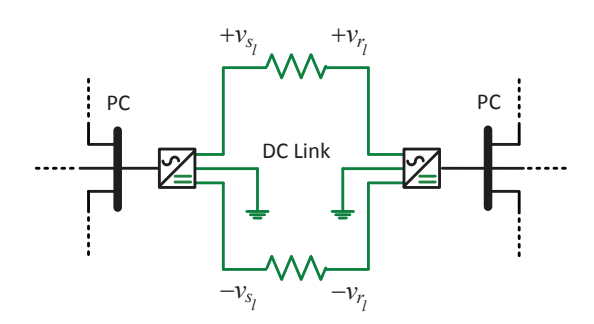


Figure 5.3: The bipolar MTDC connection

We define n_{PC} as the set of AC buses coupling with the DC buses of VSC. As it is shown in Fig. 5.1, the DC side voltage at each station is related to AC side voltage by:

$$v_n = \frac{v_n'}{2\sqrt{2}} m_{n,n'}, \ \forall n \in n_{PC}, \forall n' \in n_{DC}$$

$$(5.1f)$$

where $m_{n,n'}$ indicates the modulation index for the converter between the bus n and n'. In practice the modulation index is bounded as $0.5 \le m_{n,n'} \le 1$. Several steady state models for converter loss have been used in the literature [113], [114]. In this Chapter, we consider the loss model proposed in [114] where the converter losses are represented by a series resistor (R_{Cse}) on the AC side and a shunt resistor (R_{Csh}) on the DC side (See Fig. 5.1). The loss of the shunt resistor R_{Csh} can be calculated as:

$$p_{loss,Csh} = \frac{v_{n'}^2}{R_{Csh}}, \ \forall n' \in n_{DC}$$
 (5.1g)

The AC Side

Define l_{VSC} as the converter line (from the DC bus to the PC bus) and l_{PC} as the AC line coupling with the converter (from the PC bus to the PCC bus). The sending end power of the converter line can be obtained by:

$$p_{s_l} = p_{s_{l'}} - p_{loss,Csh}, \ \forall l \in l_{PC}, \forall l' \in l_{VSC}$$

$$(5.1h)$$

$$q_{s_l} = q_C, \ \forall l \in l_{PC}, \forall l' \in l_{VSC}$$
 (5.1i)

Where q_C is the reactive power output of the voltage converter station in the VSC-MTDC system. The constraints for the AC side of each station are derived using the

equivalent circuit shown in Fig. 5.1. As it is shown, coupling transformer and phase reactor can be simply modeled as an AC line. Therefore constraints (2.2d) and (2.2e) together with following equations can be applied to each VSC station. The $p_{loss,T}$, $p_{loss,Cse}$, $q_{loss,T}$ and $q_{loss,Cse}$ are obtained in a similar way as (2.1d) and (2.1e) in the following equations:

$$p_{loss,T} = \frac{p_{s_l}^2 + q_{s_l}^2}{v_{s_l}^2} R_T, \ \forall l \in l_{PC}$$
 (5.1j)

$$q_{loss,T} = \frac{p_{s_l}^2 + q_{s_l}^2}{v_{s_l}^2} X_T, \ \forall l \in l_{PC}$$
 (5.1k)

$$p_{loss,Cse} = \frac{p_{s_l}^2 + q_{s_l}^2}{v_{s_l}^2} R_{Cse}, \ \forall l \in l_{PC}$$
 (5.11)

where R_T and X_T are resistance and reactance of the coupling transformer.

5.2.3 FACTS Devices

The FACTS devices considered in this Chapter include static synchronous compensator (STATCOM) and static VAR compensator (SVC).

STATCOM

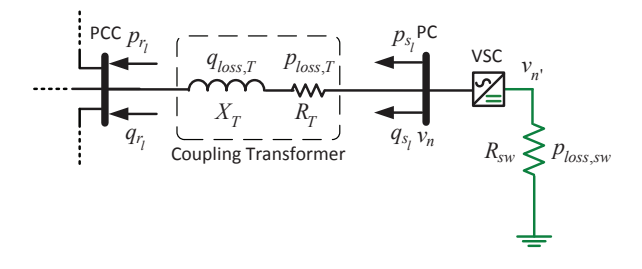


Figure 5.4: The equivalent circuit of STATCOM

The coupling transformer between the VSC in STATCOM and connecting point to the network can be modeled as an AC line (See Fig. 5.4). Similar as the MTDC model, l_{PC} is defined as the coupling transformer line from the PC bus to the PCC bus. The STATCOM can be modeled using the following set of equations.

$$q_{r_l} = q_{s_l} - q_{loss,T}, \ \forall l \in l_{PC}$$

$$(5.2a)$$

$$p_{r_l} = p_{s_l} - p_{loss,T}, \ \forall l \in l_{PC}$$

$$(5.2b)$$

$$v_{s_l}^2 - v_{r_l}^2 = 2R_T p_{s_l} + 2X_T q_{s_l} - R_T p_{loss,T} - X_T q_{loss,T}, \ \forall l \in l_{PC}$$
 (5.2c)

The losses of STATCOM are modeled by:

$$q_{loss,T} = \frac{p_{s_l}^2 + q_{s_l}^2}{v_{s_l}^2} X_T, \ \forall l \in l_{PC}$$
 (5.2d)

$$p_{loss,T} = \frac{p_{s_l}^2 + q_{s_l}^2}{v_{s_l}^2} R_T, \ \forall l \in l_{PC}$$
 (5.2e)

A shunt resistor in the DC side of the converter is used to model the switching losses. The DC side voltage of STATCOM is related to the AC side voltage as follows:

$$v_n = \frac{v_{n'}}{2\sqrt{2}} m_{n,n'}, \ \forall n \in n_{PC}, \forall n' \in n_{DC}$$

$$(5.2f)$$

The switching losses are calculated by:

$$p_{loss,sw} = \frac{v_{n'}^2}{R_{sw}}, \ \forall n' \in n_{DC}$$
 (5.2g)

SVC

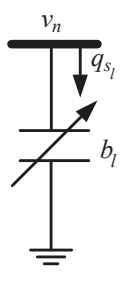


Figure 5.5: The equivalent circuit of SVC

The equivalent circuit of SVC is shown in Fig. 5.5. We define l_{SVC} as the set of SVC line (from the SVC device to the connected AC bus). The SVC is modeled as a variable susceptance with upper and lower bounds B_l^{Max} , B_l^{Min} [115]. Accordingly, the SVC constraints are:

$$q_{s_l} = -b_l v_{s_l}^2, \ \forall l \in l_{SVC}$$

$$B_l^{Min} \le b_l \le B_l^{Max}, \ \forall l \in l_{SVC}$$

$$(5.2h)$$

$$B_l^{Min} \le b_l \le B_l^{Max}, \ \forall l \in l_{SVC}$$
 (5.2i)

5.3 Convexification and Approximation

The convexification and approximation of the hybrid AC-DC network and FACTS models are derived in this Section. The convexification is based on second-order cone programming. The approximation is based on small voltage phase angle difference assumption and voltage magnitude assumption for power transmission network.

5.3.1 Formulation

We define a new variable $V_n = v_n^2$ for both AC and DC bus voltage magnitudes to linearize some constraints related with the voltage. Accordingly, $V_{s_l} = v_{s_l}^2, V_{r_l} = v_{r_l}^2$. The voltage solutions can be recovered by $v_n = \sqrt{V_n}$ from the solutions of V_n . Note we do not include $V_n = v_i^2, V_{s_l} = v_{s_l}^2, V_{r_l} = v_{r_l}^2$ in the model in order to avoid nonconvexity. As long as the voltage solutions can be recovered finally, it is not necessary to include these constraints in the model. Using V_n, V_{s_l}, V_{r_l} , constraints (5.1c) and (5.1e) are rewritten as:

$$V_{s_l} - V_{r_l} = 2p_{s_l}R_l - p_{loss_l}R_l, \forall l \in l_{DCmono}$$

$$(5.3a)$$

$$V_{s_l} - V_{r_l} = p_{s_l} R_l - p_{loss_l} R_l, \forall l \in l_{DCbi}$$

$$(5.3b)$$

Constraints (5.2c) can be rewritten as:

$$V_{s_l} - V_{r_l} = 2R_T p_{s_l} + 2X_T q_{s_l} - R_T p_{loss,T} - X_T q_{loss,T}, \forall l \in l_{PC}$$
 (5.3c)

Constraints (5.1g) and (5.2g) are rewritten as:

$$p_{loss,Csh} = \frac{V_n}{R_{Csh}}, \ \forall n \in n_{DC}$$
 (5.3d)

$$p_{loss,sw} = \frac{V_n}{R_{sw}}, \ \forall n \in n_{DC}$$
 (5.3e)

Also constraints (5.2h)-(5.2i) can be rewritten as:

$$-B_l^{Max}V_{s_l} \le q_{s_l} \le -B_l^{Min}V_{s_l}, \ \forall l \in l_{SVC}$$

$$(5.3f)$$

Squaring both sides of (5.1f) and (5.2f) and using $V_n = v_n^2$ give us:

$$V_n = \frac{V_{n'}}{8} m_{n,n'}^2, \ \forall n \in n_{PC}, \forall n' \in n_{DC}$$

$$(5.3g)$$

Considering:

$$M_{n,n'}^{Min} \le m_{n,n'}^2 \le M_{n,n'}^{Max}$$
 (5.3h)

One can obtain the following linear constraint equivalent with (5.3g)-(5.3h):

90

$$\frac{8V_n}{M_{n,n'}^{Max}} \le V_{n'} \le \frac{8V_n}{M_{n,n'}^{Min}}, \ \forall n \in n_{PC}, \forall n' \in n_{DC}$$

$$\tag{5.3i}$$

The last step is to handle the nonlinear constraints associated with power loss. First we obtain a linear relation between active power and reactive power loss:

$$p_{loss_l} X_l = q_{loss_l} R_l, \ \forall l \in l_{AC} \tag{5.3j}$$

We replace all equalities in the form of (2.1d), (5.1b), (5.1d) and (5.2d) with the following inequalities:

$$q_{loss_{l}}^{Max} \ge q_{loss_{l}} \ge \frac{p_{s_{l}}^{2} + q_{s_{l}}^{2}}{V_{s_{l}}} X_{l}, \ \forall l \in l_{AC}$$
 (5.3k)

$$p_{loss_l}^{Max} \ge p_{loss_l} \ge \frac{p_{s_l}^2}{V_{s_l}} R_l, \ \forall l \in l_{DCmono}$$
 (5.31)

$$p_{loss_l}^{Max} \ge p_{loss_l} \ge \frac{p_{s_l}^2}{4V_{s_l}} R_l, \ \forall l \in l_{DCbi}$$

$$(5.3m)$$

Where $q_{loss_l}^{Max}$ is the upper bound of reactive power loss for AC line. $p_{loss_l}^{Max}$ is the upper bound of active power loss. These bounds are security constraints. These inequalities are now in the form of rotated second-order cone [116,117] which is convex. Using the approximation $W_{s_l} \approx 1$, If K_l is the squared operation capacity of line l, $q_{loss_l}^{Max}$, $p_{loss_l}^{Max}$ are determined by:

$$q_{loss_l}^{Max} = \frac{K_l}{V_{s_l}} X_l \approx K_l X_l, \ \forall l \in l_{AC}$$
(5.3n)

$$p_{loss_l}^{Max} = \frac{K_l}{V_{s_l}} R_l \approx K_l R_l, \ \forall l \in l_{DCmono}$$
 (5.30)

$$p_{loss_l}^{Max} = \frac{K_l}{4V_{s_l}} R_l \approx \frac{K_l}{4} R_l, \ \forall l \in l_{DCbi}$$
 (5.3p)

At this stage, all constraints derived for the hybrid AC-DC network, and FACTS devices are either linear or conic constraints. With this formulation the power flow constraints has been convexified. We denote this convex ACOPF model as SOC-ACOPF.

5.4 Wind Power Scenario Generation

In this Section we propose a methodology to generate wind power scenarios based on on-site measurements of wind speed and two different wind turbine models. The proposed methodology is capable of generating scenarios for multiple wind farms, possibly owned by different companies, with any number of wind turbines. The flow chart of the wind power scenario generation methodology is illustrated by Fig. 5.6. The

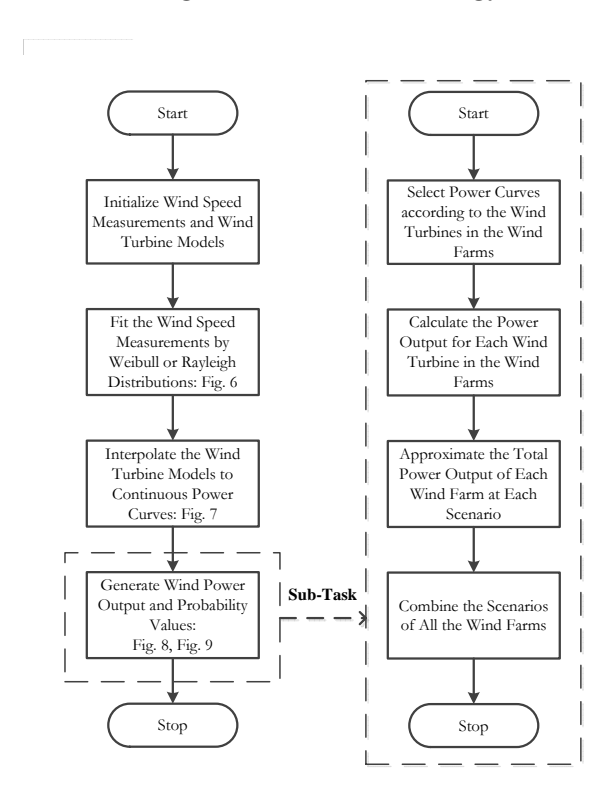


Figure 5.6: Flow chart of the wind power scenario generation methodology

first step of our wind power scenario generation methodology consists of adequately modeling the probability distribution of wind speed measurements. Both Weibull and Rayleigh distributions can be used to fit wind speed measurements data. In this Chapter, we use the wind speed measurements from Näsudden in Sweden and fit one Weibull and one Rayleigh distribution $\pi(U)$ to the measurements data. Note that U represents wind speed. The wind speed measurements and fitted distributions are demonstrated in Fig. 5.7. In the second step of our methodology we obtain the power output of wind turbines depending on the wind speed. In particular, we consider two different wind turbine models: the VESTAS-V90/3.0 [118] and the MERVENTO-3.6/118 [119]. For both wind turbine models there exist available power curve data sheets that link wind speed to power output at discrete given wind speeds. In order to generalize this information to be able to handle any value U of possible wind speeds, we interpolate these between the existing points, which yield continuous curves f(U)

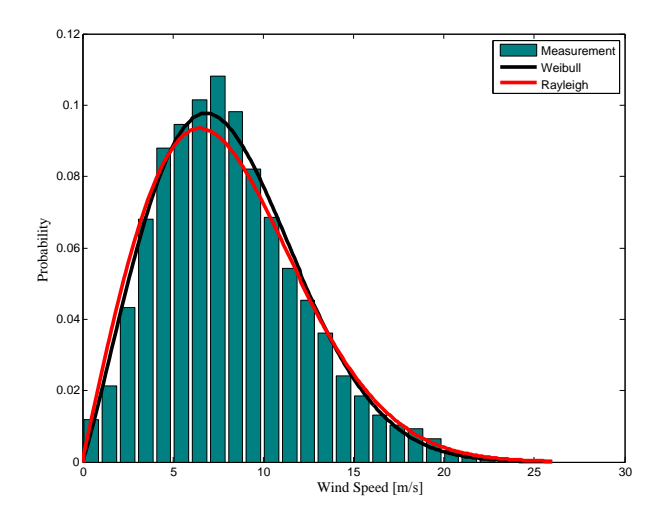


Figure 5.7: Weibull and Rayleigh distributions of wind speed measurement

that relate wind speed U to power output P. These curves are shown in Fig. 5.8. And more generally, with t being the index for wind turbines and j representing the scenario $P(t,j) = f(U_{t,j})$. Third, we want to obtain the probability of each wind

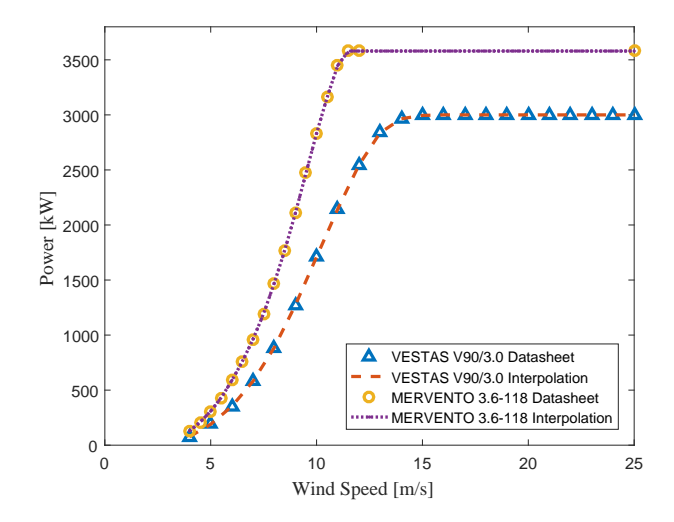


Figure 5.8: Power curves of two wind turbine models

power scenario, but in order to do so let us briefly discuss the notation. We consider different wind farms $e \in E$. Let $t \in e$ represent the wind turbines that belong to wind farm e. We assume the most general case i.e. wind farms are independent of each other. This could be interpreted as each wind farm is owned by an individual company. If the wind farms were all owned by the same company our methodology

still holds, however, the case would be less complex. Each wind farm (or company) e considers a certain set of wind power scenarios $j_e \in J_e$. Therefore, the total number of scenarios that has to be considered is the combination of all the wind power scenarios of all the independent wind farms (companies), i.e., the cardinality of J: $card(J) = \prod_e card(J_e)$. As an example, consider that we have four wind farms, and each of them considers three different power output scenarios. Then, the total number of different scenarios/combinations j of the power output of all wind farms is $3^4 = 81(j = 1, 2, ..., 81$ in this case), as shown in Fig. 5.9. Scenario j = 1 corresponds to the case where each wind farm considers its first power output scenario. In scenario j = 2 the first three wind farms consider their first power output scenario, and the last wind farm considers its second power output scenario, etc. In the following equation let $j_e(j)$ be the power output scenario of wind farm e that corresponds to combination/scenario j. Then the probability π_j of each scenario can be calculated as (5.4). The probabilities of the example of 81 scenarios are given in Fig. 5.10.

$$\pi_j = \prod_e \frac{\sum_{t \in e} \pi(U_{t, j_{e(j)}})}{\sum_{t \in e, j_e \in J_e} \pi(U_{t, j_{e(j)}})}$$
(5.4)

Note that wind speed U_{t,j_e} is generated from the fitted distributions in the first

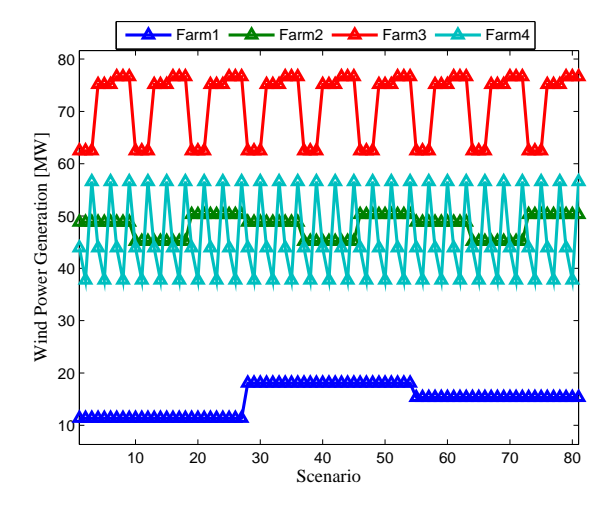


Figure 5.9: Power output of 81 wind power scenarios

step of the methodology. Then $P(t, j_e)$ is calculated according to the power output curves in the second step of the methodology. The probabilities of each scenario are calculated in the third step of the methodology. Finally, we assume that wake effects and turbulence losses of all wind farms are 15%, which yields the total maximum wind power generation of each wind farm e in scenario j as $0.85 \sum_{t \in e} P(t, j_e)$, which is the

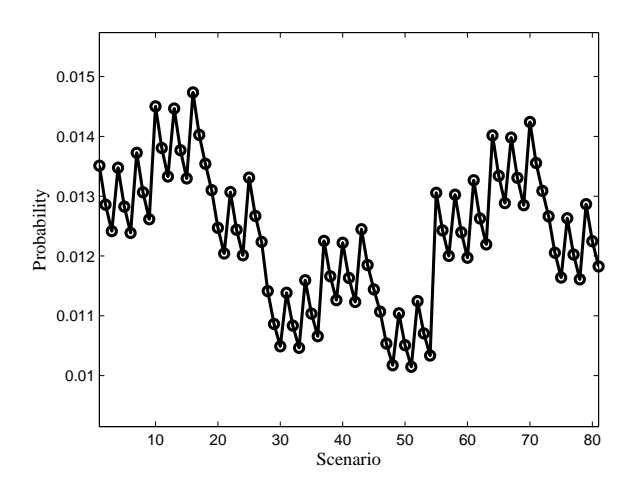


Figure 5.10: Probability values of 81 wind power scenarios

parameter $p_{e_{i,j}}^{Max}$ (maximum active power generation from wind farms) used in model (5.5a)-(5.5u). The parameter $q_{e_{i,j}}^{Max}$ (maximum reactive power generation from wind farms) in model (5.5a)-(5.5u) is generated by specifying the range of power factors of the wind farms (linear relationship between $q_{e_{i,j}}^{Max}$ and $p_{e_{i,j}}^{Max}$ is settled by the wind farms).

Finally, it is important to point out that when the number of wind farms increases, the combined wind power scenarios will increase exponentially. To deal with this challenge, we propose the M-BDA and parallel computation technique explained in Section VI.

5.5 Stochastic SOC-ACOPF Model

We formulate the problem of optimal operation of VSC-MTDC system and FACTS as a two stage stochastic programming problem in (5.5a)-(5.5u). We assume the wind power forecast is scenario-based which is a widely used approach to consider uncertainties. The objective is to minimize the expected dispatch cost $\sum_{n \in n_{AC}} C(p_n) + \sum_{j \in J, e \in E} \pi_j C_{e,j}(p_{e_{n,j}})$ in which $\sum_{i \in i_{AC}} C(p_n)$ is the dispatch cost of thermal generators and $\sum_{j \in J, e \in E, n \in n_{AC}} \pi_j C_{e,j}(p_{e_{n,j}})$ is the expected dispatch cost of all wind farms (generally all thermal generators and wind turbines are connected to AC buses). The dispatch decisions include the power generations from both thermal generators and wind farms. The first-stage decision is to dispatch the active power generations of thermal generators $\Omega_1 = \{p_n\} \in \Re$. The solution of Ω_1 is feasible for all wind power scenarios. This is because thermal generators are dispatched before the realization of

wind power. Because the reactive power generations $q_{n,j}$ of thermal generators can be adjusted fast according to each scenario, these variables are considered as the secondstage variables. The wind power generations $p_{e_{n,j}}, q_{e_{i,j}}$ (active and reactive power), operation points of VSC-MTDC system and FACTS constitute the set of second-stage decision variables as $\Omega_2 = \{q_{n,j}, q_{e_{n,j}}, q_{e_{n,j}}, p_{s_{l,j}}, q_{s_{l,j}}, \forall l \in l_{VSC} \cup l_{PC} \cup l_{SVC}\} \in \Re.$ Where $e \in E$ is the index of wind farms, J is the set of wind power generation scenarios. The set Ω_2 is solved according to each wind power scenario j with probability π_j . It is worth to mention that since we have also considered the operational cost $C_{e,j}$ of the wind farms, not all wind power $p_{e_{n,j}}^{Max}$ are dispatched in the final decisions made by the operator. The amount of dispatched wind power is constrained by network conditions represented by (5.5b)-(5.5u). Note that the wind farms are connected to the power network through the VSC-MTDC system. The power balance constraints (5.5b)-(5.5c) are also valid for these connections. Because the transmission line power flow variables $p_{s_{l,i}}, q_{s_{l,i}}$ are also scenario-based, the feasibility of power balance constraints (5.5b)-(5.5c) can be guaranteed though the first-stage decision variables p_i are fixed for all the wind power scenarios.

$$\underset{\Omega = \Omega_1 \cup \Omega_2}{\text{Minimize}} \quad Cost = \sum_{n \in n_{AC}} C(p_n) + \sum_{j \in J, e \in E, n \in n_{AC}} \pi_j C_{e,j}(p_{e_{n,j}})$$

$$(5.5a)$$

subject to

$$p_n + p_{e_{n,j}} - p_{d_n} = \sum_{l \in I_{AC}} (A_{nl}^+ p_{s_{l,j}} - A_{nl}^- p_{loss_{l,j}}) + G_n V_{n,j}, \, \forall n \in n_{AC}, j \in J$$
 (5.5b)

$$q_{n,j} + q_{e_{n,j}} - q_{d_n} = \sum_{l \in I_{AC}} (A_{nl}^+ q_{s_{l,j}} - A_{nl}^- q_{loss_{l,j}}) - B_n V_{n,j}, \, \forall n \in n_{AC}, j \in J$$
 (5.5c)

$$q_{loss_{l}}^{Max} \ge q_{loss_{l},j} \ge \frac{p_{s_{l},j}^{2} + q_{s_{l},j}^{2}}{W_{s_{l},j}} X_{l}, \ \forall l \in l_{AC}, j \in J$$
(5.5d)

$$p_{loss_{l,j}}X_l = q_{loss_{l,j}}R_l, \ \forall l \in l_{AC}, j \in J$$

$$(5.5e)$$

$$V_{s_{l,j}} - V_{r_{l,j}} = 2R_l p_{s_{l,j}} + 2X_l q_{s_{l,j}} - R_l p_{loss_{l,j}} - X_l q_{loss_{l,j}}, \forall l \in l_{AC}, j \in J$$
 (5.5f)

$$\theta_{l,j} = X_l p_{s_{l,j}} - R_l q_{s_{l,j}}, \, \forall l \in l_{AC}, j \in J$$
 (5.5g)

$$p_n = \sum_{l \in l_{DC}} (A_{nl}^+ p_{s_{l,j}} - A_{nl}^- p_{loss_{l,j}}) + G_n V_{n,j}, \, \forall n \in n_{DC}, j \in J$$
 (5.5h)

$$p_{loss_l}^{Max} \ge p_{loss_l,j} \ge \frac{p_{s_{l,j}}^2}{W_{s_{l,j}}} R_l, \ \forall l \in l_{DCmono}$$

$$(5.5i)$$

$$p_{loss_l}^{Max} \ge p_{loss_l,j} \ge \frac{p_{s_{l,j}}^2}{4W_{s_{l,j}}} R_l, \ \forall l \in l_{DCbi}$$

$$(5.5j)$$

$$V_{s_{l,j}} - V_{r_{l,j}} = 2p_{s_{l,j}}R_l - p_{loss_{l,j}}R_l, \forall l \in l_{DCmono}, j \in J$$
 (5.5k)

$$V_{s_{l,j}} - V_{r_{l,j}} = p_{s_{l,j}} R_l - p_{loss_{l,j}} R_l, \ \forall l \in l_{DCbi}, j \in J$$
 (5.51)

$$-B_l^{Max}V_{s_{l,j}} \le q_{s_{l,j}} \le -B_l^{Min}V_{s_{l,j}}, \ \forall l \in l_{SVC}, j \in J$$
 (5.5m)

$$p_{loss,Csh,j} = \frac{V_{n,j}}{R_{Csh}}, \forall n \in n_{DC}, j \in J$$
(5.5n)

$$p_{loss,sw,j} = \frac{V_{n,j}}{R_{sw}}, \ \forall n \in n_{DC}, j \in J$$

$$(5.50)$$

$$\frac{8V_{n,j}}{M_{n,n'}^{Max}} \le V_{n',j} \le \frac{8V_{n,j}}{M_{n,n'}^{Min}}, \ \forall n \in n_{PC}, \forall n' \in n_{DC}, j \in J$$
 (5.5p)

$$V_i^{Min} \le V_{n,j} \le V_i^{Max}, \ \forall n \in n_{AC} \cup n_{DC} \cup n_{PC}, j \in J$$
 (5.5q)

$$q_{e_{n,j}}^{Min} \le q_{e_{i,j}} \le q_{e_{n,j}}^{Max}, \ j \in J, e \in E$$
 (5.5r)

$$p_{e_{n,j}}^{Min} \le p_{e_{i,j}} \le p_{e_{n,j}}^{Max}, \ j \in J, e \in E$$
 (5.5s)

$$q_n^{Min} \le q_n \le q_n^{Max}, \ \forall n \in n_{AC} \cup n_{DC}$$
 (5.5t)

$$p_n^{Min} \le p_n \le p_n^{Max}, \ \forall n \in n_{AC} \cup n_{DC}$$
 (5.5u)

Parameters π_j , $p_{e_{n,j}}^{Max}$, $p_{e_{n,j}}^{Min}$, $q_{e_{n,j}}^{Max}$, $q_{e_{n,j}}^{Min}$ are generated in the wind power scenario generation methodology explained in Section IV. The optimization problem (5.5a)-(5.5u) minimizes the expected power generation cost considering the uncertainties of wind power. If we use convex (generally quadratic) cost function for Cost, because both the objective and constraints are convex, this minimization problem is convex. This is further validated by the numerical results in Section VII of this Chapter through using MOSEK solver in GAMS which can only solve convex problem. Hence, the global optimal solutions can be obtained by solving (5.5a)-(5.5u). The challenge is, when large number of wind scenarios are considered, the scale of the optimization problem (5.5a)-(5.5u) can exceed the capability of solvers. We explain in the next Section of this Chapter how to deal with this challenge by decomposition.

5.6 Decomposition of Stochastic SOC-ACOPF

If we assume the OPF problem is feasible (at least one solution exists), then strong duality holds for the formulated SOC-ACOPF model. Thus Benders decomposition is applicable here to solve the large-scale stochastic SOC-ACOPF problem in a decomposed way. In Benders decomposition, the original large-scale optimization problem is decomposed into a master problem and several subproblems. The objective solution of the master problem gives the lower bound of the original optimization problem (we consider minimization problem here). The subproblems can give upper bound of the objective in the original minimization problem. With the proceed of the iterations, the lower bound and upper bound given by the master problem and subproblems gradually

converge. The challenges are how to formulate the master problem and subproblems in the decomposition and how to accelerate the iterations. These challenges are addressed in this Section. Taking the first-stage decision variables $\Omega_1 = \{p_n\} \in \Re$ as the complicating variables in Benders decomposition, we can decompose the stochastic SOC-ACOPF (5.5a)-(5.5u). The master problem of the proposed M-BDA is formulated as:

$$\underset{\Omega_1}{\text{Minimize}} \quad Cost = \sum_{n \in n_{AC}} C(p_n) + Cost_w$$
 (5.6a)

subject to (5.5u)

$$Cost_w \ge Cost_{w,k} + \sum_{n \in n_{AC}} \mu_{n,k}^p(p_n - \hat{p}_{n,k}), \ \forall k \in K$$
 (5.6b)

Where $\hat{p}_{n,k}$ is the dispatched active power (first-stage decision) at iteration k. Constraint (5.6b) is the Benders cut which expands iteratively in order to take more information from the subproblem into account. $Cost_{w,k} = \sum_{n} Cost_{w}^{n}$ is the sum of objective solutions in the subproblems at iteration k. $Cost_{w}^{n}$ is the objective of subproblem n (the expected cost of wind power generations). $\mu_{n,k}^{p}$ is the dual variable solution of equation (5.7b) at iteration k (equal to zero in the first iteration) in the subproblem. The subproblem of the proposed M-BDA is:

$$\underset{\Omega_2}{\text{Minimize}} \quad Cost_w^n = \sum_{j \in j_n, e \in E, n \in n_{AC}} \pi_j C_{e,j}(p_{e_{n,j}})$$
 (5.7a)

subject to
$$(5.5b) - (5.5t)$$

$$p_n = \hat{p}_{n,k} : \mu_{n,k}^p, \ \forall k \in K$$

$$(5.7b)$$

Where $\bigcup_{n}^{T} j_{n} = J$ is a division of the wind power scenario set J. $N = \sum n$ is the total number of threads settled in the parallel computation. The scenarios assigned to subproblem n are included in the set j_{n} . To guarantee the feasibility of all the subproblems in M-BDA, we allow load shedding for all the buses in the network. We set the cost parameters of load shedding much larger than the most expensive generators in the network. Although some loads may not be fully met at the beginning of the iterations, the final solutions of M-BDA cover all these loads (because the cost is too expensive and will be iteratively met by generations in the original network). Our simulations show that this method is more efficient to guarantee the feasibility of the subproblems than using the method of the original feasibility cut in Benders decomposition (the MOSEK solver can not converge after several hours when using the original feasibility cut approach).

As the iterations proceed, more Benders cuts are iteratively included into the master problem. After solving the master problem (5.6), all subproblems can be

computed in parallel. The proposed parallel computation structure of stochastic SOC-ACOPF using the proposed M-BDA is illustrated in Fig. 5.11. The Master problem is responsible to give solutions of the first-stage decision variable $\Omega_1 = \{p_n\} \in \Re$ while subproblems yield solutions of the second-stage decision variable $\Omega_2 = \{q_{n,j}, p_{e_{n,j}}, q_{e_{n,j}}, p_{s_{l,j}}, q_{s_{l,j}}, \forall l \in l_{VSC} \cup l_{PC} \cup l_{SVC}\} \in \Re$. There is no communication requirement between the subproblems.

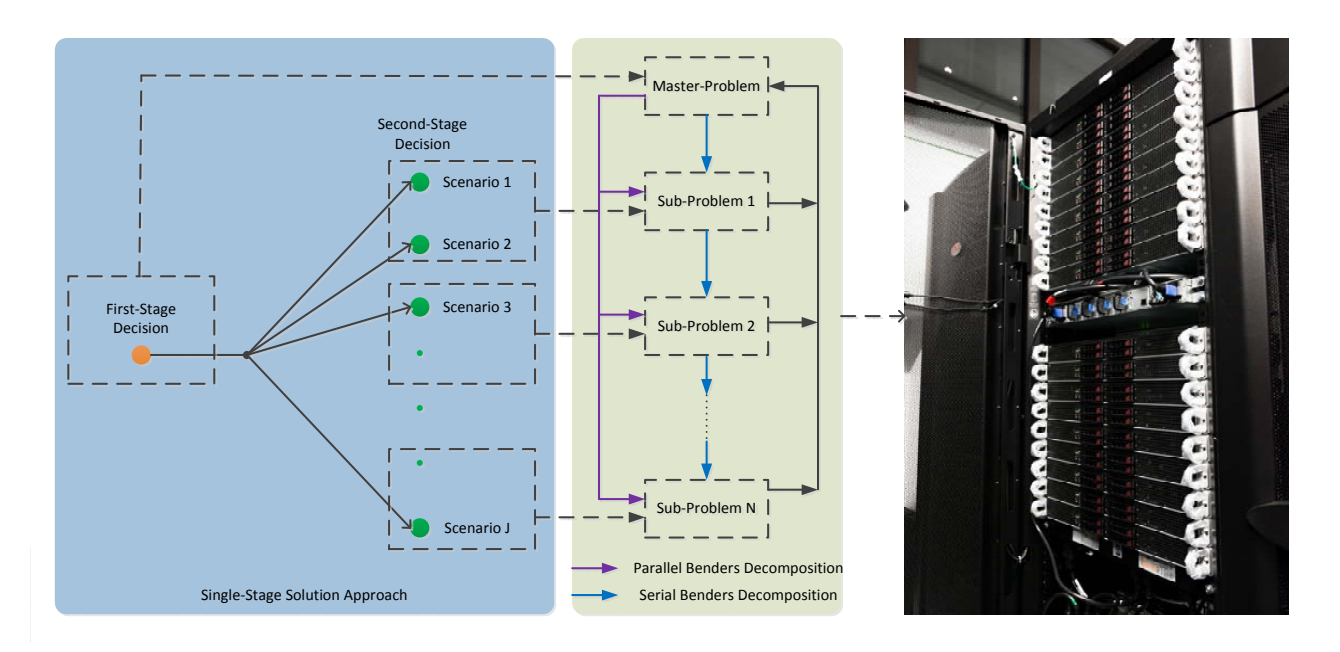


Figure 5.11: Solution approaches of the stochastic SOC-ACOPF model

5.7 Numerical Results

5.7.1 Solving Stochastic SOC-ACOPF by M-BDA and Parallel Computation

The test case network configuration is shown in Fig. 5.12. Two wind farms are connected to the IEEE30-bus network through a five-terminal VSC-MTDC system (D1-D5). The VSC-MTDC system is connected to bus 1, bus 15 and bus 30 in the IEEE30-bus network. There are twenty VESTAS-V90/3.0 wind turbines in the first wind farm and thirty MERVENTO-3.6/118 wind turbines in the second wind farm. Two STATCOM devices (located at bus 4 and bus 18) and two SVC devices (located at bus 14 and bus 21) are connected in the AC network. The proposed wind power

scenario generation methodology is implemented in MATLAB. The stochastic SOC-ACOPF model and M-BDA are coded in GAMS and solved by MOSEK [54]. The test cases with 10, 100 and 1000 wind power scenarios are run on a computer with Intel i7-2760QM 2.4 GHz CPU and 8 GB of RAM. Simulations of the 10000 wind power scenarios test case are performed at PDC Center for High Performance Computing (PDC-HPC) in KTH Royal Institute of Technology. The deployed computation node at PDC-HPC has 48 CPU cores (3.00 GHz Intel Xeon Processor E7-8857) and 1 TB of RAM in total. In order to compare the performance of different solution approaches,

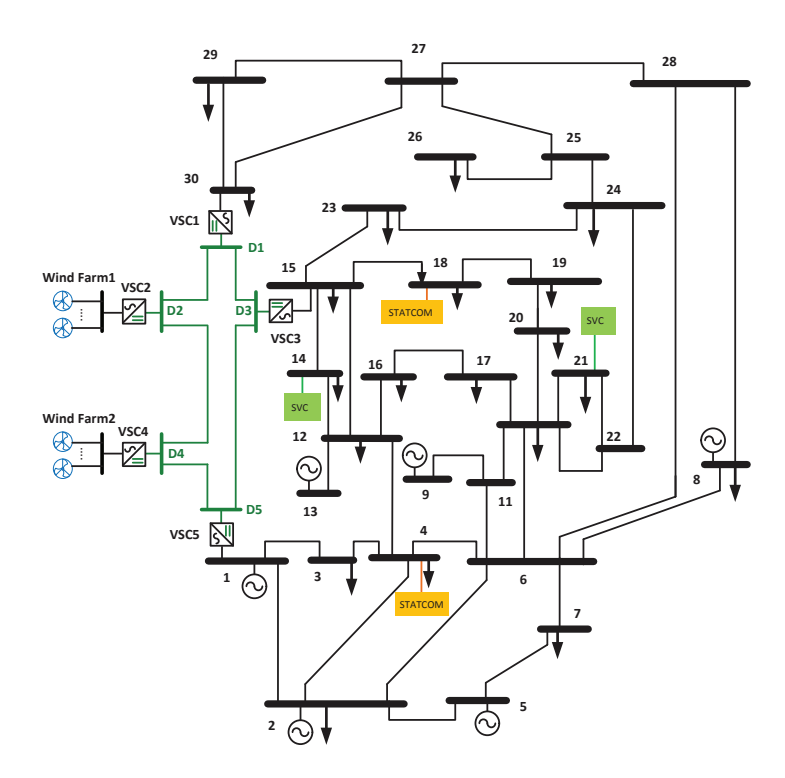


Figure 5.12: The IEEE30-bus network with two wind farms integrated by VSC-MTDC system

following solution approaches are defined:

1. **Single-Stage** solution approach. The stochastic programming for all wind power scenarios are formulated and solved as one single stochastic optimization problem. This approach is set as the benchmark to compare with the proposed M-BDA approach.

- Parallel M-BDA solution approach. The subproblems in M-BDA are solved in parallel during each iteration. This approach is proposed to improve the computational efficiency when large number of wind power scenarios are considered.
- 3. **Serial M-BDA** solution approach. The subproblems in M-BDA are solved in serial during each iteration. This solution approach is to demonstrate the efficiency of the proposed parallel computation structure in GAMS.

The proposed M-BDA stops when the upper bound and lower bound of the objective is within 2%. The solution approaches are illustrated in Fig. 5.11. In Fig. 5.11, we assign two wind power scenarios to each subproblem for ease of illustration. In the computation of large number of wind power scenarios, we can assign more scenarios to each subproblem to distribute the computation burden to each thread more evenly. The numerical results of objective values are summarized in Table 5.1. We can see that solutions by M-BDA are all very close (relative error less than 2%) to the single-stage solution. The objective solutions are different for different test cases because the generated wind power scenarios (probability values and maximum power outputs) are different. When considering 10000 wind power scenarios, MOSEK cannot converge using the single-stage approach. The proposed M-BDA shows strong convergence capability and finds all the optimal solutions.

We list the CPU computation time for the single-stage and M-BDA approaches in Table 5.2. For the test cases of 10, 100 and 1000 scenarios, we set 4 threads for the parallel computation. 30 threads are set for the parallel computation of 10000 scenarios test case. In all test cases, parallel M-BDA is faster than the serial execution. In the test case of 10000 scenarios, parallel computation outperform the single-stage approach in terms of both computation speed and convergence capability. The single-stage approach cannot converge within 184.27 seconds. Even though for small numerical examples the single-stage solution approach is faster than M-BDA, it is important to point out that for large-scale cases, the single-stage optimization problem did not converge due to the curse of dimensionality. The proposed M-BDA, however, found the global optimal solution faster than it took MOSEK to determine that if there is a convergence problem. Therefore, our solution approach is useful for large-scale computation. It is worth to mention that even though we use a small network in which there are 30 buses, the total number of wind power scenarios that we have considered here show that the scale of the stochastic SOC-ACOPF model is very large. This is demonstrated by the total number of constraints of each test case in Table 5.2. Note that the total number of constraints in Table 5.2 refers to the coded model in GAMS which, in general, has more constraints than the mathematical model represented in (5.5a)-(5.5u).

The convergence of the proposed M-BDA is shown in Fig. 5.13. When the number of wind power scenarios increases, the required number of iterations of M-BDA also

M-BDA No. of Scenarios Single-Stage[\$] No. of Threads Upper Bound[\$] Lower Bound[\$] 10 320.26 319.69 $\overline{4}$ 325.01 100 320.06 4 324.33 319.87 1000 380.65 382.77 380.46 4 10000 NA 30 378.55 371.67

Table 5.1: Objective value

Table 5.2: Computation time

No. of Scenarios	No. of Constraints	Single-Stage [s]	M-BDA [s]		
		Single-Stage [s]	Serial	Parallel	
10	450	0.23	1.94	0.59	
100	4500	1.72	11.12	3.86	
1000	45000	28.74	296.98	70.87	
10000	450000	184.27	6191.58	116.34	

increases. The efficiency of the proposed M-BDA can be observed in that even in the case of 10000 scenarios, the M-BDA converges within 13 iterations.

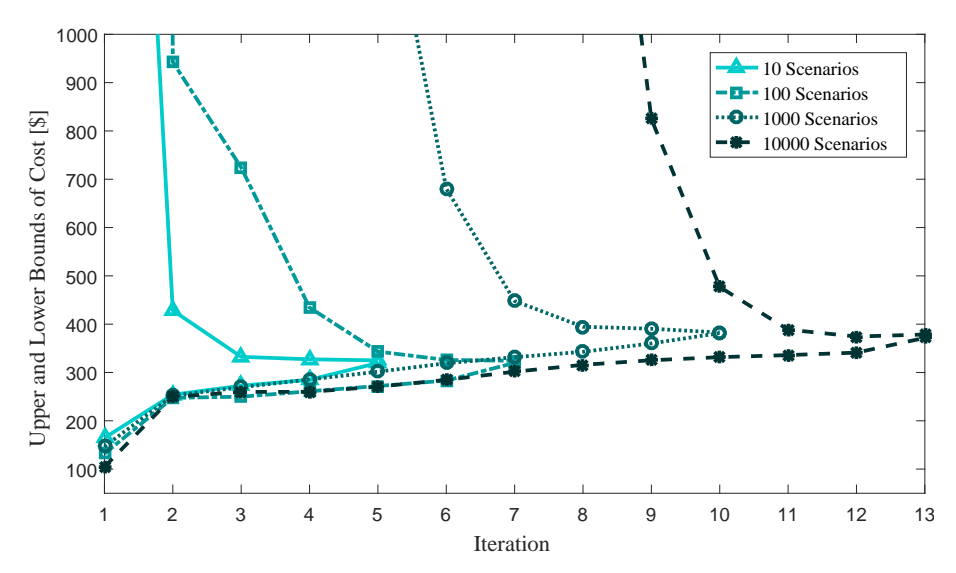


Figure 5.13: The convergence of M-BDA

To show the benefits of the stochastic programming, we calculate the Value of

Stochastic Solution (VSS) according to [120] as:

$$VSS = Cost^{D*} - Cost^{S*}$$
 (5.8a)

Where $Cost^{D*}$ is the objective value of deterministic solution, $Cost^{S*}$ is the objective value of stochastic solution. VSS is a measure of the benefits to model the uncertain power outputs of wind farms as scenario-based variables instead of using the expected values. $Cost^{D*}$ is obtained by firstly replacing the wind power maximum generation parameters $p_{e_{n,j}}^{Max}$, $q_{e_{n,j}}^{Max}$ with the expected values:

$$p_{e_{n,j_0}}^{Max} = \sum_{j} \pi_j p_{e_{n,j}}^{Max}$$
 (5.8b)

$$q_{e_{n,j_0}}^{Max} = \sum_{j} \pi_j q_{e_{n,j}}^{Max} \tag{5.8c}$$

Then we solve the model (5.5a)-(5.5u) (in this way there is only one scenario $j = j_0$ in the model) to find the deterministic solution of the first-stage decision variables p_n^{D*} . After obtaining p_n^{D*} , we fix the first-stage decision variables as:

$$p_n = p_n^{D*} \tag{5.8d}$$

Afterwards, we solve the stochastic model (5.5a)-(5.5u) again to find $Cost^{D*}$. Note, in this step, the second-stage parameters $p_{e_{n,j}}^{Max}, q_{e_{n,j}}^{Max}$ are not fixed as expressed in (5.8b)-(5.8c) and any number of wind power scenarios are allowed.

The results of VSS are listed in Table 5.3. Significant benefits of stochastic programming are observed when large number of wind power scenarios are considered. The reason for large value of VSS in cases having large number of wind power scenarios is because the value of lost load (VoLL) parameter is large in our test cases. These results show that, when large number of wind power scenarios are considered, it is very hard to find the deterministic solution $Cost^{D*}$ without load shedding. As a comparison, the stochastic programming approach can always find the optimal solutions efficiently.

	Solution		
No. of Scenarios	Deterministic	Stochastic	VSS [\$]
10	478.71	320.26	158.45
100	532.77	320.06	212.71
1000	9924.11	380.65	9543.46
10000	65960.41	378.55	65581.86

Table 5.3: Value of stochastic solution (VSS)

5.8 Conclusions

We propose a stochastic SOC-ACOPF model to optimally operate the power network incorporating VSC-MTDC system and FACTS devices in the context of scenario-based forecast of wind power. Both mono-polar and bipolar MTDC connections are modeled. STATCOM and SVC as FACTS devices are integrated in a unified modelling approach in the proposed SOC-ACOPF model. The SOC-ACOPF is a convex optimization problem which can be solved efficiently to global optimality. Using the wind speed measurements and the wind turbine models, we are able to generate representative power generation scenarios from multiple wind farms. Finally, we propose to use M-BDA to address the computational challenge of large-scale power system operations. When 10000 wind scenarios are considered, a single-stage stochastic SOC-ACOPF model is not tractable even by high performance computing. As a comparison, the proposed parallel computation in GAMS based on M-BDA is capable of solving the stochastic SOC-ACOPF model and accelerating the computations. Large values of VSS show the significant benefits of using stochastic SOC-ACOPF when large number of wind power scenarios are considered. The results of this Chapter demonstrate the great potential of stochastic conic programming, high performance computing and M-BDA in dealing with the severe challenge of integrating large-scale wind power which is inevitable in the future of power system.

Chapter 6

Coordinated Energy Dispatch for Super Grid

6.1 Introduction

Recent years have witnessed the promising development of super grid worldwide. In Europe, the e-Highway2050 project has been implemented to identify weak power transmission lines and resolve these constraints for future decarbonized economy [42]. Reference [41] finds that 228,000km of new lines are required to be cost-optimally built for the European power network before 2050. Around €200 billion investment for updating the European transmission infrastructure is expected to be in place up to the year of 2020 [39]. China is planning to install 13 to 20 extra 800kV to 1300kV HVDC lines from 2014 onwards to transmit approximately 1300GW of solar, wind and hydro-power generation to the southeast population centers [40]. It is estimated by the international energy agency (IEA) that the total investment of China on updating the transmission network reaches more than \$4 trillion by the year of 2040 [40]. Using unit commitment model, the impact analysis of inter-regional transmission power network expansion in China by authors in [121] show that large economic benefits can be achieved.

To optimally operate an ultra-large-scale super grid is challenging in many aspects. Though more flexible control can be gained through the deployment of FACTS, phase-shifting transformers (PSTs) and VSC-MTDC, the unplanned power flow is still one of the main challenges to operate the super grid [39]. By investigating the impacts of inter-regional grid transmission in China, reference [121] shows that efficient dispatch mechanism across regions accounting for generation efficiency should be established. Reference [122] proposes a decomposition-coordination algorithm to find the sub-optimal solution of the integrated electrical and heating system. The algorithm in [122] works by dividing the system into two subsystems and then iteratively adjusting the coordinated variables which are at the boundary of the electrical and heating system. The numerical results show that it requires 15 iterations to converge for a test case with 6 nodes of electrical network and 31 nodes of heating network. However, the convergence of the coordination mechanism in [122] cannot be guaranteed because of the nonconvex model. As improvements, our model used in this Chapter is convex

and the convergence is guaranteed.

The optimal operation of the power network is generally formulated as an OPF problem [123, 124]. Since the formulated OPF model of operating the super grid is a very large-scale optimization problem, distributed approaches to solve the OPF model are useful to make the problem tractable for the optimization solver. These distributed solution approaches mainly include Lagrangian relaxation [72], BD [73, 101], Dantzig-Wolfe decomposition [74] and ADMM [75] (for a comprehensive literature review of distributed or decentralized OPF solution approaches, please refer to the Introduction Section of Chapter 3).

Three main research gaps are identified from the literature review:

- 1. The coordination of energy dispatch of different nations or regions for the super grid has not been well discussed; Without an efficient coordination mechanism, it is hard to operate the super grid optimally.
- 2. The speed up of distributed solution algorithm to solve large-scale ACOPF problem is still in demand to assist real-time decision making to operate the super grid.

In this spirit, we propose in this Chapter the concept of power synergy hub (PSHub) to coordinate the energy dispatch of the super grid. We show that the mathematical foundation of energy dispatch coordination operation in PSHub is the modified BD. We propose an improved convex ACOPF model based on SOCP which is SOC-ACOPF (Model P). The proposed SOC-ACOPF model does not introduce new variables except the voltage magnitude square V_n . To obtain an equivalent linear representation of the line capacity limit (2.1h), we use the approximation $V_{s_l} \approx 1$ (per unit value). Two approximations $sin\theta_l \approx \theta_l$ and $v_{s_l}v_{r_l} \approx 1$ (per unit value) for convexifying the nonconvex constraint (2.1g) are introduced in our model. Moreover, the proposed SOC-ACOPF model is valid for both radial and mesh power networks. These are the main differences of our model compared with other SOC-ACOPF models in the literature [44,48,125]. To accelerate the coordination process in the PSHub, we propose a parallel computation structure in GAMS. The fast convergence of the energy dispatch coordination in PSHub and the proposed SOC-ACOPF model are demonstrated by numerical results for large-scale power networks up to 9241 nodes. The rest of this Chapter is organized as follows. Section II proposes the concept of PSHub. Section III formulates the modified BD as the mathematical foundation of PSHub energy dispatch coordination operations. Section IV designs the parallel computation structure in GAMS. Section V presents the numerical results and discussions. Section VI concludes the advantages of the proposed approaches in this Chapter.

6.2 Proposing the Power Synergy Hub

In this Section, we firstly show the severe challenge of operating the super grid and then propose the solution to this challenge as PSHub. An overview of the key functions of the PSHub are explained.

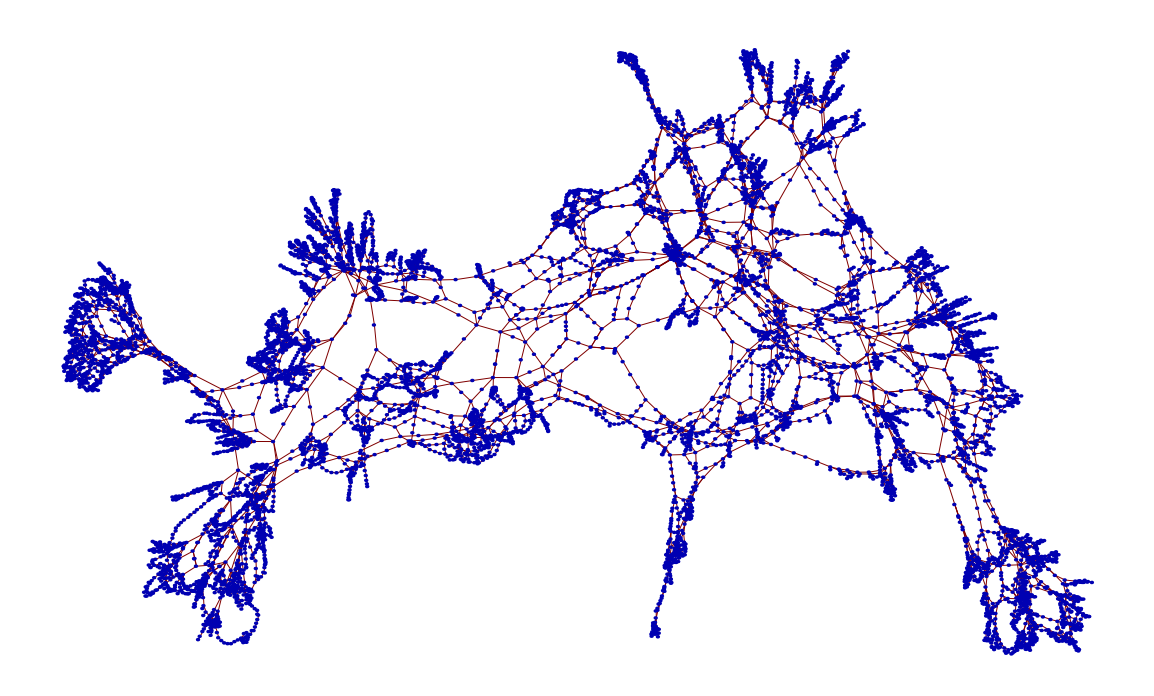


Figure 6.1: Visualizing the European super grid

To demonstrate the challenging scale of operating the super grid, we plot the network layout of the European high voltage transmission networks (750kV, 400kV, 380kV, 330kV, 220kV, 154kV, 150kV, 120kV and 110kV) in Fig. 6.1. The network data is based on the Pan European Grid Advanced Simulation and State Estimation (PEGASE) project [126]. The important metrics of the power network and the corresponding OPF model are listed in Table 6.1. It is beyond the capability of current available optimization solvers to efficiently solve one single OPF model to find the global optimal solution, not to mention the gigantic requirement of RAM capacity for the computers. For example, the LINDOGLOBAL solver which is a powerful global nonlinear programming solver in GAMS currently cannot solve optimization problems with more than 3000 variables and 2000 constraints. One practical way to deal with

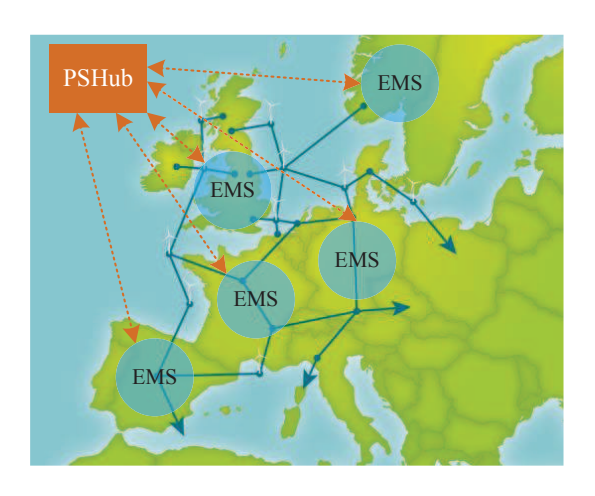


Figure 6.2: The conceptual diagram of PSHub

TD, 1, 1, C, 1	C 1 .	. C .		11		. • 1
Table 6.1:	Scale	OI O	perating	tne	super	gria

Super Grid Model	Metrics of Network Data			Metrics of OPF Model	
Super Grid Moder	Nodes	Lines	Generators	Variables	Constraints
1354pegase	1354	1991	260	11192	20393
2869pegase	2869	4582	510	25086	45590
9241pegase	9241	16049	1445	85568	155087

this challenge is to keep operating the regional power networks by current regional energy management system (EMS) centers and then coordinate the EMS in an efficient mechanism. We propose the concept of PSHub to implement the coordination mechanism of the super grid. This is illustrated in Fig. 6.2. Regional EMS represented as blue circles in Fig. 6.2 is operating the national or regional power networks. The HVDC and HVAC (represented as blue lines with arrows in Fig. 6.2) are connecting the networks of different nations or regions. While the regional EMS is operating its own power network, it is not sufficient to achieve global optimum for the super grid. It is impossible to guarantee the feasibility and security of the tie-line HVDC and HVAC connections without coordinating the operations of all the regional EMS centers. To coordinate the operations of the regional EMS centers, bi-directional communication between PSHub with regional EMS is required. The regional EMS submits information of its own network conditions to the PSHub. The PSHub then commands the operation points to each regional EMS taking the constraints of tie-line HVDC and

HVAC connections into account.

Mathematically speaking, the function of PSHub is like a global optimization algorithm which iterates the local optimal solutions obtained by the regional EMS centers and coordinates the individual EMS by determining its total power output and the power flows of the tie-lines, in order to achieve global optimality in the super grid. There are two fundamental problems to be solved by the PSHub:

- 1. What information is required to communicate from the regional EMS centers to the PSHub (represented as orange lines with arrows in Fig. 6.2)?
- 2. How to coordinate the energy dispatch of multiple regional EMS centers in order to achieve global optimal targets?

We prove in following Sections of this Chapter that the proposed modified BD is not only an efficient approach to implement the coordination mechanism in PSHub but also leads to solutions very close to the global optimal targets for the super grid. The formulated Benders cuts are the information required to be communicated from regional EMS centers to the PSHub. These constitute two main contributions of this Chapter.

6.3 Mathematical Foundation of PSHub: Modified Benders Decomposition

In this Section, we show that how modified BD can be used as the mathematical foundation of energy dispatch coordination in PSHub. In BD, the original large-scale optimization problem is decomposed to a master problem and several subproblems. The objective solution of the master problem gives the lower bound of the original optimization problem (we consider minimization problem here). The objective solutions of the subproblems can give upper bound of the objective in the original minimization problem. With the proceed of the iterations, the lower bound and upper bound given by the master problem and subproblems finally converge. The challenges are how to formulate the master problem and subproblems in the decomposition and how to accelerate the convergence. These challenges are addressed in this Section. We also propose to deal with the feasibility problem of the subproblem in the modified BD by an efficient way without using the original Benders feasibility cuts approach.

The key observation and contribution in this Chapter is that, if we take the total power generations of the regional power networks as the complicating variables in formulating the modified BD, the modified BD can serve as the mathematical foundation of the energy dispatch coordination implemented by the PSHub. The total power generations of the regional power networks are actually the operation points to be found

by the regional EMS centers. The energy dispatch of each regional power network k is a subproblem in the modified BD algorithm. The master problem of the modified BD is the energy dispatch coordination of the PSHub. The subproblem k in the modified BD is formulated in (6.1).

$$Cost_k^{EMS} = \underset{\Omega}{\text{Minimize}} \sum_{\forall n \in N_k, l \in L_k} f(p_n, q_n, p_{o_l}, q_{o_l})$$
(6.1a)

subject to
$$(2.1b) - (2.1c), (2.1j) - (2.1m), (2.2b) - (2.2e),$$

$$\forall n \in N_k, l \in L_k \tag{6.1b}$$

$$\sum_{n \in N_k} p_n = P_{k,j}^{sum} : \mu_{k,j}^P$$
 (6.1c)

$$\sum_{n \in N_k} q_n = Q_{k,j}^{sum} : \mu_{k,j}^Q$$
 (6.1d)

Where $Cost_k^{EMS}$ is the cost of energy production for regional power network k. (6.1b) refers to the power flow constraints for all lines and nodes located in regional network k. N_k and L_k are sets of the nodes and lines located in the regional power network k. $P_{k,j}^{sum}$ and $Q_{k,j}^{sum}$ are the solutions of total power generations in regional power networks from the master problem of the modified BD at iteration j. $\mu_{k,j}^P$ and $\mu_{k,j}^Q$ are dual variables for the corresponding constraints used for constructing the Benders cuts. The objective solution of the subproblem (6.1) is the upper bound of the energy dispatch for each regional EMS center.

To guarantee the feasibility of the subproblem, we have added one more generator with large capacity at each bus of the regional power networks. The marginal generation cost of the added generators is larger than the most expensive generators in the original regional power networks (note these added generators do not exist and are only used as variables in the model). In this way the final converged dispatch results do not include generations from these added generators (cheap generators are more preferred to be dispatched because we minimize the generation cost as the objective). This is another contribution of this Chapter to deal with the feasibility problems of the subproblems in the modified BD. This approach is more efficient than the traditional Benders feasibility cuts approach which cannot converge within hours in our simulations. The numerical failure of MOSEK solver [54] using the traditional Benders feasibility cut approach in solving ultra-large-scale ACOPF indicates that a modified BD should be developed. As a comparison, the proposed approach converges very fast. In this way, the power balance constraints (2.1b) and (2.1c) in (6.1b) are modified as

(6.1e) and (6.1f):

$$p_n + p_n^+ - P_{d_n} = \sum_{l \in L_k} (A_{nl}^+ p_{s_l} - A_{nl}^- p_{o_l}) + G_n V_n, \ \forall n \in N_k, l \in L_k$$
 (6.1e)

$$q_n + q_n^+ - Q_{d_n} = \sum_{l \in L_k} (A_{nl}^+ q_{s_l} - A_{nl}^- q_{o_l}) - B_n V_n, \ \forall n \in N_k, l \in L_k$$
 (6.1f)

Where p_n^+ and q_n^+ are the active power and reactive power generations from the added generators. The objective function in the subproblem (6.1) is modified as (6.1g):

$$Cost_{k,j}^{S} = \text{Minimize} \sum_{\forall n \in N_{k}, l \in L_{k}} f(p_{n}, q_{n}, p_{o_{l}}, q_{o_{l}}) + \sum_{n \in N_{k}} (C_{n}^{p+} p_{n}^{+} + C_{n}^{q+} q_{n}^{+})$$
(6.1g)

Where C_n^{p+} and C_n^{q+} are the marginal cost parameters of active power and reactive power generations from the added generators. The Benders feasibility cuts are used to remove infeasible solutions from the searching space of the solver. However, if the infeasible region of the searching space is very complex and large, using Benders feasibility cuts will be very time-consuming. This is because it is required to generate many Benders feasibility cuts in order to remove possible infeasible solutions from the searching space. Our approach to guarantee the feasibility of the subproblems can avoid detecting the feasibility procedure of BD. In this way, the computational efficiency is improved.

The lower bound of objective for energy dispatch for all the regional EMS centers is obtained by solving the master problem of the modified BD. The master problem of the modified BD is formulated in (6.2).

$$\underset{\Omega}{\text{Minimize } Cost^{PSHub}} = \sum_{k \in K} Cost_k^{EMS}$$
(6.2a)

subject to
$$(2.1b) - (2.1c), (2.1j) - (2.1m), (2.2b) - (2.2e), \forall l \in \tau$$
 (6.2b)

$$Cost_k^{EMS} \ge Cost_{k,j}^{EMS} + \mu_{k,j}^P \left(\sum_{n \in N_k} (p_n + p_n^+) - P_{k,j}^{sum} \right)$$

$$+ \mu_{k,j}^{Q} \left(\sum_{n \in N_k} (q_n + q_n^+) - Q_{k,j}^{sum} \right), \ \forall k \in K, j \in J$$
 (6.2c)

Where $Cost^{PSHub}$ refers to the total cost of energy production for the super grid. (6.2b) represents the power flow constraints of tie-lines (transmission lines connecting different EMS regions). τ is defined as the set of all tie-lines. We model each regional power network as a single virtual node in the master problem. Constraint (6.2c) includes Benders cuts from the subproblems. $\mu_{k,j}^P$ and $\mu_{k,j}^Q$ are dual variable solutions

of equations (6.1c)-(6.1d) in regional power network k (which is equal to zero at the first iteration). The master problem is responsible to give solutions of total power output of regional power networks and tie-line power flows. The subproblems are responsible to give solutions of subnetwork power flows. The master problem is always feasible because it is actually a relaxed problem of the original SOC-ACOPF model. As the iterations proceed, more Benders cuts from the regional networks are iteratively included into the master problem (this process is interpreted as the communication between PSHub and all regional EMS centers). After solving the master problem, all the subproblems can be computed in parallel which we explain in the next Section. If the original problem is convex (the proposed SOC-ACOPF model is convex), it is proved that the optimal solution can be found within finite iterations [73, 101]. The procedure of using the modified BD to operate the super grid is explained in Fig. 6.4. A graphical illustration of the relationship between the master problem and subproblems in the modified BD is plotted in Fig. 6.5. To show the difference of the modified BD with the traditional BD, we also plot the flow chart of traditional BD in Fig. 6.3. As we have mentioned, our modified BD avoids the steps of checking subproblems feasibility and generating the Benders feasibility cuts in the iterations.

6.4 Accelerating the Implementation of Modified BD by Parallel Computation

As the modified BD in PSHub is solved in an iterative way, the execution can be accelerated by parallel computation. We explain in this Section the proposed parallel computation structure in GAMS [89]. The performance of the parallel computation is validated by the numerical results in the next Section.

The proposed parallel computation structure of the energy dispatch coordination by PSHub is illustrated in Fig. 6.5. The parallel computation structure is implemented in GAMS platform and it is based on the modified BD. The parallel computation is comprised of one Parallel Loop and one Collect Loop. The Parallel Loop complies all the subproblems in the modified BD and submits each subproblem to one thread to be executed by one core of the CPU. Since the subproblems are actually the energy dispatch of regional EMS centers, we denote the threads of the subproblems in Fig. 6.5 by 'EMS-1', 'EMS-2', ..., 'EMS-k'. The Collect Loop repeatedly checks the solution status of each thread and then saves the solutions as long as the solutions are available. The threads of solved subproblems are released in order to avoid over using the computer disk capacity. Because there is no communication requirement among the subproblems, the capability of multi-CPU computers can be utilized to the most.

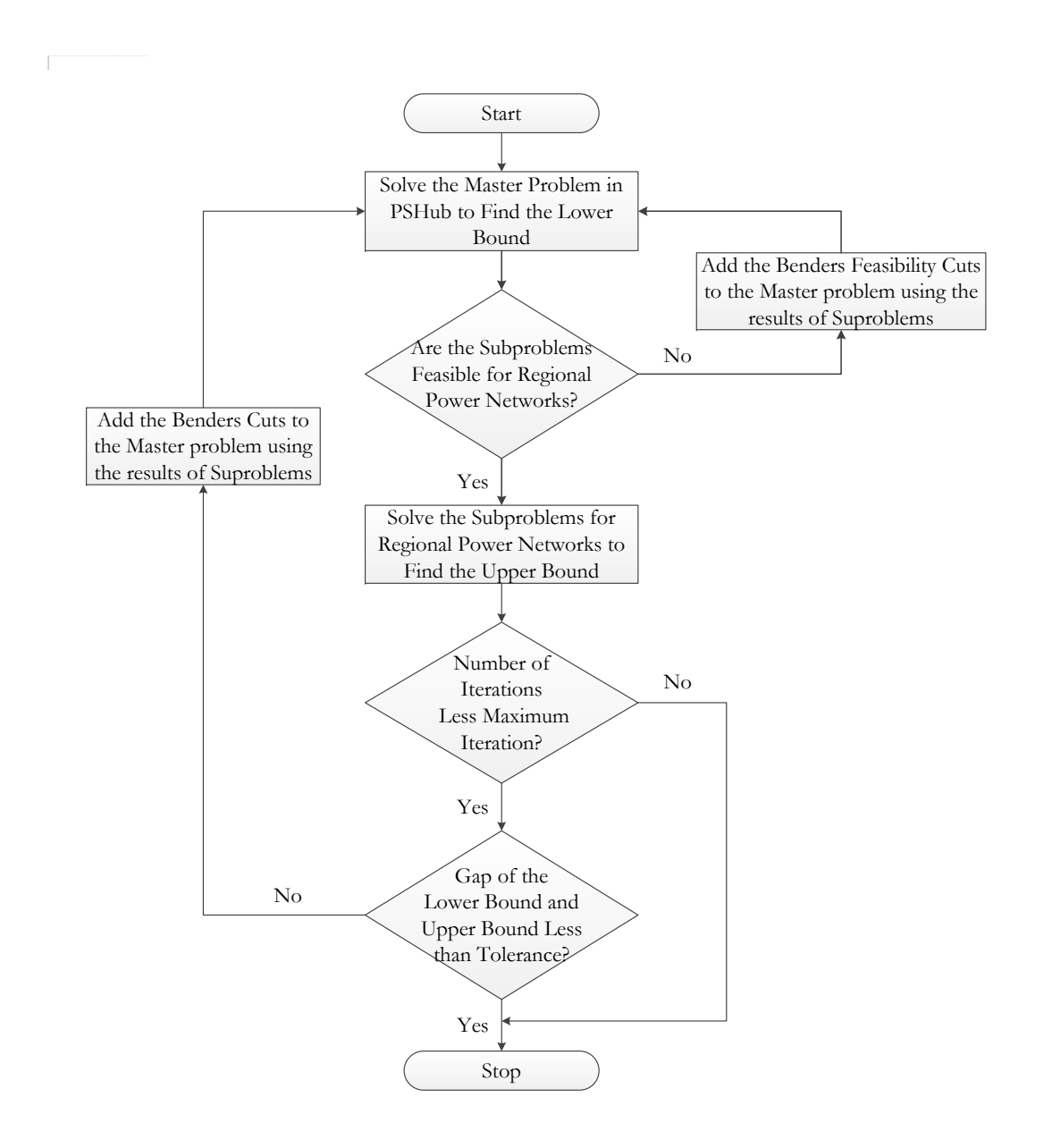


Figure 6.3: The flow chart of traditional BD

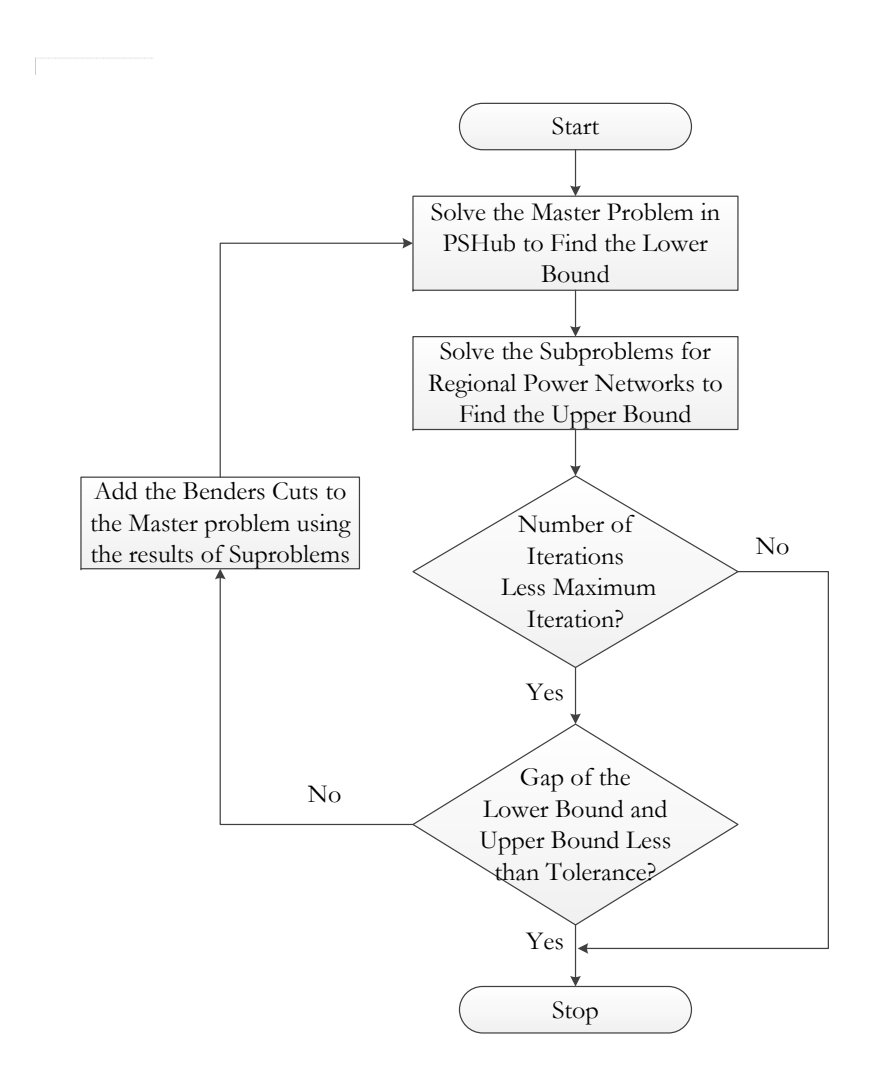


Figure 6.4: The flow chart of the modified BD

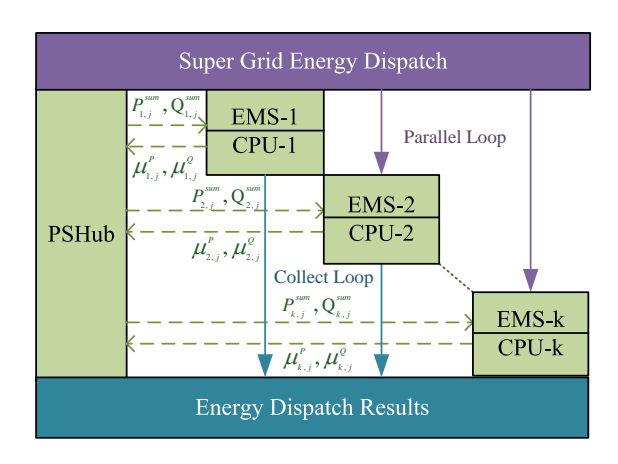


Figure 6.5: The parallel computation management in PSHub

6.5 Numerical Results

In this Section, the performance of energy dispatch coordination by PSHub accelerated by parallel computation is demonstrated. All the models are coded in GAMS and solved by the MOSEK solver. All simulations are run on a computer with Intel i7-2760QM 2.4 GHz CPU and 8 GB RAM.

6.5.1 Performance of Energy Dispatch Coordination by PSHub

To demonstrate the performance of energy dispatch coordination, we compare the results of PSHub with the centralized energy dispatch where the nonconvex ACOPF is solved as one single optimization problem in MATPOWER [70]. MATPOWER uses MATLAB built-in Interior Point Solver (MIPS) to solve nonconvex ACOPF. The solutions obtained from MATPOWER are local optimal solutions. We summarize the metrics of the regional networks in Table 6.2. The 'EMS' column lists the total number of regional EMS centers that are coordinated by the PSHub.

Base Case

In this base case, we use the power load data in the original power networks. We list the objective value results and computational CPU time in Table 6.3. The required number of iterations, generated Benders cuts and solution accuracy are summarized

Test Case	EMS	Number of Tie-Lines	Number of Nodes in Regional Networks
	2	27	828, 526
1354pegase	4	56	311, 253, 319, 471
	8	69	168, 151, 120, 243, 186, 102, 260, 124
	2	20	1899, 970
2869pegase	4	39	975, 457, 531, 906
	8	83	324, 532, 295, 214, 312, 288, 524, 350
	2	15	4122, 5119
9241pegase	4	51	1200, 1754, 3253, 3034
	8	126	1247, 735, 509, 1887, 1489, 922, 1597, 855

Table 6.2: Metrics of regional EMS and power networks

in Table 6.4. The relative gap in Table 6.4 is calculated as in (6.3):

$$Relative \ Gap = \frac{Upper \ Bound - Lower \ Bound}{Upper \ Bound} \times 100\% \tag{6.3}$$

Because the overall super grid is a fixed network, more regional EMS centers mean smaller scale for each regional power network. So the required computation time, in general, will decrease with the increasing of EMS centers. This is because each regional EMS center dispatch is computed by the proposed parallel computation. However, as we can notice from the results of the 2869pegase test case, the computation time of coordinating 4 regional EMS centers is more than the computation time of coordinating 2 regional EMS centers. This result shows that the computation time does not only depend on the network scale but also the specific network structure. The communicated Benders cuts from all the regional EMS to PSHub are equal to the number of iterations times the number of regional EMS centers.

The centralized dispatch results in Table 6.3 are obtained from MATPOWER which solves the nonconvex ACOPF model and can only guarantee local optimal solutions. The PSHub coordination results are obtained by solving our convex SOC-ACOPF model using our proposed modified BD approach. The decentralized SOC-ACOPF approach converges to very close results compared with the centralized solutions of SOC-ACOPF model in Table 6.3. The comparison in Table 6.3 is to demonstrate both the advantages of convex SOC-ACOPF model over the nonconvex ACOPF model in MATPOWER and the advantages of PSHub coordination over centralized dispatch. Since the SOC-ACOPF is convex, the solutions are guaranteed to be global optimal. The benefits of global economy improvements are because of the advantage of global optimality over local optimality. The computational efficiency improvement is because of the advantage of the modified BD using parallel computation. From a tech-

nical perspective, the regional EMS is always required to be involved to coordinate the operations with other regional EMS as long as the power grid is interconnected. Otherwise, the security of the power grid cannot be guaranteed. From an economic perspective, the results of regional EMS from PSHub coordination are very close to centralized dispatch (solve the SOC-ACOPF model as one single optimization without using the modified BD). This is guaranteed by the convergence of the modified BD. The convergence means the final results can converge to the centralized solution of the decision variables which ensure that the economic cost of regional EMS also converges to the solution of centralized solution. In summary, the fast convergence of the coordination by PSHub shows strong coordination capability. By using parallel computation, the required computation time for more EMS centers does not increase. On the contrary, the efficient parallel computation management algorithm is capable of accelerating the computations. This is highly appreciated in online decision making applications where the computation time is limited.

PSHub Coordination Centralized Dispatch Test Case Objective [\$] **EMS** CPU Time [s] Objective [\$] CPU Time [s] Upper Bound Lower Bound 74009.46 74009.45 2 1.05 1354pegase 74822.49 72726.67 4 1.47 74069.35 8.58 8 74009.47 74009.450.41 2 133902.29 133902.21 4.82 134582.33 132578.46 6.38 2869pegase 4 133999.29 18.66 134112.36 133791.95 8 1.22 314273.05 314273.03 $\overline{2}$ 58.78 316425.87 311537.62 4 29.05 315912.43 9241pegase 85.11314597.18 314597.11 8 13.79

Table 6.3: PSHub coordination results: base case

Load Scenarios

To validate the robustness of the coordination mechanism by PSHub, we simulate the power load scenarios from 70% to 90% of the original load data. Because the centralized energy dispatch by MATPOWER cannot converge for most cases when the power loads are below 70% or above 100% of the original load data, we do not show the results for these load scenarios. The results are demonstrated in Fig. 6.6, Fig. 6.7 and Fig. 6.8. For all the considered load scenarios, the coordinated energy dispatch by PSHub converge to very close objective values compared with the centralized dispatch

Test Case	EMS	No. of Iterations	No. of Benders Cuts	Relative Gap
	2	3	6	0.00%
1354pegase	4	3	12	2.80%
	8	3	24	0.00%
2869pegase	2	3	6	0.00%
	4	4	16	1.49%
	8	3	24	0.24%
9241pegase	2	3	6	0.00%
	4	3	12	1.54%
	8	3	24	0.00%

Table 6.4: Iterations, Benders cuts and solution accuracy

by MATPOWER. The required computation time of PSHub is less than the CPU time of centralized dispatch. These results show that coordinated energy dispatch by PSHub is robust against the considered load scenarios.

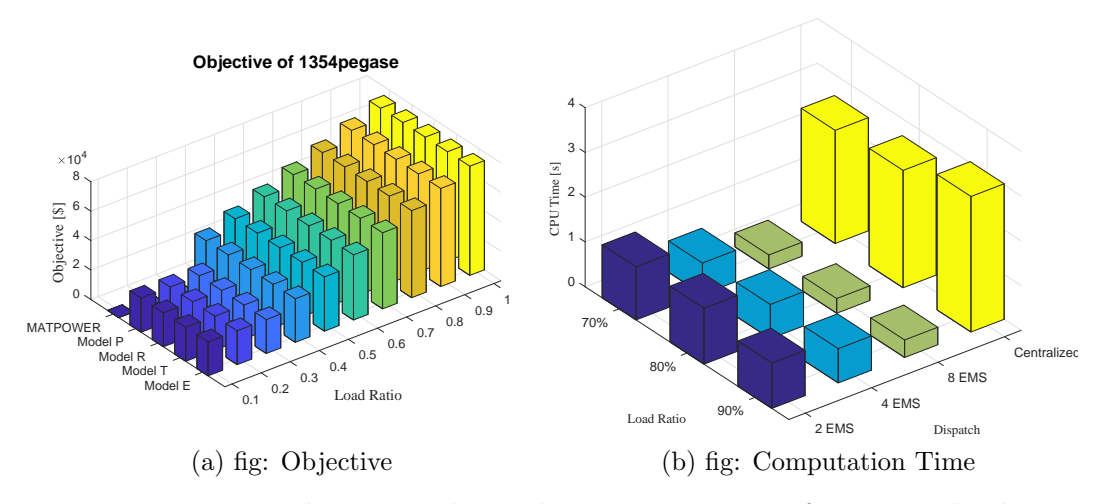


Figure 6.6: 1354pegase objective value and computation time for various load scenarios

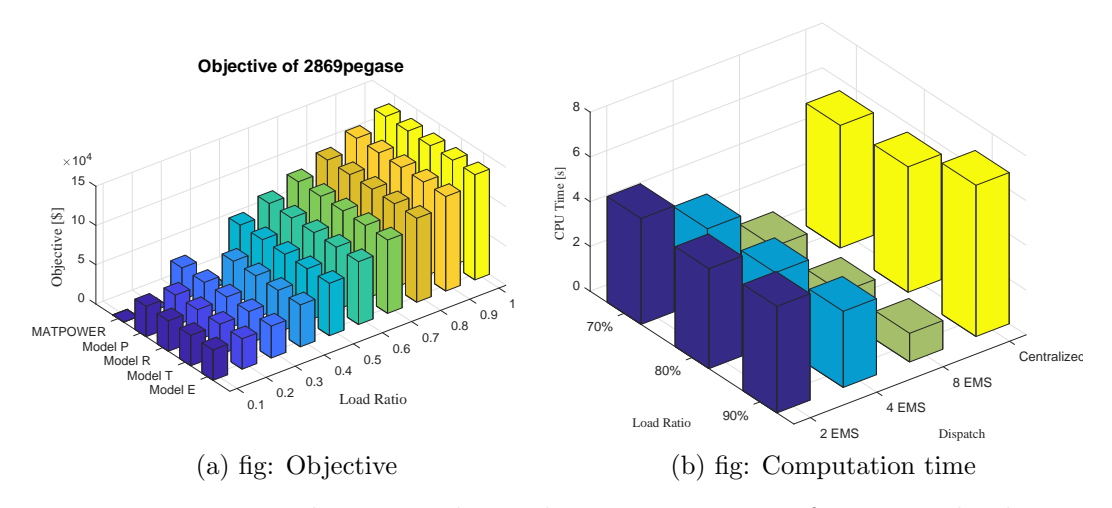


Figure 6.7: 2869pegase objective value and computation time for various load scenarios

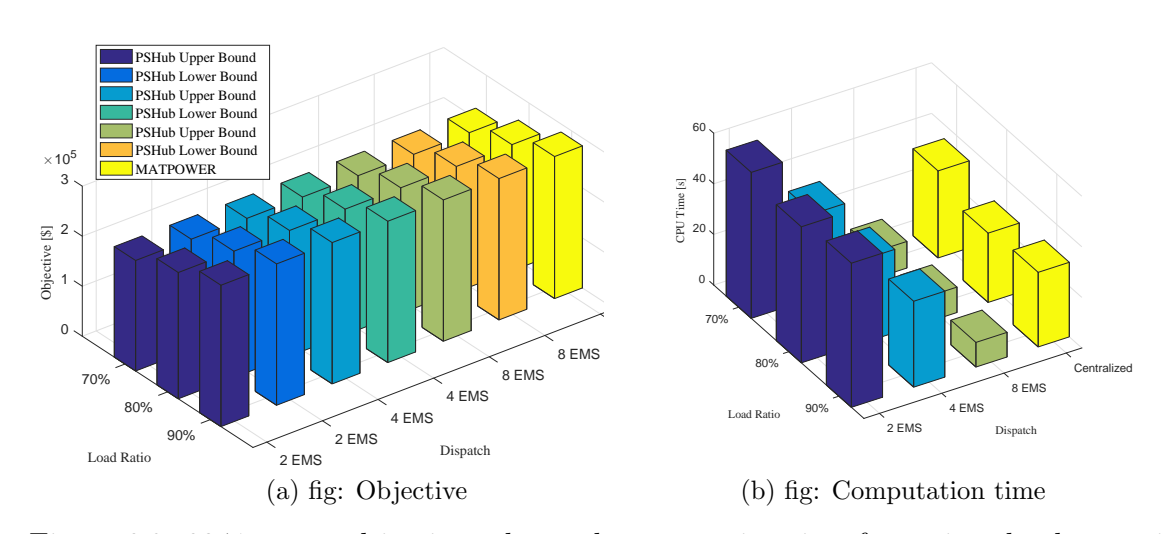


Figure 6.8: 9241pegase objective value and computation time for various load scenarios

119

6.6 Conclusions

Coordinating the energy dispatch across continent is a challenging task of future super grid operations. With the large-scale integration of renewable energy to the power system, more transmission expansions are required to connect these renewable energy resources in remote areas either onshore or offshore. It is hard to efficiently operate the super grid without an international or inter-regional coordination mechanism. This Chapter contributes to the literature by proposing the SOC-ACOPF model and the PSHub concept to solve this challenge. Specifically, we have solved three problems of operating the super grid:

- 1. How to approximately find the global optimal operating points of the power network? The solution is the improved convex SOC-ACOPF model;
- 2. How to coordinate the energy dispatch of different nations or regions and reduce the communication burden? The solution is the modified BD algorithm;
- 3. How to execute the coordination of ultra-large-scale power network fast enough to assist online decision making? The solution is the proposed parallel computation structure.

By coordinating the energy dispatch of regional EMS centers, global optimal energy dispatch targets can be achieved. The coordination in PSHub is based on the modified BD algorithm and the proposed convex SOC-ACOPF model. The advantage of using convex SOC-ACOPF model is that the convergence of modified BD can be guaranteed. The fast and strong convergence capability of the proposed coordination mechanism implemented in PSHub is demonstrated by the proposed parallel computation approach. The numerical results of various number of regional power networks and load scenarios show that the coordinated energy dispatch by PSHub is robust. Compared with other distributed ACOPF solution algorithms in the literature, the main advantages of the proposed modified BD are three-fold:

- 1. Instead of using the original Benders feasibility cuts approach, we can guarantee the feasibility of the formulated subproblems in the modified BD by adding one more generator at each node of the power network with larger marginal cost. Our approach converges within one minute CPU time for power networks up to 9241 nodes. The original Benders feasibility cuts approach cannot converge after several hours in our simulations.
- 2. Since we formulate the modified BD by taking the total power generations of the regional power networks as the complicating variables, no other detailed information except the Benders cuts is required to be communicated from the

regional power networks to the PSHub. This formulation can largely reduce the communication burden to coordinate the super grid. Since the parameters of the Benders cuts are required to be communicated from the regional power networks to the PSHub in each iteration, the reduced communication burden is also because our modified BD approach requires less iterations to converge compared with the traditional BD.

3. The privacy of information for the regional power networks can be protected since the boundaries between different regional power networks are still kept. No transfer of information between different regional power networks is required. The only two-way communication is between the PSHub and individual regional power network. This is largely due to our novel formulation of the modified BD which takes the total power outputs of the regional power networks as the complicating variables. In other words, if we take other variables as the complicating variables to formulate the master problem and subproblems of BD, the information privacy of regional power network may not be well protected.

Chapter 7

Closure

This Chapter summarizes the main conclusions of this thesis. Future research work to be conducted is directed.

7.1 Concluding Remarks

Proposing new models, solution algorithms and applications of SOC-ACOPF is the main contribution of this dissertation. One of the targets of the proposed SOC-ACOPF models and sequential tightness algorithm is to improve the solution quality of SOC-ACOPF model which can optimally operate the power system. The proposed M-BDA is to accelerate the computational efficiency to assist real-time decision making. Through various test cases based on real power networks, the applications in DLMP, wind power integration and super grid coordination, the applicability of the proposed models and algorithms are proved.

In Chapter 2, detailed mathematical formulations of the proposed SOC-ACOPF models are presented. The improvements of the solutions from SOC-ACOPF compared with the global optimal solution from the LINDOGLOBAL solver in GAMS are demonstrated numerically. Feasible solutions can be recovered from the relaxed solutions of SOC-ACOPF models by using the proposed heuristic feasible solution recovery algorithm.

Chapter 3 proposes the sequential tightness algorithm to improve the AC feasibility of the solutions from the SOC-ACOPF models. Solutions with better AC feasibility mean more realistic operation points (voltages, power flows, etc.) for the power network. For large-scale SOC-ACOPF problem, we prove analytically and numerically that the proposed M-BDA is an efficient decentralized solution approach compared with the centralized solution approach.

Chapter 4 solves two practical challenges of implementing DLMP: the computational challenge and the TSO-DSO coordination challenge. We propose the concept of GBF which can be regarded as a unified communication format between TSO and DSO. Considering the large-scale penetration of DERs, the proposed HED mechanism relaxes the energy dispatch burden by assigning the dispatch task to multiple power network operators i.e. TSO and DSO.

7.2. FUTURE WORK 123

Chapter 5 proposes a scenario decomposition based M-BDA to solve the challenge of large number of wind power scenarios when using stochastic optimization to operate the power network with VSC-MTDC system and FACTS devices. By using HPC, this M-BDA approach combined with our designed parallel computing architecture shows strong convergence capability and computational efficiency.

Chapter 6 finally uses SOC-ACOPF and M-BDA to coordinate the energy dispatch of the super grid across the continent. We actually prove that SOC-ACOPF and M-BDA can serve as the mathematical foundations of the proposed concept of PSHub coordinating the energy dispatch of multiple nations or regions.

7.2 Future Work

The power network is expanding either to connect more renewable energy from remote areas which may be far from the load centers, or to provide electricity for rural developing areas. The scale of resulted optimization model to operate the power network is growing. Improving the accuracy and computational efficiency of the proposed SOC-ACOPF models is one main direction of future research work. We are now working on accurate linearization of the SOC-ACOPF model since linear programming is more easier to solve.

The penetration of DERs in the distribution network is accelerating due to various policy supports and technology advancements. Fully activating all possible flexibilities from DERs by DLMP is very important to benefit the power network, producers and consumers. There are still some unsolved problems in implementing DLMP such as the market power issue. Investigating this issue is critical to provide insights and decision supports for the policy makers. The market power issue in the context of DLMP can be another direction of future research work.

Bibliography

- [1] M. B. Cain, R. P. O'neill, and A. Castillo, "History of optimal power flow and formulations," FERC, Tech. Rep., 2012.
- [2] R. P. O'Neill, A. Castillo, and M. B. Cain, "The IV formulation and linear approximations of the AC optimal power flow problem," FERC, Tech. Rep., 2012.
- [3] S. Frank, I. Steponavice, and S. Rebennack, "Optimal power flow: a bibliographic survey II," *Energy Systems*, vol. 3, no. 3, pp. 259–289, 2012.
- [4] M. Geidl and G. Andersson, "Optimal power flow of multiple energy carriers," *IEEE Transactions on Power Systems*, vol. 22, no. 1, pp. 145–155, 2007.
- [5] D. Gan, R. J. Thomas, and R. D. Zimmerman, "Stability-constrained optimal power flow," *IEEE Transactions on Power Systems*, vol. 15, no. 2, pp. 535–540, 2000.
- [6] E. Iggland, R. Wiget, S. Chatzivasileiadis, and G. Anderson, "Multi-Area DC-OPF for HVAC and HVDC Grids," *IEEE Transactions on Power Systems*, vol. 30, no. 5, pp. 2450–2459, Sept 2015.
- [7] J. A. Momoh, R. Adapa, and M. E. El-Hawary, "A review of selected optimal power flow literature to 1993. Part I: Nonlinear and quadratic programming approaches," *IEEE Transactions on Power Systems*, vol. 14, no. 1, pp. 96–104, 1999.
- [8] J. A. Momoh, M. El-Hawary, and R. Adapa, "A review of selected optimal power flow literature to 1993. Part II: Newton, linear programming and interior point methods," *IEEE Transactions on Power Systems*, vol. 14, no. 1, pp. 105–111, 1999.
- [9] J. Yuryevich and K. P. Wong, "Evolutionary programming based optimal power flow algorithm," *IEEE Transactions on Power Systems*, vol. 14, no. 4, pp. 1245–1250, 1999.
- [10] H. Cai, C. Chung, and K. Wong, "Application of differential evolution algorithm for transient stability constrained optimal power flow," *IEEE Transactions on Power Systems*, vol. 23, no. 2, pp. 719–728, 2008.

- [11] T. J. Overbye, X. Cheng, and Y. Sun, "A comparison of the AC and DC power flow models for LMP calculations," in *System Sciences*, 2004. Proceedings of the 37th Annual Hawaii International Conference on, Jan 2004, pp. 9 pp.—.
- [12] S. M. Amin and B. F. Wollenberg, "Toward a smart grid: power delivery for the 21st century," *Power and Energy Magazine*, *IEEE*, vol. 3, no. 5, pp. 34–41, 2005.
- [13] S. Abdelouadoud, R. Girard, F.-P. Neirac, and T. Guiot, "Optimal power flow of a distribution system based on increasingly tight cutting planes added to a second order cone relaxation," *International Journal of Electrical Power & Energy Systems*, vol. 69, pp. 9–17, 2015.
- [14] P. Lipka, S. Oren, R. O'Neill, and A. Castillo, "Running a more complete market with the SLP-IV-ACOPF," *IEEE Transactions on Power Systems*, vol. PP, no. 99, pp. 1–1, 2016.
- [15] Y. Liu, J. Li, and L. Wu, "Distribution system restructuring: Distribution LMP via unbalanced ACOPF," *IEEE Transactions on Smart Grid*, vol. PP, no. 99, pp. 1–1, 2017.
- [16] D. K. Molzahn, F. Dörfler, H. Sandberg, S. H. Low, S. Chakrabarti, R. Baldick, and J. Lavaei, "A survey of distributed optimization and control algorithms for electric power systems," *IEEE Transactions on Smart Grid*, vol. PP, no. 99, pp. 1–1, 2017.
- [17] B. Zhao, Z. Xu, C. Xu, C. Wang, and F. Lin, "Network partition based zonal voltage control for distribution networks with distributed PV systems," *IEEE Transactions on Smart Grid*, vol. PP, no. 99, pp. 1–1, 2017.
- [18] Bidding Areas of Nord Pool. [Online]. Available: http://www.nordpoolspot.com/How-does-it-work/Bidding-areas/
- [19] Electric power markets: National overview. [Online]. Available: https://www.ferc.gov/market-oversight/mkt-electric/overview.asp
- [20] E. Loukarakis, J. W. Bialek, and C. J. Dent, "Investigation of maximum possible opf problem decomposition degree for decentralized energy markets," *IEEE Transactions on Power Systems*, vol. 30, no. 5, pp. 2566–2578, Sept 2015.
- [21] E. Celebi and J. D. Fuller, "Time-of-use pricing in electricity markets under different market structures," *Power Systems, IEEE Transactions on*, vol. 27, no. 3, pp. 1170–1181, 2012.

[22] J. Aghaei and M.-I. Alizadeh, "Critical peak pricing with load control demand response program in unit commitment problem," *IET Generation, Transmission & Distribution*, vol. 7, no. 7, pp. 681–690, 2013.

- [23] P. L. Joskow and C. D. Wolfram, "Dynamic pricing of electricity," *The American Economic Review*, vol. 102, no. 3, pp. 381–385, 2012.
- [24] C. Vivekananthan, Y. Mishra, and F. Li, "Real-time price based home energy management scheduler," 2014.
- [25] M. R. H. Darryl R. Biggar, *The Economics of Electricity Markets*. IEEE Press & Wiley, 2014.
- [26] I. Pérez-Arriaga and A. Bharatkumar, "A framework for redesigning distribution network use of system charges under high penetration of distributed energy resources: New principles for new problems," CEEPR Working Paper Series no. WP-2014-006, Tech. Rep., 2014.
- [27] F. Li, "Recent developments in common distribution network pricing in Great Britain," in *Energy Market (EEM)*, 2010 7th International Conference on the European, 2010, pp. 1–5.
- [28] P. M. Sotkiewicz and J. M. Vignolo, "Nodal pricing for distribution networks: efficient pricing for efficiency enhancing dg," *Power Systems, IEEE Transactions on*, vol. 21, no. 2, pp. 1013–1014, 2006.
- [29] Y. Li, W. Li, W. Yan, J. Yu, and X. Zhao, "Probabilistic optimal power flow considering correlations of wind speeds following different distributions," *IEEE Transactions on Power Systems*, vol. 29, no. 4, pp. 1847–1854, 2014.
- [30] S. Widergren, C. Marinovici, T. Berliner, and A. Graves, "Real-time pricing demand response in operations," in *Power and Energy Society General Meeting*, 2012 IEEE, 2012, pp. 1–5.
- [31] F. Sahriatzadeh, P. Nirbhavane, and A. Srivastava, "Locational marginal price for distribution system considering demand response," in *North American Power Symposium (NAPS)*, 2012, 2012, pp. 1–5.
- [32] S. Huang, Q. Wu, S. S. Oren, R. Li, and Z. Liu, "Distribution locational marginal pricing through quadratic programming for congestion management in distribution networks," *IEEE Transactions on Power Systems*, vol. 30, no. 4, pp. 2170–2178, 2015.

- [33] G. T. Heydt, B. H. Chowdhury, M. L. Crow, D. Haughton, B. D. Kiefer, F. Meng, and B. R. Sathyanarayana, "Pricing and control in the next generation power distribution system," *Smart Grid, IEEE Transactions on*, vol. 3, no. 2, pp. 907–914, 2012.
- [34] S. Massoud Amin and B. Wollenberg, "Toward a smart grid: power delivery for the 21st century," *Power and Energy Magazine*, *IEEE*, vol. 3, no. 5, pp. 34 41, sept.-oct. 2005.
- [35] D. Van Hertem, J. Rimez, and R. Belmans, "Power flow controlling devices as a smart and independent grid investment for flexible grid operations: Belgian case study," *Smart Grid, IEEE Transactions on*, vol. 4, no. 3, pp. 1656–1664, 2013.
- [36] Y. Xiao, Y. H. Song, C.-C. Liu, and Y. Z. Sun, "Available transfer capability enhancement using facts devices," *Power Systems, IEEE Transactions on*, vol. 18, no. 1, pp. 305–312, 2003.
- [37] M. Claus, D. Retzmann, D. Sorangr, and K. Uecker, "Solutions for Smart and Super Grids with HVDC and FACTS, Technical article Published by Siemens AG," [Online]. Available: http://www.ptd.siemens.de/CEPSI08_Art.pdf, October 2008.
- [38] F. B. Alhasawi and J. V. Milanovic, "Techno-economic contribution of facts devices to the operation of power systems with high level of wind power integration," *IEEE Transactions on Power Systems*, vol. 27, no. 3, pp. 1414–1421, Aug 2012.
- [39] E. Bompard, G. Fulli, M. Ardelean, and M. Masera, "It's a Bird, It's a Plane, It's a...Supergrid!: Evolution, Opportunities, and Critical Issues for Pan-European Transmission," *IEEE Power and Energy Magazine*, vol. 12, no. 2, pp. 40–50, March 2014.
- [40] C. W. Gellings, "A globe spanning super grid," *IEEE Spectrum*, vol. 52, no. 8, pp. 48–54, August 2015.
- [41] M. Fűrsch, S. Hagspiel, C. Jägemann, S. Nagl, D. Lindenberger, and E. Trőter, "The role of grid extensions in a cost-efficient transformation of the european electricity system until 2050," *Applied Energy*, vol. 104, pp. 642 652, 2013.
- [42] G. Sanchis, B. Betraoui, T. Anderski, E. Peirano, R. Pestana, B. D. Clercq, G. Migliavacca, M. Czernie, and M. Paun, "The Corridors of Power: A Pan-European "Electricity Highway" System for 2050," *IEEE Power and Energy Magazine*, vol. 13, no. 1, pp. 38–51, Jan 2015.

[43] L. Gan, N. Li, U. Topcu, and S. H. Low, "Exact convex relaxation of optimal power flow in radial networks," *IEEE Transactions on Automatic Control*, vol. 60, no. 1, pp. 72–87, 2015.

- [44] M. Farivar and S. H. Low, "Branch Flow Model: Relaxations and Convexification: Part I, Part II," *IEEE Transactions on Power Systems*, vol. 28, no. 3, pp. 2554–2572, Aug 2013.
- [45] W. Wei, J. Wang, N. Li, and S. Mei, "Optimal power flow of radial networks and its variations: A sequential convex optimization approach," *IEEE Transactions on Smart Grid*, vol. PP, no. 99, pp. 1–1, 2017.
- [46] C. Coffrin and P. Van Hentenryck, "A linear-programming approximation of AC power flows," *INFORMS Journal on Computing*, vol. 26, no. 4, pp. 718–734, 2014.
- [47] S. Bolognani and S. Zampieri, "On the Existence and Linear Approximation of the Power Flow Solution in Power Distribution Networks," *Power Systems*, *IEEE Transactions on*, vol. 31, no. 1, pp. 163–172, Jan 2016.
- [48] C. Coffrin, H. L. Hijazi, and P. V. Hentenryck, "The QC Relaxation: A Theoretical and Computational Study on Optimal Power Flow," *IEEE Transactions on Power Systems*, vol. 31, no. 4, pp. 3008–3018, July 2016.
- [49] B. H. Kim and R. Baldick, "A comparison of distributed optimal power flow algorithms," *IEEE Transactions on Power Systems*, vol. 15, no. 2, pp. 599–604, 2000.
- [50] J. Guo, G. Hug, and O. K. Tonguz, "A case for non-convex distributed optimization in large-scale power systems," *IEEE Transactions on Power Systems*, vol. PP, no. 99, pp. 1–1, 2017.
- [51] C. Hamon, M. Perninge, and L. Soder, "A Stochastic Optimal Power Flow Problem With Stability Constraints Part I: Approximating the Stability Boundary," *IEEE Transactions on Power Systems*, vol. 28, no. 2, pp. 1839–1848, 2013.
- [52] M. Perninge and C. Hamon, "A stochastic optimal power flow problem with stability constraints— Part II: the optimization problem," *IEEE Transactions on Power Systems*, vol. 28, no. 2, pp. 1849–1857, 2013.
- [53] D. K. Molzahn, B. C. Lesieutre, and C. L. DeMarco, "A sufficient condition for global optimality of solutions to the optimal power flow problem," *IEEE Transactions on Power Systems*, vol. 29, no. 2, pp. 978–979, March 2014.

- [54] The mosek optimization software. [Online]. Available: http://www.mosek.com
- [55] M. Baradar and M. R. Hesamzadeh, "AC power flow representation in conic format," *IEEE Transactions on Power Systems*, vol. 30, no. 1, pp. 546–547, 2015.
- [56] R. Jabr et al., "Radial distribution load flow using conic programming," *IEEE Transactions on Power Systems*, vol. 21, no. 3, pp. 1458–1459, 2006.
- [57] M. Nazari, "Control and planning of multi-terminal hvdc transmission systems," Ph.D. dissertation, KTH, Electric Power and Energy Systems, 2017, qC 20170908.
- [58] X. Bai, H. Wei, K. Fujisawa, and Y. Wang, "Semidefinite programming for optimal power flow problems," *International Journal of Electrical Power & Energy Systems*, vol. 30, no. 6, pp. 383–392, 2008.
- [59] J. Lavaei and S. H. Low, "Zero duality gap in optimal power flow problem," *IEEE Transactions on Power Systems*, vol. 27, no. 1, pp. 92–107, 2012.
- [60] B. C. Lesieutre, D. K. Molzahn, A. R. Borden, and C. L. DeMarco, "Examining the limits of the application of semidefinite programming to power flow problems," in *Communication, Control, and Computing (Allerton)*, 2011 49th Annual Allerton Conference on, Sept 2011, pp. 1492–1499.
- [61] D. Molzahn, J. Holzer, B. Lesieutre, and C. DeMarco, "Implementation of a large-scale optimal power flow solver based on semidefinite programming," *IEEE Transactions on Power Systems*, vol. 28, no. 4, pp. 3987–3998, 2013.
- [62] J. Lavaei, D. Tse, and B. Zhang, "Geometry of power flows and optimization in distribution networks," *IEEE Transactions on Power Systems*, vol. 29, no. 2, pp. 572–583, 2014.
- [63] S. Low, "Convex Relaxation of Optimal Power Flow, Part I: Formulations and Equivalence," *IEEE Transactions on Control of Network Systems*, vol. 1, no. 1, pp. 15–27, March 2014.
- [64] S. H. Low, "Convex relaxation of optimal power flow, part II: Exactness," *IEEE Transactions on Control of Network Systems*, vol. 1, no. 2, pp. 177–189, June 2014.
- [65] B. Kocuk, S. S. Dey, and X. A. Sun, "Inexactness of SDP Relaxation and Valid Inequalities for Optimal Power Flow," *IEEE Transactions on Power Systems*, vol. 31, no. 1, pp. 642–651, Jan 2016.

[66] R. P. O'Neill, A. Castillo, and M. B. Cain, "The Computational Testing of AC Optimal Power Flow Using the Current Voltage Formulations," FERC, Tech. Rep., 2012.

- [67] C. Coffrin, H. L. Hijazi, and P. Van Hentenryck, "Network flow and copper plate relaxations for ac transmission systems," in *Power Systems Computation Conference (PSCC)*, 2016, 2016.
- [68] B. Kocuk, S. S. Dey, and X. A. Sun, "Strong SOCP Relaxations for the Optimal Power Flow Problem," *Operations Research*, vol. 64, no. 6, pp. 1177–1196, 2016.
- [69] M. Ghamkhari, A. Sadeghi-Mobarakeh, and H. Mohsenian-Rad, "Strategic bidding for producers in nodal electricity markets: A convex relaxation approach," IEEE Transactions on Power Systems, vol. PP, no. 99, pp. 1–1, 2016.
- [70] R. D. Zimmerman, C. E. Murillo-Sánchez, and R. J. Thomas, "MATPOWER: Steady-state operations, planning, and analysis tools for power systems research and education," *IEEE Transactions on Power Systems*, vol. 26, no. 1, pp. 12–19, 2011.
- [71] G. P. McCormick, "Computability of global solutions to factorable nonconvex programs: Part I Convex underestimating problems," *Mathematical programming*, vol. 10, no. 1, pp. 147–175, 1976.
- [72] A. J. Conejo and J. A. Aguado, "Multi-area coordinated decentralized DC optimal power flow," *IEEE Transactions on Power Systems*, vol. 13, no. 4, pp. 1272–1278, Nov 1998.
- [73] A. M. Geoffrion, "Generalized Benders decomposition," *Journal of optimization theory and applications*, vol. 10, no. 4, pp. 237–260, 1972.
- [74] V. H. Quintana, R. Lopez, R. Romano, and V. Valadez, "Constrained economic dispatch of multi-area systems using the dantzig-wolfe decomposition principle," *IEEE Transactions on Power Apparatus and Systems*, vol. PAS-100, no. 4, pp. 2127–2137, April 1981.
- [75] T. Erseghe, "Distributed optimal power flow using ADMM," *IEEE Transactions on Power Systems*, vol. 29, no. 5, pp. 2370–2380, Sept 2014.
- [76] N. Alguacil and A. J. Conejo, "Multiperiod optimal power flow using Benders decomposition," *IEEE Transactions on Power Systems*, vol. 15, no. 1, pp. 196–201, Feb 2000.

- [77] Y. Fu, M. Shahidehpour, and Z. Li, "Security-constrained unit commitment with AC constraints*," *IEEE Transactions on Power Systems*, vol. 20, no. 3, pp. 1538–1550, Aug 2005.
- [78] S. Binato, M. V. F. Pereira, and S. Granville, "A new Benders decomposition approach to solve power transmission network design problems," *IEEE Transactions on Power Systems*, vol. 16, no. 2, pp. 235–240, May 2001.
- [79] Y. Wang, L. Wu, and S. Wang, "A fully-decentralized consensus-based ADMM approach for DC-OPF with demand response," *IEEE Transactions on Smart Grid*, vol. PP, no. 99, pp. 1–11, 2017.
- [80] M. Bazrafshan and N. Gatsis, "Decentralized stochastic optimal power flow in radial networks with distributed generation," *IEEE Transactions on Smart Grid*, vol. 8, no. 2, pp. 787–801, March 2017.
- [81] W. Lu, M. Liu, S. Lin, and L. Li, "Fully decentralized optimal power flow of multi-area interconnected power systems based on distributed interior point method," *IEEE Transactions on Power Systems*, vol. PP, no. 99, pp. 1–1, 2017.
- [82] S. Arora, S. Rao, and U. Vazirani, "Geometry, flows, and graph-partitioning algorithms," *Communications of the ACM*, vol. 51, no. 10, pp. 96–105, 2008.
- [83] Y. Jia and Z. Xu, "A direct solution to biobjective partitioning problem in electric power networks," *IEEE Transactions on Power Systems*, vol. 32, no. 3, pp. 2481–2483, May 2017.
- [84] E. Cotilla-Sanchez, P. D. H. Hines, C. Barrows, S. Blumsack, and M. Patel, "Multi-attribute partitioning of power networks based on electrical distance," *IEEE Transactions on Power Systems*, vol. 28, no. 4, pp. 4979–4987, Nov 2013.
- [85] J. Guo, G. Hug, and O. K. Tonguz, "Intelligent partitioning in distributed optimization of electric power systems," *IEEE Transactions on Smart Grid*, vol. 7, no. 3, pp. 1249–1258, May 2016.
- [86] J. P. Hespanha, "An efficient matlab algorithm for graph partitioning," Department of Electrical & Computer Engineering, University of California., Tech. Rep., 2004.
- [87] K. Lehmann, A. Grastien, and P. V. Hentenryck, "AC-Feasibility on Tree Networks is NP-Hard," *IEEE Transactions on Power Systems*, vol. 31, no. 1, pp. 798–801, Jan 2016.

[88] A. Verma, "Power grid security analysis: an optimization approach," Ph.D. dissertation, Dept. Ind. Eng. Oper. Res., Columbia Univ., New York, NY, USA, 2009.

- [89] M. R. Bussieck, M. C. Ferris, and A. Meeraus, "Grid-enabled optimization with gams," *INFORMS Journal on Computing*, vol. 21, no. 3, pp. 349–362, 2009.
- [90] R. Mudumbai and S. Dasgupta, "Distributed control for the smart grid: The case of economic dispatch," in *Information Theory and Applications Workshop* (ITA), 2014, 2014, pp. 1–6.
- [91] H. Karami, M. Sanjari, S. Hosseinian, and G. Gharehpetian, "An optimal dispatch algorithm for managing residential distributed energy resources," *IEEE Transactions on Smart Grid*, vol. 5, no. 5, pp. 2360–2367, 2014.
- [92] A. Fazeli, M. Sumner, C. Johnson, and E. Christopher, "Coordinated optimal dispatch of distributed energy resources within a smart energy community cell," in *Innovative Smart Grid Technologies (ISGT Europe)*, 2012 3rd IEEE PES International Conference and Exhibition on, 2012, pp. 1–10.
- [93] A. Conejo and J. Aguado, "Multi-area coordinated decentralized DC optimal power flow," vol. 13, no. 4, pp. 1272–1278, 1998.
- [94] Y. Zhang and F. Li, "Network pricing for high voltage radial distribution networks," in *Power and Energy Society General Meeting*, 2011 IEEE, 2011, pp. 1–5.
- [95] V. Loia and A. Vaccaro, "Decentralized economic dispatch in smart grids by self-organizing dynamic agents," *IEEE Transactions on Systems, Man, and Cybernetics: Systems*, vol. 44, no. 4, pp. 397–408, 2014.
- [96] F. Meng and B. Chowdhury, "Distribution Imp-based economic operation for future smart grid," in *Power and Energy Conference at Illinois (PECI)*, 2011 *IEEE*, 2011, pp. 1–5.
- [97] P. Hallberg *et al.*, "Active distribution system management a key tool for the smooth integration of distributed generation," *Eurelectric TF Active System Management*, vol. 2, p. 013, 2013.
- [98] E. Rivero, S. Daan, A. Ramos, M. Maenhoudt, and A. Ulian, "Preliminary assessment of the future role of DSOs, future market architectures and regulatory frameworks for network integration of dres," European Project EvolvDSO, Deliverable, vol. 1, 2014.

- [99] K. Purchala, L. Meeus, D. Van Dommelen, and R. Belmans, "Usefulness of dc power flow for active power flow analysis," in *IEEE Power Engineering Society General Meeting*, 2005. IEEE, 2005, pp. 454–459.
- [100] A. V. Fiacco and J. Kyparisis, "Convexity and concavity properties of the optimal value function in parametric nonlinear programming," *Journal of Optimization Theory and Applications*, vol. 48, no. 1, pp. 95–126, 1986.
- [101] A. J. Conejo, E. Castillo, R. Minguez, and R. Garcia-Bertrand, *Decomposition techniques in mathematical programming: engineering and science applications*. Springer Science & Business Media, 2006.
- [102] K. Schneider, P. Phanivong, and J.-S. Lacroix, "IEEE 342-node low voltage networked test system," in *PES General Meeting— Conference & Exposition*, 2014 IEEE. IEEE, 2014, pp. 1–5.
- [103] X. Y. Ma, Y. Z. Sun, and H. L. Fang, "Scenario generation of wind power based on statistical uncertainty and variability," *IEEE Transactions on Sustainable Energy*, vol. 4, no. 4, pp. 894–904, Oct 2013.
- [104] P. Pinson, G. Papaefthymiou, B. Klockl, and H. A. Nielsen, "Generation of statistical scenarios of short-term wind power production," in *Power Tech*, 2007 IEEE Lausanne, July 2007, pp. 491–496.
- [105] D. H. Yoon, H. Song, G. Jang, and S. K. Joo, "Smart operation of hvdc systems for large penetration of wind energy resources," *IEEE Transactions on Smart Grid*, vol. 4, no. 1, pp. 359–366, March 2013.
- [106] E. Heydarian-Forushani, M. Moghaddam, M. Sheikh-El-Eslami, M. Shafie-khah, and J. Catalão, "A stochastic framework for the grid integration of wind power using flexible load approach," *Energy Conversion and Management*, vol. 88, pp. 985 – 998, 2014.
- [107] A. Rabiee and A. Soroudi, "Stochastic multiperiod opf model of power systems with hvdc-connected intermittent wind power generation," *IEEE Transactions on Power Delivery*, vol. 29, no. 1, pp. 336–344, Feb 2014.
- [108] A. Nasri, A. J. Conejo, S. J. Kazempour, and M. Ghandhari, "Minimizing wind power spillage using an opf with facts devices," *IEEE Transactions on Power* Systems, vol. 29, no. 5, pp. 2150–2159, Sept 2014.
- [109] List of power stations in Sweden. [Online]. Available: https://en.wikipedia.org/wiki/List_of_power_stations_in_Sweden

[110] Y. Fu, M. Liu, and L. Li, "Multiobjective stochastic economic dispatch with variable wind generation using scenario-based decomposition and asynchronous block iteration," *IEEE Transactions on Sustainable Energy*, vol. 7, no. 1, pp. 139–149, Jan 2016.

- [111] M. Baradar, M. R. Hesamzadeh, and M. Ghandhari, "Second-order cone programming for optimal power flow in vsc-type ac-dc grids," *Power Systems, IEEE Transactions on*, vol. 28, no. 4, pp. 4282–4291, 2013.
- [112] M. Baradar, "On the efficiency and accuracy of simulation methods for optimal power system operation: Convex optimization models for power system analysis, optimal utilization of vsc-type dc wind farm grids and facts devices," Ph.D. dissertation, KTH, Electric Power Systems, 2015, qC 20150521.
- [113] M. Baradar and M. Ghandhari, "A Multi-Option Unified Power Flow Approach for Hybrid AC/DC Grids Incorporating Multi-Terminal VSC-HVDC," *Power Systems, IEEE Transactions on*, vol. PP, no. 99, pp. 1–8, 2013.
- [114] B. Han, G. Karady, J. Park, and S. Moon, "Interaction analysis model for transmission static compensator with emtp," *Power Delivery, IEEE Transactions on*, vol. 13, no. 4, pp. 1297–1302, 1998.
- [115] H. Ambriz-Perez, E. Acha, and C. Fuerte-Esquivel, "Advanced svc models for newton-raphson load flow and newton optimal power flow studies," *Power Systems, IEEE Transactions on*, vol. 15, no. 1, pp. 129–136, 2000.
- [116] M. S. Lobo, L. Vandenberghe, S. Boyd, and H. Lebret, "Applications of second-order cone programming," *Linear Algebra and its Applications*, vol. 284, no. 1-3, pp. 193 228, 1998.
- [117] F. Alizadeh and D. Goldfarb, "Second-order cone programming," *Mathematical Programming (Series B)*, vol. 95, no. 1, pp. 3–51, 2003.
- [118] "V90 3.0 MW brochure," VESTAS, Tech. Rep., 2011.
- [119] "MERVENTO 3.6-118: The wind turbine reinvented," MERVENTO, Tech. Rep., 2004.
- [120] J. M. M. Antonio J. Conejo, Miguel Carrión, *Decision Making Under Uncertainty in Electricity Markets*, ser. 0884-8289. Springer US, 2010, vol. 153.
- [121] Y. Li, Z. Lukszo, and M. Weijnen, "The impact of inter-regional transmission grid expansion on china's power sector decarbonization," *Applied Energy*, vol. 183, pp. 853 873, 2016.

- [122] J. Li, J. Fang, Q. Zeng, and Z. Chen, "Optimal operation of the integrated electrical and heating systems to accommodate the intermittent renewable sources," *Applied Energy*, vol. 167, pp. 244 254, 2016.
- [123] M. Varadarajan and K. Swarup, "Solving multi-objective optimal power flow using differential evolution," *Generation, Transmission & Distribution, IET*, vol. 2, no. 5, pp. 720–730, 2008.
- [124] S. Sivasubramani and K. Swarup, "Multi-objective harmony search algorithm for optimal power flow problem," *International Journal of Electrical Power & Energy Systems*, vol. 33, no. 3, pp. 745–752, 2011.
- [125] R. A. Jabr, R. Singh, and B. C. Pal, "Minimum loss network reconfiguration using mixed-integer convex programming," *IEEE Transactions on Power Systems*, vol. 27, no. 2, pp. 1106–1115, May 2012.
- [126] S. Fliscounakis, P. Panciatici, F. Capitanescu, and L. Wehenkel, "Contingency ranking with respect to overloads in very large power systems taking into account uncertainty, preventive, and corrective actions," *IEEE Transactions on Power Systems*, vol. 28, no. 4, pp. 4909–4917, Nov 2013.

Complete List of Publications and Patents

Peer-Reviewed Journals included in the Journal Citation Report (JCR)

- [J6]. Z. Yuan, M. R. Hesamzadeh. Second-Order Cone AC Optimal Power Flow: Convex Relaxations and Feasible Solutions, Journal of Modern Power Systems and Clean Energy, 2018 (Submitted).
- [J5]. Z. Yuan, M. R. Hesamzadeh, S. Wogrin and M. Baradar. Stochastic Optimal Operation of VSC-MTDC System and FACTS Considering Large-Scale Integration of Wind Power, Computers & Operations Research, 2017 (Submitted).
- [J4]. Z. Yuan, M. R. Hesamzadeh. A Modified Benders Decomposition Algorithm to Solve Second-Order Cone AC Optimal Power Flow, IEEE Transactions on Smart Grid, 2017 (Published).
- [J3]. Z. Yuan, S. Wogrin and M. R. Hesamzadeh. Towards the Power Synergy Hub (PSHub): Coordinating the Energy Dispatch of Super Grid by Modified Benders Decomposition, Applied Energy, Volume 205, 2017, Pages 1419-1434 (Published).
- [J2]. Z. Yuan, M. R. Hesamzadeh. Hierarchical Coordination of TSO-DSO Economic Dispatch Considering Large-Scale Integration of Distributed Energy Resources, Applied Energy, Volume 195, 2017, Pages 600-615 (Published).
- [J1]. Z. Yuan, M. R. Hesamzadeh, D. Biggar. Distribution Locational Marginal Pricing by Convexified ACOPF and Hierarchical Dispatch, IEEE Transactions on Smart Grid, 2016 (Published).

Peer-Reviewed Conference Proceedings

- [C8]. Z. Yuan, M. R. Hesamzadeh. A Max-Affine Approximation Model to Solve Power Flow Problem with Controllable Accuracy, The International Conference on Innovative Smart Grid Technologies Europe, Sarajevo, October 21-25, 2018 (Submitted).
- [C7]. Z. Yuan, M. R. Hesamzadeh. Improving the Accuracy of Second-Order Cone AC Optimal Power Flow by Convex Approximations, The International Conference on Innovative Smart Grid Technologies Asia, Singapore, May 22-25, 2018 (Accepted).

- [C6]. Z. Yuan, M. R. Hesamzadeh. A Distributed Economic Dispatch Mechanism to Implement Distribution Locational Marginal Pricing, Power Systems Computation Conference, Dublin, Ireland, June 11-15, 2018 (Accepted).
- [C5]. Z. Yuan, M. R. Hesamzadeh. Applying Convex Optimal Power Flow to Distribution Locational Marginal Pricing, 21st Conference of the International Federation of Operational Research Societies, Québec City, Canada, July 17 - 21, 2017.
- [C4]. Z. Yuan, M. R. Hesamzadeh, Y. Cui, L. B. Tjernberg. Applying High Performance Computing to Probabilistic Convex Optimal Power Flow, International Conference on Probabilistic Methods Applied to Power Systems, Beijing, China, October 16 20, 2016.
- [C3]. Z. Yuan, M. R. Hesamzadeh. Implementing Zonal Pricing in Distribution Network: the Concept of Pricing Equivalence, IEEE Power and Energy Society General Meeting, Boston, USA, July 17 21, 2016.
- [C2]. Z. Yuan, M. R. Hesamzadeh. A Hierarchical Dispatch Structure for Distribution Network Pricing, 15th International Conference on Environment and Electrical Engineering, Rome, Italy, June 10 - 13, 2015.
- [C1]. M. Nilsson, L. Soder and Z. Yuan. Estimation of Power System Frequency Response based on Measured & Simulated Frequencies, IEEE Power and Energy Society General Meeting, Boston, USA, July 17 - 21, 2016.

Patents

- [P2]. Z. Yuan (Applicant and Co-Inventor), M. R. Hesamzadeh. Sequential Conic Programming Method to Solve Optimal Power Flow Problem, Sweden, 2016 (Submitted and in the Second Round Evaluation by Swedish Patent Office).
- [P1]. Z. Yuan (Applicant and Co-Inventor), M. R. Hesamzadeh. A Decomposition System to Solve AC Optimal Power Flow Problem, Sweden, 2016 (Submitted and in the Second Round Evaluation by Swedish Patent Office).

Curriculum Vitae

Zhao Yuan was born on 17th January, 1988 in Handan, People's Republic of China. From 2007 to 2011, he was studying towards the Bachelor degree majoring in Electrical Engineering at Hebei University of Technology (China). Zhao was awarded the National Second Prize in Contemporary Undergraduate Mathematical Contest in Modeling (CUMCM) by China Society for Industrial and Applied Mathematics in the year of 2010. From 2008 to 2010, the National Inspiring Scholarship was awarded to him for three consecutive years.

In 2014, Zhao obtained Double Master degree majoring in Electrical Engineering from Huazhong University of Science and Technology (China), and in Renewable Energy from ParisTech (France). He conducted the thesis internship at Mines ParisTech from March to September of 2013.

Zhao joined the Electricity Market Research Group (EMReG) of KTH as a PhD student under the program of Erasmus Mundus Joint Doctorate in Sustainable Energy Technologies and Strategies (SETS) in the September of 2014. Supervised by Dr. Mohammad Reza Hesamzadeh, he conducted research on power system optimization, distribution locational marginal pricing and renewable energy. The main research topic is the optimal power flow problem which is the fundamental mathematical model of power system operations. The joint research of Zhao Yuan, Dr. Mohammad Reza Hesamzadeh and Dr. Darryl Biggar lays the foundation of hierarchical economic dispatch mechanism which (1) solves the challenge of large-scale integration of distributed energy resources; (2) largely reduces the communication burden between transmission system operator (TSO) and distribution system operator (DSO); (3) provides an efficient parallel computation framework to calculate the distribution locational marginal price (DLMP). Zhao's research work contributes to two Sweden patents and fourteen scientific peer-reviewed publications.

From 2016 to 2017, Zhao visited the Institute for Research in Technology of Comillas pontifical University where Dr. Sonja Wogrin supervised his research. The research work result in two peer-reviewed publications which covers (1) wind power integration through voltage source converter based multi-terminal DC transmission system and flexible AC transmission system; (2) Power Synergy Hub to coordinate the energy dispatch of super grid across the continent.

Zhao's expertise includes optimization, power system operation, renewable energy integration and electricity market.

A Modified Benders Decomposition Algorithm to Solve Second-Order Cone AC Optimal Power Flow

Zhao Yuan, Student Member, IEEE, and Mohammad Reza Hesamzadeh, Senior Member, IEEE

Variables

Abstract—This paper proposes to speed up solving largescale second-order cone AC optimal power flow (SOC-ACOPF) problem by decomposition and parallelization. Firstly, we use spectral factorization to partition large power network to multiple subnetworks connected by tie-lines. Then a modified Benders decomposition algorithm (M-BDA) is proposed to solve the SOC-ACOPF problem iteratively. Taking the total power output of each subnetwork as the complicating variable, we formulate the SOC-ACOPF problem of tie-lines as the master problem and the SOC-ACOPF problems of the subnetworks as the subproblems in the proposed M-BDA. The feasibility and optimality (preserving the original optimal solution of the SOC-ACOPF model) of the proposed M-BDA are analytically and numerically proved. A GAMS grid computing framework is designed to compute the formulated subproblems of M-BDA in parallel. The numerical results show that the proposed M-BDA can solve large-scale SOC-ACOPF problem efficiently. Accelerated M-BDA by parallel computing converges within few iterations. The computational efficiency (reducing computation CPU time and computer RAM requirement) can be improved by increasing the number of partitioned subnetworks.

Index Terms—Optimal power flow, Network partitioning, Modified Benders decomposition, Feasibility and optimality proof, Parallel computing.

NOMENCLATURE

Nodes or Buses.

L	Lines.	
K	Networks.	
N_k	Nodes at subnet	twork k.
L_k	Lines at subnety	work k.
au	Tie-lines (lines	connecting different subnetworks).
N_{τ}	Nodes at the en	ds of tie-lines.
J	Iterations.	
Paran	neters:	
A_{nl}^+ ,	A_{nl}^-	Node to line incidence matrix.
X_l^{n}	766	Reactance of line l.
R_l		Resistance of line <i>l</i> .
G_n		Shunt conductance at bus n .
B_n		Shunt susceptance at bus n .
P_{d_n}		Active power demand at bus n .
Q_{d_n}		Reactive power demand at bus n .
K_l		Bound of active power loss of line l.
c_l		Partitioning cost of cutting line l .
C		Cost matrix of network partition.
$ar{n},ar{k}$		Cardinality of set N and set K .
$C_{d_n}^{P+}$	$C_{d_n}^{P-}, C_n^v, C_n^\theta$	Penalty cost parameters.

The authors are with Electricity Market Research Group (EMReG), Department of Electric Power and Energy Systems, School of Electrical Engineering. KTH Royal Institute of Technology, Stockholm, SE-10044, Sweden. Email: yuanzhao@kth.se, mrhesamzadeh@ee.kth.se

variables:	
p_n	Active power generation at bus n .
q_n	Reactive power generation at bus n .
p_{s_l}	Active power flow at the sending end of line l .
q_{s_l}	Reactive power flow at the sending end of line l .
p_{o_l}	Active power loss of line l .
q_{o_l}	Reactive power loss of line l .
v_n	Voltage magnitude at bus n (lower case).
v_{s_l}	Voltage at the sending end of line l (lower case).
v_{r_l}	Voltage at the receiving end of line l (lower case).
V_n	Voltage magnitude square at bus n (upper case).
V_{s_l}	Voltage at the sending end of line l (upper case).
V_{r_l}	Voltage at the receiving end of line l (upper case).
θ_l	Voltage phase angle difference of line l .
θ_{s_l}	Voltage phase angle at the sending end of line l .
$ heta_{r_l}$	Voltage phase angle at the receiving end of line l .
M	Network partition matrix.
$Cost^{M}$	Objective of master problem.
$Cost_{k,j}^{S}$	Objective of subnetwork k at iteration j .
$P_{k,j}^{sum}$	Total active power generation of subnetwork k
70,5	at iteration j
$Q_{k,j}^{sum}$	Total reactive power generation of subnetwork \boldsymbol{k}

I. INTRODUCTION

at iteration j

POWER network is, either historically or technically, partitioned into caveral and titioned into several zones or subnetworks to reduce the complexity of operation, control or planning tasks [1], [2]. For example, Nord Pool operates the electricity market of Sweden over four well-defined bidding areas from the north to the south [3]. Ten regions (California, MISO, New England, New York, Northwest, PJM, Southeast, Southwest, SPP and Texas) of the USA power system are separately operated by the corresponding independent system operators (ISOs) [4]. One fundamental technical reason of operating the power system by network partitions is that the dimension of the Hessian matrix and Jacobian matrix during the iterations of the optimization is reduced. It is then easier for the solver to address small-scale optimization problems. Another advantage of decentralized operation is that the optimal power flow (OPF) problems of multiple subnetworks can be solved in a parallel manner. In facing growing power network expansions and accelerating penetrations of distributed energy resources (DERs) which may exceed the capability of centralized operation, parallel and decentralized operation could be a feasible solution [5].

Early research about the feasibility, applicability and comparison of decentralized OPF algorithms using auxiliary problem principle (APP), the predictor-corrector proximal multiplier method and alternating direction method are proposed or

demonstrated by [6]-[8]. Decentralized approaches to solve the OPF problem also include Lagrangian relaxation [9], Benders decomposition (BD) [10], Dantzig-Wolfe decomposition [11] and Alternating Direction Method of Multipliers (ADMM) [12]. A comprehensive summary of distributed algorithms for optimization and control of power system can be found in [1]. Lagrangian relaxation approach relaxes the coupling constraints between the subnetworks and generally only approximated solutions can be guaranteed [9]. BD and Dantzig-Wolfe decomposition require to firstly formulate the master problem and subproblem, and then iterate until the solutions (of the master problem and subproblem) converge [10], [11]. BD is widely used to solve the security constrained unit commitment (SCUC) problem and transmission expansion planning (TEP) problem which are expanded applications of OPF [13]-[15]. In SCUC and TEP, mostly the integer variables are taken as the complicating variables to formulate the master problem and subproblem of BD [13]-[15]. Message exchanges among the subnetworks are required by ADMM [12]. Generally, when more subnetworks are partitioned, more iterations are required for ADMM to converge [12]. Reference [16] investigates three ADMM-based decentralized DCOPF solution algorithm with different communication strategies. It shows numerically that the convergence performance can be improved by enhancing the data exchange with the central controller (or coordinator). The network partitioning approach is also important for the convergence performance [16]. Authors in [17] solve the stochastic second-order cone programming (SOCP) based ACOPF by ADMM for radial distribution networks. The updates of the variables and multipliers are decomposed by each node and each scenario. As a result, it requires large number of iterations to converge (over 3000 iterations are required for a 50-node test case with 500 scenarios) [17]. Using ADMM, a comprehensive investigation of decomposing nonconvex ACOPF down to the individual node level is conducted by [5]. The results show that convergence speed of ADMM largely depends on test cases. The nonconvexity of ACOPF also requires a suitable selection of the penalty factors of ADMM to guarantee the convergence [5]. Reference [18] proposes a parametric quadratic programming approach to solve the regional correction equation in the proposed fully distributed interior point method (F-DIPM) to solve ACOPF. The power network is partitioned to several regions geographically. Then boundary variables associated with the tie-lines are duplicated for each region. A unidirectional ring communication is employed to transmit the information about boundary variables during each Newton-Raphson iteration. Various test cases show the robust convergence of F-DIPM. Authors in [19] use ADMM to solve the semi-definite rogramming (SDP) based relaxed ACOPF model for the formulated unbalanced microgrid. The fast convergence of ADMM over sub-gradient based method is demonstrated by test cases of the IEEE37-node feeder partitioned to four areas and a 10-node microgrid partitioned to three areas in [19]. As a improvement, we consider much larger power networks in this paper. By deriving and proving the closed form solutions for the OPF subproblems, [20] speed up the convergence of ADMM for radial distribution networks. Both mesh and radial power

networks are addressed in this paper.

Graph theory shows that the network-partitioning problem is NP-hard [21], [22]. Accordingly, various heuristic approaches such as geometric approach and flow-based approach have been proposed to solve the network-partitioning problem [21]. Authors in [23] define the electrical distance based on the network admittance parameter and then use it as a measure to distinguish strongly connected buses from weakly connected buses. The electrical distance between the buses within each partitioned zone are minimized while the electrical distance between buses of different partitioned zones are maximized in the multi-attribute network partitioning problem [23]. Reference [2] improves the Modularity Index in the communitydetection based network-partition algorithm such that both network topology and reactive power capability are taken into account. The goal in [2] is to control the zonal voltage of distribution network using a parallel processing approach. Authors in [24] show promising advantages of solving ACOPF by decomposing the optimality conditions. The effects of network partitioning on the computation efficiency are also investigated in [24]. However, the proposed intelligent network partitioning method in [24] requires to first solve the ACOPF problem. Considering the complexity of different networkpartitioning methods, we use spectral factorization [25] to partition the power networks in this paper.

Two challenges can be identified to solve the large-scale SOC-ACOPF problem in a decentralized way: (1) How to decompose the problem efficiently? The problem-decomposition algorithm should be computationally fast; (2) How to efficiently coordinate the objectives of the decomposed subproblems such that the final solutions converge to global optimality? Here, the global optimality means the SOC-ACOPF problem is solved in a single programming model. Accordingly, the main contributions of this paper are:

- A modified Benders decomposition algorithm (M-BDA) based on network partitions is proposed for solving large-scale SOC-ACOPF problem. The computation is accelerated by parallel computing;
- 2) The feasibility of the proposed M-BDA is analytically and numerically proved. Since the proposed M-BDA is modified from the original Benders decomposition, the feasibility proof of M-BDA is provided. We also prove that the original optimal solution of the SOC-ACOPF model is preserved by the proposed M-BDA.

The proposed solution algorithm (based on network partitions, M-BDA and parallel computing) provides an efficient framework to speed up large-scale SOC-ACOPF computations. As an important contribution, there is no message exchange requirement among the subnetworks in the proposed approach. Our decomposition approach also requires few number of iterations to converge for the test cases in this paper and it is robust to the number of partitioned subnetworks. The rest of this paper is organized as follows. Section II explains the SOC-ACOPF model. Section III presents the network partitioning approach based on spectral factorization. Section IV details the formulations of M-BDA. The feasibility and optimality of the formulated master problem and subproblem in M-

BDA is analytically proved. The parallel computing structure to accelerate the proposed M-BDA is also designed in this section. Section V discusses numerical results for various IEEE test cases and power network partitions. The power network partitions based on spectral factorization are also plotted. Section VI concludes.

II. THE SOC-ACOPF MODEL

The SOC-ACOPF model, as a convex relaxation of the nonconvex ACOPF model, is summarized here in (1) [26]. The convexity, accuracy and applicability of this model have been proved by our work in [26]. The objective function (1a)

been proved by our work in [26]. The objective function (1a) can be any convex function of the decision variables.
$$\begin{aligned} & \text{Minimize} \quad f(p_n,q_n,p_{o_l},q_{o_l}) & \text{(1a)} \\ & \text{subject to} \\ & p_n-P_{d_n}=\sum_l (A_{nl}^+p_{s_l}-A_{nl}^-p_{o_l})+G_nV_n, \ \forall n\in N \ \ \text{(1b)} \\ & q_n-Q_{d_n}=\sum_l (A_{nl}^+q_{s_l}-A_{nl}^-q_{o_l})-B_nV_n, \ \forall n\in N \ \ \text{(1c)} \\ & K_l\geq p_{o_l}\geq \frac{p_{s_l}^2+q_{s_l}^2}{V_{s_l}}R_l, \ \forall l\in L \ \ \ \text{(1d)} \end{aligned}$$

$$p_{o_l} X_l = q_{o_l} R_l, \ \forall l \in L$$
 (1e)

$$V_{s_l} - V_{r_l} = 2R_l p_{s_l} + 2X_l q_{s_l} - R_l p_{o_l} - X_l q_{o_l}, \ \forall l \in L \ (1f)$$

$$\begin{split} z_{h_{l}} &= X_{l}p_{s_{l}} - R_{l}q_{s_{l}}, \ \forall l \in L \\ z_{h_{l}} &\geqslant v_{m_{l}}^{min}z_{\theta_{l}} + z_{\theta_{l}}^{min}v_{m_{l}} - v_{m_{l}}^{min}z_{\theta_{l}}^{min}, \ \forall l \in L \\ z_{h_{l}} &\geqslant v_{m_{l}}^{max}z_{\theta_{l}} + z_{\theta_{l}}^{max}v_{m_{l}} - v_{m_{l}}^{max}z_{\theta_{l}}^{max}, \ \forall l \in L \\ z_{h_{l}} &\leqslant v_{m_{l}}^{min}z_{\theta_{l}} + z_{\theta_{l}}^{max}v_{m_{l}} - v_{m_{l}}^{max}z_{\theta_{l}}^{max}, \ \forall l \in L \\ z_{h_{l}} &\leqslant v_{m_{l}}^{min}z_{\theta_{l}} + z_{\theta_{l}}^{min}v_{m_{l}} - v_{m_{l}}^{min}z_{\theta_{l}}^{max}, \ \forall l \in L \\ z_{h_{l}} &\leqslant v_{m_{l}}^{max}z_{\theta_{l}} + z_{\theta_{l}}^{min}v_{m_{l}} - v_{m_{l}}^{min}z_{\theta_{l}}^{min}, \ \forall l \in L \\ v_{m_{l}} &\geqslant v_{s_{l}}^{min}v_{r_{l}} + v_{r_{l}}^{min}v_{s_{l}} - v_{s_{l}}^{min}v_{r_{l}}^{min}, \ \forall l \in L \\ v_{m_{l}} &\geqslant v_{s_{l}}^{min}v_{r_{l}} + v_{r_{l}}^{max}v_{s_{l}} - v_{s_{l}}^{max}v_{r_{l}}^{max}, \ \forall l \in L \\ v_{m_{l}} &\geqslant v_{s_{l}}^{min}v_{r_{l}} + v_{r_{l}}^{max}v_{s_{l}} - v_{s_{l}}^{min}v_{r_{l}}^{max}, \ \forall l \in L \\ v_{m_{l}} &\geqslant v_{s_{l}}^{min}v_{r_{l}} + v_{r_{l}}^{max}v_{s_{l}} - v_{s_{l}}^{min}v_{r_{l}}^{max}, \ \forall l \in L \\ v_{m_{l}} &\geqslant v_{s_{l}}^{min}v_{r_{l}} + v_{r_{l}}^{max}v_{s_{l}} - v_{s_{l}}^{min}v_{r_{l}}^{max}, \ \forall l \in L \\ v_{m_{l}} &\geqslant v_{s_{l}}^{min}v_{r_{l}} + v_{r_{l}}^{max}v_{s_{l}} - v_{s_{l}}^{min}v_{r_{l}}^{max}, \ \forall l \in L \\ v_{m_{l}} &\geqslant v_{s_{l}}^{min}v_{r_{l}} + v_{r_{l}}^{max}v_{s_{l}} - v_{s_{l}}^{min}v_{r_{l}}^{max}, \ \forall l \in L \\ v_{m_{l}} &\geqslant v_{s_{l}}^{min}v_{r_{l}} + v_{r_{l}}^{max}v_{s_{l}} - v_{s_{l}}^{min}v_{r_{l}}^{max}, \ \forall l \in L \\ v_{m_{l}} &\geqslant v_{s_{l}}^{min}v_{r_{l}}^{min}v_{$$

$$z_{h_l} \geqslant v_{m_l}^{min} z_{\theta_l} + z_{\theta_l}^{min} v_{m_l} - v_{m_l}^{min} z_{\theta_l}^{min}, \ \forall l \in L$$
 (1h)

$$z_{h_l} \geqslant v_{m_l}^{max} z_{\theta_l} + z_{\theta_l}^{max} v_{m_l} - v_{m_l}^{max} z_{\theta_l}^{max}, \ \forall l \in L$$
 (1i)

$$z_{h_l} \leqslant v_{m_l}^{min} z_{\theta_l} + z_{\theta_l}^{max} v_{m_l} - v_{m_l}^{min} z_{\theta_l}^{max}, \forall l \in L$$
 (1j)

$$z_{h_l} \leqslant v_{m_l}^{max} z_{\theta_l} + z_{\theta_l}^{min} v_{m_l} - v_{m_l}^{max} z_{\theta_l}^{min}, \ \forall l \in L$$
 (1k)

$$v_{m_l} \geqslant v_{s_l}^{min} v_{r_l} + v_{r_l}^{min} v_{s_l} - v_{s_l}^{min} v_{r_l}^{min}, \ \forall l \in L$$
 (11)

$$v_{m_l} \geqslant v_{s_l}^{max} v_{r_l} + v_{r_l}^{max} v_{s_l} - v_{s_l}^{max} v_{r_l}^{max}, \ \forall l \in L$$
 (1m)

$$v_{m_l} \leqslant v_{s_l}^{min} v_{r_l} + v_{r_l}^{max} v_{s_l} - v_{s_l}^{min} v_{r_l}^{max}, \forall l \in L$$

$$\tag{1n}$$

$$v_{m_l} \leqslant v_{s_l}^{max} v_{r_l} + v_{r_l}^{min} v_{s_l} - v_{s_l}^{max} v_{r_l}^{min}, \ \forall l \in L$$
 (10)

$$\begin{aligned} &v_{m_l} \leqslant v_{s_l} &v_{r_l} + v_{r_l} &v_{s_l} - v_{s_l} &v_{r_l} \\ &v_{m_l} \leqslant v_{s_l}^{max} v_{r_l} + v_{r_l}^{min} v_{s_l} - v_{s_l}^{max} v_{r_l}^{rin}, \ \forall l \in L \end{aligned} \qquad (10)$$

$$&z_{\theta_l} \geqslant cos(\frac{\theta_l^{max}}{2})(\theta_l + \frac{\theta_l^{max}}{2}) - sin(\frac{\theta_l^{max}}{2}), \ \forall l \in L \end{aligned} \qquad (12)$$

$$&z_{\theta_l} \leqslant cos(\frac{\theta_l^{max}}{2})(\theta_l - \frac{\theta_l^{max}}{2}) + sin(\frac{\theta_l^{max}}{2}), \ \forall l \in L \end{aligned} \qquad (12)$$

$$z_{\theta_l} \leqslant cos(\frac{\theta_l^{max}}{2})(\theta_l - \frac{\theta_l^{max}}{2}) + sin(\frac{\theta_l^{max}}{2}), \ \forall l \in L \quad (1q)$$

$$V_n \ge v_n^2, \ \forall n \in N$$
 (1r)

$$V_n \le (v_n^{max} + v_n^{min})v_n - v_n^{max}v_n^{min}, \ \forall n \in \mathbb{N}$$
 (1s)

$$V_n^{min} \le V_n \le V_n^{max}, \forall n \in \mathbb{N}$$

$$V_n^{min} \le V_n \le V_n^{max}, \forall n \in \mathbb{N}$$

$$V_n^{min} \le V_n^{max}, \forall n \in \mathbb{N}$$

$$p_n^{min} \le p_n \le p_n^{max}, \ \forall n \in N$$
 (1u)
$$q_n^{min} \le q_n \le q_n^{max}, \ \forall n \in N$$
 (1v)

$$q_n^{min} < q_n < q_n^{max}, \ \forall n \in N$$
 (1v)

Where $\Omega = \{p_n, q_n, p_{s_l}, q_{s_l}, p_{o_l}, q_{o_l}, V_n, \theta_l\} \in \Re$ is the set of decision variables. z_{h_l} , z_{θ_l} and v_{m_l} are the introduced auxiliary variables to derive the SOC-ACOPF model. Equations (1b) and (1c) represent the active and reactive power balance. A_{nl}^+ and A_{nl}^- are incidence matrix of the network with $A_{nl}^+=1$, $A_{nl}^-=0$ if n is the sending end of line l and $A_{nl}^+=-1$, $A_{nl}^-=1$ if n is the receiving end of line l. Constraints (1d)-(1e) represent active power and reactive power loss. Constraint (1d) is the convex relaxation of the active power loss by rotated cone. The left side of (1d) bounds p_{o_l} (which equivalently bounds capacity of line l). $V_{s_l} = v_{s_l}^2$ and $V_{r_l}=v_{r_l}^2$ are voltage magnitude squares. $\theta_l=\theta_{s_l}^2-\theta_{r_l}^3$ is the voltage phase angle difference of line l. Constraints (1g)-(1s) are convex hulls of the nonconvex AC power flow constraint $v_{s_l}v_{r_l}$ sin $\theta_l=X_lp_{s_l}-R_lq_{s_l}$. (1g)-(1s) are valid for $0<\theta_l^{max}<\frac{\pi}{2}$ and positive V_n^{min},V_n^{max} parameters. Note the term s in $p_{s_l}, q_{s_l}, v_{s_l}, V_{s_l}$ is not an index but only to imply the meaning of sending end of line l. The term r in v_{r_l}, V_{r_l} is not an index but only to imply the meaning of receiving end of line l. The term d in P_{d_n} , Q_{d_n} is not an index but only to imply the meaning of power demand. Similar reasoning holds for the term o in p_{o_l}, q_{o_l} which is to denote the meaning of power loss, the term h in z_{h_l} which is to denote the meaning of convex hull, the term θ in z_{θ} , which is to denote the meaning of auxiliary variable related to phase angle, and the term m in v_{m_l} which is to denote the meaning of auxiliary variable related to voltage. Compared with the SOCP-based ACOPF model in [27] which is valid for only radial power networks (since the model does not include constraints related with voltage phase angle variables), our model (1) is valid for both mesh and radial power networks. In section V of this paper, we give numerical comparisons and more explanations of our SOC-ACOPF model and the model in [27].

III. POWER NETWORK PARTITIONING

Power network topology can be always equivalently represented by a graph G = (N, L) with a vertex set N denoting the nodes or buses and an edge set L denoting the lines or branches. This implies we can use graph-partitioning algorithms to partition a power network. A \bar{k} partition of N defines \bar{k} disjoint subsets of N as $P = \{N_1, N_2, ..., N_{\bar{k}}\}$. If the partitioning cost of cutting line l (allocating the ends of the line to two separate subnetworks) is c_l , the total cost of partition P is $C(P) = \sum_{l \in \tau} c_l$ where τ is the set of lines with nodes belonging to different subnetworks i.e. the set of tie-lines. Higher c_l means higher possibility that line l is to be kept in one subnetwork (if we minimize the total cost of partitioning). There can be various strategies to set c_l . If all c_l parameters are equal, the network partitioning algorithm will result in least number of tie-lines. In this paper, we set $c_l = 1$ for all lines in order to obtain minimal number of tie-lines after the network partitioning. The network partitioning problem is formulated in (2) [25]:

Maximize
$$trace\left(M^{T}CM\right)$$
 (2a)

subject to
$$\|M\|_F = \sqrt{\bar{n}}$$
 (2b)

$$M^T M \le \epsilon I_{\bar{k}\bar{k}} \tag{2c}$$

$$M_{nk} \in \{0,1\}, n = 1,...,\bar{n}, k = 1,...,\bar{k}$$
 (2d)

where M is $\bar{n} \times \bar{k}$ orthogonal \bar{k} -partition matrix with $M_{nk} =$ 1 if $n \in N_k$ and $M_{nk} = 0$ if $n \notin N_k$. $||M||_F =$ $\sqrt{trace(M^TM)}$ is Frobenius norm. Constraint (2b) is valid because M is a \bar{k} -partition matrix if and only if each row of M is the canonical basic of R^k [25]. C is the $\bar{n} \times \bar{n}$ cost matrix of the network. $C_{in} = c_l$ if i and n are the connecting nodes of line l. $C_{in} = 0$ if i and n are not the connecting nodes of line l. The $I_{\bar{k}\bar{k}}$ is $\bar{k}\times\bar{k}$ unit matrix. Constraint

(2c) models an ϵ -bounded partition (the maximum number of nodes of all subnetworks to be partitioned is ϵ). $C, I_{\bar{k}\bar{k}}$ and ϵ are the parameters of optimization problem (2). The objective is to minimize the total cost of partitioning. This is valid because $C(P) = I_{\bar{n}}^T C I_{\bar{n}} - trace (M^T C M)$ [25]. The network partitioning problem (2) can be solved approximately by the spectral factorization algorithm proposed in [25]. We show in Section V that even by using the approximated solutions of network partitioning problem (2), the computation efficiency of SOC-ACOPF can still be improved. Please note by using this power network partitioning algorithm, we are not re-organizing the current operational setting of geographically partitioned power network which already exists. This power network partitioning algorithm is executed in the computer and the aim is to solve large-scale SOC-ACOPF problem more efficiently when centralized solution approach requires much computational time and computer RAM capacity.

IV. PROPOSING M-BDA AND THE PARALLEL COMPUTING

The SOC-ACOPF model explained in Section II is used here to formulate the M-BDA. The key contribution is that we decompose SOC-ACOPF by taking the total power generation of each subnetwork as the complicating variable in formulating the proposed M-BDA. This formulation shows very fast convergence performance. We first decompose the large-scale power network to \bar{k} subnetworks using the power network partitioning algorithm described in Section III. The SOC-ACOPF of each subnetwork is taken as a subproblem in the proposed M-BDA. The subproblem k of the proposed M-BDA is formulated in (3).

$$\begin{split} Cost_{k,j}^S &= \text{Minimize} \sum_{\forall n \in N_k, l \in L_k} f(p_{g_n}, q_{g_n}, p_{o_l}, q_{o_l}) & \text{(3a)} \\ &\text{subject to } (1b) - (1v), \, \forall n \in N_k, l \in L_k & \text{(3b)} \\ &\sum_{n \in N_k} p_n = P_{k,j}^{sum} : \mu_{k,j}^P, \, \forall k \in K, j \in J \\ &\sum_{n \in N_k} q_n = Q_{k,j}^{sum} : \mu_{k,j}^Q, \, \forall k \in K, j \in J \end{split}$$

Where (3b) refers to the power flow constraints for all lines and nodes located in subnetwork k. N_k and L_k are the sets of nodes and lines located in the subnetwork k. $P_{k,j}^{sum}$ and $Q_{k,j}^{sum}$ are the solutions of subnetwork total power generation from the master problem of the proposed M-BDA in iteration j. $\mu_{k,j}^P$ and $\mu_{k,j}^Q$ are the dual variables for corresponding constraints used for constructing Benders cuts. To guarantee the feasibility of all the subproblems in M-BDA, we allow load increments or decrements for all the nodes in the network. Thus the power balance constraints (1b)-(1c) in (3b) are modified as:

$$p_{n} - P_{d_{n}} = \Delta P_{d_{n}}^{+} - \Delta P_{d_{n}}^{-} + \sum_{l \in L_{k}} (A_{nl}^{+} p_{s_{l}} - A_{nl}^{-} p_{o_{l}})$$

$$+ G_{n} V_{n}, \ \forall n \in N_{k}, l \in L_{k}$$

$$q_{n} - Q_{d_{n}} = \Delta Q_{d_{n}}^{+} - \Delta Q_{d_{n}}^{-} + \sum_{l \in L_{k}} (A_{nl}^{+} q_{s_{l}} - A_{nl}^{-} q_{o_{l}})$$

$$- B_{n} V_{n}, \ \forall n \in N_{k}, l \in L_{k}$$
(3f)

Where non-negative variables $\Delta P_{d_n}^+$ and $\Delta Q_{d_n}^+$ are the load increments. Non-negative variables $\Delta P_{d_n}^-$ and $\Delta Q_{d_n}^-$ are the load decrements. The load increments and decrements are penalized in the objective function using the penalty parameters $C_{d_n}^{P^+}$, $C_{d_n}^{P^-}$, $C_{d_n}^{Q^+}$ and $C_{d_n}^{Q^-}$. Note the solutions of tieline variables are obtained by solving the formulated master problem (4) of M-BDA. To force the solutions of tie-line voltage variables to be same as the solutions from the master problem (4), we also include penalty terms for the tie-line voltage variables in the objective function of the subproblem. C_n^v , C_n^θ are positive penalty parameters. Minimizing quadratic objective function over a convex feasible region is a convex optimization problem. This is formulated as:

$$\begin{split} Cost_{k,j}^{S} = & \operatorname{Minimize} \sum_{\forall n \in N_{k}, l \in L_{k}} f(p_{n}, q_{n}, p_{o_{l}}, q_{o_{l}}) \\ &+ \sum_{n \in N_{k}} (C_{d_{n}}^{P+} \Delta P_{d_{n}}^{+} + C_{d_{n}}^{P-} \Delta P_{d_{n}}^{-} \\ &+ C_{d_{n}}^{Q+} \Delta Q_{d_{n}}^{+} + C_{d_{n}}^{Q-} \Delta Q_{d_{n}}^{-}) \\ &+ \sum_{n \in N_{k} \cap N_{r}, j \in J} [C_{n}^{v} (v_{n} - v_{n,j}^{M})^{2} \\ &+ C_{n}^{\theta} (\theta_{n} - \theta_{n,j}^{M})^{2}] \end{split} \tag{3g}$$

Where $v_{n,j}^M, \theta_{n,j}^M$ are the voltage and phase angle solutions from the master problem (4) at iteration j. Although some load increments or decrements may exist at the beginning of the iterations, the final solution of the proposed M-BDA does not have these increments or decrements. This is because the cost of these increments and decrements are very high and they will iteratively converge to zero. Our simulations show that this method is more efficient to guarantee the feasibility of the subproblems than using the feasibility cut approach in the original Benders decomposition (the MOSEK solver can not converge after several hours for the test cases in our paper when using the original feasibility cut approach. we believe the numerical failure of MOSEK using the original Benders feasibility cuts approach is because the infeasible region of the SOC-ACOPF is very complex and hard to be removed by the feasibility cuts)

The master problem of the proposed M-BDA is formulated in (4):

$$Minimize \ Cost^M = \sum_{k \in K} Cost_k^S \tag{4a}$$

subject to
$$(1b) - (1v), \forall l \in \tau$$
 (4b)

$$Cost_{k}^{S} \ge Cost_{k,j-1}^{S} + \mu_{k,j-1}^{P} \left(P_{k,j}^{sum} - P_{k,j-1}^{sum} \right) + \mu_{k,j-1}^{Q} \left(Q_{k,j}^{sum} - Q_{k,j-1}^{sum} \right), \forall k \in K, j \in J$$
 (4c)

Where (4b) refers to the power flow constraints of all the tie-lines. $P_{k,j-1}^{sum}$ and $Q_{k,j-1}^{sum}$ are the decisions of the previous iteration which are considered as parameter in the current iteration. The decisions of $P_{k,j}^{sum}$ and $Q_{k,j}^{sum}$ are made in the master problem (4) by considering the expanding Benders cuts (4c) and tie-line constraints (4b). We model each subnetwork as a single virtual node in the master problem. This is conceptually illustrated in Fig. 2, 3 and 4 in Section V. Constraints (4c) are Benders cuts from the subproblems.

 $\mu^P_{k,j-1}$ and $\mu^Q_{k,j-1}$ are dual variable solutions of equations (3c)-(3d) in subnetwork k at the previous iteration j-1. As the iterations proceed, more Benders cuts from solving the subproblems are iteratively included into the master problem. After solving the master problem, all the subproblems can be solved in parallel. The proposed parallel computing structure using the proposed M-BDA is illustrated in Fig. 1. The master problem is responsible for giving solutions of tie-line power flows and lower bound of the objective function. The solutions of subnetwork power flows and upper bound of the objective function are given by the subproblems. There is no communication requirement between the subproblems. In each iteration, firstly the master problem is solved and then all the subproblems are solved in parallel. Since we assign the same partitioning cost c_i to all lines, the number of tielines of the network partitions are minimized which in turn minimizes the size of the master problem. We summarize the parallel computing management algorithm in Algorithm 1. The parallelization of the subproblems include one Parallel Loop which generates threads of all the subproblems and one Collect Loop which repeatedly checks the status of the threads and stores the solutions when available. To avoid overloading of the computer disk capacity, the subproblem thread Thread-k is released after the solutions are collected.

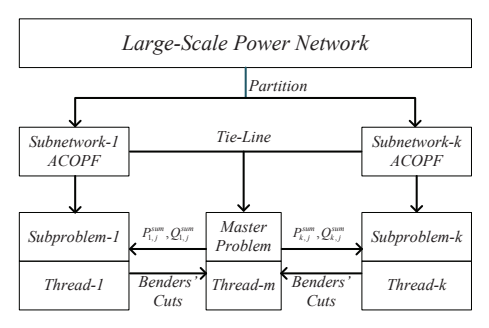


Fig. 1. The proposed parallel computing structure using M-BDA

Theorem 1. If the original SOC-ACOPF model (without decomposition) is feasible, the formulated master problem (4) of the proposed M-BDA is feasible.

Proof. We prove theorem 1 by mathematical induction. We prove firstly the formulated master problem (4) is feasible at iteration j = 1. Afterwards, we prove for any iteration $j' \in J$, if the formulated master problem (4) is feasible for j = j'then it is feasible for the next iteration j = j' + 1.

Step 1: The formulated master problem (4) is feasible for j=1. We prove this by constructing one feasible solution for the formulated master problem (4) of the proposed M-BDA. Assume $\Omega_0 = \{p_{n,0}, q_{n,0}, p_{s_{l,0}}, q_{s_{l,0}}, p_{o_{l,0}}, q_{o_{l,0}}, v_{n,0}, \theta_{l,0}\} \in$ R is one feasible solution of the original SOC-ACOPF model, Ω_0 is also feasible for constraints (4b) in the master problem (4) of the proposed M-BDA. Note it is not necessarily required that the feasible solution Ω_0 is optimal for the original SOC-ACOPF model.

We construct the feasible solution $P_{k,j,0}^{sum}, Q_{k,j,0}^{sum}, P_{k,j-1,0}^{sum}$

```
Algorithm 1: Parallel Computing Management Algorithm
 Initialization: j = 1;
     Generate SOC-ACOPF model (4) for the tie-lines:
      SOC-ACOPF-Master;
      Assign SOC-ACOPF-Master to Thread-m;
     Execute Thread-m;
     Broadcast P_{k,j}^{sum} and Q_{k,j}^{sum} to Thread-k for k \in K;
         Generate SOC-ACOPF model (3) for the
          subnetwork-k: SOC-ACOPF-k;
         Assign SOC-ACOPF-k to Thread-k;
         k = k + 1;
     while k < k^{max};
         if thread-k is ready then
            Collect Solutions from Thread-k;
     Send Cost_{k,j}^S, \mu_{k,j}^P and \mu_{k,j}^Q to Thread-m; Release Thread-k; while SOC\text{-}ACOPF thread is nonempty;
     j = j + 1;
 Release Thread-m;
```

and $Q_{k,j-1,0}^{sum}$ as:

$$P_{k,j,0}^{sum} = \sum p_{n,0}$$
 (5a)

$$Q_{k,j,0}^{sum} = \sum_{k,j} q_{n,0}$$
 (5b)

$$P_{k,j-1,0}^{sum} = \sum_{i} p_{n,0}$$
 (5c)

$$\begin{split} P_{k,j,0}^{sum} &= \sum_{n \in N_k} p_{n,0} & \text{(5a)} \\ Q_{k,j,0}^{sum} &= \sum_{n \in N_k} q_{n,0} & \text{(5b)} \\ P_{k,j-1,0}^{sum} &= \sum_{n \in N_k} p_{n,0} & \text{(5c)} \\ Q_{k,j-1,0}^{sum} &= \sum_{n \in N_k} q_{n,0} & \text{(5d)} \end{split}$$

If we use $\Omega_0, P_{k,j,0}^{sum}, Q_{k,j,0}^{sum}, P_{k,j-1,0}^{sum}$ and $Q_{k,j-1,0}^{sum}$, then constraint (4c) becomes:

$$\begin{split} Cost_{k}^{S} &\geq Cost_{k,j-1}^{S} + \mu_{k,j-1}^{P} \left(P_{k,j,0}^{sum} - P_{k,j-1,0}^{sum} \right) \\ &+ \mu_{k,j-1}^{Q} \left(Q_{k,j,0}^{sum} - Q_{k,j-1,0}^{sum} \right), \, \forall k \in K \end{split} \tag{5e}$$

Which is:

$$Cost_k^S \ge Cost_{k,j-1}^S, \, \forall k \in K$$
 (5f)

No matter what values $\mu_{k,j-1}^P$ and $\mu_{k,j-1}^Q$ are chosen at j=1, constraint (5f) is always feasible since we do not have upper bound for $Cost_k^S$. The feasible objective solution is:

$$Cost^{M,0} = Min[\sum_{k \in K} Cost_k^S] = \sum_{k \in K} Cost_{k,j-1}^S \qquad \textbf{(5g)}$$

Which is actually the lower bound of the non-negative term $\sum_{k \in K} Cost_{k,j-1}^{S}$. Thus we successfully construct a feasible solution of the master problem as $\Omega_0, P_{k,j,0}^{sum}, Q_{k,j,0}^{sum}$ with objective value of $Cost^{M,0}$. This means the master problem is feasible for j = 1.

Step 2: If the formulated master problem (4) is feasible for j = j', then it is feasible for j = j' + 1. We prove this step by showing that there is at least one feasible solution for iteration j = j' + 1 which can always be constructed by using the feasible solution for $j=j^{'}$. Suppose one feasible solution for iteration $j=j^{'}$ is $\Omega_{j^{'}}, P_{k,j^{'},0}^{sum}, Q_{k,j^{'},0}^{sum}$ with master problem

and subproblem objective values as $Cost^{M,j^{'},0}, Cost_{k}^{S,j^{'},0}.$ We construct the feasible solution for $j = j^{'} + 1$ as:

$$\begin{split} P_{k,j'+1,0}^{sum} &= P_{k,j',0}^{sum} & \text{(5h)} \\ Q_{k,j'+1,0}^{sum} &= Q_{k,j',0}^{sum} & \text{(5i)} \end{split}$$

$$Q_{k,i'+1,0}^{sum} = Q_{k,i',0}^{sum} \tag{5i}$$

The added Benders cut at iteration j = j' + 1 is:

$$Cost_{k}^{S} \geq Cost_{k,j'}^{S} + \mu_{k,j'}^{P} \left(P_{k,j'+1,0}^{sum} - P_{k,j',0}^{sum} \right) + \mu_{k,j'}^{Q} \left(Q_{k,j'+1,0}^{sum} - Q_{k,j',0}^{sum} \right), \forall k \in K$$
 (5j)

Or equivalently:

$$Cost_k^S \ge Cost_{k,j'}^S, \forall k \in K$$
 (5k)

We show in following that no matter what value $Cost_{k}^{S}$ takes, we can always construct a feasible solution for the master problem (4). If there exists:

$$Cost_{k,i'}^{S} \ge Cost_{k}^{S,j',0}, \forall k \in K$$
 (51)

The feasible solution of $Cost_k^S$ for j = j' + 1 is $Cost_{k,j'}^S$. Accordingly, feasible objective solution is $Cost^{M,j'+1,0} =$ $\sum_{k \in K} Cost_{k,i'}^S$

Otherwise, if there exists $k \in K' \subset K$ such that:

$$Cost_{k,j'}^{S} \le Cost_{k}^{S,j',0}, \forall k \in K' \subset K$$
 (5m)

We replace these $Cost_k^S$ by $Cost_k^{S,j'}$,0 $(\forall k \in K' \subset K)$. The feasible solution of $Cost_k^S$ is $\left\{Cost_{k,j'}^S, \forall k \notin K' \subset K\right\} \cup$ $\left\{Cost_k^{S,j',0}, \forall k \in K' \subset K\right\}$. Accordingly, the feasible objection tive solution of the master problem (4) for iteration j = j' + 1

$$Cost^{M,j^{'}+1,0} = \sum_{k \notin K^{\prime} \subset K} Cost^{S}_{k,j^{'}} + \sum_{k \in K^{\prime} \subset K} Cost^{S,j^{'},0}_{k}$$
 (5)

Combining Step 1 and Step 2, we have proven that the formulated master problem (4) is always feasible as long as the original SOC-ACOPF model is feasible.

Theorem 2. If the original SOC-ACOPF model (without decomposition) is feasible, the necessary and sufficient condition for the feasibility of the formulated subproblem (3) of the

$$\sum_{n \in N_k} p_n^{min} \le P_{k,j}^{sum} \le \sum_{n \in N_k} p_n^{max}, \forall k \in K, j \in J \quad (6a)$$

$$\sum_{n \in N_k} p_n^{min} \le P_{k,j}^{sum} \le \sum_{n \in N_k} p_n^{max}, \forall k \in K, j \in J \qquad \text{(6a)}$$

$$\sum_{n \in N_k} q_n^{min} \le Q_{k,j}^{sum} \le \sum_{n \in N_k} q_n^{max}, \forall k \in K, j \in J \qquad \text{(6b)}$$

Proof. We firstly prove (6) is necessary for the feasibility of subproblem (3) i.e. if subproblem (3) is feasible then (6) holds. Suppose the feasible solution of subproblem (3) at iteration $j \in J \text{ is } \Omega_j = \{p_{n,j}, q_{n,j}, p_{s_{l,j}}, q_{s_{l,j}}, p_{o_{l,j}}, q_{o_{l,j}}, v_{n,j}, \theta_{l,j}\} \in$ \Re , from (3c)-(3d) of (3) we have:

$$\sum_{n \in N_k} p_{n,j} = P_{k,j}^{sum}, \, \forall k \in K, j \in J$$
 (7a)

$$\sum_{n \in N_k} q_{n,j} = Q_{k,j}^{sum}, \forall k \in K, j \in J$$
 (7b)

 Ω_i is feasible for constraints (4b) of (4), so:

$$p_n^{min} \le p_{n,j} \le p_n^{max}, \, \forall n \in N_k \tag{7c}$$

$$q_n^{min} \le q_{n,j} \le q_n^{max}, \, \forall n \in N_k$$
 (7d)

Obviously,

$$\sum_{n} p_n^{min} \le \sum_{n} p_{n,j} \le \sum_{n} p_n^{max}$$
 (7e)

$$\sum_{n \in N_k} p_n^{min} \le \sum_{n \in N_k} p_{n,j} \le \sum_{n \in N_k} p_n^{max}$$

$$\sum_{n \in N_k} q_n^{min} \le \sum_{n \in N_k} p_{n,j} \le \sum_{n \in N_k} q_n^{max}$$
(7e)

From (7a)-(7b) and (7e)-(7f), the expression (6) holds.

Next, we prove (6) is sufficient for the feasibility of subproblem (3) i.e. if (6) holds, subproblem (3) is feasible. Again, we assume $\Omega_0 = \{p_{n,0}, q_{n,0}, p_{s_{l,0}}, q_{s_{l,0}}, p_{o_{l,0}}, q_{o_{l,0}}, V_{n,0}, \theta_{l,0}\} \in$ \Re is one feasible solution of the original SOC-ACOPF model. Obviously, $\{p_{s_{l,0}}, q_{s_{l,0}}, p_{o_{l,0}}, q_{o_{l,0}}, v_{n,0}, \theta_{l,0}\}$ is feasible for constraints (1d)-(1v) in constraint (3b) of (3). The remaining constraints are (1b)-(1c) (which are modified as (3e)-(3f)) and (3c)-(3d). We construct the feasible solution of p_n, q_n at iteration j as $p_{n,j}, q_{n,j}$:

$$p_{n,j} = p_{n,0} + \Delta P_{d_n}^+ - \Delta P_{d_n}^-, \ \forall n \in N_k, l \in L_k \eqno(7\mathrm{g})$$

$$q_{n,j} = q_{n,0} + \Delta Q_{d_n}^+ - \Delta Q_{d_n}^-, \ \forall n \in N_k, l \in L_k$$
 (7h)

Substitute (7g)-(7h) in (3e)-(3f), we have:

$$\begin{aligned} p_{n,0} + \Delta P_{d_n}^+ - \Delta P_{d_n}^- - P_{d_n} &= \Delta P_{d_n}^+ - \Delta P_{d_n}^- + G_n V_{n,0} \\ &+ \sum_{l \in L_k} (A_{nl}^+ p_{s_{l,0}} - A_{nl}^- p_{o_{l,0}}), \, \forall n \in N_k, l \in L_k \end{aligned} \tag{7i}$$

$$q_{n,0} + \Delta Q_{d_n}^+ - \Delta Q_{d_n}^- - Q_{d_n} = \Delta Q_{d_n}^+ - \Delta Q_{d_n}^- - B_n V_{n,0} + \sum_{l \in L} (A_{nl}^+ q_{s_{l,0}} - A_{nl}^- q_{o_{l,0}}), \, \forall n \in N_k, l \in L_k \quad (7j)$$

Or equivalently:

$$\begin{split} p_{n,0} - P_{d_n} &= \sum_{l} (A_{nl}^+ p_{s_{l,0}} - A_{nl}^- p_{o_{l,0}}) \\ &+ G_n V_{n,0}, \ \forall n \in N_k, l \in L_k \\ q_{n,0} - Q_{d_n} &= \sum_{l} (A_{nl}^+ q_{s_{l,0}} - A_{nl}^- q_{o_{l,0}}) \\ &- B_n V_{n,0}, \ \forall n \in N_k, l \in L_k \end{split} \tag{71}$$

Which are feasible since Ω_0 is a feasible solution. To construct the feasible solutions of the power load increments or

decrements variables, we consider feasibility of the constraints

$$\sum_{n \in N_k} p_{n,j} = \sum_{n \in N_k} (p_{n,0} + \Delta P_{d_n}^+ - \Delta P_{d_n}^-)$$

$$= P_{k,j}^{sum}, \ \forall k \in K, j \in J$$

$$\sum_{n \in N_k} q_{n,j} = \sum_{n \in N_k} (q_{n,0} + \Delta Q_{d_n}^+ - \Delta Q_{d_n}^-)$$

$$= Q_{k,j}^{sum}, \ \forall k \in K, j \in J$$
(7n)

Since (6) holds, we can express $P_{k,j}^{sum}$ and $Q_{k,j}^{sum}$ as:

$$P_{k,j}^{sum} = \lambda_{k,j}^{P} \sum_{n} p_{n}^{max} + (1 - \lambda_{k,j}^{P}) \sum_{n} p_{n}^{min}$$
 (70)

$$\begin{split} P_{k,j}^{sum} &= \lambda_{k,j}^{P} \sum_{n \in N_{k}} p_{n}^{max} + (1 - \lambda_{k,j}^{P}) \sum_{n \in N_{k}} p_{n}^{min} \\ Q_{k,j}^{sum} &= \lambda_{k,j}^{Q} \sum_{n \in N_{k}} q_{n}^{max} + (1 - \lambda_{k,j}^{Q}) \sum_{n \in N_{k}} q_{n}^{min} \end{split} \tag{7p}$$

Where $0 \le \lambda_{k,j} \le 1$. Similarly, we can express $p_{n,0}, q_{n,0}$ as:

$$p_{n,0} = \lambda_{n,0}^{P} p_n^{max} + (1 - \lambda_{n,0}^{P}) p_n^{min}$$
 (7q)

$$q_{n,0} = \lambda_{n,0}^{Q} q_{n}^{max} + (1 - \lambda_{n,0}^{Q}) q_{n}^{min}$$
 (7r)

Where $0 \leq \lambda_{n,0} \leq 1$. By which we can construct the feasible solution of $\Delta P_{d_n}^+, \Delta P_{d_n}^-, \Delta Q_{d_n}^+$ and $\Delta Q_{d_n}^-$. If $\lambda_{k,j}^P \geq \lambda_{n,0}^P$ and $\lambda_{k,j}^Q \geq \lambda_{n,0}^Q$, we have:

$$\begin{split} \Delta P_{d_n}^+ &= (\lambda_{k,j}^P - \lambda_{n,0}^P)(p_n^{max} - p_n^{min}), \, \forall n \in N_k \\ \Delta P_{d_n}^- &= 0, \, \forall n \in N_k \end{split} \tag{7s}$$

$$\begin{split} &\Delta P_{d_n}^- = 0, \, \forall n \in N_k \\ &\Delta Q_{d_n}^+ = (\lambda_{k,j}^Q - \lambda_{n,0}^Q)(q_n^{max} - q_n^{min}), \, \forall n \in N_k \\ &\Delta Q_{\overline{d}_n}^- = 0, \, \forall n \in N_k \end{split} \tag{7u}$$

$$\Delta Q_{d_n}^+ = (\lambda_{k,j}^Q - \lambda_{n,0}^Q)(q_n^{max} - q_n^{min}), \ \forall n \in N_k$$
 (7u)

$$\Delta Q_{d_n}^- = 0, \, \forall n \in N_k \tag{7v}$$

Otherwise If $\lambda_{k,i}^P < \lambda_{n,0}^P$ or $\lambda_{k,i}^Q < \lambda_{n,0}^Q$, then:

$$\Delta P_{d_n}^+ = 0, \, \forall n \in N_k \tag{7w}$$

$$\Delta P_{d_n}^- = 0, \ \forall n \in N_k$$
 (7x)
$$\Delta P_{d_n}^- = (\lambda_{n,0}^P - \lambda_{k,j}^P)(p_n^{max} - p_n^{min}), \ \forall n \in N_k$$
 (7x)
$$\Delta Q_{d_n}^+ = 0, \ \forall n \in N_k$$
 (7y)

$$\Delta Q_{d_n}^+ = 0, \, \forall n \in N_k \tag{7y}$$

$$\Delta Q_d^- = (\lambda_{n,0}^Q - \lambda_{k,i}^Q)(q_n^{max} - q_n^{min}), \forall n \in N_k$$
 (7z)

(7s)-(7z) guarantee the non-negativity of $\Delta P_{d_n}^+, \Delta P_{d_n}^-, \Delta Q_{d_n}^+, \Delta Q_{d_n}^-, \quad \text{the feasibility of} \quad \text{(3c)-(3d)}$ (equality) as well as the feasibility of $p_{n,j}$ and $q_{n,j}$ expressed in (7g)-(7h) (satisfying the constraints (1u)-(1v)).

Theorem 3. If the original SOC-ACOPF model (without decomposition) is feasible and condition (6) holds, the optimal solution of the original SOC-ACOPF model is preserved by the proposed M-BDA.

Proof. Since the convergence of M-BDA is guaranteed by the convexity of the SOC-ACOPF model which has been proved by [10], the remaining task is to prove the convergent optimal solution of M-BDA is exactly the optimal solution of the original SOC-ACOPF model. The proof of Theorem 3 is straightforward based on the Theorem 1 and Theorem 2. Note we have actually proved in Theorem 1 that any feasible solution of the original SOC-ACOPF model is also feasible for the formulated master problem (4) of M-BDA. We denote the optimal solution of the original SOC-ACOPF model as $\Omega_*=\{p_{n,*},q_{n,*},p_{s_{l,*}},q_{s_{l,*}},p_{o_{l,*}},q_{o_{l,*}},V_{n,*},\theta_{l,*}\}\in\Re.$ Since Ω_* is also feasible for the original SOC-ACOPF model, we can set the feasible solutions Ω_0 used in the proof of Theorem

$$\Omega_0 = \Omega_*$$
 (8a)

Again, we can use mathematical induction to prove Ω_* is always feasible for the master problem (4). Firstly, we prove Ω_* is feasible for the master problem (4) at iteration j=1. According to the Step 1 of the proof for Theorem 1, if we set $\Omega_0 = \Omega_*$, we can construct the feasible solution $P_{k,j,*}^{sum}, Q_{k,j,*}^{sum}, P_{k,j-1,*}^{sum}$ and $Q_{k,j-1,*}^{sum}$ as:

$$P_{k,j,*}^{sum} = \sum_{n \in N} p_{n,*}$$
 (8b)

$$P_{k,j,*}^{sum} = \sum_{n \in N_k} p_{n,*}$$

$$Q_{k,j,*}^{sum} = \sum_{n \in N_i} q_{n,*}$$
(8b)

$$P_{k,j-1,*}^{sum} = \sum_{n \in N_k} p_{n,*}$$
 (8d)

$$P_{k,j-1,*}^{sum} = \sum_{n \in N_k} p_{n,*}$$

$$Q_{k,j-1,*}^{sum} = \sum_{n \in N_k} q_{n,*}$$
(8d)

Same reasoning through the $Step\ 1$ of the proof for Theorem 1, we can prove Ω_* , $P_{k,j,*}^{sum}$, $Q_{k,j,*}^{sum}$ is feasible for the master problem (4) at iteration j=1. Then we prove Ω_* is feasible for the master problem (4) at iteration j = j' + 1 if Ω_* is feasible at iteration j = j'. Since Ω_* is feasible at iteration j = j', at **Step 2** of the proof for Theorem 1, we can set:

$$\Omega_{s'} = \Omega_*$$
(8f)

$$P_{k,j',0}^{sum} = P_{k,j'+1,0}^{sum} = \sum_{n \in N_b} p_{n,*}$$
 (8g)

$$Q_{k,j',0}^{sum} = P_{k,j'+1,0}^{sum} = \sum_{n \in \mathbb{N}} q_{n,*}$$
 (8h)

Same reasoning through Step 2 of the proof for Theorem 1, we can prove Ω_* is feasible for the master problem (4) at iteration j = j' + 1. Up to now, we have proved Ω_* is always feasible for the master problem (4).

Next, we prove Ω_* is the optimal convergent solution of M-BDA by contradiction. Suppose the convergent solution of M-BDA is $\Omega_{\prime} \neq \Omega_{*}$. Since Ω_{*} is the optimal solution of the original SOC-ACOPF model, we have:

$$\sum_{k \in K} Cost_k^{S*} < \sum_{k \in K} Cost_k^{S'} = Cost^{M'}$$
 (8i)

Where $Cost_k^{S*}$ is the optimal objective solution for the subproblem (3) using Ω_* . $Cost_k^{S'}$ is the convergent optimal objective solution for the subproblem (3) using Ω . \hat{Cost}^M is the convergent optimal objective solution for the master problem (4). Because we have proved Ω_* is always feasible for the master problem (4) (and thus still feasible when M-BDA converges), and we know:

$$Cost^{M*} < Cost^{M'}$$
 (8j)

Where $Cost^{M*}$ is the feasible objective solution for the master problem (4) using Ω_* . Relationship expressed by (8j) contradicts with the assumption that $Cost^{M'}$ is the optimal objective solution of the master problem (4) $(\Omega_{\prime}$ is the convergent

optimal solution). Thus $\Omega' \neq \Omega_*$ cannot hold. The convergent optimal solution must be Ω_* . Note it is not required that Ω_* is feasible for all iterations of the subproblem (3). As long as the master problem (4) can converge to Ω_* and gives $P^{sum}_{k,j,*} = \sum_{n \in N_k} p_{n,*}, Q^{sum}_{k,j,*} = \sum_{n \in N_k} q_{n,*}$ as parameters to the subproblem (3) (in the final iterations of M-BDA), the final convergent optimal solution is Ω_* .

V. NUMERICAL RESULTS

All computations are run on a computer with 2.4GHz CPU and 8GB RAM. We use the power network data from MAT-POWER directly [28]. The network partitioning algorithm is implemented in MATLAB [25]. The GAMS Grid Computing Facility [29] is employed for implementing the proposed parallel computing.

A. Comparison of SOC-ACOPF models

To compare our SOC-ACOPF model with the SOCP-based ACOPF model in [27], we implement both models in GAMS and solve the models for various IEEE test cases by MOSEK solver. Note we implement the active power loss constraint (1d) in GAMS coding of the SOC-ACOPF model which is different from the implementation in our work in [26]. Accordingly, there are some minor numerical differences compared with the results in [26]. As benchmarks of the comparisons, we use the results from MATPOWER which gives local optimal solutions of the nonconvex ACOPF model and the results from LINDOGLOBAL solver in GAMS which can give global optimal solutions of the nonconvex ACOPF model. MATPOWER uses MATLAB built-in Interior Point Solver (MIPS) to solve nonconvex ACOPF. The LINDOGLOBAL solver employs branch-and-cut methods to find the global optimal solution. If a solution is not found, we denote the corresponding result as 'NA'.

The results are listed in Table I. For all test cases, our SOC-ACOPF model can give very close results compared with LINDOGLOBAL. Compared to MATPOWER and LIN-DOGLOBAL results, the objective value of IEEE14-bus from our SOC-ACOPF model is bit higher. The reason of this is that the voltage phase angle constraint $0 < \overline{\theta_l} < \frac{\pi}{2}$ is included in our SOC-ACOPF model (this constraint is required by the convex envelopes expressed by constraint (1g) to (1q)) while this is not necessary for the nonconvex ACOPF model in MATPOWER and GAMS solved by LINDOGLOBAL (the reason can also be due to numerical accuracy tolerance differences of different solvers). For IEEE300-bus, 1354pegase and 2869pegase, LINDOGLOBAL cannot solve these test cases since the model scale exceed the limit of LINDOGLOBAL. In these test cases, we compare the results with MATPOWER which are still very close to our results. It is worth to mention that the results of mesh power networks from the model in [27] are much relaxed solutions since this model does not include constraints related to voltage phase angle. It can be seen from the results in Table I that lower objective values are obtained from the model in [27] compared with our SOC-ACOPF model. However, less AC feasibility can be guaranteed from the solutions of the model in [27]. In terms of computation

time, the model in [27] requires the least computation time since this model has the least number of constraints. LIN-DOGLOBAL requires the most the computation time to find a global optimal solution. Our model takes less computation time than MATPOWER. Because we have included the voltage phase angle constraints (1g) to (1q) in our SOC-ACOPF model to make it valid for both mesh and radial power networks, the computation time is larger than the model in [27].

B. The power network partitioning

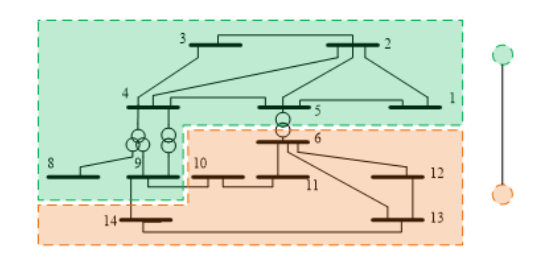


Fig. 2. IEEE14-bus network partitions (two subnetworks) and the master problem representation $\,$

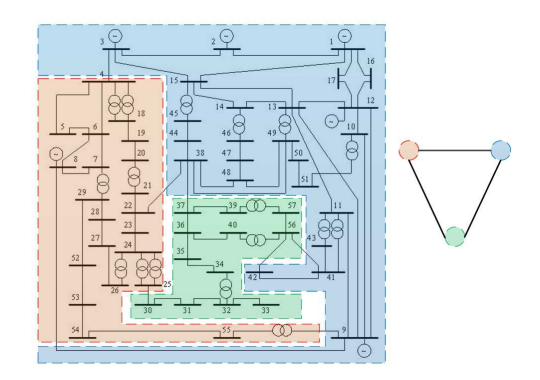


Fig. 3. IEEE57-bus network partitions (three subnetworks) and the master problem representation

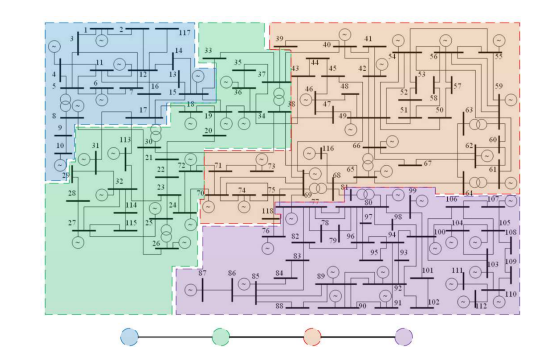


Fig. 4. IEEE118-bus network partitions (four subnetworks) and the master

1 Fansactions on Smart Grid

1 IEEE TRANSACTIONS ON SMART GRID

9

TABLE I COMPARISON OF SOC-ACOPF MODELS

Test Case		Objectiv	e Value [\$]		Computation CPU Time [s]			
Test Case	SOC-ACOPF	Model in [27]	MATPOWER	LINDOGLOBAL	SOC-ACOPF	Model in [27]	MATPOWER	LINDOGLOBAL
IEEE14-bus	8092.32	8072.42	8081.53	8081.54	0.09	0.08	0.11	0.20
IEEE57-bus	41711.78	41673.10	41737.79	41737.93	0.17	0.11	0.12	2.31
IEEE118-bus	129376.00	129330.74	129660.70	129660.54	0.36	0.13	0.30	27.10
IEEE300-bus	718546.27	718091.78	719725.11	NA	0.64	0.25	0.48	NA
1354pegase [30]	74040.99	74006.84	74069.35	NA	2.50	0.64	8.58	NA
2869pegase [30]	133934.70	133866.95	133999.29	NA	9.72	1.23	18.66	NA

TABLE II RESULTS OF POWER NETWORK PARTITIONING

Test Case	Partition	Number of Nodes in Subnetworks	Number of Lines in Subnetworks	Number of Tie-lines	CPU Time [s]
	2	6, 8	11, 6	3	0.02
	3	3, 5, 6	2, 7, 6	5	0.02
	4	4, 2, 3, 5	4, 1, 2, 7	6	0.03
IEEE14-bus	5	2, 2, 5, 3, 2	1, 1, 7, 2, 1	8	0.03
	6	3, 3, 2, 2, 2, 2	3, 3, 1, 1, 1, 1	10	0.03
	7	2, 1, 3, 2, 2, 1, 3	1, 0, 2, 1, 1, 0, 3	12	0.04
	8	3, 1, 2, 2, 1, 2, 2, 1	3, 0, 1, 1, 0, 0, 1, 0	14	0.05
	2	18, 39	19, 55	6	0.03
	3	12, 21, 24	12, 25, 35	8	0.03
	4	27, 11, 10, 9	38, 13, 10, 9	10	0.04
IEEE57-bus	5	11, 10, 7, 9, 20	11, 12, 6, 9, 29	13	0.04
	6	6, 7, 20, 8, 10, 6	6, 8, 29, 7, 12, 5	13	0.04
	7	7, 6, 10, 10, 9, 5, 10	7, 7, 12, 14, 7, 4, 10	19	0.05
	8	6, 9, 5, 7, 9, 4, 6, 11	5, 10, 6, 7, 9, 3, 5, 15	20	0.05
	2	79, 39	121, 60	5	0.03
	3	38, 35, 45	51, 55, 70	10	0.04
	4	25, 38, 37, 18	29, 60, 57, 23	17	0.04
IEEE118-bus	5	22, 16, 27, 19, 34	27, 17, 45, 23, 51	23	0.05
	6	23, 16, 18, 17, 30, 14	29, 23, 25, 21, 48, 18	22	0.05
	7	15, 12, 8, 18, 16, 16, 33	19, 16, 10, 27, 19, 19, 47	29	0.06
	8	21, 15, 6, 16, 15, 12, 16, 17	29, 20, 6, 19, 19, 16, 19, 25	33	0.06
	2	116, 184	159, 246	6	0.06
	3	116, 89, 95	159, 113, 127	12	0.06
	4	35, 87, 98, 80	37, 117, 132, 114	11	0.07
IEEE300-bus	5	80, 105, 45, 33, 37	105, 135, 62, 39, 52	18	0.07
	6	54, 52, 48, 33, 60, 53	74, 59, 65, 39, 84, 69	21	0.09
	7	34, 59, 35, 37, 81, 21, 33	47, 80, 37, 52, 113, 25, 39	18	0.09
	8	34, 33, 53, 35, 35, 21, 35, 54	47, 39, 77, 42, 50, 25, 37, 74	20	0.12
	2	828, 526	1211, 753	27	0.56
	3	585, 428, 341	830, 644, 479	38	0.59
	4	311, 253, 319, 471	481, 352, 443, 659	56	0.66
1354pegase [30]	5	178, 377, 297, 246, 256	253, 536, 460, 337, 355	50	0.65
	6	363, 87, 67, 217, 319, 301	510, 135, 85, 293, 446, 465	57	0.67
	7	120, 255, 72, 288, 152, 225, 242	180, 363, 97, 443, 211, 311, 322	64	0.72
	8	168, 151, 120, 243, 186, 102, 260, 124	242, 210, 180, 331, 274, 138, 354, 193	69	0.92
	2	1899, 970	2929, 1633	20	1.20
	3	600, 903, 1366	1026, 1526, 2010	20	1.25
	4	975, 457, 531, 906	1512, 647, 852, 1532	39	1.43
2869pegase [30]	5	377, 509, 528, 789, 666	536, 818, 849, 1213, 1108	58	1.51
1 6 [44]	6	562, 355, 412, 392, 771, 377	944, 585, 644, 621, 1187, 536	65	1.45
	7	354, 312, 579, 322, 508, 580, 214	501, 485, 915, 535, 754, 972, 354	66	1.62
	8	324, 532, 295, 214, 312, 288, 554, 350	544, 791, 491, 354, 485, 464, 876, 494	83	2.10

The results of power network partitioning by spectral factorization are listed in Table II. For each test case, we partition the power network from two to eight subnetworks. The 'Partition' column in Table II lists the total number of subnetworks which is the parameter used in the power network partitioning problem (2). Subnetworks are formed such that collection of them constructs the original power network. For small power networks, when more subnetworks are partitioned, there can be only one bus for some partitioned subnetworks. Thus, there is no line inside these single-bus subnetworks. The spectral factorization algorithm is capable of partitioning all test cases

in reasonable time. Generally, the computation time increases when more subnetworks are partitioned. The CPU time of partitioning large power networks is higher than the one for partitioning small power networks. Fig. 2, Fig. 3 and Fig. 4 are plotted to visualize some representative partitions for IEEE14-bus, IEEE57-bus and IEEE118-bus test cases. We use different colors to distinguish different partitioned subnetworks in Fig. 2, Fig. 3 and Fig. 4. The corresponding master problem of the proposed M-BDA for each partitioned power network is also conceptually illustrated. Note we do not plot all the tie-lines in the representative master problems in Fig. 2, Fig. 3 and Fig.

TABLE III
ACCELERATED M-BDA BY GAMS PARALLEL COMPUTING

Test Case		lution Approach			Accelerated M-BDA		
iesi Case	Objective [\$]	CPU Time [s]	Partition	Upper Bound [\$]	Lower Bound [\$]	Relative Gap	CPU Time [s]
			2	8156.28	8067.17	1.09%	0.16
			3	8115.84	8043.42	0.89%	0.20
			4	8107.18	8043.43	0.79%	0.14
IEEE14-bus	8092.32	0.09	5	8102.82	8057.13	0.56%	0.20
			6	8127.95	8080.57	0.58%	0.28
			7	8099.13	7967.99	1.62%	0.31
			8	8119.83	8073.33	0.57%	0.28
			2	41801.64	41647.12	0.37%	0.30
			3	41871.87	41428.57	1.06%	0.25
			4	41798.99	41624.31	0.42%	0.22
IEEE57-bus	41711.78	0.17	5	41924.35	41675.16	0.59%	0.44
			6	41814.77	41445.73	0.88%	0.45
			7	41956.47	41376.34	1.38%	0.25
			8	41848.47	41518.08	0.79%	0.37
			2	130025.49	129261.01	0.59%	0.33
			3	130847.44	128976.06	1.43%	0.76
			4	130066.45	129182.29	0.68%	0.39
IEEE118-bus	129376.00	0.36	5	130201.72	128631.17	1.21%	0.63
			6	131015.94	129089.14	1.47%	0.36
			7	130725.29	128393.25	1.78%	0.39
			8	129620.15	128955.16	0.51%	0.59
			2	722485.13	712303.53	1.41%	0.86
			3	721442.74	709941.27	1.59%	0.55
			4	724036.39	717468.50	0.91%	1.03
IEEE300-bus	718546.27	0.64	5	724084.83	712925.47	1.54%	0.59
			6	724038.39	709888.48	1.95%	0.70
			7	719765.51	716539.87	0.45%	0.52
			8	720591.14	714182.86	0.89%	0.47
			2	74041.62	74041.60	0.00%	3.98
			3	74198.12	74038.80	0.21%	4.17
			4	74040.36	74040.36	0.00%	1.51
1354pegase [30]	74040.99	2.50	5	74040.91	74040.91	0.00%	1.51
			6	74040.42	74040.42	0.00%	1.30
			7	74040.82	74040.82	0.00%	1.61
			8	74041.01	74040.99	0.00%	0.91
			2	133938.47	133886.16	0.04%	11.83
			3	134455.42	133409.29	0.78%	14.26
			4	133940.19	133869.50	0.05%	6.72
2869pegase [30]	133934.70	9.72	5	134122.31	131618.32	1.87%	8.70
			6	133915.61	133915.57	0.00%	3.42
			7	133928.71	133928.70	0.00%	3.15
			8	135021.76	132710.79	1.71%	5.34

4. Detailed results about the tie-lines are listed in Table II.

C. Accelerated M-BDA using GAMS parallel computing

The MOSEK solver in GAMS is used to solve the SOC-ACOPF model, the master problem and subproblem in the proposed M-BDA. The results of accelerated M-BDA using GAMS parallel computing are listed in Table III. For comparison, the results of centralized solution approach (without decomposition) of SOC-ACOPF are also listed. The 'Relative Gap' column shows the gap between the upper bound and lower bound of M-BDA calculated as Relative Gap = Upper Bound Lower Bound \times 100%. For all these test cases, M-BDA converges to very close solutions to single-stage SOC-ACOPF without decomposition. With the increase of partition depth (more subnetworks and fewer nodes in each subnetwork), the SOC-ACOPF problem complexity is decreasing. All test cases converge within few iterations. Compared with the computation time of the centralized solution approach, the computational efficiency improvement is more prominent in large test cases. Our results of improved computational efficiency by varying the power network partitions show

promising approach of using sufficient off-line simulations to identify the most efficient power network partitions for a given power network.

VI. CONCLUSION

An accelerated M-BDA using parallel computing is proposed to tackle the complexity of large-scale SOC-ACOPF problem. The formulation, feasibility and optimality proof, and fast convergence of the proposed M-BDA are the main contributions of the current paper. The numerical results show that the M-BDA accelerated by GAMS grid computing can reduce SOC-ACOPF problem scale (reduce the RAM requirement for the computer) as well as computation time. The advantage of solving SOC-ACOPF in a decomposed way is that we reduce the dimension of Hessian matrix and Jacobian matrix during the iterations of interior point method. This is very useful for large-scale power networks where the number of variables and constraints of the formulated SOC-ACOPF exceed the solver limit. Another advantage of the proposed decomposition is that, by keeping the boundaries between different subnetworks or zones in the power system, the data

privacy of each operation zone can be protected. A coordinator who is solving the master problem of the proposed M-BDA does not need to know the detailed network configuration of the subnetworks. All the required information (from the subnetworks) by the coordinator is communicated through the Benders cuts. We prove the feasibility and optimality of M-BDA analytically and numerically. The convergence of the proposed approach is guaranteed by the convexity of the SOC-ACOPF model [10]. Future research can be directed on examining the proposed approaches for larger power networks.

ACKNOWLEDGMENT

The authors would like to thank the support from SETS Erasmus Mundus Joint Doctorate Fellowship funded by the European Commission for this research project on optimal power flow. The editors' and reviewers' great efforts of reviewing this paper are highly appreciated by the authors.

REFERENCES

- D. K. Molzahn, F. Drfler, H. Sandberg, S. H. Low, S. Chakrabarti, R. Baldick, and J. Lavaei, "A survey of distributed optimization and control algorithms for electric power systems," *IEEE Transactions on Smart Grid*, vol. PP, no. 99, pp. 1–1, 2017.
 B. Zhao, Z. Xu, C. Xu, C. Wang, and F. Lin, "Network partition based zonal voltage control for distribution networks with distributed and control of the control of t
- PV systems," IEEE Transactions on Smart Grid, vol. PP, no. 99, pp. 1-1. 2017.
- [3] Bidding Areas of Nord Pool. [Online]. Available: http://www. nordpoolspot.com/How-does-it-work/Bidding-areas/

 [4] Electric power markets: National overview. [Online]. Available:
- https://www.ferc.gov/market-oversight/mkt-electric/overview.asp
 [5] E. Loukarakis, J. W. Bialek, and C. J. Dent, "Investigation of maximum
- possible opf problem decomposition degree for decentralized energy markets," *IEEE Transactions on Power Systems*, vol. 30, no. 5, pp. 2566-2578, Sept 2015.
- [6] B. H. Kim and R. Baldick, "Coarse-grained distributed optimal power flow," IEEE Transactions on Power Systems, vol. 12, no. 2, pp. 932-939,
- [7] R. Baldick, B. H. Kim, C. Chase, and Y. Luo, "A fast distributed implementation of optimal power flow," *IEEE Transactions on Power Systems*, vol. 14, no. 3, pp. 858–864, Aug 1999.

 B. H. Kim and R. Baldick, "A comparison of distributed optimal power flow algorithms," *IEEE Transactions on Power Systems*, vol. 15, no. 2, pp. 599–604, May 2000.
- A. J. Conejo and J. A. Aguado, "Multi-area coordinated decentralized DC optimal power flow," *IEEE Transactions on Power Systems*, vol. 13, no. 4, pp. 1272–1278, Nov 1998. [10] A. M. Geoffrion, "Generalized Benders decomposition,"
- optimization theory and applications, vol. 10, no. 4, pp. 237–260, 1972. V. H. Quintana, R. Lopez, R. Romano, and V. Valadez, "Constrained
- economic dispatch of multi-area systems using the dantzig-wolfe decomposition principle," *IEEE Transactions on Power Apparatus and Systems*,
- vol. PAS-100, no. 4, pp. 2127–2137, April 1981.

 [12] T. Erseghe, "Distributed optimal power flow using ADMM," *IEEE* Transactions on Power Systems, vol. 29, no. 5, pp. 2370-2380, Sept
- [13] N. Alguacil and A. J. Conejo, "Multiperiod optimal power flow using Benders decomposition," *IEEE Transactions on Power Systems*, vol. 15,
- no. 1, pp. 196–201, Feb 2000. Y. Fu, M. Shahidehpour, and Z. Li, "Security-constrained unit com-[14] T. Fu, M. Shaindenpour, and Z. Li, Security-Constanted unit commitment with AC constraints*," *IEEE Transactions on Power Systems*, vol. 20, no. 3, pp. 1538–1550, Aug 2005.
 [15] S. Binato, M. V. F. Pereira, and S. Granville, "A new Benders decomponing."
- sition approach to solve power transmission network design problems, IEEE Transactions on Power Systems, vol. 16, no. 2, pp. 235-240, May 2001.
- [16] Y. Wang, L. Wu, and S. Wang, "A fully-decentralized consens based ADMM approach for DC-OPF with demand response," *IE Transactions on Smart Grid*, vol. PP, no. 99, pp. 1–11, 2017.

- [17] M. Bazrafshan and N. Gatsis, "Decentralized stochastic optimal power flow in radial networks with distributed generation," IEEE Transactions on Smart Grid, vol. 8, no. 2, pp. 787–801, March 2017. W. Lu, M. Liu, S. Lin, and L. Li, "Fully decentralized optimal power
- flow of multi-area interconnected power systems based on distributed interior point method," *IEEE Transactions on Power Systems*, vol. PP, no. 99, pp. 1–1, 2017. E. Dall'Anese, H. Zhu, and G. B. Giannakis, "Distributed optimal power
- flow for smart microgrids," *IEEE Transactions on Smart Grid*, vol. 4, no. 3, pp. 1464–1475, Sept 2013.
- Q. Peng and S. H. Low, "Distributed Optimal Power Flow Algorithm for Radial Networks, I: Balanced Single Phase Case," *IEEE Transactions* on Smart Grid, vol. PP, no. 99, pp. 1-11, 2017. S. Arora, S. Rao, and U. Vazirani, "Geometry, flows, and graph-
- partitioning algorithms," Communications of the ACM, vol. 51, no. 10, pp. 96–105, 2008.
- Y. Jia and Z. Xu, "A direct solution to biobjective partitioning problem in electric power networks," IEEE Transactions on Power Systems, vol. 32, no. 3, pp. 2481–2483, May 2017. E. Cotilla-Sanchez, P. D. H. Hines, C. Barrows, S. Blumsack, and
- M. Patel, "Multi-attribute partitioning of power networks based on electrical distance," *IEEE Transactions on Power Systems*, vol. 28, no. 4, pp. 4979-4987, Nov 2013
- [24] J. Guo, G. Hug, and O. K. Tonguz, "Intelligent partitioning in distributed optimization of electric power systems," *IEEE Transactions on Smart Grid*, vol. 7, no. 3, pp. 1249–1258, May 2016.

 J. P. Hespanha, "An efficient matlab algorithm for graph partitioning,"
- Department of Electrical & Computer Engineering, University of California., Tech. Rep., 2004.
- Torma, 1ecn. Rep., 2004.
 Z. Yuan, M. R. Hesamzadeh, and D. Biggar, "Distribution locational marginal pricing by convexified ACOPF and hierarchical dispatch," *IEEE Transactions on Smart Grid*, vol. PP, no. 99, pp. 1–1, 2016.
 M. Farivar and S. H. Low, "Branch Flow Model: Relaxations and Convexification: Part I," *IEEE Transactions on Power Systems*, vol. 28,
- no. 3, pp. 2554–2564, Aug 2013. R. D. Zimmerman, C. E. Murillo-Sánchez, and R. J. Thomas, "MAT-
- POWER: Steady-state operations, planning, and analysis tools for power systems research and education," *IEEE Transactions on Power Systems*,
- vol. 26, no. 1, pp. 12–19, 2011. M. R. Bussieck, M. C. Ferris, and A. Meeraus, "Grid-enabled optimization with GAMS," INFORMS Journal on Computing, vol. 21, no. 3, pp. 349–362, 2009.
- S. Fliscounakis, P. Panciatici, F. Capitanescu, and L. Wehenkel, "Contingency ranking with respect to overloads in very large power systems taking into account uncertainty, preventive, and corrective actions," *IEEE* Transactions on Power Systems, vol. 28, no. 4, pp. 4909-4917, Nov 2013



Zhao Yuan received B.E. in Electrical Engineering from Hebei University of Technology in 2011, double M.E. in Electrical Engineering from Huazhong University of Science and Technology, and in Renewable Energy from ParisTech in 2014. Zhao is awarded the National Second Prize in 2010 China Undergraduate Contest of Mathematical Modelling by China Society for Industrial and Applied Mathematics. He is currently pursuing the PhD degree in Electricity Market Research Group (EMReG) of KTH Royal Institute of Technology, Sweden. His

research interests include optimal power flow, power system operation and electricity market.



Mohammad Reza Hesamzadeh (IEEE-SM13) received his Docent from KTH Royal Institute of Technology, Sweden, and his PhD from Swinburne University of Technology, Australia, in 2013 and 2010 respectively. He was a post-doctoral fellow at KTH in 2010-2011 where he is currently a faculty member. His Special fields of interests include Electricity market modeling, analysis, and design and mathematical modelling and computing. Dr Hesamzadeh is a member of International Association for Energy Economics (IAEE) and a Member

of Cigre, Sweden Section.

Distribution Locational Marginal Pricing by Convexified ACOPF and Hierarchical Dispatch

Zhao Yuan, Student Member, IEEE, Mohammad Reza Hesamzadeh, Senior Member, IEEE, and Darryl R. Biggar

Abstract-This paper proposes a hierarchical economic dispatch (HED) mechanism for computing distribution locational marginal prices (DLMPs). The HED mechanism involves three levels: The top level is the national (regional) transmission network, the middle level is the distribution network, while the lowest level reflects local embedded networks or microgrids. Each network operator communicates its generalized bid functions (GBFs) to the next higher level of the hierarchy. The GBFs approximate the true cost function of a network by a series of affine functions. The concept of Benders cuts are employed in simulating the GBFs. The AC optimal power flow (ACOPF) is convexified and then used for dispatching generators and calculating GBFs and DLMPs. The proposed convexification is based on the second order cone reformulation. A sequential optimization algorithm is developed to tighten the proposed second order cone relaxation of ACOPF. The properties of the sequential tightness algorithm are discussed and proved. The HED is implemented in the GAMS grid computing platform. The GBFs and DLMPs are calculated for the modified IEEE 342 node low voltage test system. The numerical results show the utility of the proposed HED and GBF in implementing DLMP.

Index Terms—Convexified ACOPF, Hierarchical economic dispatch, Generalized bid function, DLMP.

NOMENCLATURE

Sets:

N Node	es.
L Line	S.
Paramete	rs:
A_{nl}, B_{nl}	Node to line incidence matrix.
x_l, r_l	Reactance and resistance.
g_n, b_n	Shunt conductance and susceptance.
K_l	Squared power capacity of line <i>l</i> .
p_n^{min}, p_n^{mo}	Lower and upper bound of p_n .
q_n^{min}, q_n^{mi}	^{n} Lower and upper bound of q_n .
p_{d_n}, q_{d_n}	Active and reactive power demand.
Variables	
p_n, q_n	Active and reactive power generation.
p_{s_l}, q_{s_l}	Active and reactive power injection.
p_{o_l}, q_{o_l}	Active and reactive power loss.
v_n, V_n	Voltage magnitude and voltage square.
v_{s_l}, v_{r_l}	Sending and receiving end voltage.
V_{s_l}, V_{r_l}	Sending and receiving end voltage square.
$ heta_l$	Voltage phase angle difference.
$\theta_{s_l}, \theta_{r_l}$	Sending end and receiving end phase angle.

Z. Yuan and M. R. Hesamzadeh are with Electricity Market Research Group (EMReG), School of Electrical Engineering, KTH Royal Institute of Technology, Stockholm, SE-10044, Sweden. Email: yuanzhao@kth.se, mrhesamzadeh@ee.kth.se

I. INTRODUCTION

MART GRID advocates envisage a future in which small customers are responsive to local market conditions with devices that reduce electricity consumption at times of high prices and increase consumption at times of low prices. The increasing penetration of devices capable of responding to market prices is increasing the need for, and the utility of, improved distribution pricing signals. Efficient distribution pricing signals reflect both losses and congestion on the distribution network. Such prices vary across both time and locations and reflect the short-run marginal cost of the transportation of electricity from one point on the distribution network to another.

In recent years there has been rapidly increasing interest in locational marginal pricing of distribution networks, especially to facilitate integration of distributed energy resources [1]. The benefit of distribution locational marginal prices (DLMPs) for charging management of electric vehicles is discussed in [2]. References [3], [4] discuss boosting of demand-side responses using DLMPs. Reference [5] demonstrates how DLMPs can alleviate congestion caused by high penetration of electric vehicles (EV) and heat pumps (HP). Reference [6] proposes to integrate DLMPs and optimization in controlling future distribution networks where electronic devices are enabled to receive control signals generated from DLMP.

Given the very large number of nodes in typical distribution networks, the complexity involved in calculating DLMPs must be properly addressed. Decentralized dispatch is an attractive solution in smart grids [7]–[9]. To address the complexity, a decentralized optimal power flow (OPF) calculated by a Lagrangian-based decomposition procedure is proposed in [10]. Reference [11] reduces high-voltage radial distribution networks to simple networks by feeder reduction techniques. Reference [12] proposes the decentralized economic dispatch for smart grids using the concept of self-organizing dynamic agents. A distributed multi-agent paradigm is proposed in [13] to calculate DLMPs.

Reference [13] reports the DLMPs in a 12-bus distribution network calculated by both direct current OPF (DCOPF) and alternating current OPF (ACOPF). The results show that DLMPs from ACOPF are higher than the ones from DCOPF (this is partly because marginal loss costs are included in the ACOPF approach). The DLMP difference between DCOPF and ACOPF is larger in congestion cases (DLMP of bus 1 is 78.33\$/MWh by DCOPF but 149.99\$/MWh by ACOPF). On the other hand, reference [2] calculates DLMPs by DCOPF because of the ACOPF complexity in distribution networks

D. R. Biggar is with the Australian Competition and Consumer Commission, Melbourne, Australia.

with a large number of nodes.

Limitations on the ability to share network information is another issue in calculating DLMPs. The importance of coordination between the distribution and transmission network layer is discussed in [14] and [15]. This issue is significant for the operation of a power system with large-scale integration of distributed energy resources.

We can distinguish two main challenges in implementing DLMPs: (1) Computational complexity: The DCOPF assumptions are not often valid in distribution grids with high resistance to reactance (R/X) ratio [16]. On the other hand, the ACOPF in distribution networks with a large number of nodes might not be computationally tractable. This demands an OPF formulation which is accurate enough and at the same time which can be solved efficiently for distribution networks with a large number of nodes. (2) Sharing of network information: the correct calculation of DLMPs needs full information of the whole transmission, distribution and local network. Sharing of detailed network information between different network layers might not be feasible or practical. In this paper, these two challenges of implementing DLMPs are addressed.

For the computation complexity challenge, we propose a convexified ACOPF based on second order cone relaxation (SOC-ACOPF) [17]–[19]. The tightness of the employed relaxation is enforced by a sequential tightness algorithm. Though Semi-Definite Programming (SDP) based ACOPF ([20]-[22]) is also one approach to solve ACOPF, the computational limits of SDP are shown in [23]. Efficient algorithms for solving SDP-based ACOPF model remains to be found [20]. SDP relaxations are exact only for limited types of problems [24]-[26]. Even for a 2-bus 1-generator system, SDP-based ACOPF can be infeasible and inexact [27]. [28] formulate the load flow problem of radial distribution network as conic programming by defining new variables. Our formulations do not need to define these new variables. [29] make use of polynomial optimization problem (POP) based ACOPF and then relaxed the POP model by second order cone programming. A hierarchy of SOCP problems is solved to obtain the bounds of ACOPF. The constraints in the hierarchy [29] are increasing during the solution process. On the contrast, the number of the constraints in the sequential tightness algorithm proposed in our paper does not grow in the solution process. By replacing the positive semidefinite condition with its necessary SOCP constraints, reference [30] formulate a mixed SDP/SOCP approach to improve the computational performance of the moment relaxations of ACOPF. But the numerical computation results from [30] show that the mixed SDP/SOCP are still not as fast as pure SOCP based ACOPF compared with our results. [31] use current square variables to formulate the SOCP relaxation of ACOPF and then recover voltage phase angle from solutions of other variables. In our SOC-ACOPF formulation, we explicitly include voltage phage angle variables. Thus the voltage phase angle solutions can be obtained directly.

To address the issue of sharing information between different network layers, the concept of GBF is proposed. The convexified ACOPF and the GBF are placed in a proposed HED mechanism. We prove that if the GBFs are communicated, the proposed HED achieves results very close to the global

economic dispatch. We demonstrate the proposed solutions to implementing DLMP by numerical simulations using a GAMS model. The rest of this paper is organized as follows. Section II explains the convex SOC-ACOPF model and sequential tightness algorithm. Two theorems are presented in this sections to show important properties of SOC-ACOPF. Section III introduces the concept of HED mechanism and GBF. Section IV present the numerical results and discussions. The convergence of HED mechanism is proved numerically. As the communication requirement between network operators, the capacity of GBF is shown to be small. Section V concludes the advantages of the proposed SOC-ACOPF approach, HED mechanism and GBF.

II. CONVEXIFIED ACOPF

A. Second order cone and convex envelope

The original nonconvex ACOPF (based on branch flow model [17], [19]) is formulated in optimization problem (1).

$$\underset{\Omega}{\text{Minimize}} \quad f(p_n, q_n, p_{o_l}, q_{o_l}) \tag{1a}$$

$$p_{n} - p_{d_{n}} = \sum_{l} (A_{nl}p_{s_{l}} - B_{nl}p_{o_{l}}) + g_{n}V_{n}, \ \forall n \in N$$
 (1b)
$$q_{n} - q_{d_{n}} = \sum_{l} (A_{nl}q_{s_{l}} - B_{nl}q_{o_{l}}) - b_{n}V_{n}, \ \forall n \in N$$
 (1c)

$$q_n - q_{d_n} = \sum_{l} (A_{nl}q_{s_l} - B_{nl}q_{o_l}) - b_n V_n, \ \forall n \in N$$
 (1c)

$$p_{o_{l}} = \frac{p_{s_{l}}^{2} + q_{s_{l}}^{2}}{V_{s_{l}}} r_{l}, \ \forall l \in L$$
 (1d)

$$p_{o_l} x_l = q_{o_l} r_l, \ \forall l \in L$$
 (1e)

$$V_{s_l} - V_{r_l} = 2r_l p_{s_l} + 2x_l q_{s_l} - r_l p_{o_l} - x_l q_{o_l}, \ \forall l \in L$$
 (1f)

$$v_{s_l}v_{r_l}\sin\theta_l = x_l p_{s_l} - r_l q_{s_l}, \ \forall l \in L$$
(1g)

$$p_{s_l}^2 + q_{s_l}^2 \le K_l, \ \forall l \in L$$

$$\begin{aligned} & V_n = v_n^2, \ \forall n \in N \\ & V_n = v_n^2, \ \forall n \in N \\ & v_n^{min} \leq v_n \leq v_n^{max}, \ \forall n \in N \\ & \theta_l^{min} \leq \theta_l \leq \theta_l^{max}, \ \forall l \in L \end{aligned} \tag{1}$$

$$\theta_l^{min} < \theta_l < \theta_l^{max}, \ \forall l \in L$$
 (1k)

$$p_n^{min} \le p_n \le p_n^{max}, \ \forall n \in N$$

$$q_n^{min} \le q_n \le q_n^{max}, \ \forall n \in N$$

Where $\Omega = \{p_n, q_n, p_{s_l}, q_{s_l}, p_{o_l}, q_{o_l}, V_n, v_n, \theta_l\} \in \Re$ is the set of decision variables. Equations (1b) and (1c) represent the active and reactive power balance. A_{nl} and B_{nl} are the incidence matrices of the network with $A_{nl} = 1$, $B_{nl} = 0$ if n is sending end of branch l, and $A_{nl} = -1$, $B_{nl} = 1$ if n is receiving end of branch l. Equations (1d)-(1e) represent active power and reactive power loss. Equations (1f)-(1g) are derived by taking the magnitude and phase angle of voltage drop phasor along line l respectively [17], [19]. Constraints (1j)-(1m) are bounds for voltage magnitude, voltage phase angle difference, active power generation and reactive power generation. Constraints (1d), (1g) and (1i) are nonconvex constraints in the optimization problem (1). Using second order cones [19], constraint (1d) can be relaxed to the rotated second order cone constraint in (2).

$$p_{o_l} \ge \frac{p_{s_l}^2 + q_{s_l}^2}{V_{s_l}} r_l, \ \forall l \in L$$
 (2)

The nonconvex constraint (1g) can be written as $z_{h_l} = x_l p_{s_l}$ – $r_lq_{s_l}$ where $z_{h_l}=v_{m_l}z_{\theta_l},\ v_{m_l}=v_{s_l}v_{r_l}$ and $z_{\theta_l}=\sin\theta_l.$ The nonconvex terms $v_{m_l}z_{\theta_l}, \ v_{s_l}v_{r_l}$ and $\sin\theta_l$ can be replaced by their convex hulls. We assume $v_{m_l}^{min}$, $z_{\theta_l}^{min}$, $z_{\theta_l}^{min}$, $v_{r_l}^{min}$, are lower bounds and v_{ml}^{max} , $z_{\theta_l}^{max}$, $v_{r_l}^{max}$, $v_{r_l}^{max}$ are upper bounds for the corresponding variables. The convex hull of the nonconvex terms are derived in (3) which are linear and convex. Equations (3i)-(3j) are valid for $0 < \theta_l^{max} < \frac{\pi}{2}$ [32]. Bounds of the variables can be determined a priori. The convex hull of $v_{s_l}v_{r_l}\sin\theta_l$ is expressed by three parts in (3). The first part include constraints (3a)-(3d). These constraints are the convex hull of $z_{h_l} = v_{m_l} z_{\theta_l}$. The second part include constraints (3e)-(3h). These constraints are the convex hull of $v_{m_l} = v_{s_l} v_{r_l}$. The third parts include (3i)-(3j). These constraints are the convex hull of $z_{\theta_l} = \sin \theta_l$.

$$z_{h_l} \geqslant v_{m_l}^{min} z_{\theta_l} + z_{\theta_l}^{min} v_{m_l} - v_{m_l}^{min} z_{\theta_l}^{min}, \ \forall l \in L$$
 (3a)

$$z_{h_l} \geqslant v_{m_l}^{max} z_{\theta_l} + z_{\theta_l}^{max} v_{m_l} - v_{m_l}^{max} z_{\theta_l}^{max}, \ \forall l \in L$$
 (3b)

$$z_{h_l} \leqslant v_{m_l}^{min} z_{\theta_l} + z_{\theta_l}^{max} v_{m_l} - v_{m_l}^{min} z_{\theta_l}^{max}, \ \forall l \in L$$
 (3c)

$$z_{h_l} \leqslant v_{m_l}^{max} z_{\theta_l} + z_{\theta_l}^{min} v_{m_l} - v_{m_l}^{max} z_{\theta_l}^{min}, \ \forall l \in L$$
 (3d)

$$v_{m_l} \geqslant v_{s_l}^{min} v_{r_l} + v_{r_l}^{min} v_{s_l} - v_{s_l}^{min} v_{r_l}^{min}, \ \forall l \in L$$
 (3e)

$$v_{m_l} \geqslant v_{s_l}^{max} v_{r_l} + v_{r_l}^{max} v_{s_l} - v_{s_l}^{max} v_{r_l}^{max}, \ \forall l \in L$$
 (3)

$$v_{m_l} \leqslant v_{s_l}^{min} v_{r_l} + v_{r_l}^{max} v_{s_l} - v_{s_l}^{min} v_{r_l}^{max}, \ \forall l \in L$$
 (3g)

$$v_{m_l} \leqslant v_{s_l}^{max} v_{r_l} + v_{r_l}^{min} v_{s_l} - v_{s_l}^{max} v_{r_l}^{min}, \forall l \in L$$

$$\tag{3h}$$

$$z_{\theta_l} \geqslant cos(\frac{\theta_l^{\text{max}}}{2})(\theta_l + \frac{\theta_l^{\text{max}}}{2}) - sin(\frac{\theta_l^{\text{max}}}{2}), \ \forall l \in L$$
 (3i)

onstraints are the convex hull of
$$z_{\theta_l} = \sin \theta_l$$
.
$$z_{h_l} \geqslant v_{m_l}^{min} z_{\theta_l} + z_{\theta_l}^{min} v_{m_l} - v_{m_l}^{min} z_{\theta_l}^{min}, \ \forall l \in L \qquad (3a)$$

$$z_{h_l} \geqslant v_{m_l}^{mix} z_{\theta_l} + z_{\theta_l}^{max} v_{m_l} - v_{m_l}^{max} z_{\theta_l}^{max}, \ \forall l \in L \qquad (3b)$$

$$z_{h_l} \leqslant v_{m_l}^{min} z_{\theta_l} + z_{\theta_l}^{max} v_{m_l} - v_{m_l}^{min} z_{\theta_l}^{max}, \ \forall l \in L \qquad (3c)$$

$$z_{h_l} \leqslant v_{m_l}^{min} z_{\theta_l} + z_{\theta_l}^{min} v_{m_l} - v_{m_l}^{max} z_{\theta_l}^{min}, \ \forall l \in L \qquad (3d)$$

$$v_{m_l} \leqslant v_{m_l}^{min} v_{r_l} + v_{r_l}^{min} v_{s_l} - v_{m_l}^{min} v_{r_l}^{min}, \ \forall l \in L \qquad (3e)$$

$$v_{m_l} \geqslant v_{s_l}^{min} v_{r_l} + v_{r_l}^{mix} v_{s_l} - v_{s_l}^{min} v_{r_l}^{min}, \ \forall l \in L \qquad (3f)$$

$$v_{m_l} \leqslant v_{s_l}^{min} v_{r_l} + v_{r_l}^{max} v_{s_l} - v_{s_l}^{min} v_{r_l}^{max}, \ \forall l \in L \qquad (3g)$$

$$v_{m_l} \leqslant v_{s_l}^{min} v_{r_l} + v_{r_l}^{min} v_{s_l} - v_{s_l}^{min} v_{r_l}^{max}, \ \forall l \in L \qquad (3h)$$

$$z_{\theta_l} \geqslant cos(\frac{\theta_l^{max}}{2})(\theta_l + \frac{\theta_l^{max}}{2}) - sin(\frac{\theta_l^{max}}{2}), \ \forall l \in L \qquad (3i)$$

$$z_{\theta_l} \leqslant cos(\frac{\theta_l^{max}}{2})(\theta_l - \frac{\theta_l^{max}}{2}) + sin(\frac{\theta_l^{max}}{2}), \ \forall l \in L \qquad (3j)$$
In a similar way the convex bull of constraint (1i) is derived.

In a similar way the convex hull of constraint (1i) is derived in (4).

$$V_n \ge v_n^2, \ \forall n \in N$$
 (4a)

$$V_n \le (v_n^{max} + v_n^{min})v_n - v_n^{max}v_n^{min}, \ \forall n \in \mathbb{N}$$
 (4b)

Using (2), (3) and (4), the optimization problem (1) can now be reformulated as a second order cone (SOC) program. This proposed SOC-ACOPF represented by [(1a)-(1c),(1e)-(1f),(1j)-(1m)] can be solved efficiently using interior point method (IPM) [33].

B. Sequential tightness algorithm

The conic relaxations in (2) are not guaranteed to be tight. To deal with this problem, we propose a sequential algorithm to improve the tightness. This sequential algorithm is based on Theorem 1 and Theorem 2 below:

Theorem 1

Assume that:

(1). the objective function of nonconvex ACOPF (1) and the proposed SOC-ACOPF is convex;

(2). nonconvex ACOPF (1) has exactly one global optimal solution $(p_{s_l}^*, q_{s_l}^*, p_{o_l}^*);$

(3). non-exact optimal solution (if exists) of SOC-ACOPF $p'_{o_l} > p^*_{o_l}$.

Then, constraint $p_{o_l} \leq p_{o_l}^*$ guarantees the tightness of constraint (2).

Proof. Firstly, we consider the case that SOC-ACOPF is exact (the relaxations in (2)-(4) are tight). The proof of theorem 1 is based on theorem 3 in reference [18] which proves that second order conic optimal power flow (SOPF) has at most one optimal solution when SOPF is exact for a radial network. Because our SOC-ACOPF model has one more constraint (1g) (to make our model valid for both radial and meshed networks) than the SOPF model described in reference [18], we are actually reducing the feasible region of SOPF in reference [18]. This means that either we keep the unique optimal solution in the feasible region or we exclude the optimal solution. For both cases, the conclusion that there is at most one global optimal solution of SOC-ACOPF when SOC-ACOPF is exact is still valid. Assume the exact optimal solution of SOC-ACOPF is $p_{o_l}^e$. If $p_{o_l}^e \neq p_{o_l}^*$, then $p_{o_l}^e$ must be the global optimal solution of the nonconvex ACOPF since $f^e \leq f^*$. Where f^e and f^* are the value of objective function for SOC-ACOPF and the nonconvex ACOPF respectively. This contradicts our assumption that there is exactly one global optimal solution of the nonconvex ACOPF. So $p_{ol}^e \neq p_{ol}^*$ is not valid. Constraint $p_{o_l} \leq p_{o_l}^*$ is feasible for SOC-ACOPF when it is exact.

When SOC-ACOPF is not exact, assume $(p_{s_{l}}^{'}, q_{s_{l}}^{'}, p_{o_{l}}^{'}, V_{s_{l}}^{'})$ is the optimal solution of SOC-ACOPF after we have put the constraint $p_{o_l} \leq p_{o_l}^*$:

$$p_{o_l}^* \ge p_{o_l}^{'} \ge \frac{p_{s_l}^{'2} + q_{s_l}^{'2}}{V_{\cdot}^{'}} r_l$$
 (5)

If $p_{o_{l}}^{'} \neq \frac{p_{s_{l}}^{'2} + q_{s_{l}}^{'2}}{V_{s_{l}}^{'}} r_{l}$, then:

$$p_{o_{l}}^{'} > p_{o_{l}}^{*}$$
 (6)

(6) contradicts (5). So $p_{o_l}^{'} \neq \frac{p_{s_l}^{'2} + q_{s_l}^{'2}}{V_{s_l}^{'}} r_l$ is not valid. Constraint (2) must be tight.

Theorem 1 shows that as long as we have a good estimation of p_{α}^* , then we can tighten constraint (2). The problem is that it is difficult to estimate $p_{o_t}^*$ before solving nonconvex ACOPF. We propose the following theorem to design the tightness algorithm.

Theorem 2

If the assumptions in theorem 1 hold and the decreasing sequence $p_{o_l,i} \leq p_{o_l,i-1}$ converges to $p_{o_l}^*$ which is the optimal solution of nonconvex ACOPF, then sequential constraints $p_{o_l} \leq p_{o_l,i}$ guarantee the tightness of constraint (2).

Proof. The proof of theorem 2 is based on theorem 1 and L'Hopital's rule. We denote here the sequential optimization problem constrained by $p_{o_l} \leq p_{o_l,i}$ as SOC-ACOPF- $\!i$ where i is the index for the sequence. Because SOC-ACOPF is assumed to be feasible for $p_{o_l} \leq p_{o_l}^*$ and $p_{o_l,i} \geq p_{o_l}^*$, SOC-ACOPF-i is always feasible. If the solution of SOC-ACOPF-i is denoted as $(p_{s_{1},i}^{*}, q_{s_{1},i}^{*}, p_{o_{1},i}^{*}, V_{s_{1},i}^{*})$, we have:

$$p_{o_l,i} \ge p_{o_l,i}^* \ge \frac{p_{s_l,i}^{*2} + q_{s_l,i}^{*2}}{V_{s_l,i}^*} r_l \tag{7}$$

.

From theorem 1, $p_{o_l} \leq p_{o_l}^*$ guarantees the tightness of equation (2):

$$\lim_{i \to +\infty} \frac{p_{s_l,i}^{*2} + q_{s_l,i}^{*2}}{V_{s_t,i}^{*}} r_l = p_{o_l}^{*}$$
 (8)

And we have assumed in theorem 2 that sequence $p_{o_l,i-1} \le p_{o_l,i-1}$ converges to $p_{o_l}^*$:

$$\lim_{i \to +\infty} p_{o_l,i} = p_{o_l}^* \tag{9}$$

According to L'Hopital's rule, (7)-(9) imply:

$$\lim_{i \to +\infty} p_{o_l,i}^* = p_{o_l}^* \tag{10}$$

In other words, the solutions of sequential optimization SOC-ACOPF-i converge to where equation (2) is tight.

Theorem 2 suggests we can find optimal solution of SOC-ACOPF by solving sequential SOC-ACOPF-i. The challenge is how to design or calculate the proper sequence $p_{o_l,i}$ converging to $p_{o_l,i}^*$. Here we propose to begin with a rather rough estimation of $p_{o_l}^*$ and then iteratively improve the estimation quality. The numerical results show that the proposed tightness algorithm can make the relaxation in constraint (2) tight.

Given (1h), the initial estimation $K_{o_l,0}$ is simply calculated by (11):

$$K_{o_l,0} = \frac{K_l}{V_{s_l}^{min}} r_l \tag{11}$$

Where $V_{s_l}^{min}$ is the lower bound of V_{s_l} . The sequential SOC-ACOPF-i is then constrained by (12):

$$p_{o_l} \le K_{o_l,i}, \ \forall l \in L \tag{12}$$

Where $K_{ol,i}, i \in \{0,1,2,...,M\}$ is the i^{th} estimation of p_{ol}^* . The tightness algorithm works by iteratively reducing the upper bounds $K_{ol,i}$ of power loss constraints that violate tightness criterion ε . If $p_{ol} - \frac{p_{sl}^2 + q_{sl}^2}{V_{sl}} r_l > \varepsilon$, $K_{ol,i+1} = \alpha_l K_{ol,i}$, where $0 < \alpha_l < 1$ is the decreasing parameter. The proposed sequential tightness algorithm is summarized in algorithm 1. This algorithm is illustrated in Fig. 1 where X^* denotes the

final solution. M denotes the maximum number of iterations

specified a priori. The original nonconvex feasible region of ACOPF is plotted with a solid line in Fig. 1. The convex feasible region of proposed SOC-ACOPF is plotted with a dashed line in Fig. 1. We will show the performance of this algorithm in Section 3 of this paper. It is worth to mention that the proposed sequential tightness algorithm is only tight for the relaxation in (2). Because there are additional relaxations we have introduced in (3a)-(4b), the final solutions of the proposed SOC-ACOPF model are generally not tight for the constraint (1g) in ACOPF. Using interior point method to solve the proposed SOC-ACOPF model in polynomial time does not violate the NP-hardness proof [34], [35] of ACOPF because the proposed SOC-ACOPF is still a relaxed model of ACOPF.

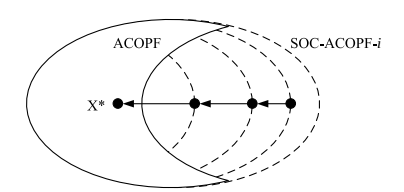


Fig. 1. The conceptual diagram of the proposed sequential tightness algorithm

III. THE HIERARCHICAL ECONOMIC DISPATCH

To define hierarchical economic dispatch (HED), we should firstly explain the traditional centralized economic dispatch (CED). We assume here centralized economic dispatch as one system operator dispatching all generations in transmission, distribution and local networks. To fulfill this dispatch task, the system operator should obtain all network information about his responsible area. Mathematically, CED is to solve ACOPF problem (1) or SOC-ACOPF [(1a)-(1c),(1e)-(1f),(1j)-(1m)]. The CED is a very large scale optimization problem considering the enormous nodes, lines and DERs. To release the complexity of CED, we propose the HED mechanism in this paper. HED actually decompose CED by Benders decomposition. We show that Benders cuts in this proposed hierarchical economic dispatch have specific economic meanings in the defined GBF.

A. The hierarchical economic dispatch mechanism

We propose a three-level dispatch mechanism with each network operator responsible for its own network. The network layers are connected through tie lines. At the third level, local network or microgrid operators (LNOs) carry out their own dispatch considering local network constraints. LNOs communicate dispatch results through the proposed GBFs to the second level of hierarchy. At the second level, the distribution network operators (DNOs) run another optimization problem taking into account the submitted GBFs from all connected LNOs and the second-level network constraints. The results of the second level optimization is packed in the form of GBFs and submitted to the first level of hierarchy. At the first level of hierarchy, transmission network operator (TNO) solves the dispatch problem of transmission network taking into account

the submitted GBFs from DNOs. Once the top level of the hierarchy is completed, the dispatch results are determined and the resulting nodal prices can be computed and communicated back down to the hierarchy. This is illustrated in Fig. 2.

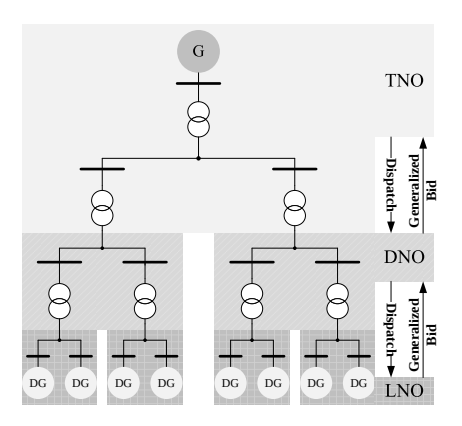


Fig. 2. The conceptual diagram of the proposed HED mechanism

B. Generalized bid function

The concept of GBF is proposed to avoid communicating detailed network and regional bid information between dispatch levels. The HED problem for LNOs contingent on the total power generation is set out in (13).

$$\begin{split} F_k(P_{k,j}^{sum}) = & \text{Minimize} \quad \sum_{n \in N_k} f(p_n,q_n) \\ & \text{subject to} \quad (1b), (1c), (1e), (1f), (1j) - (1m) \\ & (2), (3), (4), (12) \\ & \sum_{n \in N_k} p_n = P_{k,j}^{sum} : (\alpha_{k,j}) \end{split} \tag{13b}$$

Where F_k is the cost of local network dispatch as a function of its total power generation $P_{k,j}^{sum}$. $k \in K$ is the index of the LNO. $f(p_n,q_n)$ is the generation cost of the local DGs. N_k is the set of local nodes. $j \in J_k$ is the index of GBFs. If we use $S(P_{k,j}^{sum})$ to denote the feasible region of (p_n,q_n) as a function of $P_{k,j}^{sum}$. The optimization value function $F_k(P_{k,j}^{sum})$ is convex because: (1). $f(p_n,q_n)$ is jointly convex on $\left\{(p_n,q_n,P_{k,j}^{sum})\,|\,(p_n,q_n)\in S(P_{k,j}^{sum}),\,P_{k,j}^{sum}\in\Re^+\right\};$ (2). $S(P_{k,j}^{sum})$ is convex on $\Re^+;$ and (3). \Re^+ is convex (see proposition 2.1 in reference [36]). F_k can be approximated from below by a set of affine functions as in (14) shown by Fig. 3.

$$F_k(P_{k,j}^{sum}) \ge \hat{F}_{k,j} + \hat{\alpha}_{k,j} \left(\sum_{n \in N_k} p_n - \hat{P}_{k,j}^{sum} \right)$$

$$\forall j \in J_k, \forall k \in K$$
(14)

We define GBF as the set of parameters of the affine approximator (14). These parameters are communicated through set $LNO_k = \{(\hat{F}_{k,j},\hat{\alpha}_{k,j},\hat{F}_{k,j}^{sum}): j \in J_k\}$ to the DNO. Once all

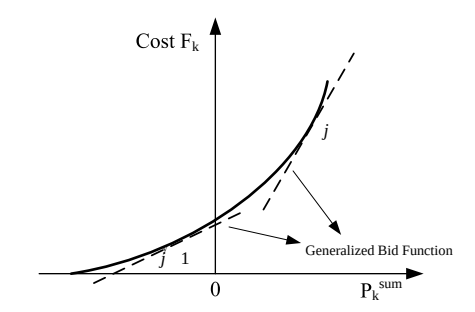


Fig. 3. Approximation of a convex cost function by affine functions

 LNO_k sets are communicated, the DNO solves the following dispatch problem (15).

$$G_v(P_{v,j}^{sum}) = \text{Minimize } \sum_{n \in N_v} f(p_n, q_n) + \sum_{k \in K} F_k$$
 (15a)

subject to
$$(1b), (1c), (1e), (1f), (1j) - (1m)$$

 $(2), (3), (4), (12), (14)$

$$\sum_{n \in \mathbb{N}_{-}} p_n = P_{v,j}^{sum} : (\alpha_{v,j})$$
(15b)

Same as F_k , G_v is also a convex optimization value function based on proposition 2.1 in reference [36]. G_v can be approximated from below by affine functions (16b). $v \in V$ is the index of the DNO. The parameters of these affine functions are communicated through set $DNO_v = \{(\hat{G}_{v,j}, \hat{\alpha}_{v,j}, \hat{P}_{v,j}^{sum}): j \in J_v\}$ to TNO. TNO solves the optimization problem (16).

$$\begin{aligned} & \text{Minimize} \quad \sum_{n \in N_t} f_t(p_n, q_n) + \sum_{v \in V} G_v \\ & \text{subject to} \quad (1b), (1c), (1e), (1f), (1j) - (1m) \\ & (2), (3), (4), (12) \\ & G_v(P^{sum}_{v,j}) \geq \hat{G}_{v,j} + \hat{\alpha}_{v,j} \left(\sum_{n \in N_v} p_n - P^{sum}_{v,j} \right) \\ & \forall j \in J_v, \, \forall v \in V \end{aligned} \tag{16b}$$

Once optimization problem (16) is solved, TNO finds the nodal prices. It also communicates the total power generation requirement $\hat{P}_{v,\hat{j}}^{sum}$ to DNOs (\hat{j}) is the index of final GBF for which the HED converges). Given $\hat{P}^{sum}_{...2}$, DNOs find the nodal prices for their networks. The DNO also communicates $\hat{P}_{L,2}^{sum}$ to the connected LNOs. LNOs then calculate the nodal prices for their local networks. The underlying mathematical structure behind the HED mechanism is the Benders decomposition approach. The proposed HED relaxes the decomposition of economic dispatch by taking $P_{k(v),j}^{sum}$ as the complicating variables instead of the tie-line power flows p_{sl},q_{sl} . This leads to fewer GBFs when multiple tie-lines exist. In this way, DNOs or LNOs do not need to submit GBFs for each tie-line (F_k and G_v are not functions of tie-line power flows). Constraints (14) and (16b) are actually Benders cuts for aggregated tie lines. If the problem is convex, it is proved that optimal solution can be found within finite iterations [37].

Algorithm 2: Hierarchical Economic Dispatch Mechanism

Initialization:

TNO solve transmission network dispatch (16);

TNO broadcast $\hat{P}_{v,\hat{j}}^{sum}$ to DNOs;

DNOs solve distribution network dispatch (15);

DNOs broadcast $\hat{P}_{v,\hat{j}}^{sum}$ to LNOs; DNOs submit DNO_k to TNO;

LNOs solve local network dispatch (14);

LNOs submit LNO_k to DNO;

IV. NUMERICAL RESULTS AND DISCUSSION

The proposed SOC-ACOPF and its tightness algorithm are examined through several case studies. Then the proposed HED is simulated. All the models are coded in GAMS. MATPOWER and LINDOGLOBAL are used for comparison. Simulations are run on a PC with Intel i7-2760QM 2.4 GHz CPU and 8 GB of RAM.

A. The performance of proposed SOC-ACOPF

The results of SOC-ACOPF with sequential tightness algorithm are reported in Table I and Table II. The relaxation gap of constraints (2) is calculated as:

$$Gp_{o_l} = \max_{l} \left\{ p_{o_l} - \frac{p_{s_l}^2 + q_{s_l}^2}{V_{s_l}} r_l \right\}$$
 (17)

The stopping criteria for the SOC-ACOPF iteration is Gp_{o_l} < 10^{-9} . In all reported cases, the Gp_{o_l} indicator is less than 10^{-9} . The optimality gap of the proposed SOC-ACOPF is measured in $Gp_f = \frac{f^* - f}{f^*} \times 100\%$. In the calculation of Gp_f , f^* is the global solution of nonconvex ACOPF calculated by LINDOGLOBAL and f is the solution of proposed SOC-ACOPF found by MOSEK solver.

TABLE I THE PERFORMANCE OF SEQUENTIAL TIGHTNESS ALGORITHM: OBJECTIVE SOLUTION

Case		Objective [\$]		Glabal Gpor		
Case	SOC	matpower	Global	Gp_{o_l}	Gp_f [%]	
IEEE14	8076.99	8081.53	8078.80	0	0.02	
IEEE57	41673.08	41737.79	41698.64	0	0.06	
IEEE118	129619.60	129660.70	129626.45	0	0.01	
IEEE300	718109.18	719725.11	719459.62	0	0.18	

TABLE II THE PERFORMANCE OF SEQUENTIAL TIGHTNESS ALGORITHM: COMPUTATION TIME

Case	CPU time [s]				
Case	SOC	matpower	Global		
IEEE14	0.10	0.11	0.20		
IEEE57	0.19	0.12	2.31		
IEEE118	0.33	0.30	27.1		
IEEE300	3.10	0.40	257.68		

As we can see from Table I, the results from SOC-ACOPF is very close to the global solutions obtained by LINDOGLOBAL.

B. Convergence of hierarchical economic dispatch

The IEEE 342 node network [38] is modified here to illustrate the operation of the proposed HED. This test case has transmission network (nodes P1-P4, P7-P8), distribution network (nodes P5-P6, P9-P390) and local networks (nodes S193-S240 in the eight spot 277/480V networks). The local networks are connected to the distribution network by transformers denoted as X3, X4 to X22 in Fig. 6. One 50 MW generator is located in the transmission network. Each 13.2 kV distribution feeder is equipped with one 7.5 MW distributed generator (DG). We distribute 48 DGs among all nodes of the local networks (one 3 MW DG at each node). To simulate congestion in the distribution network and local networks, we increase the load levels in all the local networks by four times and then reduce the tieline transformer capacity (X10-X18 is reduced to 3 MVA and X21-X22 is reduced to 4 MVA). We assume all generators are dispatchable. To accelerate computation, we design a GAMS grid computing structure to assign the dispatch task of each network to different threads as demonstrated in Fig. 5.

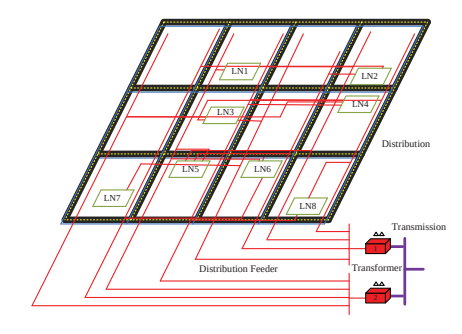


Fig. 4. The hierarchy of the modified IEEE 342 node test system

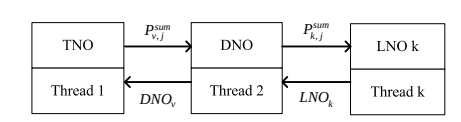


Fig. 5. The GAMS grid computing structure of hierarchical economic dispatch

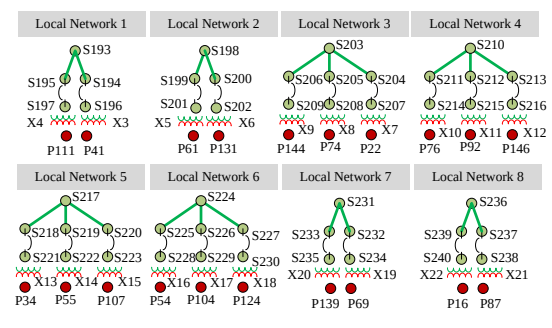


Fig. 6. Local low voltage networks

The dispatch results of HED are listed in Table III. We denote the case of no congestion as the base case in this paper. CED results denoted as 'C' are also listed. The HED results (denoted as 'H') converge to the solution very close to centralized dispatch dispatch cost. All cases converge within three iterations shown in Fig. 7. Because of approximations used in HED mechanism, the final cost of HED is a bit different from centralized dispatch (the difference is within 1% after three iterations). The CPU time for computation is within 1.8 second. If the LNOs and DNO submit their GBFs (i.e. parameters of three affine approximators in one package) to the next higher hierarchy, the HED converges in one iteration. It is worth to mention that Benders decomposition is a way to build GBFs in HED. HED does not work in an iterative way.

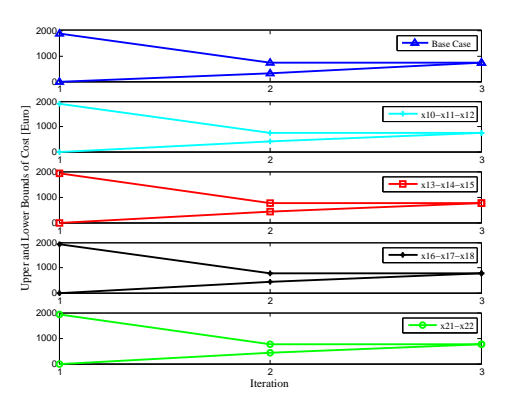


Fig. 7. The convergence of the proposed HED mechanism

C. Distribution locational marginal price

The nodal prices are shown in Fig. 8. All nodal prices are very close to each other in the base case. The only differences in the nodal prices are due to the marginal cost of energy loss. This can be clearly observed from the small price spikes at the ending nodes (S193, S198, S203, S210, S217, S224, S231 and S236) of each local network. The congested distribution transformers are indicated in the legend of Fig. 8. When congestion happens, the nodes located in the local network have higher prices. The consumers with priceresponsive load can response to these higher prices. This can be observed by comparing consumer payment and DG income when congestion happens with the ones in the base case. We plot the total payment of consumers in the local networks in Fig. 9. The payment difference as compared to the base-case payments is also shown in Fig. 9. The congestion management potential of DLMP can be further demonstrated by the income increase of DGs when congestion happens. This is shown in Fig. 10. When congestion happens, the increased nodal prices give local DGs strong incentive to produce more energy.

D. The generalized bid function

The GBFs are listed in Tables IV-VIII. We sum the $\hat{F}_{k,j}$ and $\hat{G}_{v,j}$ parameters in the GBFs for all networks and list the

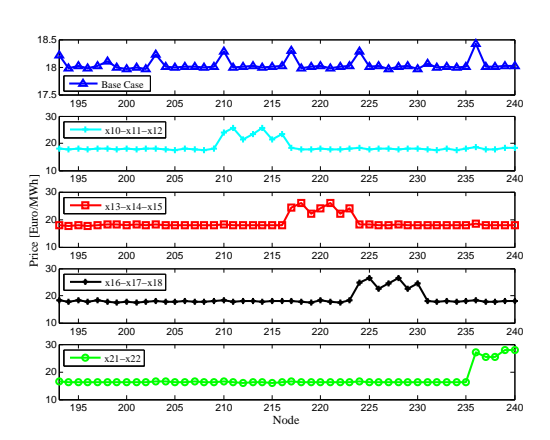


Fig. 8. The nodal prices in local networks

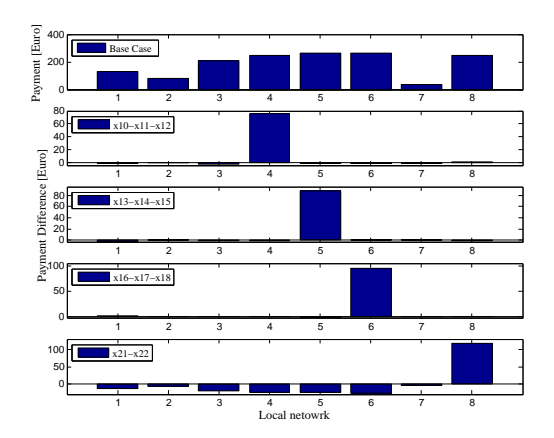


Fig. 9. The total payment of consumers in local networks

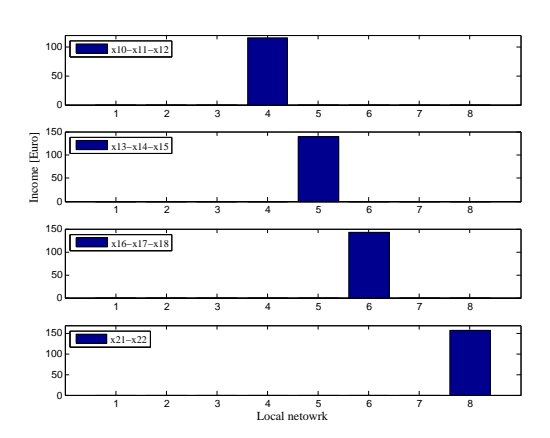


Fig. 10. The total income of DGs in local networks

TABLE III
THE RESULTS OF THE ACTIVE POWER DISPATCH FROM HED MECHANISM, C: CENTRALIZED DISPATCH, H: HED

Network	Generator	Base Cas	se [MW]	x10-x11-	x12 [MW]	x13-x14-x15 [MW]		x16-x17-x18 [MW]		x21-x22 [MW]	
	Generator	C	H	С	H	C	H	С	H	С	H
Transmission	1	50.00	50.00	50.00	50.00	50.00	50.00	50.00	50.00	50.00	50.00
	2	7.50	7.50	7.50	7.50	7.50	7.50	7.50	7.50	7.50	7.50
	3	7.50	7.50	7.50	7.50	7.50	7.50	7.50	7.50	7.50	7.50
	4	7.50	7.50	7.50	7.50	7.50	7.50	7.50	7.50	7.50	7.50
Distribution	5	7.50	7.50	7.50	7.50	7.50	7.50	7.50	7.50	7.50	7.50
Distribution	6	7.50	7.50	7.50	7.50	7.50	7.50	7.50	7.50	7.50	7.50
	7	7.50	7.50	7.50	7.50	7.50	7.50	7.50	7.50	7.50	7.50
	8	7.50	7.50	7.50	7.50	7.50	7.50	7.50	7.50	7.50	7.50
	9	5.93	5.96	0.99	0.94	0.14	0.15	0.10	0.10	0.05	0.04
Local 4	29	0.00	0.00	2.89	3.00	0.00	0.00	0.00	0.00	0.00	0.00
Local 4	30	0.00	0.00	1.40	2.07	0.00	0.00	0.00	0.00	0.00	0.00
Local 5	36	0.00	0.00	0.00	0.00	2.44	3.00	0.00	0.00	0.00	0.00
Local 5	37	0.00	0.00	0.00	0.00	0.17	2.86	0.00	0.00	0.00	0.00
	38	0.00	0.00	0.00	0.00	0.18	0.00	0.00	0.00	0.00	0.00
	43	0.00	0.00	0.00	0.00	0.00	0.00	2.44	3.00	0.00	0.00
Local 6	44	0.00	0.00	0.00	0.00	0.00	0.00	2.87	2.97	0.00	0.00
	45	0.00	0.00	0.00	0.00	0.00	0.00	0.65	0.00	0.00	0.00
	53	0.00	0.00	0.00	0.00	0.00	0.00	0.00	0.00	2.98	3.00
Local 8	54	0.00	0.00	0.00	0.00	0.00	0.00	0.00	0.00	3.00	3.00
	55	0.00	0.00	0.00	0.00	0.00	0.00	0.00	0.00	0.00	0.13
Total Co	st [€]	731.67	732.25	757.91	755.09	766.93	762.38	769.15	766.96	769.15	776.38

accumulated results in the last row of the Tables IV-VIII. As in Tables III-VII, the LNOs submit their calculated GBFs to the DNO. Accordingly, the DNO takes into account submitted GBFs from LNOs and prepars its GBFs to be submitted to the TNO. The TNO calculates the dispatch instructions and nodal prices will be communicated back down to the hierarchy. Note that LNOs only need to submit their GBFs to the DNO. Bids from the 48 local DGs are not required to be submitted to the DNO. In other words, with GBFs, the network layers would not need to share their detailed network information between each others. Table IV - Table VIII demonstrate the communication burden of HED is small.

TABLE IV THE GBFS IN BASE CASE

Network	j = 1		j = 2		j = 3	
Network	P^{sum}	α	P^{sum}	α	P^{sum}	α
DNO	21.60	8.00	58.46	18.00	58.46	18.00
LNO1	7.20	24.00	0.00	20.00	0.00	19.98
LNO2	6.64	24.50	0.00	20.50	0.00	20.48
LNO3	10.17	26.50	0.00	21.00	0.00	20.98
LNO4	10.67	27.00	0.00	21.50	0.00	21.47
LNO5	10.86	27.50	0.00	22.00	0.00	21.98
LNO6	10.88	28.00	0.00	22.50	0.00	22.48
LNO7	6.25	27.00	0.00	23.00	0.00	22.95
LNO8	8.37	27.50	0.00	23.50	0.00	23.45
Cost [€]	1825.28		632.25		632	.25

V. CONCLUSION

This paper proposes solutions to practical challenges with implementing locational marginal prices in distribution networks. The challenges considered here include (1) the computational complexity of nodal prices in AC optimal power flow and (2) the network information which potentially must be communicated. We propose a SOC-ACOPF to calculate nodal prices in a distribution network. The proposed SOC-ACOPF can be solved efficiently to global optimality while it has more

 $\begin{tabular}{ll} TABLE~V\\ THE~GBFs~in~case~of~x10-x11-x12~congestion \end{tabular}$

Network	j = 1			: 2	j = 3	
Network	P^{sum}	α	P^{sum}	α	P^{sum}	α
DNO	20.32	8.00	53.44	18.00	53.44	18.00
LNO1	7.10	24.00	0.00	19.98	0.00	20.00
LNO2	6.55	24.50	0.00	20.48	0.00	20.49
LNO3	10.00	26.50	0.00	20.98	0.00	20.99
LNO4	13.77	27.50	5.07	23.50	5.07	23.50
LNO5	10.69	27.50	0.00	21.98	0.00	21.99
LNO6	10.71	28.00	0.00	22.48	0.00	22.49
LNO7	6.16	27.00	0.00	22.98	0.00	22.98
LNO8	8.28	27.50	0.00	23.48	0.00	23.48
Cost [€]	1876.40		655.09		655.09	

TABLE VI
THE GBFs in case of x13-x14-x15 congestion

Network	j = 1		j = 2		j = 3	
INCLWOIR	P^{sum}	α	P^{sum}	α	P^{sum}	α
DNO	20.03	8.00	52.65	18.00	52.65	18.00
LNO1	7.08	24.00	0.00	20.00	0.00	20.00
LNO2	6.53	24.50	0.00	20.50	0.00	20.50
LNO3	9.97	26.50	0.00	21.00	0.00	21.00
LNO4	10.47	27.00	0.00	21.50	0.00	21.50
LNO5	14.58	28.00	5.86	24.00	5.86	24.00
LNO6	10.68	28.00	0.00	22.50	0.00	22.49
LNO7	6.14	27.00	0.00	23.00	0.00	22.99
LNO8	8.27	27.50	0.00	23.50	0.00	23.49
Cost [€]	1888.70		662.38		662.38	

accurate results than DCOPF. The tightness of the relaxation from the power loss constraints in the SOC-ACOPF can be guaranteed by the proposed sequential tightness algorithm. The issue of network information sharing is addressed through the proposed concept of GBF. The HED mechanism is also proposed to decompose the dispatch task of multiple connected networks. A three-level network is considered. At the third level, LNOs communicate the dispatch cost of their networks through the proposed GBFs. At the second level, DNO runs another optimization considering its own network conditions

TABLE VII THE GBFs in case of x16-x17-x18 congestion

Network	j = 1		j = 2		j = 3	
	P^{sum}	α	P^{sum}	α	P^{sum}	α
DNO	20.03	8.00	52.60	18.00	0.00	18.00
LNO1	7.08	24.00	0.00	20.00	0.00	20.00
LNO2	6.53	24.50	0.00	20.50	0.00	20.50
LNO3	9.97	26.50	0.00	21.00	0.00	21.00
LNO4	10.47	27.00	0.00	21.50	0.00	21.49
LNO5	10.66	27.50	0.00	22.00	5.97	21.99
LNO6	14.66	28.50	5.97	24.50	0.00	24.50
LNO7	6.14	27.00	0.00	23.00	0.00	22.99
LNO8	8.27	27.50	0.00	23.50	0.00	23.49
Cost [€]	1892.15		666	666.96		.96

TABLE VIII THE GBFs IN CASE OF X21-X22 CONGESTION

Network	j = 1			: 2	j = 3	
Network	P^{sum}	α	P^{sum}	α	P^{sum}	α
DNO	20.00	8.00	52.54	18.00	52.54	18.00
LNO1	7.08	24.00	0.00	19.96	0.00	20.00
LNO2	6.53	24.50	0.00	20.46	0.00	20.49
LNO3	9.96	26.50	0.00	20.97	0.00	20.99
LNO4	10.47	27.00	0.00	21.47	0.00	21.49
LNO5	10.65	27.50	0.00	21.94	0.00	21.99
LNO6	10.67	28.00	0.00	22.44	0.00	22.49
LNO7	6.14	27.00	0.00	22.95	0.00	22.99
LNO8	12.45	31.50	6.13	27.50	6.13	27.50
Cost [€]	1900).90	676.38		676.38	

and submitted GBFs of the LNOs. The results of this optimization are packed in the form of GBFs and communicated to the first level of hierarchy i.e. TNO. Once the optimization problem of the first level of hierarchy is solved, the dispatch results and nodal prices are communicated back down to the hierarchy. The convergence of HED mechanism is guaranteed by the convexity of the SOC-ACOPF. The simulation results show the utility of proposed mechanism for implementing nodal pricing in distribution and local networks. The proposed mechanism is tested in a stationary environment. Studying the impact of uncertainty is a possible future extension of this work.

ACKNOWLEDGMENT

The authors would like to thank the support from SETS Erasmus Mundus Joint Doctorate Fellowship for this research project on distribution pricing. We want to express our special thanks to Konstantin Staschus who is the Secretary-General of the European Network of Transmission System Operators (ENTSO-E). Dr. Konstantin Staschus provides many insightful and highly motivating comments on this paper when the first draft is ready. These comments help the authors to improve the paper before the final submission to IEEE. All the careful reviews on this paper by the editors and reviewers of this journal are sincerely appreciated by the authors

REFERENCES

- P. M. Sotkiewicz and J. M. Vignolo, "Nodal pricing for distribution networks: efficient pricing for efficiency enhancing DG," *Power Systems, IEEE Transactions on*, vol. 21, no. 2, pp. 1013–1014, 2006.
 R. Li, Q. Wu, and S. Oren, "Distribution locational marginal pricing for
- optimal electric vehicle charging management," *Power Systems, IEEE Transactions on*, vol. 29, no. 1, pp. 203–211, 2014.

- [3] S. Widergren, C. Marinovici, T. Berliner, and A. Graves, "Real-time pricing demand response in operations," in *Power and Energy Society General Meeting*, 2012 IEEE, 2012, pp. 1–5.
 [4] F. Sahriatzadeh, P. Nirbhavane, and A. Srivastava, "Locational marginal
- price for distribution system considering demand response," in *North American Power Symposium (NAPS)*, 2012, 2012, pp. 1–5.

 [5] S. Huang, Q. Wu, S. S. Oren, R. Li, and Z. Liu, "Distribution locational
- marginal pricing through quadratic programming for congestion management in distribution networks," *IEEE Transactions on Power Systems*, vol. 30, no. 4, pp. 2170–2178, 2015. [6] G. T. Heydt, B. H. Chowdhury, M. L. Crow, D. Haughton, B. D. Kiefer,
- G. T. Heydt, B. H. Chowdhury, M. L. Crow, D. Haughton, B. D. Kiefer, F. Meng, and B. R. Sathyanarayana, "Pricing and control in the next generation power distribution system," *Smart Grid, IEEE Transactions on*, vol. 3, no. 2, pp. 907–914, 2012.

 R. Mudumbai and S. Dasgupta, "Distributed control for the smart grid: The case of economic dispatch," in *Information Theory and Applications Workshop (ITA)*, 2014, 2014, pp. 1–6.

 H. Karami, M. Sanjari, S. Hosseinian, asid G. Gharehpetian, "An optimal distributed energy."
- optimal dispatch algorithm for managing residential distributed energy resources," *IEEE Transactions on Smart Grid*, vol. 5, no. 5, pp. 2360– 2367, 2014.
- [9] A. Fazeli, M. Sumner, C. Johnson, and E. Christopher, "Coordinated optimal dispatch of distributed energy resources within a smart energy community cell," in *Innovative Smart Grid Technologies (ISGT Europe)*, 2012 3rd IEEE PES International Conference and Exhibition on, 2012,
- A. J. Conejo and J. A. Aguado, "Multi-area coordinated decentralized DC optimal power flow," *IEEE Transactions on Power Systems*, vol. 13, no. 4, pp. 1272-1278, 1998.
- [11] Y. Zhang and F. Li, "Network pricing for high voltage radial distribution networks," in *Power and Energy Society General Meeting*, 2011 IEEE, 2011, pp. 1-5.
- V. Loia and A. Vaccaro, "Decentralized economic dispatch in smart grids by self-organizing dynamic agents," *IEEE Transactions on Systems, Man, and Cybernetics: Systems*, vol. 44, no. 4, pp. 397–408, 2014.
- F. Meng and B. Chowdhury, "Distribution LMP-based economic operation for future smart grid," in *Power and Energy Conference at Illinois (PECI)*, 2011 IEEE, 2011, pp. 1–5.
 P. Hallberg *et al.*, "Active distribution system management a key tool for
- the smooth integration of distributed generation," Eurelectric TF Active System Management, vol. 2, p. 013, 2013.
- E. Rivero, S. Daan, A. Ramos, M. Maenhoudt, and A. Ulian, "Preliminary assessment of the future role of DSOs, future market architectures and regulatory frameworks for network integration of dres," European Project EvolvDSO, Deliverable, vol. 1, 2014.
- K. Purchala, L. Meeus, D. Van Dommelen, and R. Belmans, "Usefulness of DC power flow for active power flow analysis," in *IEEE Power Engineering Society General Meeting*, 2005. IEEE, 2005, pp. 454–
- [17] M. Farivar and S. H. Low, "Branch flow model: Relaxations and convexification Part I," *IEEE Transactions on Power Systems*, vol. 28, no. 3, pp. 2554–2564, 2013.
- L. Gan, N. Li, U. Topcu, and S. H. Low, "Exact convex relaxation of optimal power flow in radial networks," *Automatic Control, IEEE*
- Transactions on, vol. 60, no. 1, pp. 72–87, 2015.

 M. Baradar and M. R. Hesamzadeh, "AC power flow representation in conic format," *IEEE Transactions on Power Systems*, vol. 30, no. 1, pp. 546–547, 2015.
- X. Bai, H. Wei, K. Fujisawa, and Y. Wang, "Semidefinite programming for optimal power flow problems," *International Journal of Electrical Power & Energy Systems*, vol. 30, no. 6, pp. 383–392, 2008.
- J. Lavaei and S. H. Low, "Zero duality gap in optimal power flow problem," *Power Systems, IEEE Transactions on*, vol. 27, no. 1, pp. 92-107, 2012
- R. Madani, M. Ashraphijuo, and J. Lavaei, "Promises of conic relaxation for contingency-constrained optimal power flow problem," *IEEE Transactions on Power Systems*, vol. 31, no. 2, pp. 1297–1307, March
- B. C. Lesieutre, D. K. Molzahn, A. R. Borden, and C. L. DeMarco, "Examining the limits of the application of semidefinite programming to power flow problems," in *Communication, Control, and Computing* (Allerton), 2011 49th Annual Allerton Conference on. IEEE, 2011, pp. 1492-1499.
- [24] J. Lavaei, D. Tse, and B. Zhang, "Geometry of power flows and optimization in distribution networks," *Power Systems, IEEE Transactions on*, vol. 29, no. 2, pp. 572–583, 2014.

- [25] S. Low, "Convex relaxation of optimal power flow, part i: Formulations and equivalence," Control of Network Systems, IEEE Transactions on, vol. 1, no. 1, pp. 15-27, March 2014.
- -, "Convex relaxation of optimal power flow, part ii: Exactness," [26] Control of Network Systems, IEEE Transactions on, no. 2, pp. 177-189, June 2014.
- B. Kocuk, S. Dey, and X. Sun, "Inexactness of sdp relaxation and valid inequalities for optimal power flow," *Power Systems, IEEE Transactions on*, to be published, early Access. [Online]. Available: http://ieeexplore.ieee.org/stamp/stamp.jsp?arnumber=7056568
- R. Jabr et al., "Radial distribution load flow using conic programming," Power Systems, IEEE Transactions on, vol. 21, no. 3, pp. 1458–1459,
- [29] X. Kuang, L. F. Zuluaga, B. Ghaddar, and J. Naoum-Sawaya, "Approximating the acopf problem with a hierarchy of socp problems," in 2015 IEEE Power Energy Society General Meeting, July 2015, pp. 1–5.
- D. K. Molzahn and I. A. Hiskens, "Mixed sdp/socp moment relaxations of the optimal power flow problem," in *PowerTech, 2015 IEEE Eindhoven*, June 2015, pp. 1–6.
 S. Bose, S. H. Low, T. Teeraratkul, and B. Hassibi, "Equivalent relax-
- T311 [31] S. Bose, S. H. Low, I. Teeraatakui, and B. Frassloi, Equivalent relaxations of optimal power flow," *IEEE Transactions on Automatic Control*, vol. 60, no. 3, pp. 729–742, March 2015.
 [32] B. Kocuk, S. S. Dey, and X. A. Sun, "Strong socp relaxations for the optimal power flow problem," *Operations Research*, 2016.
- [33] A. Mosek, "The MOSEK optimization software," Online at http://www. mosek. com, vol. 54, 2010.
- [34] K. Lehmann, A. Grastien, and P. V. Hentenryck, "AC-Feasibility on Tree Networks is NP-Hard," *IEEE Transactions on Power Systems*, vol. 31,
- no. 1, pp. 798–801, Jan 2016.

 A. Verma, "Power grid security analysis: an optimization approach," Ph.D. dissertation, Dept. Ind. Eng. Oper. Res., Columbia Univ., New York, NY, USA, 2009.
- A. V. Fiacco and J. Kyparisis, "Convexity and concavity properties of the optimal value function in parametric nonlinear programming," Journal of Optimization Theory and Applications, vol. 48, no. 1, pp. 95-126, 1986.
- [37] A. J. Conejo, E. Castillo, R. Minguez, and R. Garcia-Bertrand, De
- composition techniques in mathematical programming: engineering and science applications. Springer Science & Business Media, 2006.

 [38] K. Schneider, P. Phanivong, and J.-S. Lacroix, "IEEE 342-node low voltage networked test system," in PES General Meeting— Conference & Exposition, 2014 IEEE. IEEE, 2014, pp. 1–5.



Zhao Yuan received B.E. in Electrical Engineering Zhao Yuan received B.E. in Electrical Engineering from Hebei University of Technology in 2011, double M.E. in Electrical Engineering from Huazhong University of Science and Technology and in Renewable Energy from Paris Tech in 2014. He is currently pursuing the PhD degree in Electricity Market Research Group (EMReG) of KTH Royal Institute of Technology, Sweden. His research interests include optimal power flow, power system operation and electricity market.



Mohammad Reza Hesamzadeh (IEEE-SM13) received his Docent from KTH Royal Institute of Technology, Sweden, and his PhD from Swinburne University of Technology, Australia, in 2013 and 2010 respectively. He was a post-doctoral fellow at KTH in 2010-2011 where he is currently a faculty member. His Special fields of interests include Electricity market modeling, analysis, and design and mathematical modelling and computing. Dr Hesamzadeh is a member of International Associ-ation for Energy Economics (IAEE) and a Member

of Cigre, Sweden Section.



Darryl R. Biggar is an economist with the Australian Competition and Consumer Commission and the Australian Energy Regulator. He specializes in the economics of regulation, including issues such as the design of incentive mechanisms, foundations of regulation, and the design of electricity markets and water markets. He has a particular interest in electricity markets including issues of nodal and zonal pricing and the measurement and control of market power. Prior to the ACCC, he worked for

the OECD in Paris, the New Zealand government, and for University College, London. Biggar has a PhD in economics from Stanford University and an MA in Mathematics from Cambridge University. He is a native of New Zealand.

Ш



Contents lists available at ScienceDirect

Applied Energy

iournal homepage: www.elsevier.com/locate/apenergy



Hierarchical coordination of TSO-DSO economic dispatch considering large-scale integration of distributed energy resources



Zhao Yuan*, Mohammad Reza Hesamzadeh

Department of Electric Power and Energy Systems, KTH Royal Institute of Technology, Stockholm, Sweden

HIGHLIGHTS

- A hierarchical coordination mechanism to coordinate the dispatch of TSO and DSO.
- A convex AC optimal power flow (AC OPF) model to calculate power flows.
- A unified communication format for TSO and DSO communication.
- A parallel computation algorithm to accelerate the coordinated dispatch.
- The effect of DERs on the voltage amplitude and phase angle are investigated.

ARTICLE INFO

Article history: Received 9 November 2016 Received in revised form 8 February 2017 Accepted 10 March 2017

Keywords:
DERS
Economic dispatch
Hierarchical coordination
Generalized bid function
Benders decomposition
Grid computing

ABSTRACT

This paper proposes a hierarchical coordination mechanism for coordinating the economic dispatch of transmission system operator (TSO) and distribution system operator (DSO). The challenge of dispatching large-scale distributed energy resources (DERs) is addressed. The coordination problem of dispatching energy and reserve is formulated. Benders decomposition is the underlying mathematical foundation of the proposed hierarchical coordination mechanism. We define the generalized bid function to approximate the dispatch cost of distribution network by a series of affine functions. The generalized bid function is communicated from DSO to TSO. By using convex AC optimal power flow model, the convergence of hierarchical coordination is guaranteed. A grid computing structure in General Algebraic Modeling System (GAMS) to accelerate the computation is proposed. The generalized bid function is simulated for various test cases. We also demonstrate the effect of DERs on the voltage magnitude and phase angle. The numerical results show that the hierarchical coordination using the generalized bid function converges to very close results compared with the results of centralized dispatch. Hierarchical coordination is capable of managing various network congestion scenarios and power loads. The generalized bid function provides a unified format of communication between TSO and DSO.

© 2017 Elsevier Ltd. All rights reserved.

1. Introduction

The large scale integration of distributed energy resources (DERs) in the distribution network is profoundly reshaping the operation of entire power system [1–3]. Due to the great technical and economic benefits from DERs [2,4], various support schemes for DERs such as tax reduction, feed-in tariff and subsidy have been implemented around the world [1]. As a good example, electric vehicle (EV) owners in the Netherlands can save around 5300¢ over four years because of the incentive policies from the government [1]. The support schemes from the government together with

* Corresponding author.

E-mail address: yuanzhao@kth.se (Z. Yuan).

technology advancement create an inevitable future of large-scale integration of DERs in distribution network.

Despite the proved benefits that DERs can provide [5,6], DERs are also challenging TSO and DSO to operate the power network in a more coordinated mode [7–10]. It is critical to coordinate the access of resources and data management between TSO and DSO to fully release the potential flexibilities from DERs [7,8]. These flexibilities include balancing supply and demand, network congestion management and voltage control. Ref. [10] investigates six grid operation challenges and possible future cooperations between TSO and DSO. The operation challenges mentioned in [10] include congestion of transmission-distribution interface, congestion of transmission lines, balancing, voltage support, black start and protection. By analyzing the Generalized Nash Equilibriums (GNEs) of incremental coordination scenarios between the

Nomenclature $\begin{array}{l} \theta_l^{min} \\ \theta_l^{max} \end{array}$ Sets lower bound of θ_l set of nodes upper bound of θ_l active power demand at node nset of lines p_{d_n} K set of networks reactive power demand at node n q_{d_n} **Parameters** Variables node to line incidence matrix active power generation at node n p_n B_{nl} node to line incidence matrix reactive power generation at node n q_n p_n^r q_n^r x_l reactance of line I active power reserve at node nresistance of line l r_l reactive power reserve at node n shunt conductance at node nactive power injection at the sending end of line l g_n b_n K_l p_{s_l} shunt susceptance at node n q_{s_l} p_{o_l} reactive power injection at the sending end of line l power capacity of line l active power loss of line l upper bound of p_{o_i} reactive power loss of line l q_{o_l} v_n V_n upper bound of q_{s_i} voltage magnitude of node nlower bound of p_n voltage magnitude square of node n θ_l θ_{s_l} upper bound of p_n voltage phase angle difference of line l voltage phase angle at the sending end of line llower bound of q_n upper bound of q_n voltage phase angle at the receiving end of line l

TSO and the DSO, Ref. [9] shows that significant cost reductions can be achieved if the degree of TSO-DSO coordination is high for providing the ancillary services. In Portugal, the Inter Control Centre Protocol (ICCP) link enables the TSO and the DSO to share network information for improving visibility of both transmission network and distribution network [11]. It is demonstrated in [12] that reactive power exchange between the operating areas of the TSO and the DSO can converge within a few iterations if grid models of both sides are iteratively updated. In order to optimize the charging and discharging behaviors of EVs, Ref. [13] proposes to let the TSO coordinate the generations in the temporal dimension while the DSO optimize the spatial distribution of EVs. Up to now, incorporating energy and reserve dispatch of DERs into the coordination mechanism between TSO and DSO capable of managing network congestions has not been well discussed in the literature. In this paper, the resource access and data management problem of TSO-DSO coordination mentioned in [7,8] are addressed.

Another critical issue of coordinating the economic dispatch of TSO and DSO is the optimal power flow (OPF) problem. OPF is an important tool to optimize the operations of power system [14,15]. The objective functions of OPF range from power losses [16,17], operation or investment cost [18,19], renewable energy spillage [20] to stability margin of the power system [21,22]. The constraints of OPF can include physics, security [23,24], stability [25] and operation [26] conditions. Traditionally, DC OPF is widely used in transmission network operations. Because the resistance to reactance (R/X) ratio of distribution line is high, the assumptions of DC OPF are not valid in distribution network [27]. In order to optimize the operation of both transmission and distribution network, an OPF tool which can be used by both TSO and DSO is necessary. In fact, the AC OPF model is the only proper approach in optimizing the operations of distribution network. However, current nonlinear programming solver is not able to find the global optimal solution of the AC OPF model because it is nonconvex. To deal with this challenge, different relaxation and appoximation techniques have been recently proposed in the literature for the AC OPF model [28-31]. Second order cone programming (SOCP) based convex AC OPF is a promising approach with good results [32]. Semi-Definite Programming (SDP) is another convexification approach for AC OPF [33-35]. Ref. [36] shows various limits of SDP computation. It is demonstrated by Ref. [33] that efficient algorithms for solving SDP-based AC OPF remains to be found. Furthermore, only limited types of problems are exact for SDP relaxations [37–39]. In cases where the exactness is not guaranteed, SDP rarely gives solutions with physical meanings. Considering the advantages of SOCP over SDP, we improve the SOCP based AC OPF formulation in [32] and use the improved model for dispatching both the transmission network and the distribution network.

Past research have shown the capability of hierarchical framework to coordinate CHP units and demand responses in the local community level [40]. For the network operation level, our research on hierarchical economic dispatch based on DC OPF also proves convergent results [41,42]. [43] proposes a hierarchical control architecture to coordinate simultaneously different demand responses. This hierarchical control architecture comprises three loops exhibiting different response delay. As a comparison, our approach have two coordination levels and the communication between the coordination levels is unified. [44] proposes a hierarchical market structure by formulating the market participants' profit maximization problem and market settlement problem in a bi-level optimization framework. The interactions of microgrids, load aggregators, generation companies and network operators are investigated by solving the formulated dynamic game. However, as we have mentioned, [44] ignores that DC OPF is not valid in distribution network. In this paper, we propose a hierarchical mechanism to efficiently coordinate the dispatch decisions of TSO and DSO for energy and reserve considering large scale integration of DERs. The proposed hierarchical coordination mechanism works by communicating the generalized bid function (GBF) from DSO to TSO. The GBF is defined as a unified communication format between TSO and DSO. We demonstrate that the proposed hierarchical coordination mechanism is capable of dealing with various network congestion scenarios. These scenarios include congestions in the transmission network, congestions in the distribution network and congestions in the transmission-distribution interface. The proposed hierarchical framework based on the improved convex AC OPF model is coded in GAMS platform. A grid computing structure in GAMS is proposed to improve the computational efficiency of the proposed hierarchical coordination mechanism. The main contributions of this paper are: (1) we formulate a convex AC OPF model because DC OPF is not valid in distribution network even though DC OPF is used by some references in our paper; (2) our coordination mechanism have a solid mathematical foundation which is Benders decomposition and thus the convergence of

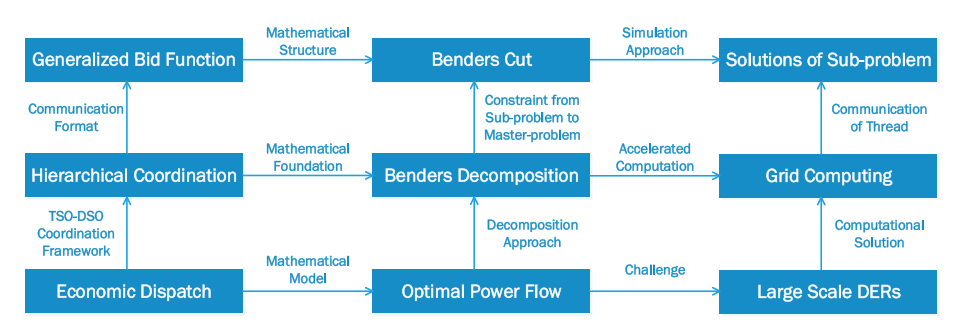


Fig. 1. Relationship of the proposed methods

coordination is guaranteed; (3) the proposed concept of generalized bid function actually is a unified communication format between TSO and DSO. The relationship of the proposed methods are summarized in Fig. 1. The rest of this paper is organized as follows. Section II explains the proposed convex AC OPF model. The economic dispatch of energy and reserve are formulated. Section III introduces the hierarchical coordination mechanism and defines the GBF. A flexible parallel computation management algorithm is designed in GAMS. Section IV presents the numerical results and discussions to validate the proposed methods. Section V concludes the advantages of the proposed hierarchical coordination mechanism

2. Convex AC OPF model based on SOCP

In this section, we present the mathematical model of convex AC OPF for economic dispatch. To deal with the uncertainties of DERs by providing sufficient reserve, the dispatch of the reserve service is also formulated.

We present here the convex AC OPF model based on the SOCP approach [32]. This model can be solved efficiently by industrialscale interior point method solver such as MOSEK [45]. The accuracy of this model have been proved by Ref. [32].

The power balance constraints. The active power and reactive power balance constraints are represented in Eqs. (1a) and (1b). These constraints are linear equations because we use voltage magnitude square variable V_n in the model. The actual voltage magnitude can be recovered from the solutions of this model as $v_n = \sqrt{V_n}$. A_{nl} and B_{nl} are the incidence matrices of the network with $A_{nl} = 1, B_{nl} = 0$ if n is the sending end of branch l, and $A_{nl} = -1, B_{nl} = 1$ if *n* is the receiving end of branch *l*. These parameters are determined by the topology of the network.

$$p_n - p_{d_n} = \sum_l (A_{nl} p_{s_l} - B_{nl} p_{o_l}) + g_n V_n, \quad \forall n \in \mathbb{N}$$
 (1a)

$$q_n - q_{d_n} = \sum_{l} (A_{nl}q_{s_l} - B_{nl}q_{o_l}) - b_n V_n, \quad \forall n \in N \eqno(1b)$$

The power loss constraints. Eqs. (1c) and (1d) represent active power and reactive power losses of transmission or distribution

$$\begin{split} p_{o_l} &= \frac{p_{s_l}^2 + q_{s_l}^2}{V_{s_l}} r_l, \quad \forall l \in L \\ q_{o_l} &= \frac{p_{s_l}^2 + q_{s_l}^2}{V_{s_l}} x_l, \quad \forall l \in L \end{split} \tag{1c}$$

$$q_{o_l} = \frac{p_{s_l}^2 + q_{s_l}^2}{V_{s_l}} x_l, \quad \forall l \in L$$
 (1d)

These quadratic equality constraints are nonconvex. We propose to relax (1d) to rotated cones expressed in (1e) in order to obtain a convex model. The active power loss p_{o_l} can be obtained from the linear relationship shown in (1f).

$$\begin{split} q_{o_l}^{max} \geqslant q_{o_l} \geqslant \frac{p_{s_l}^2 + q_{s_l}^2}{V_{s_l}} x_l, & \forall l \in L \\ p_{o_l} x_l = q_{o_l} r_l, & \forall l \in L \end{split} \tag{1e}$$

$$p_{\alpha}x_l = q_{\alpha}r_l, \quad \forall l \in L$$
 (1f)

The upper bound of reactive power loss $q_{o_i}^{max}$ is estimated from the upper bound of line capacity as shown in (1g). The approximation in (1g) is based on $V_{s_1} \approx 1$ (per unit value) which is valid in normal power system operations.

$$q_{o_{l}}^{max} = \frac{[p_{s_{l}}^{max}]^{2} + [q_{s_{l}}^{max}]^{2}}{V_{s_{l}}} x_{l} = \frac{K_{l}^{2}}{V_{s_{l}}} x_{l} \approx K_{l}^{2} x_{l}$$
(1g)

The voltage constraints. Eqs. (1h) and (1i) are derived by taking the magnitude and phase angle of the voltage drop phasor of line l, respectively. θ_l is the voltage phase angle difference of line l expressed in (1j).

$$V_{s_l} - V_{r_l} = 2r_l p_{s_l} + 2x_l q_{s_l} - r_l p_{o_l} - x_l q_{o_l}, \quad \forall l \in L \eqno(1h)$$

$$v_{s_l}v_{r_l}\theta_l = x_lp_{s_l} - r_lq_{s_l}, \quad \forall l \in L$$

$$\tag{1i}$$

$$\theta_l = \theta_{s_l} - \theta_{r_l}, \quad \forall l \in L$$
 (1j)

Eq. (1i) is nonconvex. If we assume $v_{s_l}v_{r_l}\approx 1$ (per unit value), Eq. (1i) can be linearized as (1k).

$$\theta_l = x_l p_{s_l} - r_l q_{s_l}, \quad \forall l \in L$$
 (1k)

The bounds of variables. Constraints (11)-(10) are the upper and lower bounds for the considered variables.

$$V_n^{min} \leqslant V_n \leqslant V_n^{max}, \quad \forall n \in N$$
 (11)

$$\theta_l^{min} \leqslant \theta_l \leqslant \theta_l^{max}, \quad \forall l \in L$$
 (1m)

$$p_n^{min} \leqslant p_n \leqslant p_n^{max}, \quad \forall n \in N$$
 (1n)

$$q_n^{min} \leqslant q_n \leqslant q_n^{max}, \quad \forall n \in N$$
 (10)

The reserve service. To mitigate real time unbalance of power system or the uncertainty of renewable energy, it is very important to schedule sufficient generation reserves. The constraints of generation reserve can be formulated as (1p) and (1q):

$$p_n + p_n^r \leqslant p_n^{max}, \quad \forall n \in N$$
 (1p)

$$\begin{aligned} p_n + p_n^r &\leqslant p_n^{\max}, & \forall n \in N \\ q_n + q_n^r &\leqslant q_n^{\max}, & \forall n \in N \end{aligned} \tag{1p}$$

where p_n^r, q_n^r are active power and reactive power reserve. One common practice is to determine the generation reserve requirement according to the capacity of the largest generator in the network

$$\sum p_n^r \geqslant Max[p_n^{max}], \quad \forall n \in N$$
 (1r)

$$\sum_{n} p_{n}^{r} \geqslant Max[p_{n}^{max}], \quad \forall n \in \mathbb{N}$$

$$\sum_{n} q_{n}^{r} \geqslant Max[q_{n}^{max}], \quad \forall n \in \mathbb{N}$$

$$(1r)$$

The convex AC OPF model. The proposed convex AC OPF model is set out in (2). $\Omega=\{p_n,q_n,p_n^r,q_n^r\}\in\Re$ is the set of decision variables of the economic dispatch. We use quadratic objective function to represent the cost of active power generation and the cost of reserve here. α_n^E,β_n^E are parameters of the energy cost function. α_n^R,β_n^R are parameters of the reserve cost function. This minimization problem is convex because both the objective and constraints are convex. The improvements in (2) compared to the OPF model in [32] are three folds. Firstly, we explicitly include the voltage phase angle variables. The solutions of these variables can be directly obtained by solving (2). Secondly, the capacity of lines are constrained by implicitly constraining the reactive power loss variable q_{o_i} in (2) while in [32] there are no constraints for the capacity of lines. Thirdly, the generation reserves are considered and formulated.

Minimize
$$f(p_n) = \alpha_n^E p_n^2 + \beta_n^E p_n + \alpha_n^R [p_n^r]^2 + \beta_n^R p_n^r$$

subject to (1a)-(1b); (1e)-(1f); (1h)-(1j)-(1k); (1l)-(1o)

If generation reserves are considered, constraints (1n) and (1o) can be replaced by constraints (1p), (1q), (1r) and (1s).

3. The hierarchical coordination mechanism

3.1. Coordination of TSO-DSO dispatch

The proposed hierarchical coordination mechanism of TSO-DSO economic dispatch is explained in this section. The generalized bid function as a unified communication format between the TSO and the DSO is defined. We show in this section that the mathematical foundation of the hierarchial coordination mechanism is actually Benders decomposition. The underlying mathematical structure of the generalized bid function is Benders cut. To accelerate the computation, a grid computing structure with an efficient parallel computation management algorithm in GAMS is designed.

To investigate the problem of TSO-DSO coordination in the context of large scale integration of DERs, It is important to firstly analyze the roles of various market players and network operators. Generally, the distribution company (DISCO) owns and operates the distribution network. DISCO can also sell electricity to the energy consumers in its local area. DSO is same as DISCO. Network operator is responsible for reliable and secure operation of the power network. The TSO is responsible for the transmission network. The distribution network is operated by the DSO. Microgrid is defined as a local electric network with DERs and loads connected. The microgrid can either connect with the main power system or disconnect with the main power system [48]. In this paper, we use the definition of the aggregator in Ref. [49] as a company who acts as an intermediary between electricity end-users and DER owners and the power system participants who wish to serve these end-users or exploit the services provided by these DERs. Load aggregator is a company who aggregate a group of loads and participates the market by using the flexibilities of the load (responsive load). Both microgrid and aggragator help operate the DERs in a cluster. The difference between the microgrid and the aggregator is that network operations are normally required in the microgrid while the aggregator does not engage in the network operations. Generation company is a company providing energy, reserve or other relevant services to the power system. Electricity retailer purchases energy from the wholesale market and then sells the energy to the customers by offering contract of fixed price or variable price. Current market setting allows the participation of DERs and the direction of power flow is from the transmission network to the distribution network. However, If large scale DERs are connected to the distribution network, It is almost impossible for one centralized network operator (e.g. TSO) to operate a power system in such scale. The economic dispatch problem is very hard to solve if all the network constraints of the distribution network are included. Without an efficient coordination mechanism between TSO and DSO, the available services from the DERs in distribution network are not visible for TSO. It is very hard for a market participant to provide the coordination service for the transmission and distribution network. The potential approach is to design a coordination mechanism for TSO and DSO.

There are two fundamental problems for the coordination of TSO-DSO economic dispatch. The first problem is how to decompose the dispatch responsibility of transmission and distribution network. In the hierarchical coordination mechanism, we propose to assign the dispatch task of each network to the corresponding system operator i.e. TSO is responsible to dispatch resources located in the transmission network while the DERs located in the distribution network are dispatched by DSO. The reliability standards of the connected network should be strictly followed by the owners of the DERs. If the DERs are not owned by DSO, some form of contract between the owners of DERs and DSO should be made in order to guarantee the reliability. In this arrangement, DSO is carrying on the dispatch responsibility and active distribution network management (ADNM). Current operations of DSO are mostly passive and only deal with uni-direction of power flow from transmission network to distribution network. The overinvested distribution network is rarely congested. However, the increasing development of DERs in the distribution network not only can cause bi-directional power flows between transmission and distribution network but also can lead to congestions in the distribution network. These challenges are pushing DSO to deploy ADNM techniques. The proposed convex AC OPF model formulated in (2) provides one of the most important tools for ADNM. The second problem is what information should be communicated between TSO and DSO in order to achieve efficient dispatch of the whole system including both transmission and distribution network. To address this problem, we propose the concept of generalized bid function (GBF) as a unified communication format between the TSO and the DSO. The GBF is defined and explained in detail in the following subsections. The hierarchical coordination mechanism is illustrated in Fig. 2. In Fig. 2, the distribution networks are interfacing with the transmission network by stepdown transformers. Each DSO fulfills the power generation requirement P^{sum} from TSO. Because the capacities of DERs are generally small, we can assume they are price takers. Higher prices caused by DERs when they are price makers can also be reflected in the proposed GBF. It is worth to mention that the market power

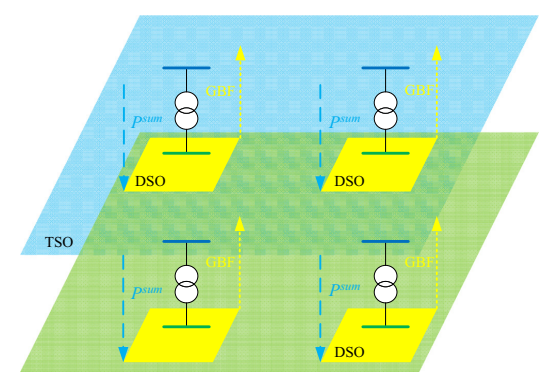


Fig. 2. The hierarchical coordination mechanism.

of DERs is a problem of market regulation and do not affect the formulation of the hierarchical coordination mechanism in this paper.

3.2. Generalized bid function

To avoid communicating detailed network data and regional bid information of DERs between TSO and DSO, the concept of GBF is proposed. The underlying mathematical structure of GBF is the Benders cut in Benders decomposition [50].

The economic dispatch for DSO contingent on the total power generation requirement of its network is set out in (3).

$$D_k(P_{k,j}^{sum}) = \text{Minimize} \sum_{n \in N_k} f(p_n, q_n)$$
(3a)

subject to (1a)-(1b); (1e)-(1f); (1h)-(1j)-(1k); (1l)-(1o) $\forall n \in N_k, l \in L_k$

$$\sum_{n \in \mathcal{N}_{i}} p_{n} = P_{k,j}^{\text{sum}} : (\alpha_{k,j})$$

$$\tag{3b}$$

where D_k is the dispatch cost of the distribution network as a function of its total power generation $P_{k,j}^{sum}$. $k \in K$ is the index of the DSO. $f(p_n,q_n)$ is the cost of power generation from the local DERs. N_k is the set of nodes in distribution network k. L_k is the set of lines in distribution network k. $j \in J_k$ is the index of the GBF. D_k can be approximated by a set of affine functions in (4) which is illustrated by Fig. 3.

$$D_{k}(P_{k,j}^{sum}) \geqslant \widehat{D}_{k,j} + \widehat{\alpha}_{k,j} \left(\sum_{n \in N_{k}} p_{n} - \widehat{P}_{k,j}^{sum} \right), \quad \forall j \in J_{k}, \ \forall k \in K$$
 (4)

Definition 1. Generalized Bid Function. We define generalized bid function as the set of parameters of the affine approximator expressed in (4). These parameters are used by TSO to incorporate the marginal cost of DERs located in distribution network to the dispatch of the entire power system. In the proposed hierarchical coordination mechanism, the generalized bid function is communicated from DSO through the set $DSO_k = \{(\widehat{D}_{kj}, \widehat{\alpha}_{kj}, \widehat{P}_{k,j}^{sum}): j \in J_k\}$ to TSO.

It is important to distinguish the GBF from the cumulative bids of DERs. Firstly, GBF implicitly includes all the bids from DERs. Given $\widehat{P}_{k,j}^{\text{sum}}$, it reflects the marginal cost of the power generation from the distribution network (where the DERs are located) as a whole. Secondly, GBF is communicated from DSO to TSO while bids of DERs are from DERs to DSO. In this sense, we assume there is a

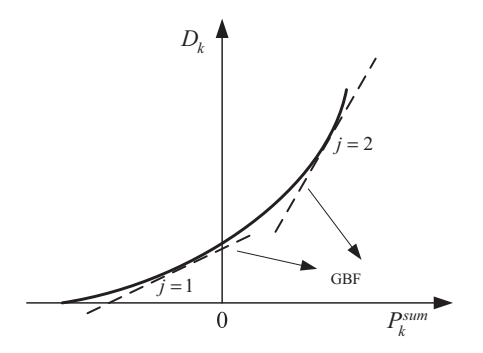


Fig. 3. Approximation of a convex cost function by affine functions.

market in the distribution network level for DERs. Thirdly, the information size of GBF is generally much less than the cumulative bids from DERs.

Once DSO_k are communicated, the TSO solves the following dispatch problem (5).

$$T_{\nu} = \text{Minimize} \sum_{n \in N_{\nu}} f(p_n, q_n) + \sum_{k \in K} D_k$$
 (5)

subject to (1a)-(1b); (1e)-(1f); (1h)-(1j)-(1k); (1l)-(1o); (4)
$$\forall n \in N_v, l \in L_v$$

where $v \in V$ is the index of the TSO. N_v is the set of nodes in transmission network v. L_v is the set of lines in the transmission network v. After optimization problem (5) is solved, the TSO communicates the total power generation requirement $\widehat{P}_{k,j}^{sum}$ to the corresponding DSO. (\widehat{j} the cardinality of the DSO_k set). Given $\widehat{P}_{k,j}^{sum}$, all the DSOs find the dispatch results of their networks. The underlying mathematical foundation of the hierarchical coordination mechanism is Benders decomposition. The optimization problem (5) is actually the master problem in Benders decomposition. The solution of the objective in (5) is the lower bound of the dispatch cost. The upper bound of distribution network dispatch cost is obtained by solving (4) which is actually the subproblem in Benders decomposition. Constraints (4) are Benders cuts. Because we use convex AC OPF model, it is proved that the optimal solution can be found within finite number of iterations [51].

It is worth to mention that the ownership problem of distribution lines is in the distribution electricity market level. Bid strategies related to different types of distribution line ownership and the impacts are not in the TSO-DSO coordination level. Thus we do not need to consider this problem in the proposed hierarchical coordination mechanism.

3.3. Accelerated hierarchical coordination by grid computing

Generally, one transmission network is providing energy to multiple distribution networks. The proposed hierarchical coordination mechanism is capable of coordinating TSO with multiple DSOs. This is clearly shown in dispatch problem (5) where we use the index k to differentiate multiple DSOs. Considering the complexity of distribution networks and large scale penetration of DERs, computation burden is one of the main challenges in coordinating TSO with multiple DSOs. The solution proposed in this paper to this computational challenge is grid computing. We design a grid computing structure in GAMS to assign the dispatch task of each network to one thread as demonstrated in Fig. 4. In this way, the hierarchical coordination is accelerated.

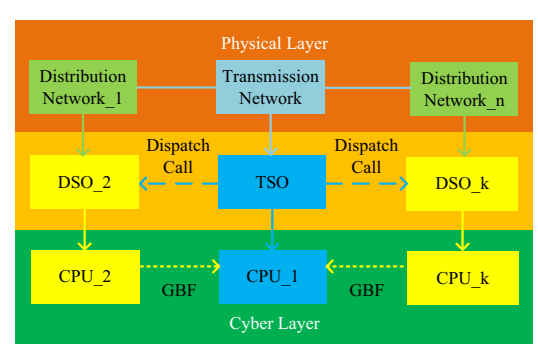


Fig. 4. GAMS grid computing structure of TSO-DSO hierarchical coordination

The dispatch problem is firstly decomposed to parallel independent threads by the Parallel Loop. This parallelization is based on assigning the convex AC OPF models to different threads. The thread of dispatching transmission network is firstly executed. The solutions of dispatching transmission network are broadcasted to other CPUs executing dispatch task of distribution networks. The dispatch problems of distribution networks are solved by different threads in parallel. During the Collect Loop, all the solutions of dispatch problems of distribution networks from the assigned threads will be collected. The GBFs are then communicated to the thread of dispatching transmission network which is in the status of waiting for input. Because there is no communication requirement between the threads executing DSO dispatch, the capability of grid computing can be exploited to the most. The proposed grid computing structure demonstrated in Fig. 4 is detailed in the grid computing management Algorithm 1. The grid computing management algorithm comprises one Parallel Loop and one Collect Loop. We propose to design the parallelization based on the total number of networks (transmission and distribution network). If the total number of networks is k^{max} , an parallelization management loop of k^{max} iterations is executed. The Collect Loop is responsible to repeatedly check the solution status of each handle (of thread) and collect available solutions. To avoid overloading of disk capacity, the handles (of threads) which have been executed are released. The frequency of handle release depends on available disk space of the computer. The Collect Loop continues until all the handles have been executed.

Algorithm 1. Grid Computing Management Algorithm

```
Initialization:
j = 1;
do
    Generate OPF model (5) for the transmission network: OPF-1;
   Assign OPF-1 to handle-1:
   Assign handle-1 to CPU-1;
   Execute handle-1:
   Broadcast P_{k,j}^{sum} To CPU-k for k > 1;
   k = 2:
   do
       Generate OPF model (3) for the distribution-k: OPF-k;
       Assign OPF-k to handle-k;
       Assign handle-k to CPU-k;
       k = k + 1;
   while k < k^{max}:
       if handle-k is ready then
           Collect Solutions from CPU-k;
           if network-k is distribution network then
              Send DSO_k to CPU-1;
           Release handle-k;
    while handle is nonempty;
while \frac{\sum_{k \in K} D_{k,j} - \sum_{k \in K} D_k}{\sum_{k \in K} D_{k,j}} > 2\% and j < j^{max};
Release handle-1:
```

4. Numerical results and discussions

In this section, the performance of the convex AC OPF model for economic dispatch is examined by several IEEE test cases [52]. The hierarchical coordination mechanism for TSO-DSO economic dispatch is firstly validated by an intuitive 38-node test case for various network congestion scenarios. The effect of DERs on the voltage magnitude and phase angles are analyzed. A large scale IEEE network test case is then used to show the potential of the proposed hierarchical coordination mechanism in practical applications. Moreover, the accurate results under various power loads show that the proposed hierarchical coordination mechanism is robust. All the models are coded in GAMS. Simulations are run on a PC with Intel 17-2760QM 2.4 GHZ CPU and 8 GB of RAM.

4.1. Performance of convex AC OPF model

We test the proposed SOCP based convex AC OPF model in (2) by several IEEE network cases [52]. Data of the test cases are from MATPOWER [53]. The results are listed in Tables 1 and 2. We use MOSEK in GAMS to solve the proposed convex AC OPF model. MATPOWER uses MATLAB built-in Interior Point Solver (MIPS) to solve the nonconvex AC OPF model. The proposed convex AC OPF model converges for all these test cases reported in Tables 1 and 2. The results of the proposed convex AC OPF model are very close to those obtained from MATPOWER. The differences are due to the approximations and relaxations used in the proposed convex AC OPF model. The computation time of convex AC OPF in GAMS is less than MATPOWER. This advantage of computation efficiency is more prominent in large network test cases. These results show that the convex AC OPF model is robust to network topology, power loads and transmission line parameters.

4.2. Dispatch results of hierarchical coordination mechanism

The IEEE 14-node [52] transmission network (which represent TSO network) is connected with two IEEE 13-node [52] feeders as distribution networks (each IEEE 13-node feeder represents one DSO network). The network configuration is shown in Fig. 5. Note that IEEE 13-node test feeder is modified here for ease of illustration and we assume the parameters of each branch are

Table 1
AC OPF objective.

Case	Objective function value [\$]		
	Convex AC OPF	MATPOWER	
IEEE14	8078.84	8081.53	
IEEE57	41696.94	41735.91	
IEEE118	129619.50	129626.20	
IEEE300	719381.80	719834.40	
1354pegase [54]	74101.36	74062.97	
2869pegase [54]	133877.00	133978.50	

Table 2 Computation time

Case	CPU time [s]	
	Convex AC OPF	MATPOWER
IEEE14	0.08	0.11
IEEE57	0.09	0.12
IEEE118	0.09	0.30
IEEE300	0.25	0.40
1354pegase [54]	0.76	8.58
2869pegase [54]	1.97	18.66

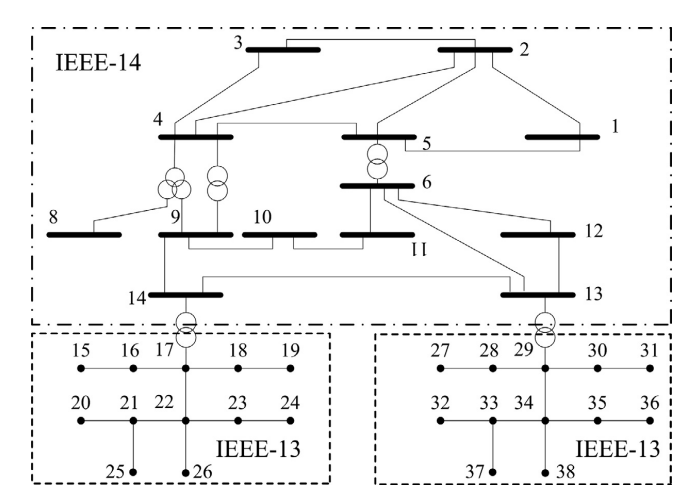


Fig. 5. Network configuration.

equal. Five generators are located in the transmission network. Ten DERs are located randomly in the two distribution networks. The power factors of DERs range from 0.71 to 1.00. We assume all generators are fully dispatchable. The base case means no congestion in any network. The congestions are caused by increasing the power loads in both transmission and distribution networks and reducing the capacity of lines or transformers in corresponding networks. Centralized dispatch results are calculated by assuming that one dispatch center has full access to both transmission and distribution network resources. Accordingly, the central dispatcher runs the convex AC OPF model for the whole system including transmission and distribution networks. The results of hierarchical coordination is compared with the results of centralized dispatch to show the performance of the hierarchical coordination. It is worth to mention that Benders decomposition is a way to build GBFs in the simulation of hierarchical coordination mechanism. The hierarchical coordination does not work in an iterative way. Each DSO calculates its GBFs and submit all of them in one package to the TSO.

4.2.1. Base case

The dispatch results of hierarchical coordination mechanism are listed in Table 3. The results of hierarchical coordination mechanism are very close to those from the centralized dispatch. Because of approximations used in the hierarchical coordination mechanism, the final cost of dispatch is a bit different from centralized

Active power dispatch results base case.

Generator	Dispatch [MW]	
	Centralized	Coordinated
1	34.14	38.74
2	140.00	140.00
3	100.00	100.00
6	10.00	10.00
8	9.68	5.88
11	10.00	10.00
12	20.00	20.00
Cost [€]	4875.76	4884.26
CPU time [s]	0.13	0.51

dispatch. The relative difference of final dispatch costs between hierarchical coordination and centralized dispatch is within 1%. The CPU computation time of simulated hierarchical coordination in the base case is 0.51 s which is longer compared with centralized dispatch. If the DSOs submit their GBFs (i.e. parameters of affine approximators of their cost functions in one package) to TSO, the hierarchical coordination converges in one iteration. Thus, the CPU time of the real hierarchical coordination is around one third of the CPU time in the simulations.

We report the parameters of the GBFs for all the DSOs and list the results in Table 4. As shown in Table 4, the DSOs prepare their GBFs to be submitted to the TSO. The TSO calculates the dispatch instructions and power dispatch requirements will be communicated back down to the DSO. Bids from the local DERs are not required to be submitted to the TSO. In other words, by using GBF, the TSO and the DSO do not need to share their detailed network information with each other.

We show the impact of DERs on the voltage amplitude and phase angle in Fig. 6. Because most energy are dispatched from the generators in the transmission network, the voltage amplitude and phase angle of the nodes in the transmission network are high. The voltage rise due to the dispatch of DERs in the second distribution network is clearly demonstrated in Fig. 6.

To demonstrate how the marginal cost parameters affect the results, we reduce the marginal cost of DERs in the second distribution network and increase the marginal cost of generators in the transmission network. The dispatch results of hierarchical coordination mechanism are listed in Table 5. In this scenario, more active power from DERs are dispatched (see Table 7). The GBFs are listed in Table 6.

Table 4Generalized bid functions in the base case.

k	j	$\widehat{D}_{k,j}\left[\epsilon\right]$	$\hat{\alpha}_{k,j}$ [ϵ /MWh]	$\widehat{P}_{k,j}^{sum}$ [MW]
1	1	1509.74	32.00	55.62
	2	126.56	15.00	8.44
	3	279.41	22.00	15.88
2	1	911.34	36.00	40.59
	2	250.28	19.00	15.28
	3	530.00	19.03	30.00

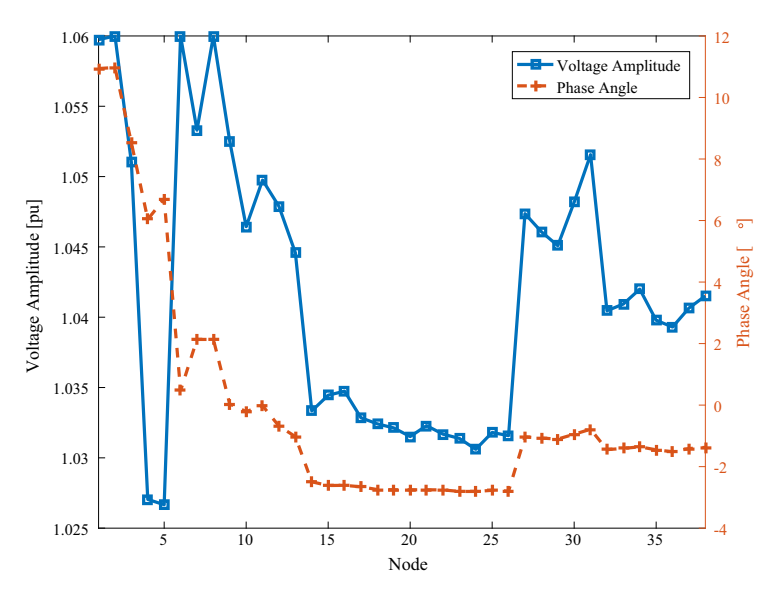


Fig. 6. Voltage amplitude and phase angle in the base case.

Table 5Active power dispatch results lower marginal cost of DERs.

Generator	Dispatch [MW]	
	Centralized	Coordinated
1	29.29	29.07
6	10.00	10.00
12	20.00	12.50
13	15.00	15.00
Cost [€]	5024.10	5007.75
CPU time [s]	0.11	0.22

Table 6Generalized bid functions lower marginal cost of DERs.

k	j	$\widehat{D}_{k,j}$ [ϵ]	$\hat{\alpha}_{k,j}$ [ϵ /MWh]	$\widehat{P}_{k,j}^{sum}$ [MW]
1	1	1409.72	32.00	52.49
	2	1265.63	15.00	8.44
	3	279.41	22.00	15.88
2	1	553.80	20.00	38.69
	2	132.00	12.00	11.00
	3	367.50	15.00	27.50

The impact of DERs on the voltage amplitude and phase angle are shown by Fig. 7. Compared with the base case, more voltage rise in the second distribution network is observed. This is because more DERs are dispatched in the distribution network due to lower marginal cost of DERs.

4.2.2. Congestion of transmission-distribution interface

The first congested transformer is located between node 14 and node 17. The second one is located between node 13 and node 29. The capacities of both transformers are reduced to 30 MVA. Congestion of Transmission-Distribution Interface [10] is modeled

by these two congested transformers. The results show that the proposed hierarchical coordination mechanism is capable of managing network interface congestions. It can be observed that when congestions happen, more DERs are activated to balance the local loads. Moreover, in this congestion scenario, the CPU computation time of the hierarchical coordination does not increase compared with the Base Case. These numerical results demonstrate the efficiency of the proposed parallel computation algorithm.

The GBFs for this congestion scenario are listed in Table 8. Congestion management of transmission-distribution interface by the proposed hierarchical coordination mechanism does not necessarily cause the DSO to submit more information to the TSO. Compared with the Base Case, $\hat{\alpha}_{kj}$ parameters in GBFs show that more expensive DERs in distribution networks are dispatched in this congestion scenario. \hat{P}_{kj}^{sum} parameters in Table 8 also show that more power generatine requirements of DERs are called by the TSO to release the congestions.

The impact of DERs on the voltage amplitude and phase angle by Fig. 8. It is interesting in this congestion scenario that the voltage amplitude in the distribution networks are lower compared with the Base Case. Even without sufficient energy from the transmission network due to the congestion of transmission-distribution interface, the DERs are capable to support the voltage in the distribution networks.

4.2.3. Congestion of transmission lines

The congestion of transmission lines are modeled by increasing the power demand of both transmission and distribution networks. Then, we reduce the capacity of the transmission line between node 1 and node 2 to 100 MVA. The capacity of the transmission line between node 6 and node 13 is reduced to 50 MVA. Because these two lines are both located in the transmission network, we refer this congestion scenario as congestion of transmission lines [10]. These two lines are congested when the dispatch models are solved. The results of centralized dispatch and the hierarchical

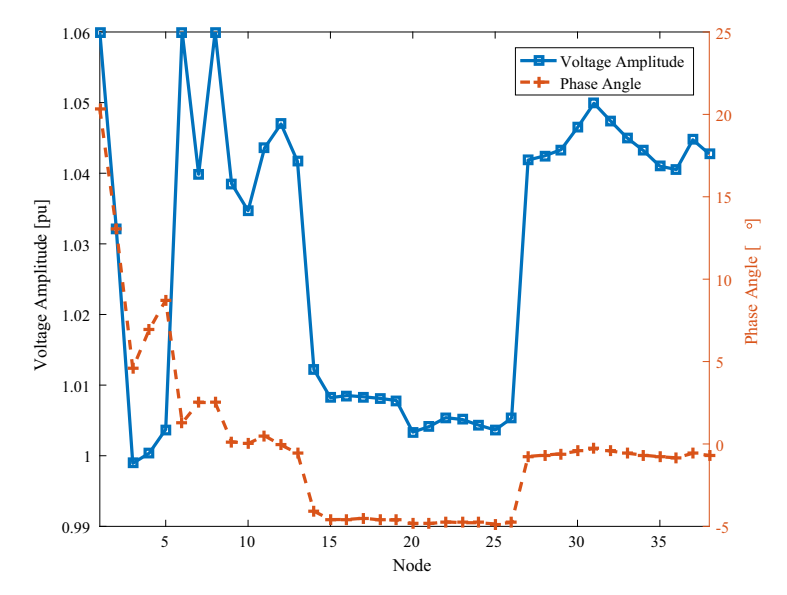


Fig. 7. Voltage amplitude and phase angle lower marginal cost of DERs.

Table 7Active power dispatch results in congestion of transmission-distribution interface.

Generator	Dispatch [MW]		
	Centralized	Hierarchical	
1	160.67	184.03	
2	140.00	140.00	
3	100.00	100.00	
4	41.67	12.17	
6	10.00	10.00	
7	23.94	28.84	
8	10.00	10.00	
10	30.00	28.85	
11	10.00	10.00	
12	20.00	20.00	
13	15.00	15.00	
14	15.00	15.00	
15	7.97	11.44	
Cost [€]	11679.75	11685.80	
CPU time [s]	0.14	0.24	

Table 8Generalized bid functions in congestion of transmission-distribution interface.

k	j	$\widehat{D}_{k,j}\left[\epsilon\right]$	$\hat{\alpha}_{k,j}$ [ϵ /MWh]	$\widehat{P}_{k,j}^{sum}$ [MW]
1	1	2421.16	35.00	83.75
	2	1568.01	32.00	57.44
	3	2215.98	32.00	77.69
2	1	2438.01	45.00	77.07
	2	2184.94	45.00	71.44
	3	2184.94	45.00	71.44

coordinated dispatch are listed in Table 9. More expensive generators in the transmission network are dispatched because of the congestion. The increase of dispatch cost can be observed in both centralized and coordinated dispatch.

Table 9 Active power dispatch results in congestion of transmission lines

Generator	Dispatch [MW]		
	Centralized	Hierarchica	
1	176.13	178.31	
2	140	140	
3	100	100	
4	100	100	
5	19.10	95.93	
6	10	10	
7	30	0	
8	10	5.88	
10	30	0	
11	10	10	
12	20	20	
14	9.11	0	
Cost [€]	13043.61	13053.53	
CPU time [s]	0.13	0.25	

Table 10 lists the GBFs in congestion of transmission lines. Compared with the congestion of transmission-distribution interface, this congestion scenario does not require to dispatch more expensive DERs in the distribution networks. This can be clearly observed from the $\hat{\alpha}_{kj}$ parameters of the GBF results.

We show the impact of DERs on the voltage amplitude and phase angle in Fig. 9. Both voltage amplitude rise and reduction of nodes in the transmission can be observed because of the congestions. These congested transmission lines do not prevent power flows from the transmission to the distribution network. The voltage in the distribution networks are supported by the energy from transmission network and DERs in the distribution networks.

4.2.4. Congestion of distribution feeders

This congestion scenario can happen when large number of EVs are charged at the same time. The congestion of distribution feeders are modeled by increasing the power demand of the transmission and the distribution networks. Then, we reduce the capacity of

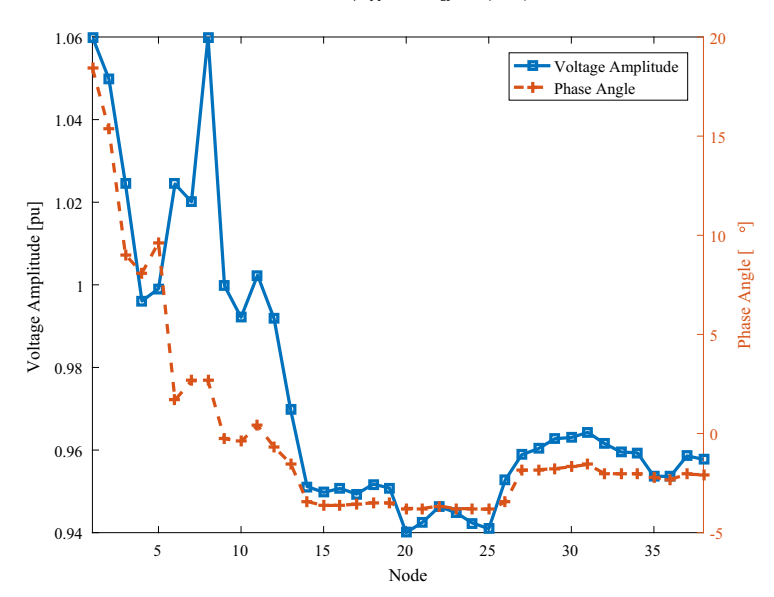


Fig. 8. Voltage amplitude and phase angle in congestion of transmission-distribution interface.

Table 10Generalized bid functions in congestion of transmission lines.

k	j	$\widehat{D}_{k,j}\left[\epsilon\right]$	$\hat{\alpha}_{k,j}$ [ϵ /MWh]	$\widehat{P}_{k,j}^{sum}$ [MW]
1	1	1680.74	32.00	60.96
	2	126.56	15.00	8.44
	3	279.41	22.00	15.88
2	1	1018.59	36.00	43.57
	2	250.28	19.00	15.28
	3	530.00	36.00	30.00

the distribution feeder between node 17 and node 22 to 10 MVA. The capacity of the distribution line between node 29 and node 34 is reduced to 10 MVA. Because these two feeders are both located in the distribution network, we refer this congestion scenario as congestion of distribution feeders. These two feeders are congested when the dispatch models are solved. The results of centralized dispatch and the hierarchical coordinated dispatch are listed in Table 11. Compared with the Base Case, this congestion scenario causes more expensive generators and DERs in the transmission and the distribution networks to be dispatched. After three

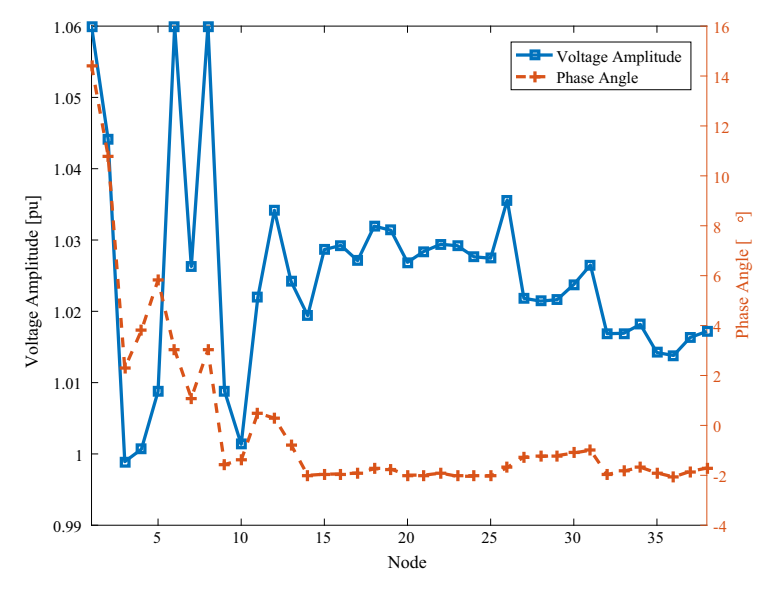


Fig. 9. Voltage amplitude and phase angle in congestion of transmission lines.

Table 11Active power dispatch results in congestion of distribution feeders

Generator	Dispatch [MW]	
	Centralized	Hierarchical
1	196.79	275.07
2	140.00	140.00
3	100.00	100.00
4	100.00	78.20
6	10.00	5.32
7	20.48	0.00
8	10.00	10.00
10	19.41	13.50
11	10.00	10.00
12	20.00	20
13	15.00	13.00
14	15.00	15
15	0.25	0.00
Cost [€]	13063.56	13078.30
CPU time [s]	0.12	0.23

Table 12Generalized bid functions in congestion of distribution feeders.

k	j	$\widehat{D}_{k,j}\left[\epsilon\right]$	$\hat{\alpha}_{k,j} \ [\epsilon/MWh]$	$\widehat{P}_{k,j}^{sum}$ [MW]
1	1	1698.04	32.00	61.50
	2	126.56	15.00	8.44
	3	731.82	15.00	28.82
2	1	1313.90	18.96	43.96
	2	2570.00	45.00	80.00
	3	1590.19	40.00	58.00

iterations, the relative difference of dispatch cost for the centralized dispatch and coordinated dispatch is less than 1%.

The GBFs in the congestion of distribution lines scenario are listed in Table 12. We can see that GBFs are capable of reflecting

the congestion information in the distribution network. $\hat{\alpha}_{kj}$ parameters in the GBFs show that the most expensive DERs are dispatched. \hat{P}^{sum}_{kj} parameters in the GBFs show that more power generation requirements from DERs are called by the TSO to release the congestion of distribution lines and fulfill local power demand.

We show the impact of DERs on the voltage amplitude and phase angle in Fig. 10. In this congestion scenario, the voltage of the nodes located afterwards the congested feeders in the distribution networks are supported mostly by the local DERs. We can see that the voltage amplitudes of these nodes are well in the range of [0.99 1.03] (per unit value).

4.3. Convergence of hierarchical coordination mechanism

The convergence characteristics of hierarchical coordination mechanism are shown in Fig. 11. After three iterations in the simulation, the relative differences of the upper bounds and lower bounds of all test cases are within 2%. The fast convergence of Benders decomposition based simulation of the hierarchical coordination proves that the required information volume of GBF is small. The hierarchical coordination of TSO-DSO dispatch is very efficient. Because we use Benders decomposition in the simulation of hierarchical coordination, the simulation works in an iterative way. However, as we have mentioned, the hierarchical coordination converges in one iteration as long as the GBFs are submitted from the DSO to the TSO as one package.

4.4. Coordination of both active power and generation reserves

The generation reserves are provided from all generators including DERs to mitigate real time power unbalance and uncertainty of renewable energy. The active power and reserve dispatch results are listed in Table 13. The dispatch cost is higher compared with the case of not providing generation reserves. The GBFs are shown in Table 14. The cost information of both the active power

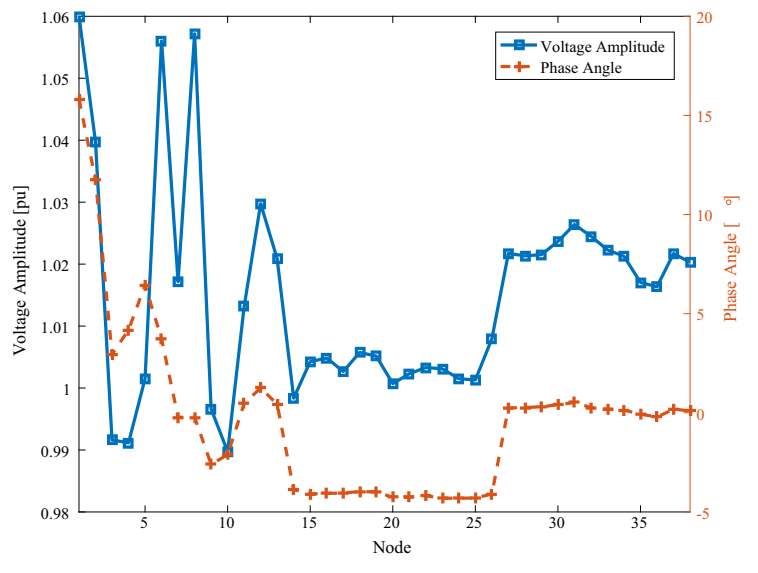


Fig. 10. Voltage amplitude and phase angle in congestion of distribution feeders.

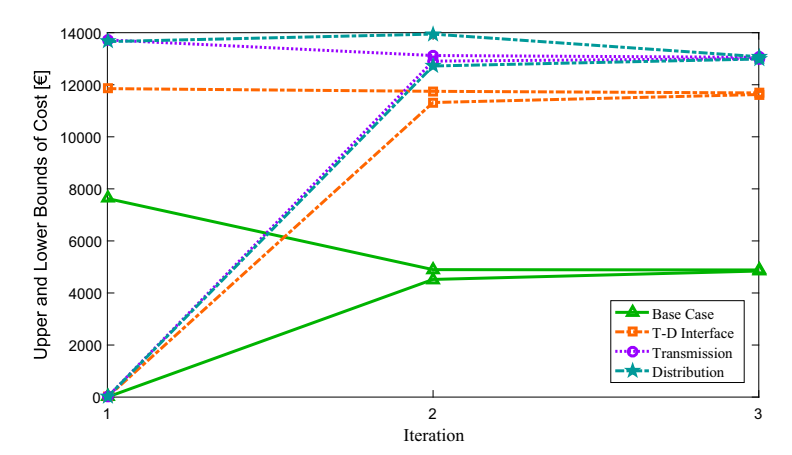


Fig. 11. The convergence of the proposed hierarchical coordination mechanism.

Table 13Dispatch results in coordination of both active power and generation reserves.

Generator	Centraliz	Centralized [MW]		ical [MW]
	Energy	Reserve	Energy	Reserve
1	138.02	0.00	148.69	0.00
2	31.93	248.07	147.60	132.40
3	115.67	84.33	0.00	200.00
6	0.00	25.00	0.00	2.50
8	20.00	5.00	6.25	5.00
11	4.36	15.64	0.00	20.00
12	15.64	4.36	20.00	0.00
14	0.00	0.00	2.86	0.00
Cost [€]	11242.09		112	37.74
CPU time [s]	0.11		0.28	

Table 14Generalized bid functions in coordination of both active power and generation reserves.

k	j	$\widehat{D}_{k,j}\left[\epsilon\right]$	$\hat{\alpha}_{k,j}$ [ϵ /MWh]	$\widehat{P}_{k,j}^{sum}$ [MW]
1	1	2283.26	32.00	61.69
	2	509.25	17.00	5.44
	3	646.75	22.00	6.25
2	1	1582.11	40.00	43.68
	2	393.38	19.00	4.12
	3	797.86	36.00	2.29

and reserve have been captured in the parameters of the GBF. We can see that the proposed hierarchical coordination mechanism is capable of coordinating both active power and generation reserves. The fast convergence of the hierarchical coordination in this test case shows the strong capability of the proposed parallel computation approach.

4.5. Application in large scale power network

The IEEE 342 node network [55] is modified here to illustrate the application of the proposed hierarchical coordination mechanism. The network is from the United Electric Light & Power

Company of New York. This test case has one 230 kV transmission network (nodes P1-P4, P7-P8) and one 277/480 V distribution network (nodes P5-P6, P9-P390, S193-S240). The meshed distribution network is connected to the transmission network by two step-down transformers (230/132 kV Δ/Δ connection) shown in Fig. 12. One 50 MW generator is located in the transmission network. Each 13.2 kV distribution feeder is equipped with one 7.5 MW DG. To simulate the large scale integration of DERs, we distribute in total 48 DGs among all nodes of the local community networks (one 3 MW DG at each node). The power factors of DERs range from 0.89 to 1.00. The active power dispatch results are listed in Table 15. The results of the GBFs are shown in Table 16. We can see in this real network test case, the performance of the hierarchical coordination mechanism is fast and accurate compared with centralized dispatch. We show the impact of DERs on the voltage amplitude and phase angle in Fig. 13. The voltage spikes in the distribution network show clearly DERs in the distribution feeders are dispatched. The meshed distribution network also shows a very complex voltage profile.

To investigate the effect of power load on the results, we change the power loads of all the 390 nodes (note the total number of nodes in this test case is 390 not 342) in the network from 10% to 100% of the load levels in the base case (because in the base case we have increased the power loads to 5 times of the loads in the original network data set, the power loads actually vary from 50% to 500% of the original loads.). Then the economic dispatch problem is solved under different load levels. The results of the dispatch cost for centralized dispatch and hierarchical coordination mechanism are shown in Fig. 14. The dispatch cost increases with the increase of the power loads. For all the load levels, hierarchical coordination mechanism converge to very close results compared with the centralized dispatch. To demonstrate the accuracy of the hierarchical coordination mechanism, we calculate the *relative error* ε of the results by:

$$\varepsilon = \frac{\cos t_H - \cos t_C}{\cos t_C} \times 100\% \tag{6}$$

where $cost_H$ is the dispatch cost of hierarchical coordination, $cost_C$ is the dispatch cost of centralized dispatch. The results of relative error are shown in Fig. 15. In this large scale network test case, the relative errors of the proposed hierarchical coordination mechanism for all the power load levels are less than 0.4%.

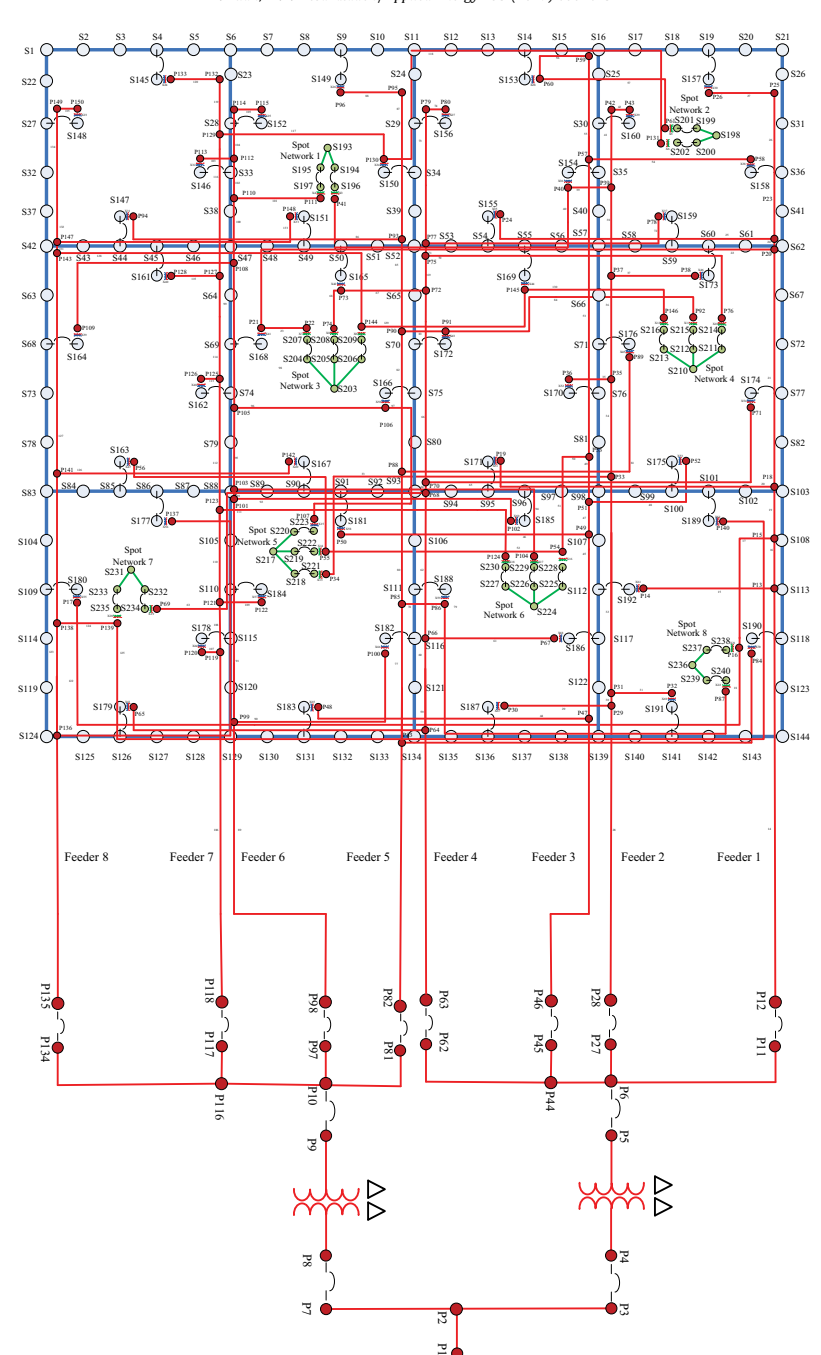


Fig. 12. The IEEE342-node network.

Table 15Active power dispatch results in large scale power network.

Generator	Dispato	h [MW]
	Centralized	Hierarchica
1	50.00	50.00
2	7.50	7.50
3	7.50	7.50
4	7.50	7.50
5	7.50	7.50
6	7.50	7.50
7	7.50	7.50
8	7.50	7.50
9	5.93	5.96
Cost [€]	73168.05	73234.11
CPU time [s]	0.12	0.23

Table 16
Generalized bid functions in large scale power network.

k	j	$\widehat{D}_{k,j}\left[\epsilon\right]$	$\hat{\alpha}_{k,j}$ [ϵ /MWh]	$\widehat{P}_{k,j}^{sum}$ [MW]
1	1	147.75	10.00	2.37
	2	501.44	16.00	5.14
	3	632.25	18.00	5.96

5. Conclusions

This paper proposes a hierarchical coordination mechanism to coordinate the economic dispatch of TSO and DSO. This is motivated by the fact that more and more DERs are integrated to the distribution network. Meanwhile the visibility of DERs to TSO is very limited. Creating a coordination mechanism to loop both TSO and DSO in activating the flexibilities from the DERs is essential. The issue of network information exchange between TSO and DSO is addressed through the proposed concept of GBF. The hierarchical coordination mechanism is proposed to decompose the dispatch task of transmission network and distribution network. Two

levels are considered in the proposed hierarchy. At the second level, DSO solves the economic dispatch considering its own network constraints and DERs. The results of DSO dispatch are packaged in the form of GBFs and communicated to the first level of hierarchy i.e. TSO. Once the economic dispatch of the first level of hierarchy is solved, the dispatch results are communicated back down to the DSO in the second hierarchy. The convergence of hierarchical coordination mechanism is guaranteed by the convexity of the proposed SOCP based AC OPF. We simulate different scenarios of possible network congestions in both transmission and distribution networks. The simulation is accelerated by the proposed grid computing structure in GAMS environment, Results show that the simulation of the proposed hierarchical coordination mechanism can achieve very close results compared with centralized dispatch within three iterations. This means if DSO submit the GBFs in one package, the real hierarchical coordination converge in one iteration. The results of GBFs in all test cases demonstrate a unified format of TSO-DSO dispatch communication. By formulating the problem of scheduling generation reserves in the proposed convex ACOPF model, we are able to demonstrate that the proposed hierarchical coordination mechanism is capable of coordinating both energy and reserves at the same time. The scheduled reserves are useful to balance power system in real time considering the uncertainty of renewable energy. The numerical results of IEEE342-node test case show the potential of practical applications of the proposed hierarchical coordination mechanism. The robustness of the proposed hierarchical coordination mechanism is proved by the accurate results under different load levels in the IEEE342node test case. Because the proposed hierarchical coordination mechanism is based on the bids of DERs in the market and the bids are generally in the same format, the implementation of this coordination mechanism does not depend on what types of DERs are connected in the distribution network. Using dynamic price signals is one market mechanism to release the network congestions and activating the flexibilities from DERs. For the aggregator, the potential to profit by participating the retail market is large if dynamic price signals are provided. The proposed hierarchical

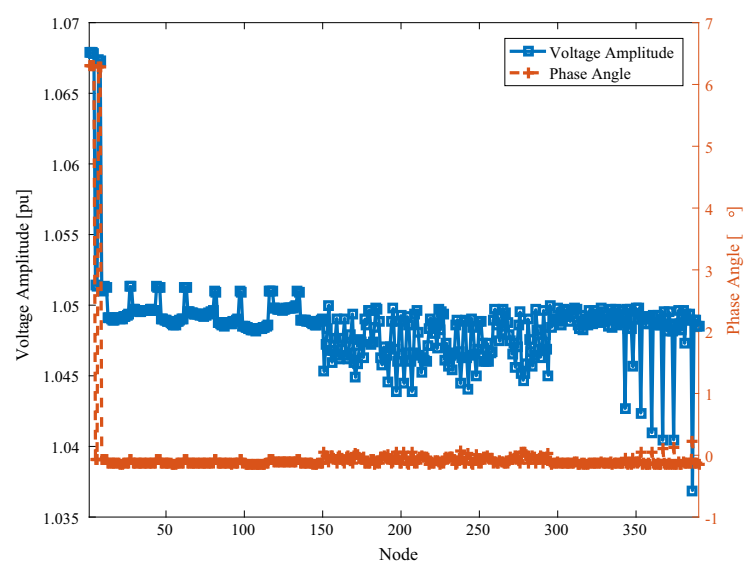


Fig. 13. Voltage amplitude and phase angle in large network.

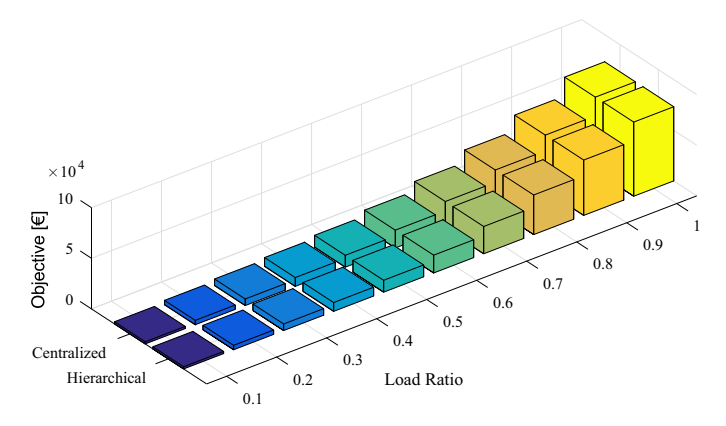


Fig. 14. Dispatch cost under different load levels.

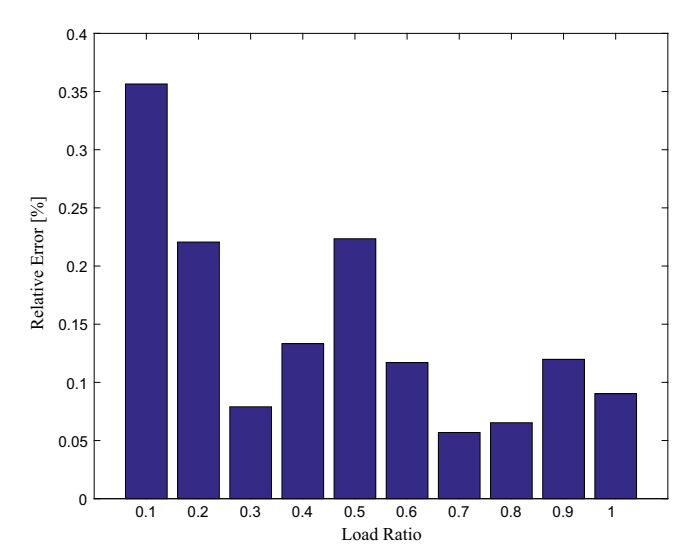


Fig. 15. Relative error of hierarchical coordination.

coordination mechanism for TSO and DSO provides a way to guarantee the market is efficient for both transmission network and distribution network.

Acknowledgment

The authors would like to thank the support from SETS Erasmus Mundus Joint Doctorate Fellowship for this research project on TSO-DSO coordination. We want to express our special thanks to Dr. Konstantin Staschusand and Dr. Darryl R. Biggar for all the insightful and motivating discussions. Dr. Konstantin Staschusand is the Secretary-General of the European Network of Transmission System Operators (ENTSO-E). Dr. Darryl R. Biggar is with the Australian Competition and Consumer Commission. All the careful reviews on this paper by the editors and reviewers of this journal are sincerely appreciated by the authors.

References

- [1] Kärkkäinen S et al. Integration of demand-side management, distributed [1] Karkkalnien S et al. Integration of unfailut-side infallagement, distributed generation, renewable energy sources and energy storages. Report task XVII integration of demand-side management, distributed generation. Renew Energy Sources Energy Storages 2008;1:77.
 [2] Driesen J, Katiraei F, Design for distributed energy resources. Power Energy Mag, IEEE 2008;6(3):30–40.
- [3] Pérez-Arriaga I, Bharatkumar A. A framework for redesigning distribution network use of system charges under high penetration of distributed energy
- network use of system charges under nigh penetration of distributed energy resources: new principles for new problems. Tech. rep., CEEPR Working Paper Series no, WP-2014-006; 2014.

 [4] Akorede MF, Hizam H, Pouresmaeil E. Distributed energy resources and benefits to the environment. Renew Sustain Energy Rev 2010;14(2):724-34.

 [5] Lakshmanan V, Marinelli M, Hu J, Bindner HW. Provision of secondary frequency control via demand response activation on thermostatically controlled loads: solutions and experiences from denmark. Appl Energy 2016;123-473-80. 2016;173:470-80.
- [6] Cheng M, Sami SS, Wu J. Benefits of using virtual energy storage system for power system frequency response. Appl Energy 2016.
 [7] EDSO. General guidelines for improving TSO-DSO cooperation. Tech. rep.;

- [8] EDSO. TSO-DSO data management report. Tech. rep.; 2015.
- [9] Zipf M, Mst D. Cooperation of TSO and DSO to provide ancillary services. In: 2016 13th International conference on the European energy market (EEM);
- [10] Helfried Brunner AZ, TSO-DSO interaction; an overview of current interaction between transmission and distribution system operators and an assessment of their cooperation in smart grids. Tech. rep., International Smart Grid Action Network (ISAGN) Discussion Paper Annex 6 Power T&D Systems, Task 5.
- ISAGN, Paris; September 2014. [11] Silva N, Pinto CM, Bernardo AM, Carrapatoso A, Pestana R, Dias S. The interaction between DSO and TSO to increase DG penetration: the Portuguese example. In: Integration of renewables into the distribution grid, CIRED 2012
- orkshop; 2012. p. 1–4. Marten F, Lwer L, Tbermann JC, Braun M. Optimizing the reactive power balance between a distribution and transmission grid through iteratively updated grid equivalents. In: Power systems computation conference (PSCC), 2014; 2014. p. 1–7.
 [13] He L, Yang J, Yan J, Tang Y, He H. A bi-layer optimization based temporal and
- spatial scheduling for large-scale electric vehicles. Appl Energy 2016:168:179-92.
- [14] Varadarajan M, Swarup K. Solving multi-objective optimal power flow using differential evolution. Gener Transm Distrib IET 2008;2(5):720-30.
- [15] Sivasubramani S, Swarup K, Multi-objective harmony search algorithm for optimal power flow problem. Int J Electr Power Energy Syst 2011;33 (3):745–52.
- (3):745-52.
 [16] Noroozian M, Ăngquist L, Ghandhari M, Andersson G. Use of upfc for optimal power flow control. IEEE Trans Power Deliv 1997;12(4):1629-34.
 [17] Mamandur K, Chenoweth R. Optimal control of reactive power flow for improvements in voltage profiles and for real power loss minimization. IEEE Trans Power Appar Syst 1981(7):3185-94.
 [18] Hesamzadeh MR, Biggar DR, Hosseinzadeh N, Wolfs PJ. Transmission augmentation with mathematical modeling of market power and strategic generating expansion Part LIEEE Trans Power Syst 2011;32(4):2040.
- generation expansion Part I, IEEE Trans Power Syst 2011;26(4):2040-8.
- [19] Lu H, Cao M, Li J, Huang G, He L. An inexact programming approach for urban electric power systems management under random-interval-parameter uncertainty. Appl Math Modell 2015;39(7):1757–68.
- [20] Li Z, Qiu F, Wang J. Data-driven real-time power dispatch for maximizing variable renewable generation. Appl Energy 2016;170:304–13.
 [21] Venkatesh B, Sadasivam G, Khan MA. A new optimal reactive power scheduling method for loss minimization and voltage stability margin maximization using successive multi-objective fuzzy lp technique. IEEE Trans Power Syst 2000;15(2):844–51.
- trans rower Syst 2000;15(2):844–51.

 [22] Song H, Lee B, Kwon S-H, Ajjarapu V. Reactive reserve-based contingency constrained optimal power flow (recopf) for enhancement of voltage stability margins. IEEE Trans Power Syst 2003;18(4):1538–46.

 [23] Alsac O, Stott B. Optimal load flow with steady-state security. IEEE Trans Power Appar Syst 1074(2):745. 51
- Power Appar Syst 1974(3):745–51.

 [24] Thomas JJ, Grijalva S. Flexible security-constrained optimal power flow. IEEE Trans Power Syst 2015;30(3):1195–202.
- [25] Condren J, Gedra TW. Expected-security-cost optimal power flow with small-signal stability constraints. IEEE Trans Power Syst 2006;21(4):
- [26] Niknam T, Narimani M, Aghaei J, Tabatabaei S, Nayeripour M. Modified honey bee mating optimisation to solve dynamic optimal power flow considering generator constraints. Gener Transm Distrib IET 2011;5(10):989–1002.
 Purchala K, Meeus L, Van Dommelen D, Belmans R. Usefulness of dc power
- flow for active power flow analysis. In: IEEE power engineering society general
- meeting, 2005. IEEE; 2005. p. 454–9.

 [28] Gan L, Low SH. Convexification of AC optimal power flow. In: Power systems computation conference (PSCC), 2014; 2014. p. 1–11.
- [29] Farivar M, Low SH. Branch flow model: relaxations and convexification: Part I. IEEE Trans Power Syst 2013:28(3):2554-64
- [30] ONeill RP, Castillo A, Cain MB. The IV formulation and linear approximations of the AC optimal power flow problem. Tech. rep., FERC; 2012.

- [31] Baradar M, Hesamzadeh MR, Ghandhari M. Second-order cone programming for optimal power flow in vsc-type ac-dc grids. IEEE Trans Power Syst 2013;28
- (d):4282-91.

 Baradar M, Hesamzadeh MR. Ac power flow representation in conic format
- [32] baladai M, resalifazader MR. Ac power low representation in Conic format.
 [33] Bai X, Wei H, Fujisawa K, Wang Y. Semidefinite programming for optimal power flow problems. Int J Electr Power Energy Syst 2008;30(6):383–92.
 [34] Lavaei J, Low SH. Zero duality gap in optimal power flow problem. IEEE Trans Power Syst 2012;27(1):92–107.
 [35] Jubril A, Olaniyan O, Komolafe O, Ogunbona P. Economic-emission dispatch problems.
- problem: a semi-definite programming approach. Appl Energy 2014;134: 446_55
- [36] Lesieutre BC, Molzahn DK, Borden AR, DeMarco CL. Examining the limits of the application of semidefinite programming to power flow problems. In: 2011 49th Annual Allerton conference on communication, control, and computing
- (Allerton); 2011. p. 1492–9. Lavaei J, Tse D, Zhang B. Geometry of power flows and optimization in distribution networks. IEEE Trans Power Syst 2014;29(2):572–83.
- [38] Low S. Convex relaxation of optimal power flow, Part I: Formulations and
- equivalence. IEEE Trans Control Netw Syst 2014;1(1):15–27.

 [39] Low S. Convex relaxation of optimal power flow, part II: Exactness. IEEE Trans Control Netw Syst 2014(2):177–89.
- [40] Xu X, Jin X, Jia H, Yu X, Li K. Hierarchical management for integrated community energy systems. Appl Energy 2015;160:231–43.
 [41] Biggar Darryl R, Hesamzadeh Mohammad Reza. The economics of electricity

- [41] Biggar Darryi K, Hesamzaden Monammad Reza. The economics of electricity markets. IEEE Press & Wiley; 2014.
 [42] Yuan Z, Hesamzadeh MR. A hierarchical dispatch structure for distribution network pricing. In: 2015 IEEE 15th international conference on environment and electrical engineering (EEEIC). IEEE; 2015. p. 1631-6.
 [43] Bhattarai B, Levesque M, Bak-Jensen B, Pillai J, Maier M, Tipper D, et al. Design and co-simulation of hierarchical architecture for demand response control and coordination. IEEE Trans Indust Inform 2016;PP(99). http://dx.doi.org/10.1109/III.2016.524582.
 [41] La Hatri-Jida dei cord/10.1109/III.2016.524582
- 10.1109/TII.2016.2634582. p. 1-1 http://dx.doi.org/10.1109/TII.2016.2634582. [44] Manshadi SD, Khodayar ME. A hierarchical electricity market structure for the smart grid paradigm. IEEE Trans Smart Grid 2016;7(4):1866–75. http://dx.doi.
- org/10.1109/TSG.2015.2428194. http://dx.doi.org/10.1109/TSG.2015.2428194. [45] The mosek optimization software. http://www.mosek.com>. [46] Liu F, Bie Z, Liu S, Ding T. Day-ahead optimal dispatch for wind integrated power system considering zonal reserve requirements. Appl Energy 2017:188:399-408.
- [47] Nistor S, Wu J, Sooriyabandara M, Ekanayake J. Capability of smart appliances to provide reserve services. Appl Energy 2015;138:590–7.
 [48] Hatziargyriou N, Asano H, Iravani R, Marnay C. Microgrids. IEEE Power Energy
- Mag 2007;5(4):78-94. http://dx.doi.org/10.1109/MPAE.2007.376583. http://dx.doi.org/10.1109/MPAE.2007.376583. [49] Scott Burger CB, Chaves-vila Jose Pablo, Prez-Arriaga I.J. The value of
- aggregators in electricity systems. Tech. rep.; 2016.
 Geoffrion AM. Generalized benders decomposition. J Optim Theory Appl 1972;10(4):237–60.
- [51] Coneio Al, Castillo E, Minguez R, Garcia-Bertrand R, Decomposition techniques in mathematical programming: engineering and science applications. Springer Science & Business Media; 2006.
- [52] The University of Washington Power Systems Test Case Archive, <a href="http://www.
- [52] The University of Washington Power Systems Test Case Archive. http://www.ee.washington.edu/research/pstca/.
 [53] Zimmerman RD, Murillo-Sánchez CE, Thomas RJ. Matpower: steady-state operations, planning, and analysis tools for power systems research and education. IEEE Trans Power Syst 2011;26(1):12–9.
 [54] Fliscounakis S, Panciatici P, Capitanescu F, Wehenkel L. Contingency ranking with respect to overloads in very large power systems taking into account uncertainty, preventive, and corrective actions. IEEE Trans Power Syst 2013;28 (4):400-17 (4):4909-17
- [55] Schneider K, Phanivong P, Lacroix J-S. leee 342-node low voltage networked test system. In: 2014 IEEE PES general meeting conference & exposition. IEEE; 2014. p. 1–5.

IV

Applied Energy xxx (xxxx) xxx-xxx



Contents lists available at ScienceDirect

Applied Energy

journal homepage: www.elsevier.com/locate/apenergy



Towards the Power Synergy Hub (PSHub): Coordinating the energy dispatch of super grid by modified Benders decomposition

Zhao Yuan^{a,*}, Sonja Wogrin^b, Mohammad Reza Hesamzadeh^a

- Department of Electric Power and Energy Systems, KTH Royal Institute of Technology, Stockholm, Sweden
- stitute for Research in Technology, ICAI School of Engineering, Comillas Pontifical University, Madrid, Spair

HIGHLIGHTS

- Propose the concept of Power Synergy Hub (PSHub) to operate the super grid.
- Compare the SOC-ACOPF model with DC OPF model and other convex AC OPF models.
- Formulate the modified Benders decomposition as the mathematical foundation of PSHub.
- Assist real-time operation of super grid by parallel computation in GAMS.
- Speed up the convergence of the modified Benders decomposition.

ARTICLE INFO

Keywords: Super grid Power synergy hub Energy dispatch Optimal power flow Modified Benders decomposition Parallel computation

ABSTRACT

The challenge of operating ultra-large-scale power system or super grid is addressed in this paper. We set up the concept of power synergy hub (PSHub) serving as the operation hub coordinating the energy dispatch of multiple nations or regions across the continent to achieve global optimal targets. An efficient mechanism based on the modified Benders decomposition (BD) is proposed to coordinate the operations of national or regional power networks. The key contribution is that we take the total power outputs of regional power networks as the complicating variables to formulate the master problem and subproblems in the modified BD. Instead of using DC optimal power flow model (DC OPF), we propose to use convex AC optimal power flow model based on second-order cone programming (SOC-ACOPF) to operate the super grid. A comprehensive investigation proves that the SOC-ACOPF outperforms DC OPF in terms of accuracy. Numerical evaluations also show that our SOC-ACOPF model has stronger convergence capability and computational efficiency over other considered SOC-ACOPF models. The convergence of the modified BD is guaranteed by the convexity of SOC-ACOPF. A parallel computation framework in GAMS is proposed to assist real-time operation of the super grid. Compared with operating super grid in a centralized way, the modified BD approach shows stronger convergence capability, computational efficiency and robustness.

1. Introduction

The European ultra-high voltage power grid is evolving to a super grid with more high voltage AC (HVAC) and high voltage DC (HVDC) interconnections [1]. The major advantage of building a super grid is balancing energy consumption and generation across the continent [2]. Larger transmission capacity between renewable energy abundant areas and load centers means more efficient complementary energy use in dimension of both location and time. It is cost beneficial to fully exploit the renewable energy resources by expanding the power transmission network throughout Europe [3]. In facing the Energy Roadmap 2050 issued by the European Commission, an ambitious 80% reduction of green house gas emissions (GHG) by the year of 2050 compared with 1990 has been set out [1,4]. Since electricity covers around 20% of energy consumption [1], exploiting the huge potential of the electricity sector in achieving the EU2050 target is critical.

Recent years have witnessed the promising development of super grid worldwide. In Europe, the e-Highway2050 project has been implemented to identify weak power transmission lines and resolve these constraints for future decarbonized economy [4]. Ref. [3] finds that 228,000 km of new lines are required to be cost-optimally built for the European power network before 2050. Around €200 billion investment for updating the European transmission infrastructure is expected to be in place up to the year of 2020 [1]. China is planning to install 13 to 20

* Corresponding author.

E-mail address: yuanzhao@kth.se (Z. Yuan).

http://dx.doi.org/10.1016/j.apenergy.2017.09.086 Received 24 June 2017; Received in revised form 12 September 2017; Accepted 13 September 2017 0306-2619/ © 2017 Elsevier Ltd. All rights reserved.

Please cite this article as: Yuan, Z., Applied Energy (2017), http://dx.doi.org/10.1016/j.apenergy.2017.09.086

ARTICLE IN PRESS

Z. Yuan et al. Applied Energy xxxx (xxxxx) xxxx-xxxx

Nome	nclature	β_n	cost parameter of active power generation at node n
Sets		$C_n^{p^+}$	cost parameter of active power generation at node
Sets		-+	(added generator)
3.7		$C_n^{q^+}$	cost parameter of reactive power generation at node
N	set of nodes or buses		(added generator)
L	set of lines or branches		
K	set of regional or national power networks	Variables	
J	set of iterations		
τ	set of tie-lines (connecting different national or regional	p_n	active power generation at node n
	power networks)	q_n	reactive power generation at node n
N_k	set of nodes or buses located in regional power network k	p_n^+	active power generation at node n (added generator)
L_k	set of lines or branches located in regional power network	q_n^+	reactive power generation at node n (added generator)
	k	p_{s_l}	active power injection at the sending end of line l
_		q_{s_l}	reactive power injection at the sending end of line l
Parame	eters	p_{ol}	active power loss of line l
		q_{o_l}	reactive power loss of line l
A_{nl}^+	node to line incidence matrix	v_n	voltage magnitude of node n (note this symbol is in the
A_{nl}^-	node to line incidence matrix		lower case)
X_l	reactance of line l	v_{s_l}	voltage magnitude at the sending end of line l
R_l	resistance of line l	v_{r_l}	voltage magnitude at the receiving end of line l
G_n	shunt conductance at node n	V_n	voltage magnitude square of node <i>n</i> (note this symbol is
B_n	shunt susceptance at node n		the upper case)
K_l	squared power capacity of line l	V_{s_l}	voltage magnitude square at the sending end of line l
$q_{o_i}^{max}$	upper bound of reactive power loss of line l	V_{r_l}	voltage magnitude square at the receiving end of line l
$p_{s_i}^{max}$	upper bound of active power flow of line l	θ_l	voltage phase angle difference of line l
q_{o}^{max}	upper bound of reactive power flow of line l	θ_{s_l}	voltage phase angle at the sending end of line l
n^{min}	lower bound of active power generation at node n	θ_{r_l}	voltage phase angle at the receiving end of line l
n ^{max}	upper bound of active power generation at node <i>n</i>	$P_{k,j}^{sum}$	total active power output of regional network k at iter
$egin{array}{ll} q_{o_l}^{max} & & & & & & & & & & & & & & & & & & &$	lower bound of reactive power generation at node n		tion j
a _{max}	upper bound of reactive power generation at node n	$Q_{k,j}^{sum}$	total reactive power output of regional network k
θ_l^{min}	lower bound of voltage phase angle difference of line <i>l</i>		iteration j
θ _l Θι ^{max}	upper bound of voltage phase angle difference of line <i>l</i>	$\mu_{k,j}^{P}$	dual variable of regional network k at iteration j in the
•	active power demand at node n		modified BD
p_{d_n}	reactive power demand at node n	$\mu_{k,j}^Q$	dual variable of regional network k at iteration j in the
q_{d_n} α_n	cost parameter of active power generation at node n		modified BD

extra 800 kV to 1300 kV HVDC lines from 2014 onwards to transmit approximately 1300GW of solar, wind and hydro-power generation to the southeast population centers [2]. It is estimated by the international energy agency (IEA) that the total investment of China on updating the transmission network reaches more than \$4 trillion by the year of 2040 [2]. Using unit commitment model, the impact analysis of interregional transmission power network expansion in China by authors in [5] show that large economic benefits can be achieved.

To optimally operate an ultra-large-scale super grid is challenging in many aspects. Though more flexible control can be gained through the deployment of flexible AC transmission system (FACTS), phase-shifting transformers (PSTs) and voltage source converter based multi-terminal DC transmission (MTDC), the unplanned power flow is still one of the main challenges to operate the super grid [1]. By investigating the impacts of inter-regional grid transmission in China, Ref. [5] shows that efficient dispatch mechanism across regions accounting for generation efficiency should be established. Ref. [6] proposes a decompositioncoordination algorithm to find the sub-optimal solution of the integrated electrical and heating system. The algorithm in [6] works by dividing the system into two subsystems and then iteratively adjusting the coordinated variables which are at the boundary of the electrical and heating system. The numerical results show that it requires 15 iterations to converge for a test case with 6 nodes of electrical network and 31 nodes of heating network. However, the convergence of the coordination mechanism in [6] cannot be guaranteed because of the nonconvex model. As improvements, our model in this paper is convex and the convergence is guaranteed.

The optimal operation of the power network is generally formulated

as an optimal power flow problem (OPF) [7,8]. The objective functions of OPF can be minimizing the power losses [9,10], minimizing the operation or investment cost [11,12], maximizing the renewable energy penetration [13] or maximizing the stability margin of the power system [14,15]. OPF is constrained by network physics, security [16,17], stability [18] and operation [19] conditions. In general, DC OPF [20] formulation as an approximation of the AC OPF model is widely used in transmission network operations. One major reason of replacing the AC OPF model by DC OPF model is because current nonlinear programming solvers are unable to efficiently find the global optimal solution of the AC OPF model mainly because of its nonconvex structure. There have been promising developments recently as various relaxation and approximation techniques are proposed in the literature for the AC OPF model [21-24]. Second-order cone programming (SOCP) based convex AC OPF is a useful approach with good results [25]. Semi-Definite Programming (SDP) is another convexification approach for AC OPF [26-28]. Ref. [29] shows various limits of SDP computation. It is proved by authors in [26] that efficient algorithms for solving SDP-based AC OPF remain to be found. Moreover, only limited types of problems are exact for SDP relaxations [30-32]. In cases where the exactness is not guaranteed, SDP rarely gives solutions with physical meanings. Taking into account the advantages of SOCP over SDP, we improve the SOCP-based AC OPF formulation in [25] and use the improved model for the operation of super grid in this paper. Compared with the AC OPF model in [25], we explicitly include voltage phase angle variables in our model and thus the solutions of these variables can be obtained directly by solving the model. In addition, the bounds of power flow variables are equivalently formulated as the Z. Yuan et al. Applied Energy xxx (xxxxx) xxx-xxx

bounds of the power loss variables in our model.

Since the formulated OPF model of operating the super grid is a very large-scale optimization problem, distributed approaches to solve the OPF model are useful to make the problem tractable for the optimization solver. These distributed solution approaches mainly include Lagrangian relaxation [33], BD [34,35], Dantzig-Wolfe decomposition [36] and Alternating Direction Method of Multipliers (ADMM) [37]. Ref. [38] gives a comprehensive summary of distributed algorithms for optimization and control of power system. Lagrangian relaxation approach relaxes the coupling constraints between the regional power networks and generally only approximated solutions can be guaranteed [33]. BD is widely used to solve the security constrained unit commitment (SCUC) problem and transmission expansion planning (TEP) problem which can be regarded as expanded applications of OPF [39-42]. It is required to firstly formulate the master problem and subproblem and then iterate until the solutions converge in BD and Dantzig-Wolfe decomposition [34,36]. For SCUC and TEP, mostly the integer variables are taken as the complicating variables to formulate the master problem and subproblem of BD [39-41]. ADMM requires message exchanges among the regional power networks [37]. Generally, when more regional power networks are to be operated, more iterations are required for ADMM to converge [37]. Three ADMM-based distributed DC OPF solution algorithms with different communication strategies are investigated by [43]. It shows numerically that the convergence performance can be improved by enhancing the data exchange with the central controller (or coordinator). Authors in [44] solve the stochastic second-order cone programming (SOCP) based AC OPF by ADMM for radial distribution networks. The updates of the variables and multipliers are decomposed by each node and each scenario. Due to the large number of scenarios and the decomposition depth (down to each node and each scenario) considered in [44], it requires more iterations to converge (over 3000 iterations are required for a 50-node test case with 500 scenarios). The results of [45] demonstrate that convergence speed of ADMM largely depends on test cases. A suitable selection of the penalty factors of ADMM is also required because of the nonconvexity of AC OPF to guarantee the convergence [45]. Ref. [46] proposes a parametric quadratic programming approach to solve the regional correction equation in the proposed fully distributed interior point method (F-DIPM) to solve AC OPF. The power network is partitioned to several regions geographically. Then boundary variables associated with the tie-lines are duplicated for each region. A unidirectional ring communication is employed to transmit the information about boundary variables during each Newton-Raphson iteration. Recent developments of using ADMM-based approaches to solve the gas-electric integrated optimal power flow problem (GEOPF) [47] and comparisons with Lagrange Relaxation (LR) and augmented LR based decentralized methods by [48] show that it is better to solve large-scale GEOPF in a decentralized way than a centralized approach in terms of information privacy, multiple system operators coordination or computational efficiency. To address the convergence issue of ADMM in dealing with nonconvex GEOPF model, authors in [47] proposes a tailored ADMM approach in which the binary variables in the GEOPF model are firstly relaxed and then a feasible solution around the neighborhood of the relaxed solution is found by the objective feasibility pump (OFP) method. Using SOCP relaxation and McCormick envelope, the mixed integer nonlinear programming (MINLP) GEOPF model is reformulated in [48] to a mixed integer SOCP model (MISOCP) which is easier to be solved by using the CPLEX solver. Ref. [49] solves the multi-area generation unit and tieline scheduling (MAUTS) problem in the context of wind power penetration by using robust optimization (RO). The formulated RO model in [49] is decomposed by augmented Lagrange decomposition and then solved by ADMM. The nonconvexity in the formulated RO model due to the integer variables is addressed by a heuristic alternating optimization procedure (AOP) in which the generation unit commitment states and tie-line phase angles are optimized and fixed alternately until convergence [49].

Three main research gaps are identified from the literature review:

- The coordination of energy dispatch of different nations or regions for the super grid has not been well discussed; Without an efficient coordination mechanism, it is hard to operate the super grid optimally
- Though past research has validated the SOCP-based convex AC OPF model, the AC feasibility of the convex AC OPF model is not thoroughly examined. Especially, the applicability compared with the widely used DC OPF model.
- The speed up of distributed solution algorithm to solve large-scale AC OPF problem is still in demand to assist real-time decision making to operate the super grid.

In this spirit, we propose in this paper the concept of power synergy hub (PSHub) to coordinate the energy dispatch of the super grid. We show that the mathematical foundation of energy dispatch coordination operation in PSHub is the modified BD. We propose an improved convex AC OPF model based on SOCP which is SOC-ACOPF. A comprehensive investigation of various IEEE test cases shows that the proposed SOC-ACOPF model is better than the DC OPF model in terms of AC feasibility performance. This means the operation points (power flows, voltages, etc.) obtained by solving the proposed SOC-ACOPF model can satisfy the real power network constraints better. The proposed SOC-ACOPF model does not introduce new variables except the voltage magnitude square V_n . To obtain an equivalent linear representation of the line capacity limit (1h), we use the approximation $V_{s_l} \approx 1$ (per unit value). Two approximations $\sin \theta_l \approx \theta_l$ and $v_{s_l} v_{r_l} \approx 1$ (per unit value) for convexifying the nonconvex constraint (1g) are introduced in our model. Moreover, the proposed SOC-ACOPF model is valid for both radial and mesh power networks. These are the main differences of our model compared with other SOC-ACOPF models in the literature [22,50,51]. A numerical comparison with other SOC-A-COPF models in the literature is conducted to demonstrate the advantages of our model. To accelerate the coordination process in the PSHub, we propose a parallel computation structure in GAMS. The fast convergence of the energy dispatch coordination in PSHub and the proposed SOC-ACOPF model are demonstrated by numerical results for large-scale power networks up to 9241 nodes. The rest of this paper is organized as follows. Section 2 proposes the concept of PSHub. Section 3 presents the exact AC OPF model, the SOC-ACOPF model and the decoupled DC OPF model. Section 4 formulates the modified BD as the mathematical foundation of PSHub energy dispatch coordination operations. Section 5 designs the parallel computation structure in GAMS. Section 6 presents the numerical results and discussions. Section 7 concludes the advantages of the proposed approaches in this paper.

2. Proposing the power synergy hub

In this section, we firstly show the severe challenge of operating the super grid and then propose the solution to this challenge as PSHub. An overview of the key functions of the PSHub are explained.

To demonstrate the challenging scale of operating the super grid, we plot the network layout of the European high voltage transmission networks (750 kV, 400 kV, 380 kV, 330 kV, 220 kV, 154 kV, 150 kV, 120 kV and 110 kV) in Fig. 1. The network data is based on the Pan European Grid Advanced Simulation and State Estimation (PEGASE) project [52]. The important metrics of the power network and the corresponding OPF model are listed in Table 1. It is beyond the capability of current available optimization solvers to efficiently solve one single OPF model to find the global optimal solution, not to mention the gigantic requirement of RAM capacity for the computers. For example, the LINDOGLOBAL solver which is a powerful global nonlinear programming solver in GAMS currently cannot solve optimization problems with more than 3000 variables and 2000 constraints. One

Z. Yuan et al. Applied Energy xxxx (xxxxx) xxxx-xxxx

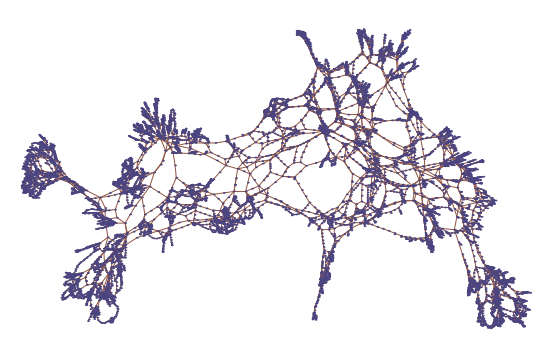


Fig. 1. Visualizing the European super grid.

Table 1 Scale of operating the super grid.

Super grid model	Metrics of network data			Metrics o	of OPF model
	Nodes	Lines	Generators	Variables	Constraints
1354pegase ^a	1354	1991	260	11192	20393
2869pegase	2869	4582	510	25086	45590
9241pegase	9241	16049	1445	85568	155087

^a Pan European Grid Advanced Simulation and State Estimation project.

practical way to deal with this challenge is to keep operating the regional power networks by current regional energy management system (EMS) centers and then coordinate the EMS in an efficient mechanism. We propose the concept of PSHub to implement the coordination mechanism of the super grid. This is illustrated in Fig. 2. Regional EMS represented as blue circles in Fig. 2 is operating the national or regional power networks. The high voltage DC lines (HVDC) as well as AC lines (HVAC) (represented as blue lines with arrows in Fig. 2) are connecting the networks of different nations or regions. While the regional EMS is operating its own power network, It is not sufficient to achieve global optimum for the super grid. It is impossible to guarantee the feasibility and security of the tie-line HVDC and HVAC connections without coordinating the operations of all the regional EMS centers. To coordinate the operations of the regional EMS centers, bi-directional communication between PSHub with regional EMS is required. The regional EMS submits information of its own network conditions to the PSHub. The PSHub then commands the operation points to each regional EMS taking the constraints of tie-line HVDC and HVAC connections into account.

Mathematically speaking, the function of PSHub is like a global optimization algorithm which iterates the local optimal solutions obtained by the regional EMS centers and coordinates the individual EMS by determining its total power output and the power flows of the tielines, in order to achieve global optimality in the super grid. There are two fundamental problems to be solved by the PSHub:

- What information is required to communicate from the regional EMS centers to the PSHub (represented as orange lines with arrows in Fig. 2)?
- 2. How to coordinate the energy dispatch of multiple regional EMS centers in order to achieve global optimal targets?

We prove in following sections of this paper that the proposed modified BD is not only an efficient approach to implement the coordination mechanism in PSHub but also leads to solutions very close to the global optimal targets for the super grid. The formulated Benders cuts are the information required to be communicated from regional EMS centers to the PSHub. These constitute two main contributions of

this paper.

3. The optimal power flow model

The fundamental mathematical models of optimal power system operations are presented in this section. The OPF models are generally solved in the EMS centers frequently to find the optimal operation points of the power network. We firstly present the full AC OPF model which is nonconvex and difficult to find the global optimality. Then we propose to use SOCP to convexify this AC OPF model. Finally, the widely used decoupled DC OPF model is presented. This DC OPF model is set as the benchmark in our paper to show the better AC feasibility of the proposed SOC-ACOPF model.

3.1. Full AC optimal power flow model

The full AC OPF model (based on the validated branch flow model [22,25]) is formulated in optimization problem (1). Note p_{s_l},q_{s_l} represent receiving end power flows in [25] which are different in our formulation. So some constraints are accordingly different. The term s in $p_{s_l},q_{s_l},v_{s_l},v_{s_l}$ is not an index but only to imply the meaning of sending end of line l. The term r in v_{r_l},v_{r_l} is not an index but only to imply the meaning of receiving end of line l. The term d in p_{d_n},q_{d_n} is not an index but only to imply the meaning of power demand. Similar reasoning holds for the term o in p_{o_l},q_{o_l} which is to denote the meaning of power loss

$$\underset{\Omega}{\text{Minimize }} f\left(p_{n}, q_{n}, p_{o_{l}}, q_{o_{l}}\right) \tag{1a}$$

subject to

$$p_{n}-p_{d_{n}}=\sum_{l}(A_{nl}^{+}p_{s_{l}}-A_{nl}^{-}p_{o_{l}})+G_{n}V_{n}\;,\;\;\forall\;n\in\mathbb{N}$$
 (1b)

$$q_{n}-q_{d_{n}}=\sum_{l}\left(A_{nl}^{+}q_{s_{l}}-A_{nl}^{-}q_{o_{l}}\right)-B_{n}V_{n}\;,\;\;\forall\;n\in\mathbb{N}$$
 (1c)

$$q_{ol} = \frac{p_{sl}^2 + q_{sl}^2}{V_{sl}} X_l \;, \quad \forall \; l \in L$$
 (1e)

$$V_{s_l} - V_{r_l} = 2R_l p_{s_l} + 2X_l q_{s_l} - R_l p_{o_l} - X_l q_{o_l} , \quad \forall \ l \in L$$
 (1f)

$$v_{s_l}v_{r_l}\sin\theta_l = X_lp_{s_l} - R_lq_{s_l} , \quad \forall \ l \in L$$
 (1g)

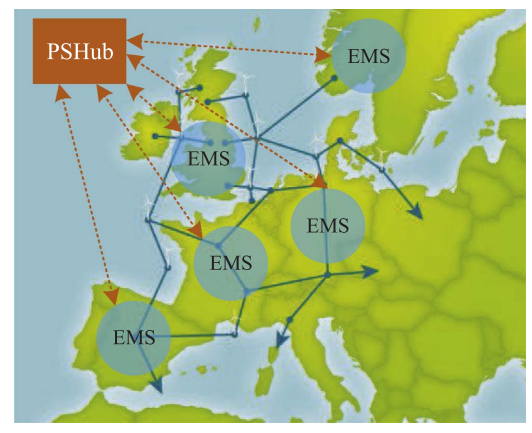


Fig. 2. The conceptual diagram of PSHub.

Z. Yuan et al. Applied Energy xxx (xxxxx) xxx-xxx

$$p_{sl}^2 + q_{sl}^2 \leqslant K_l, \quad \forall \ l \in L \tag{1h}$$

$$V_n = v_n^2 \,, \quad \forall \ n \in N \tag{1i}$$

$$v_n^{min} \le v_n \le v_n^{max}, \quad \forall \ n \in N$$
 (1j)

$$\theta_l^{min} \le \theta_l \le \theta_l^{max}, \quad \forall \ l \in L$$
 (1k)

$$p_n^{min} \le p_n \le p_n^{max}$$
, $\forall n \in N$ (11)

$$q_n^{min} \le q_n \le q_n^{max}$$
, $\forall n \in N$ (1m)

where $\Omega=\{p_n,q_n,p_{s_l},q_{s_l}p_{o_l},q_{o_l},V_n,v_n,\theta_l\}\in\Re$ is the set of decision variables. Depending on the applications, the objective function $f(p_n,q_n,p_{o_l},q_{o_l})$ can be the economic cost of energy production, network power loss or security margin. In this paper, we use the quadratic or linear cost function of energy production in MATPOWER [53] directly. Eqs. (1b) and (1c) represent the active and reactive power balance. A_{nl}^{+} and A_{nl}^- are the incidence matrices of the network with $A_{nl}^+=1, A_{nl}^-=0$ if *n* is the sending end of line *l*, and $A_{nl}^+ = -1, A_{nl}^- = 1$ if *n* is the receiving end of line l. Eqs. (1d) and (1e) represent active power and reactive power loss. Eqs. (1f) and (1g) are derived by taking the magnitude and phase angle of the voltage drop phasor along line l respectively [22,25]. Constraints (1j), (1k), (1l), (1m) are bounds for voltage magnitude, voltage phase angle difference, active power generation and reactive power generation. This model is nonconvex because of the nonconvex constraints (1d), (1e), (1g) and (1i). Current available nonlinear programming solvers are unable to efficiently find the global optimal solution of this nonconvex model.

3.2. Second-order cone AC optimal power flow model

The convexification and approximation of the full AC OPF model are derived in this section. The convexification is based on SOCP. The approximation is based on small voltage phase angle difference assumption and voltage magnitude assumption for power transmission network. Compared with the convex AC OPF model in [25], the improvements of the proposed SOC-ACOPF model in current paper are twofold:

- Voltage phase angle variables are explicitly included in the SOC-ACOPF model so that the solutions of these variables can be obtained directly by solving the proposed SOC-ACOPF model.
- 2. The upper bound of power flow for each line is constrained equivalently by constraint (2c).

Note that in the proposed SOC-ACOPF model, we only use the squared voltage variable V_n instead of the voltage variable v_n in order to exclude the nonconvex constraint (1i). The solution of v_n can be recovered by $v_n = \sqrt{V_n}$ in which V_n is solved directly from the proposed SOC-ACOPF model.

Constraints (1d), (1e), (1g) and (1i) are nonconvex constraints in the optimization problem (1). Using second-order cone [25], constraint (1e) can be relaxed to the rotated second-order cone constraint in (2a).

$$q_{o_l} \ge \frac{p_{s_l}^2 + q_{s_l}^2}{V_{s_l}} X_l$$
, $\forall l \in L$ (2a)

Constraint (1h) can be equivalently replaced by:

$$q_{ol} \leq q_{ol}^{max}, \quad \forall \ l \in L$$
 (2b)

where the upper bound of reactive power loss $q_{ij}^{\it max}$ is estimated from the upper bound of line capacity as shown in (2c). The approximation in (2c) is based on $V_{sj}\approx 1$ (per unit value) which is valid in normal power system operations.

$$q_{ij}^{max} = \frac{[p_{s_i}^{max}]^2 + [q_{s_i}^{max}]^2}{V_{s_i}} X_l = \frac{K_l}{V_{s_i}} X_l \approx K_l X_l$$
 (2c)

Nonconvex constraint (1d) can be replaced by the linear relationship between $p_{\rm or}$ and $q_{\rm or}$:

$$p_{0l}X_l = q_{0l}R_l , \quad \forall \ l \in L$$
 (2d)

We use two approximations $\sin\theta_l \approx \theta_l$ and $v_{sl}v_{rl} \approx 1$ (per unit value) for linearizing the equation given in (1g). These assumptions are valid for transmission network under normal operations. Note that these assumptions are only used to linearize (1g)–(2e):

$$\theta_l = X_l p_{s_l} - R_l q_{s_l} , \quad \forall \ l \in L$$
 (2e)

Using (2a), (2b), (2d) and (2e), the optimization problem (1) can now be reformulated as a SOCP problem. This proposed SOC-ACOPF model represented by {(1a)-(1c), (1f), (1j)-(1m), (2a)-(2b), (2d)-(2e)} can be solved efficiently to global optimum using interior point method (IPM) [54]. The convexity of the proposed SOC-ACOPF model is further validated by the solutions from the MOSEK solver (an efficient convex programming solver which can only solve convex models and detect any nonconvexity in the model) in GAMS.

The objective function f of typical economic dispatch is quadratic:

$$f(p_n) = \sum_{n} \alpha_n p_n^2 + \beta_n p_n \tag{2f}$$

where α_n, β_n are cost parameters of the active power generation. Minimizing quadratic objective function over a convex feasible region is a convex optimization problem.

3.3. Decoupled DC optimal power flow model

The decoupled DC OPF model is a widely used approximation of the exact AC OPF model. It is set as the benchmark to validate the AC feasibility of the proposed SOC-ACOPF model. We present the decoupled DC OPF model in (3) [55].

$$\underset{\circ}{\text{Minimize }} f(p_n, q_n) \tag{3a}$$

subject to

$$p_n - p_{d_n} = \sum_{l} (A_{nl} p_{s_l}) + G_n, \quad \forall \ n \in \mathbb{N}$$
 (3b)

$$p_{s_l} = \frac{\theta_l}{X_l}, \quad \forall l \in L$$
 (3d)

$$q_{s_l} = \frac{v_{s_l} - v_{r_l}}{X_l}$$
, $\forall l \in L$ (3e)

where constraints (3b)–(3e) and (1j)–(1m) are linear. Constraint (1h) is convex. So, if we use convex objective function (generally the objective function is either linear or quadratic), this minimization model is convex. This OPF model is decoupled because the active power flow P_{s_l} is only approximated by the voltage phase angle difference variable \mathfrak{S}_l while the reactive power flow q_{s_l} is calculated by voltage magnitude variable v_n . However, as we demonstrate later by the numerical results of this paper, the AC feasibility of model (3) is worse compared with the proposed SOC-ACOPF model.

${\bf 4.} \ \ {\bf Mathematical} \ \ {\bf foundation} \ \ {\bf of} \ \ {\bf PSHub:} \ \ {\bf modified} \ \ {\bf Benders} \ \ \\ {\bf decomposition}$

In this section, we show that how modified BD can be used as the mathematical foundation of energy dispatch coordination in PSHub. In BD, the original large-scale optimization problem is decomposed to a master problem and several subproblems. The objective solution of the master problem gives the lower bound of the original optimization

Z. Yuan et al. Applied Energy xxxx (xxxxx) xxxx—xxx

problem (we consider minimization problem here). The objective solutions of the subproblems can give upper bound of the objective in the original minimization problem. With the proceed of the iterations, the lower bound and upper bound given by the master problem and subproblems finally converge. The challenges are how to formulate the master problem and subproblems in the decomposition and how to accelerate the convergence. These challenges are addressed in this section. We also propose to deal with the feasibility problem of the subproblem in the modified BD by an efficient way without using the original Benders feasibility cuts approach.

The key observation and contribution in this paper is that, if we take the total power generations of the regional power networks as the complicating variables in formulating the modified BD, the modified BD can serve as the mathematical foundation of the energy dispatch coordination implemented by the PSHub. The total power generations of the regional power networks are actually the operation points to be found by the regional EMS centers. The energy dispatch of each regional power network k is a subproblem in the modified BD algorithm. The master problem of the modified BD is the energy dispatch coordination of the PSHub. The subproblem k in the modified BD is formulated in (4).

$$Cost_k^{EMS} = \text{Minimize} \sum_{\forall n \in N_k, l \in L_k} f(p_n, q_n, p_{o_l}, q_{o_l})$$
 (4a)

subject to (1a)-(1c), (1f), (1j)-(1m)

(2a)-(2b), (2d)-(2e)
$$\forall n \in N_k, l \in L_k$$
 (4b)

$$\sum_{n \in N_k} p_n = P_{k,j}^{sum} : \mu_{k,j}^P$$
(4c)

$$\sum_{n \in \mathbb{N}_b} q_n = Q_{k,j}^{sum} : \mu_{k,j}^Q$$
(4d)

where $Cost_k^{EMS}$ is the cost of energy production for regional power network k. (4b) refers to the power flow constraints for all lines and nodes located in regional network k. N_k and L_k are sets of the nodes and lines located in the regional power network k. $P_{k,j}^{sum}$ and $Q_{k,j}^{sum}$ are the solutions of total power generations in regional power networks from the master problem of the modified BD at iteration j. $\mu_{k,j}^P$ and $\mu_{k,j}^Q$ are dual variables for the corresponding constraints used for constructing the Benders cuts. The objective solution of the subproblem (4) is the upper bound of the energy dispatch for each regional EMS center.

To guarantee the feasibility of the subproblem, we have added one more generator with large capacity at each bus of the regional power networks. The marginal generation cost of the added generators is larger than the most expensive generators in the original regional power networks (note these added generators do not exist and are only used as variables in the model). In this way the final converged dispatch results do not include generations from these added generators (cheap generators are more preferred to be dispatched because we minimize the generation cost as the objective). This is another contribution of this paper to deal with the feasibility problems of the subproblems in the modified BD. This approach is more efficient than the traditional Benders feasibility cuts approach which cannot converge within hours in our simulations. The numerical failure of MOSEK solver [54] using the traditional Benders feasibility cut approach in solving ultra-largescale AC OPF indicates that a modified BD should be developed. As a comparison, the proposed approach converges very fast. In this way, the power balance constraints (1b) and (1c) in (4b) are modified as (4e)

$$p_n + p_n^+ - P_{d_n} = \sum_{l \in L_k} \; (A_{nl}^+ p_{s_l} - A_{nl}^- p_{o_l}) + G_n V_n \;, \; \; \forall \; n \in N_k, l \in L_k$$
 (4e)

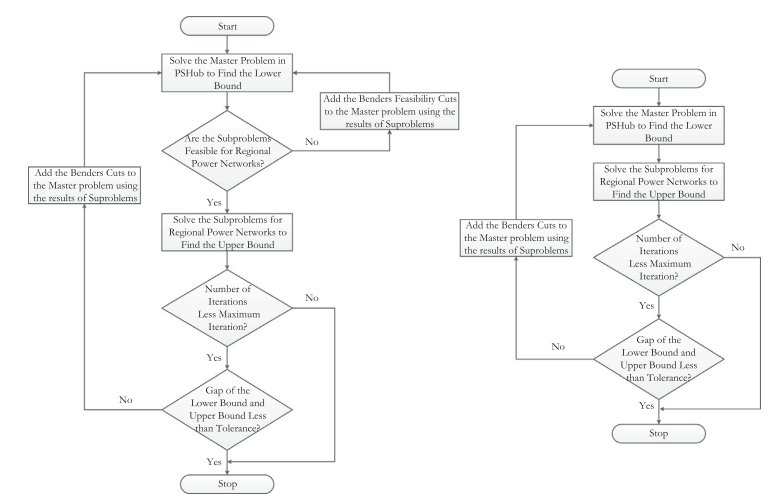
$$q_n + q_n^+ - Q_{d_n} = \sum_{l \in I_k} (A_{nl}^+ q_{s_l} - A_{nl}^- q_{o_l}) - B_n V_n, \quad \forall n \in N_k, l \in L_k$$
(4f)

where p_n^+ and q_n^+ are the active power and reactive power generations from the added generators. The objective function in the subproblem (4) is modified as (4g):

$$Cost_{k,j}^{S} = \text{Minimize} \sum_{\forall n \in N_{k}, l \in L_{k}} f(p_{n}, q_{n}, p_{o_{l}}, q_{o_{l}}) + \sum_{n \in N_{k}} (C_{n}^{p+} p_{n}^{+} + C_{n}^{q+} q_{n}^{+})$$
(4g)

where C_n^{p+} and C_n^{q+} are the marginal cost parameters of active power and reactive power generations from the added generators. The Benders feasibility cuts are used to remove infeasible solutions from the searching space of the solver. However, if the infeasible region of the searching space is very complex and large, using Benders feasibility cuts will be very time-consuming. This is because it is required to generate many Benders feasibility cuts in order to remove possible infeasible solutions from the searching space. Our approach to guarantee the feasibility of the subproblems can avoid detecting the feasibility procedure of BD. In this way, the computational efficiency is improved.

Fig. 3. The flow charts of traditional BD and the modified BD.



Traditional Benders Decomposition Algorithm

Modified Benders Decomposition Algorithm

Z. Yuan et al. Applied Energy xxx (xxxxx) xxx-xxx

The lower bound of objective for energy dispatch for all the regional EMS centers is obtained by solving the master problem of the modified BD. The master problem of the modified BD is formulated in (5).

$$\underset{\Omega}{\text{Minimize } Cost^{PSHub} = \sum_{k \in V} Cost_k^{EMS}} \tag{5a}$$

subject to (1a)-(1c), (1f), (1j)-(1m)

(2a)–(2b), (2d)–(2e),
$$\forall l \in \tau$$
 (5b)

$$Cost_{k}^{EMS} \ge Cost_{k,j}^{EMS} + \mu_{k,j}^{P} \left(\sum_{n \in N_{k}} (p_{n} + p_{n}^{+}) - P_{k,j}^{sum} \right)$$
(5c)

$$+ \mu_{k,j}^{Q}(\sum_{n \in N_{k}} (q_{n} + q_{n}^{+}) - Q_{k,j}^{sum}), \quad \forall k \in K, j \in J$$
 (5d)

where $Cost^{PSHub}$ refers to the total cost of energy production for the super grid. (5b) represents the power flow constraints of tie-lines (transmission lines connecting different EMS regions), τ is defined as the set of all tie-lines. We model each regional power network as a single virtual node in the master problem. Constraint (5d) includes Benders cuts from the subproblems. $\mu_{k,j}^P$ and $\mu_{k,j}^Q$ are dual variable solutions of Eqs. (4c) and (4d) in regional power network k (which is equal to zero at the first iteration). The master problem is responsible to give solutions of total power output of regional power networks and tieline power flows. The subproblems are responsible to give solutions of subnetwork power flows. The master problem is always feasible because it is actually a relaxed problem of the original SOC-ACOPF model. As the iterations proceed, more Benders cuts from the regional networks are iteratively included into the master problem (this process is interpreted as the communication between PSHub and all regional EMS centers). After solving the master problem, all the subproblems can be computed in parallel which we explain in the next section. If the original problem is convex (the proposed SOC-ACOPF model is convex), it is proved that the optimal solution can be found within finite iterations [34,35]. The procedure of using the modified BD to operate the super grid is explained in Fig. 3. A graphical illustration of the relationship between the master problem and subproblems in the modified BD is plotted in Fig. 4. To show the difference of the modified BD with the traditional BD, we also plot the flow chart of traditional BD in Fig. 4. As we have mentioned, our modified BD avoids the steps of checking subproblems feasibility and generating the Benders feasibility cuts in the iterations.

5. Accelerating the implementation of modified BD by parallel computation $% \left(1\right) =\left(1\right) \left(1\right)$

As the modified BD in PSHub is solved in an iterative way, the execution can be accelerated by parallel computation. We explain in this section the proposed parallel computation structure in GAMS [56]. The performance of the parallel computation is validated by the numerical results in the next section.

The proposed parallel computation structure of the energy dispatch coordination by PSHub is illustrated in Fig. 4. The parallel computation structure is implemented in GAMS platform and it is based on the modified BD. The parallel computation is comprised of one Parallel Loop and one Collect Loop. The Parallel Loop complies all the subproblems in the modified BD and submits each subproblem to one thread to be executed by one core of the CPU. Since the subproblems are actually the energy dispatch of regional EMS centers, we denote the threads of the subproblems in Fig. 4 by 'EMS-1', 'EMS-2', ..., 'EMS-k'. The Collect Loop repeatedly checks the solution status of each thread and then saves the solutions as long as the solutions are available. The threads of solved subproblems are released in order to avoid over using the computer disk capacity. Because there is no communication requirement among the subproblems, the capability of multi-CPU computers can be utilized to the most.

6. Numerical results

In this section, we firstly investigate comprehensively the AC feasibility of the proposed SOC-ACOPF model and the decoupled DC OPF model. A numerical comparison of our SOC-ACOPF model with other convex AC OPF models is also provided. The performance of energy dispatch coordination by PSHub accelerated by parallel computation is then demonstrated. All the models are coded in GAMS and solved by the MOSEK solver. All simulations are run on a PC with Intel i7-2760QM 2.4 GHz CPU and 8 GB RAM.

6.1. Comparison of SOC-ACOPF and decoupled DC OPF

We compare the AC feasibility of SOC-ACOPF and decoupled DC OPF by various IEEE test cases [57]. These test cases are based on real world power network configuration data. The AC feasibility is shown by the gap of the equality constraints (1b)-(1g) between the full AC OPF model and the SOC-ACOPF model or the decoupled DC OPF model. A smaller absolute value of the gap means better AC feasibility. Zero gap means the solutions are fully feasible. For IEEE14-Bus, IEEE57-Bus, IEEE118-Bus and IEEE300-Bus, the absolute values of the AC feasibility gaps are plotted directly, whereas for 1354pegase and 2869pegase [52], we plot the histogram to summarize the statistics of the absolute values of the AC feasibility gaps. Note that the left-side Y-axis denotes the AC feasibility gap for the proposed SOC-ACOPF model. The rightside Y-axis denotes the AC feasibility gap for the decoupled DC OPF model. The X-axis of the histogram distributes the absolute values of the AC feasibility gaps to 50 intervals. The Y-axis of the histogram is the number of instances in each interval of the X-axis. The total number of instances is equal to the total number of constraints for the corresponding test case.

For ease of illustration, we categorize the equality constraints (1b)–(1g) representing the AC feasibility into three groups:

- Kirchhoff's Current Law (KCL) constraints: active power balance (1b) as KCL-P and reactive power balance (1c) as KCL-Q. The AC feasibility gaps of these constraints are summarized in Figs. 5, 8, 11, 14, 17 and 20. These figures show the AC feasibility gap of the KCL constraint at each bus:
- 2. Power Loss constraints: active power loss (1d) as P_{loss} and reactive power loss (1e) as Q_{loss} . The AC feasibility gap of these constraints are summarized in Figs. 6, 9, 12, 15, 18 and 21. These figures show the AC feasibility gap of the Power Loss constraint at each transmission line:
- 3. Voltage Drop constraints: voltage drop magnitude (1f) as $\Delta \nu$ and voltage drop phase angle (1g) as $\theta_{\Delta \nu}$. The AC feasibility gap of these

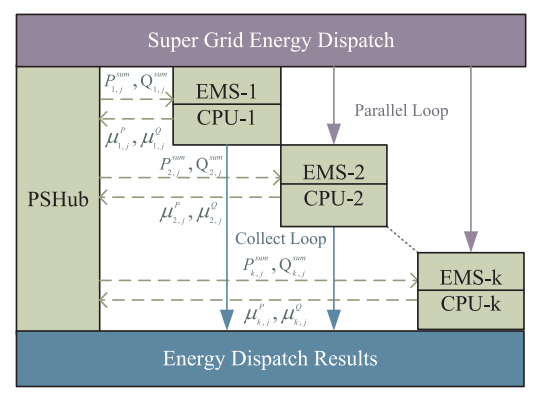


Fig. 4. The parallel computation management in PSHub

Z. Yuan et al. Applied Energy xxx (xxxxx) xxxx—xxx

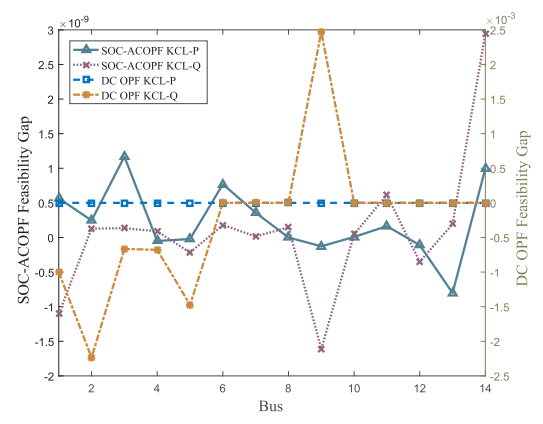


Fig. 5. IEEE14-Bus AC feasibility of KCL constraints.

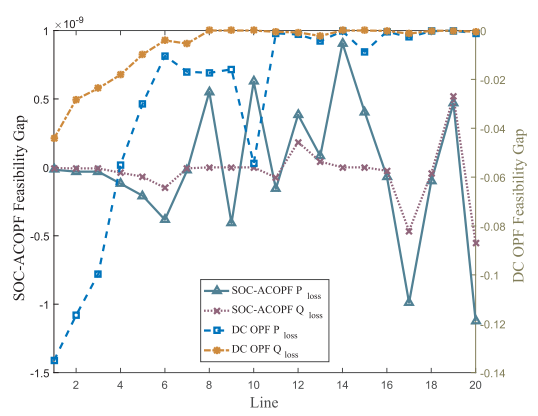


Fig. 6. IEEE14-Bus AC feasibility of power loss constraints.

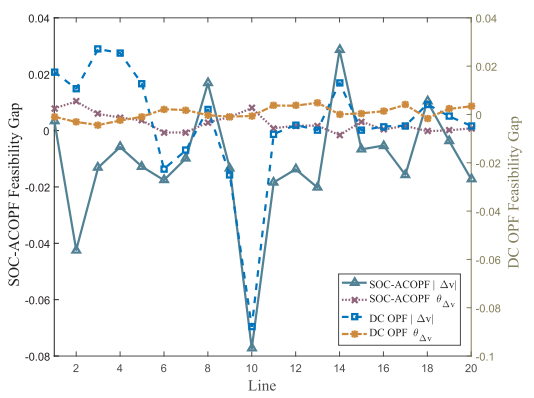


Fig. 7. IEEE14-Bus AC feasibility of voltage drop constraints

constraints are summarized in Figs. 7, 10, 13, 16, 19 and 22. These figures show the AC feasibility gap of the Voltage Drop constraint at each transmission line.

Finally, to give an overall comparison, we list the maximum

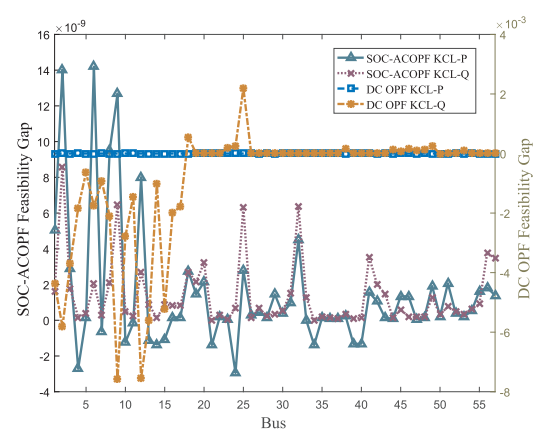


Fig. 8. IEEE57-Bus AC feasibility of KCL constraints.

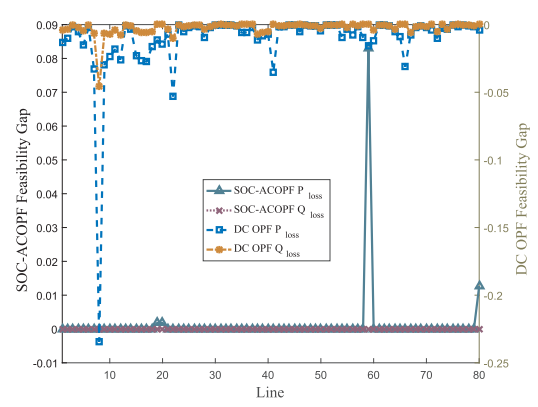
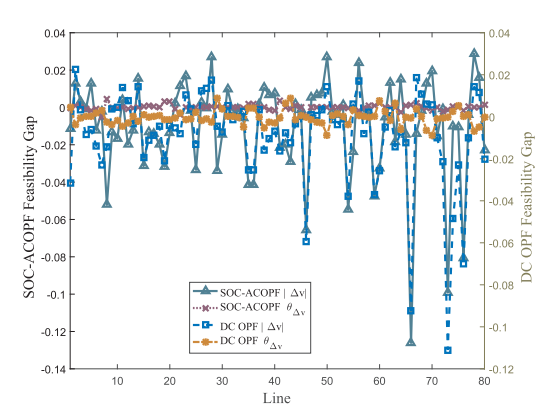


Fig. 9. IEEE57-Bus AC feasibility of power loss constraints.



 $\textbf{Fig. 10.} \ \textbf{IEEE57-Bus} \ \textbf{AC} \ \textbf{feasibility} \ \textbf{of} \ \textbf{voltage} \ \textbf{drop} \ \textbf{constraints}.$

absolute values of AC feasibility gaps of the proposed SOC-ACOPF model and decoupled DC OPF model in Table 2. In all the test cases, the AC feasibility of the proposed SOC-ACOPF model is much better than the decoupled DC OPF model for the KCL and Power Loss constraints. For the KCL and Power Loss constraints, AC feasibility of the proposed SOC-ACOPF model is better than the decoupled DC OPF model. For the

Z. Yuan et al. Applied Energy xxxx (xxxxx) xxxx-xxxx

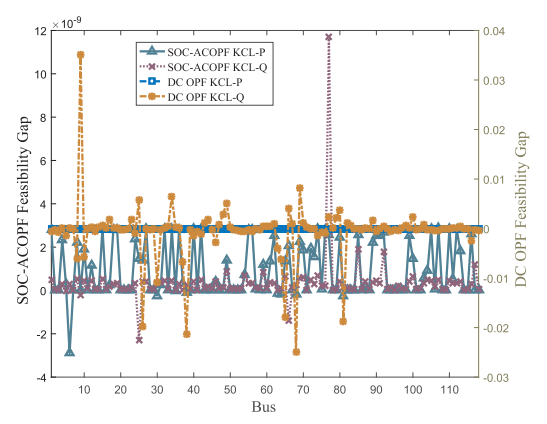


Fig. 11. IEEE118-Bus AC feasibility of KCL constraints.

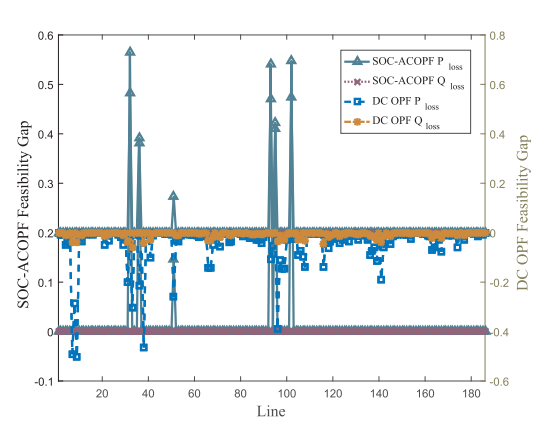


Fig. 12. IEEE118-Bus AC feasibility of power loss constraints.

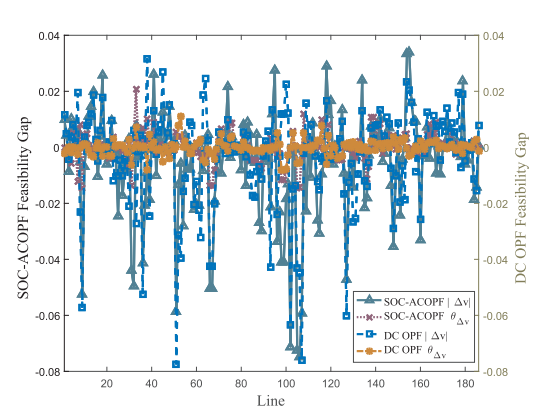


Fig. 13. IEEE118-Bus AC feasibility of voltage drop constraints.

Voltage Drop constraints, there is no significant AC feasibility difference between the SOC-ACOPF model and the decoupled DC OPF model. In summary, AC feasibility of the proposed SOC-ACOPF model is better than the decoupled DC OPF model.

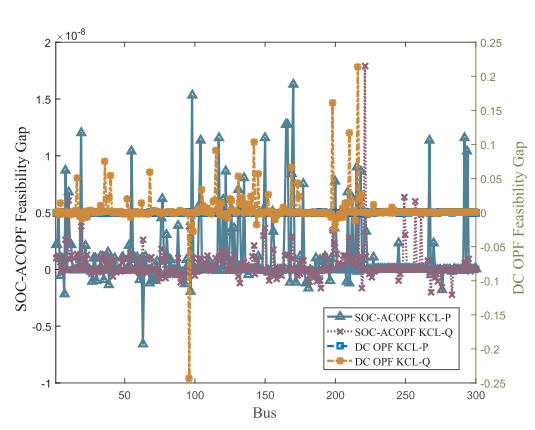


Fig. 14. IEEE300-Bus AC feasibility of KCL constraints.

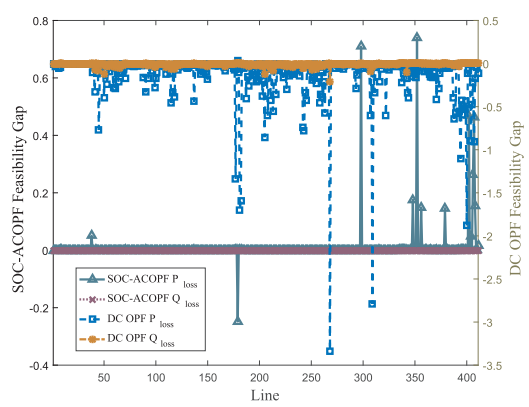


Fig. 15. IEEE300-Bus AC feasibility of power loss constraints.

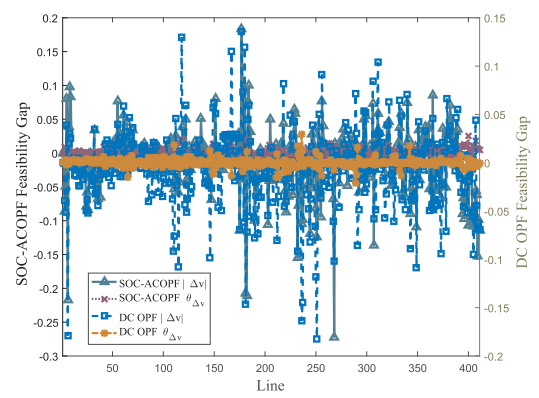


Fig. 16. IEEE300-Bus AC feasibility of voltage drop constraints.

6.2. Comparison of SOC-ACOPF and other convex AC OPF models

To evaluate the performance of our SOC-ACOPF model with other convex OPF models, we have also implemented the SOCP-based AC OPF models in [22,51]. The results from nonconvex AC OPF model in MA-TPOWER are used as the benchmark for the comparison. The results of

Z. Yuan et al. Applied Energy xxxx (xxxxx) xxxx-xxx

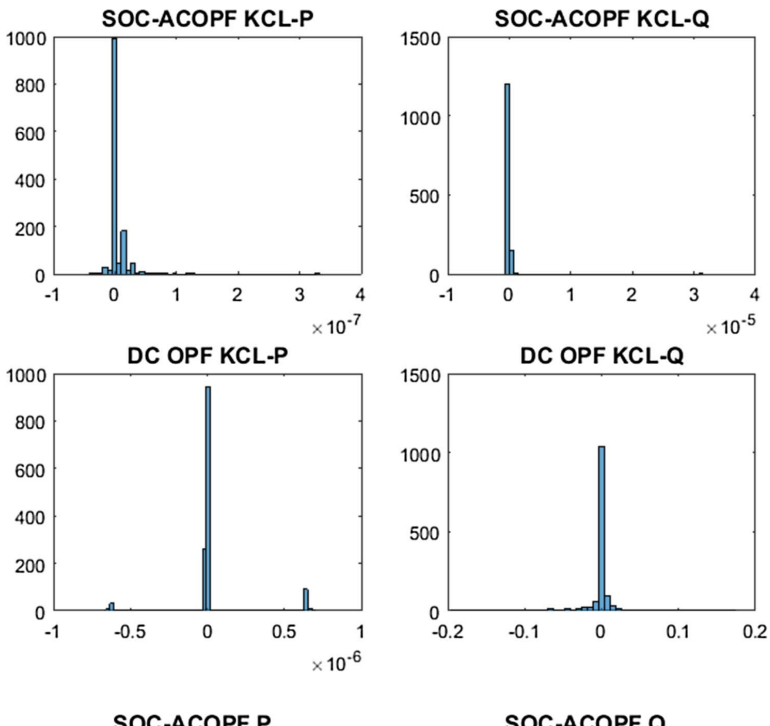


Fig. 17. 1354pegase AC feasibility of KCL constraints.

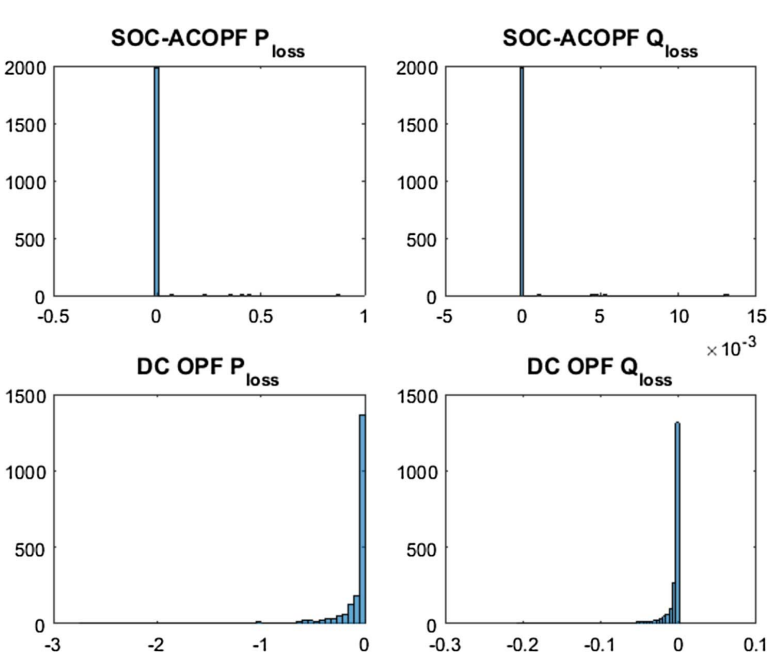
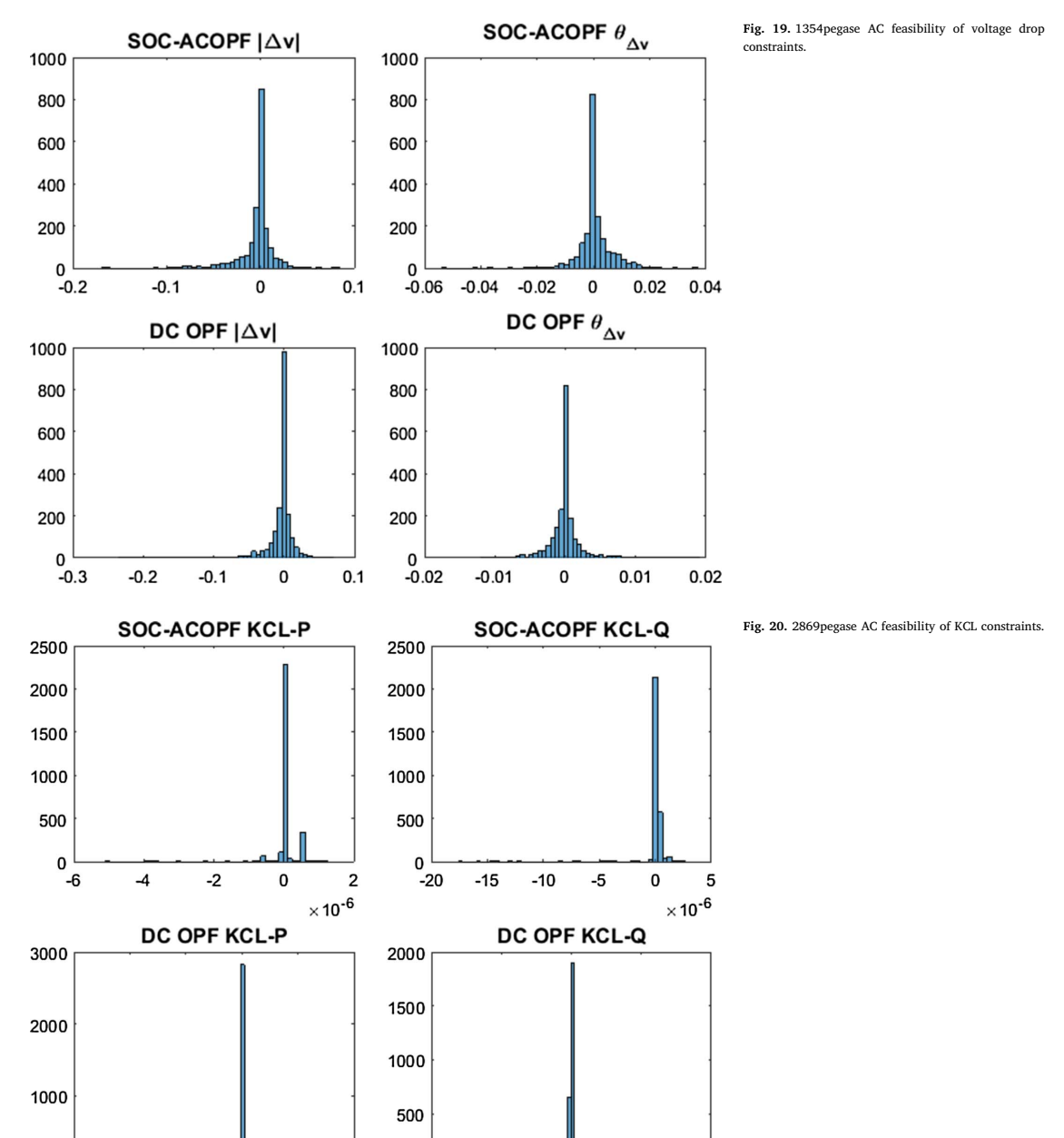


Fig. 18. 1354pegase AC feasibility of power loss constraints

various IEEE test cases are listed in Tables 3 and 4. Note the model in [22] is only valid for radial power networks and the objective values listed in Table 3 for this model are much relaxed solutions (lower objective values serving as the lower bounds of the objective solutions but no guarantee of AC feasibility for mesh power networks) compared with

our SOC-ACOPF model and the model in [51] which are both valid for mesh and radial power networks. The model in [22] requires less computation time because there are less constraints in the model (no voltage phase angle constraints and thus solutions of voltage phase angle variables cannot be directly obtained from solving this model).

Z. Yuan et al. Applied Energy xxx (xxxxx) xxxx—xxx



For IEEE57-Bus and 9241 pegase, MOSEK cannot converge for the model in [51]. As a comparison, MOSEK can always converge to solutions for our SOC-ACOPF model with acceptable computation time.

2

×10⁻⁴

0 ^L

-4

-2

0

6.3. Performance of energy dispatch coordination by PSHub

0.4

0.2

To demonstrate the performance of energy dispatch coordination, we compare the results of PSHub with the centralized energy dispatch where the nonconvex AC OPF is solved as one single optimization

0 ^{_} -0.4

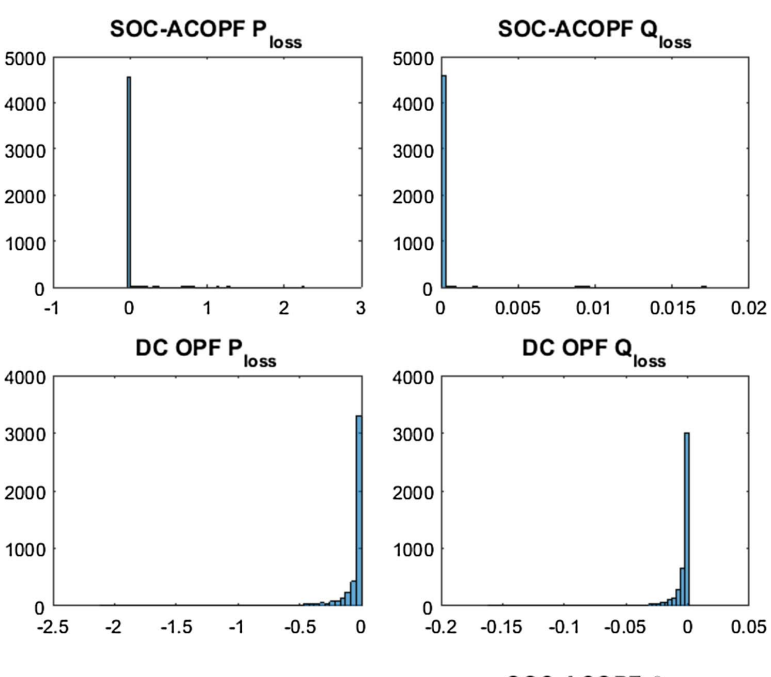
-0.2

0

Z. Yuan et al.

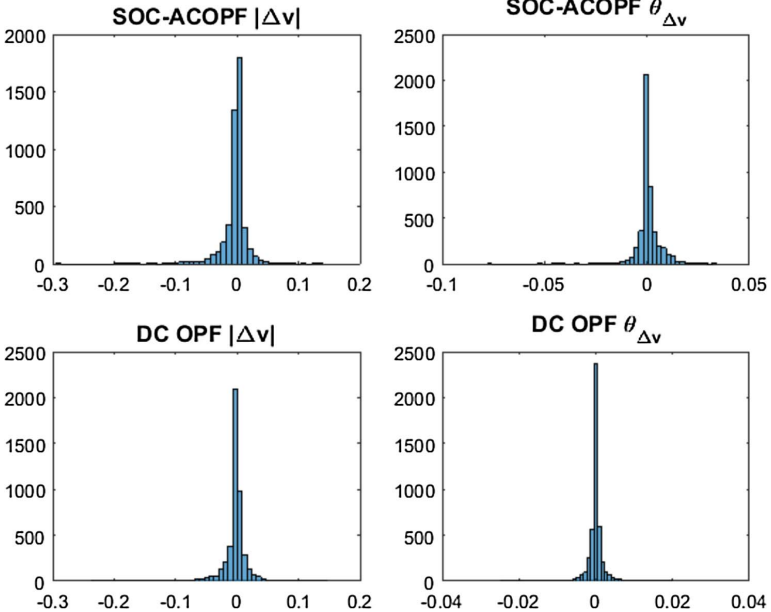
Applied Energy xxx (xxxx) xxx-xxx

Fig. 21. 2869pegase AC feasibility of power loss con-



 $\mathsf{SOC}\text{-}\mathsf{ACOPF}\;\theta_{\Delta \mathsf{V}}$

Fig. 22. 2869pegase AC feasibility of voltage drop



problem in MATPOWER [53]. MATPOWER uses MATLAB built-in Interior Point Solver (MIPS) to solve nonconvex AC OPF. The solutions obtained from MATPOWER are local optimal solutions. We summarize the metrics of the regional networks in Table 5. The 'EMS' column lists the total number of regional EMS centers that are coordinated by the PSHub.

6.3.1. Base case

In this base case, we use the power load data in the original power networks. We list the objective value results and computational CPU time in Table 6. The required number of iterations, generated Benders cuts and solution accuracy are summarized in Table 7. The relative gap in Table 7 is calculated as in (6):

ARTICLE IN PRESS

Z. Yuan et al. Applied Energy xxx (xxxxx) xxxx—xxx

 $\begin{tabular}{ll} \textbf{Table 2} \\ \textbf{Summary of the maximum absolute values of the AC feasibility gap.} \\ \end{tabular}$

Test case	Model	AC feasibility gap					
		KCL-P	KCL-Q	$ \Delta v $	$\theta_{\Delta u}$	P_{loss}	Q_{loss}
IEEE14	SOC-ACOPF	1.17E-09	2.95E-09	7.73E - 02	1.03E - 02	1.12E-09	5.51E-10
	Decoupled DC OPF	1.42E - 09	2.47E-03	8.80E - 02	4.87E - 03	1.35E-01	4.43E-02
IEEE57	SOC-ACOPF	1.00E - 08	8.59E-09	1.26E-01	5.35E - 03	8.30E-02	2.91E-09
	Decoupled DC OPF	1.68E - 09	7.59E - 03	1.11E-01	8.90E - 03	2.34E-01	4.59E - 02
IEEE118	SOC-ACOPF	2.89E - 09	1.00E-08	7.48E-02	2.07E - 02	5.65E-01	2.87E-10
	Decoupled DC OPF	2.00E - 08	3.51E - 02	7.75E - 02	1.12E - 02	5.00E-01	5.88E - 02
IEEE300	SOC-ACOPF	2.00E - 08	2.00E-08	2.72E-01	2.57E - 02	7.40E-01	1.70E-09
	Decoupled DC OPF	4.86E-05	2.43E-01	1.82E - 01	2.97E - 02	3.34E + 00	2.09E-01
1354pegase	SOC-ACOPF	3.30E-07	3.11E-05	1.70E-01	5.34E-02	8.78E-01	1.32E-02
1 0	Decoupled DC OPF	7.00E - 07	1.95E - 01	2.31E - 01	1.88E-02	2.73E + 00	2.07E-01
2869pegase	SOC-ACOPF	5.08E - 06	1.76E-05	2.89E-01	7.63E - 02	2.26E+00	1.72E-02
	Decoupled DC OPF	4.01E - 04	2.61E-01	2.32E-01	2.41E-02	2.10E+00	1.61E-01

Table 3
Objective value [\$].

Test case	SOC-ACOPF	Model in [22]	Model in [51]	MATPOWER
IEEE14	8078.84	8072.42	8073.16	8081.53
IEEE57	41696.94	41673.10	NA	41737.79
IEEE118	129619.50	129330.74	129325.68	129660.70
IEEE300	719381.80	718091.78	719451.23	719725.11
1354pegase	74040.99	74006.84	73974.56	74069.35
2869pegase	133934.70	133866.95	133823.28	133999.29
9241pegase	313692.87	312212.00	NA	315912.43

Table 4
Computation CPU time [s].

Test case	SOC-ACOPF	Model in [22]	Model in [51]	MATPOWER
IEEE14	0.08	0.08	0.07	0.11
IEEE57	0.09	0.11	NA	0.12
IEEE118	0.09	0.13	0.09	0.30
IEEE300	0.25	0.25	0.22	0.48
1354pegase	0.76	0.64	2.56	8.58
2869pegase	1.97	1.23	6.82	18.66
9241pegase	14.73	4.98	NA	85.11

Table 5
Metrics of regional EMS and power networks.

Test case	EMS	Number of tie- lines	Number of nodes in regional networks
1354pegase	2	27	828, 526
	4	56	311, 253, 319, 471
	8	69	168, 151, 120, 243, 186, 102, 260, 124
2869pegase	2	20	1899, 970
	4	39	975, 457, 531, 906
	8	83	324, 532, 295, 214, 312, 288, 524, 350
9241pegase	2	15	4122, 5119
	4	51	1200, 1754, 3253, 3034
	8	126	1247, 735, 509, 1887, 1489, 922, 1597, 855

$$Relative \ Gap = \frac{Upper \ Bound-Lower \ Bound}{Upper \ Bound} \times 100\% \eqno(6)$$

Because the overall super grid is a fixed network, more regional EMS

Table 6
PSHub coordination results: base case.

Test case	PS	SHub coordination	Centralized dispatch			
	Objective [\$]		EMS	CPU	Objective [\$]	CPU
	Upper bound	Lower bound		time [s]		time [s]
1354pegase	74009.46	74009.45	2	1.05	74069.35	8.58
	74822.49	72726.67	4	1.47		
	74009.47	74009.45	8	0.41		
2869pegase	133902.29	133902.21	2	4.82	133999.29	18.66
	134582.33	132578.46	4	6.38		
	134112.36	133791.95	8	1.22		
9241pegase	314273.05	314273.03	2	58.78	315912.43	85.11
	316425.87	311537.62	4	29.05		
	314597.18	314597.11	8	13.79		

Table 7
Iterations, Benders cuts and solution accuracy.

Test case	EMS	Number of iterations	Number of Benders cuts	Relative gap
1354pegase	2	3	6	0.00%
	4	3	12	2.80%
	8	3	24	0.00%
2869pegase	2	3	6	0.00%
	4	4	16	1.49%
	8	3	24	0.24%
9241pegase	2	3	6	0.00%
	4	3	12	1.54%
	8	3	24	0.00%

centers mean smaller scale for each regional power network. So the required computation time, in general, will decrease with the increasing of EMS centers. This is because each regional EMS center dispatch is computed by the proposed parallel computation. However, as we can notice from the results of the 2869pegase test case, the computation time of coordinating 4 regional EMS centers is more than the computation time of coordinating 2 regional EMS centers. This result shows that the computation time does not only depend on the network scale but also the specific network structure. The communicated Benders cuts from all the regional EMS to PSHub are equal to

ARTICLE IN PRESS

Z. Yuan et al. Applied Energy xxx (xxxxx) xxx-xxx

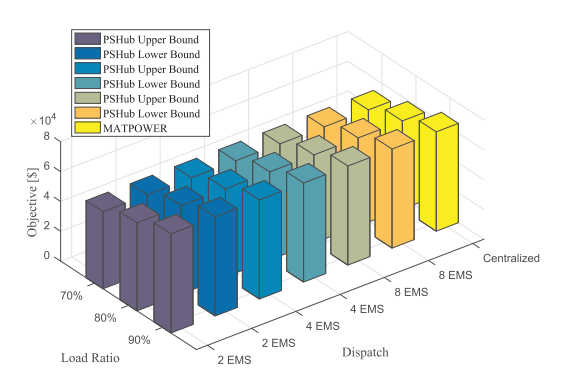


Fig. 23. 1354pegase objective values for various load scenarios.

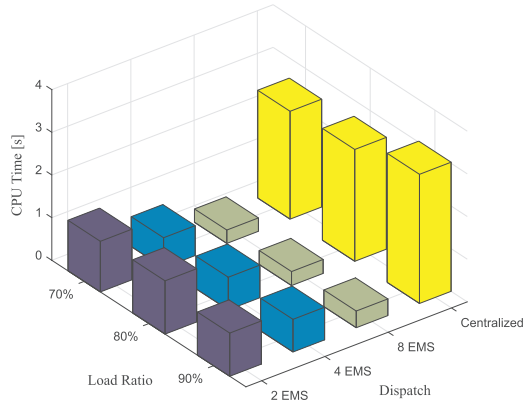


Fig. 24. 1354pegase computation time for various load scenarios.

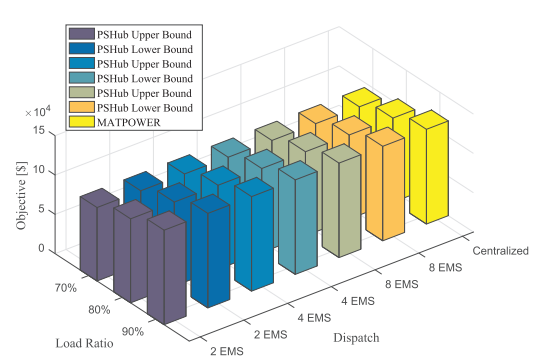


Fig. 25. 2869pegase objective values for various load scenarios.

the number of iterations times the number of regional EMS centers.

The centralized dispatch results in Table 6 are obtained from MATPOWER which solves the nonconvex AC OPF model and can only guarantee local optimal solutions. The PSHub coordination results are obtained by solving our convex SOC-ACOPF model using our proposed modified BD approach. The decentralized SOC-ACOPF approach converges to very close results compared with the centralized solutions of SOC-ACOPF model in Table 3. The comparison in Table 6 is to demonstrate both the advantages of convex SOC-ACOPF model over the nonconvex AC OPF model in MATPOWER and the advantages of PSHub

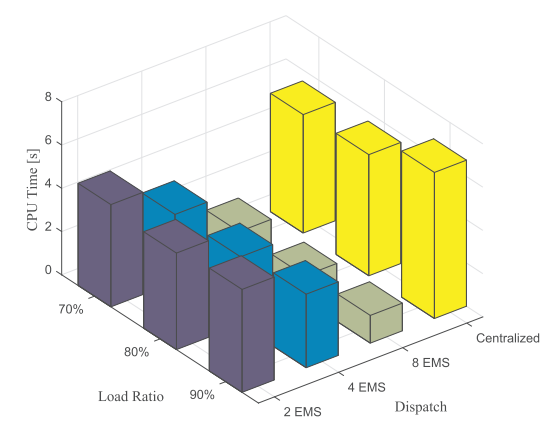


Fig. 26. 2869pegase computation time for various load scenarios.

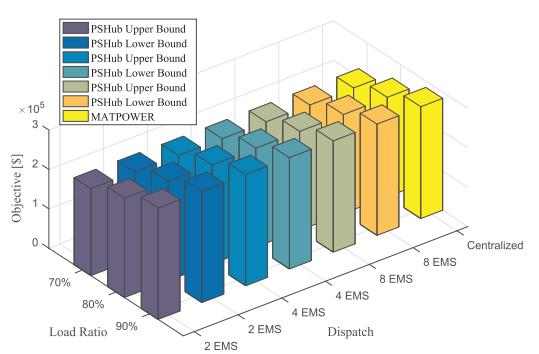


Fig. 27. 9241pegase objective values for various load scenarios.

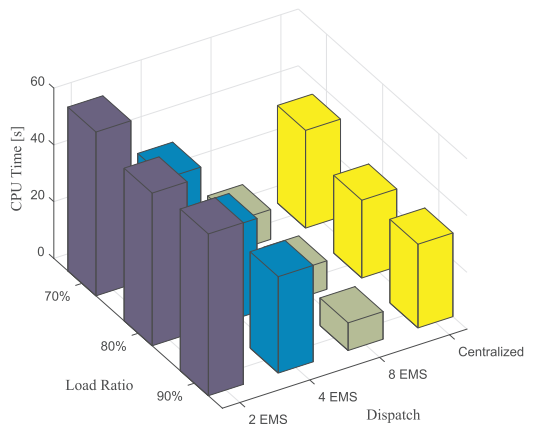


Fig. 28. 9241pegase computation time for various load scenarios.

coordination over centralized dispatch. Since the SOC-ACOPF is convex, the solutions are guaranteed to be global optimal. The benefits of global economy improvements are because of the advantage of global optimality over local optimality. The computational efficiency improvement is because of the advantage of the modified BD using parallel computation. From a technical perspective, the regional EMS is

Z. Yuan et al. Applied Energy xxx (xxxx) xxx-xxx

always required to be involved to coordinate the operations with other regional EMS as long as the power grid is interconnected. Otherwise, the security of the power grid cannot be guaranteed. From an economic perspective, the results of regional EMS from PSHub coordination are very close to centralized dispatch (solve the SOC-ACOPF model as one single optimization without using the modified BD). This is guaranteed by the convergence of the modified BD. The convergence means the final results can converge to the centralized solution of the decision variables which ensure that the economic cost of regional EMS also converges to the solution of centralized solution. In summary, the fast convergence of the coordination by PSHub shows strong coordination capability. By using parallel computation, the required computation time for more EMS centers does not increase. On the contrary, the efficient parallel computation management algorithm is capable of accelerating the computations. This is highly appreciated in online decision making applications where the computation time is limited.

6.3.2. Load scenarios

To validate the robustness of the coordination mechanism by PSHub, we simulate the power load scenarios from 70% to 90% of the original load data. Because the centralized energy dispatch by MATPOWER cannot converge for most cases when the power loads are below 70% or above 100% of the original load data, we do not show the results for these load scenarios. The objective value results are demonstrated in Figs. 23, 25 and 27. We also show the CPU time of the computations in Figs. 24, 26 and 28. For all the considered load scenarios, the coordinated energy dispatch by PSHub converge to very close objective values compared with the centralized dispatch by MA-TPOWER. The required computation time of PSHub is less than the CPU time of centralized dispatch. These results show that coordinated energy dispatch by PSHub is robust against the considered load scenarios.

7. Conclusions

Coordinating the energy dispatch across continent is a challenging task of future super grid operations. With the large-scale integration of renewable energy to the power system, more transmission expansions are required to connect these renewable energy resources in remote areas either onshore or offshore. It is hard to efficiently operate the super grid without an international or inter-regional coordination mechanism. This paper contributes to the literature by proposing the SOC-ACOPF model and the PSHub concept to solve this challenge. Specifically, we have solved three problems of operating the super grid:

- 1. How to approximately find the global optimal operating points of the power network? The solution is the improved convex SOC-ACOPF model:
- 2. How to coordinate the energy dispatch of different nations or regions and reduce the communication burden? The solution is the modified BD algorithm;
- 3. How to execute the coordination of ultra-large-scale power network fast enough to assist online decision making? The solution is the proposed parallel computation structure.

The accuracy of the proposed SOC-ACOPF model is proved by a comprehensive investigation of the numerical results from various IEEE test cases. Compared with the widely used decoupled DC OPF model, the AC feasibility of the proposed SOC-ACOPF model is better. This means the solutions obtained by the proposed SOC-ACOPF model are more accurate and realistic. A numerical comparison with other SOC-ACOPF models in the literature also shows the computational advantages of our model. Thus, we demonstrate that the proposed SOC-ACOPF model can be a good candidate for applications in operating the large-scale super grid in real time.

By coordinating the energy dispatch of regional EMS centers, global optimal energy dispatch targets can be achieved. The coordination in

PSHub is based on the modified BD algorithm and the proposed convex SOC-ACOPF model. The advantage of using convex SOC-ACOPF model is that the convergence of modified BD can be guaranteed. The fast and strong convergence capability of the proposed coordination mechanism implemented in PSHub is demonstrated by the proposed parallel computation approach. The numerical results of various number of regional power networks and load scenarios show that the coordinated energy dispatch by PSHub is robust. Compared with other distributed AC OPF solution algorithms in the literature, the main advantages of the proposed modified BD are threefold:

- 1. Instead of using the original Benders feasibility cuts approach, we can guarantee the feasibility of the formulated subproblems in the modified BD by adding one more generator at each node of the power network with larger marginal cost. Our approach converges within one minute CPU time for power networks up to 9241 nodes. The original Benders feasibility cuts approach cannot converge after several hours in our simulations.
- 2. Since we formulate the modified BD by taking the total power generations of the regional power networks as the complicating variables, no other detailed information except the Benders cuts is required to be communicated from the regional power networks to the PSHub. This formulation can largely reduce the communication burden to coordinate the super grid. Since the parameters of the Benders cuts are required to be communicated from the regional power networks to the PSHub in each iteration, the reduced communication burden is also because our modified BD approach requires less iterations to converge compared with the traditional BD.
- 3. The privacy of information for the regional power networks can be protected since the boundaries between different regional power networks are still kept. No transfer of information between different regional power networks is required. The only two-way communication is between the PSHub and individual regional power network. This is largely due to our novel formulation of the modified BD which takes the total power outputs of the regional power networks as the complicating variables. In other words, if we take other variables as the complicating variables to formulate the master problem and subproblems of BD, the information privacy of regional power network may not be well protected.

Acknowledgment

The authors would like to thank the support from SETS Erasmus Mundus Joint Doctorate Fellowship for this research project on super grid. All the careful reviews on this paper by the editors and reviewers of this journal are sincerely appreciated by the authors.

References

- [1] Bompard E, Fulli G, Ardelean M, Masera M. It's a Bird, It's a Plane, It's a... Supergrid!: Evolution, opportunities, and critical issues for pan-European transmission. IEEE Power Energy Mag 2014;12(2):40–50. http://dx.doi.org/10.1109/MPE.2013.2294813.
- [2] Gellings CW, A globe spanning super grid, IEEE Spect 2015;52(8):48-54, http://dx.
- [3] Fűrsch M, Hagspiel S, Jägemann C, Nagl S, Lindenberger D, Trőter E. The role of grid extensions in a cost-efficient transformation of the European electricity system intil 2050. Appl Energy 2013:104:642-52.
- [4] Sanchis G, Betraoui B, Anderski T, Peirano E, Pestana R, Clercq BD, et al. The corridors of power: a pan-European electricity highway system for 2050. IEEE Power Energ Mag 2015;13(1):38-51. http://dx.doi.org/10.1109/MPE.2014.
- [5] Li Y, Lukszo Z, Weijnen M. The impact of inter-regional transmission grid expansion on China's power sector decarbonization. Appl Energy 2016;183:853-73. http://dx doi.org/10.1016/j.apenergy.2016.09.006. Li J, Fang J, Zeng Q, Chen Z. Optimal operation of the integrated electrical and
- eating systems to accommodate the intermittent renewable sources. Appl Energy 2016:167:244-54.
- [7] Varadarajan M, Swarup K. Solving multi-objective optimal power flow using differential evolution. IET Gener, Transm Distrib 2008;2(5):720–30.
 [8] Sivasubramani S, Swarup K. Multi-objective harmony search algorithm for optimal

Z. Yuan et al. Applied Energy xxx (xxxx) xxx-xxx

- power flow problem. Int J Electr Power Energy Syst 2011;33(3):745-52.
- [9] Noroczian M, Anguist L, Ghandhari M, Andersson G. Use of upfc for optimal power flow control. IEEE Trans Power Deliv 1997;12(4):1629–34.
 [10] Mamandur K, Chenoweth R. Optimal control of reactive power flow for improve-
- ments in voltage profiles and for real power loss minimization. IEEE Trans Power Apparat Syst 1981(7):3185–94.

 [11] Hesamzadeh MR, Biggar DR, Hosseinzadeh N, Wolfs PJ. Transmission augr
- tion with mathematical modeling of market power and strategic generation expansion Part I. IEEE Trans Power Syst 2011;26(4):2040-8.

 [12] Lu H, Cao M, Li J, Huang G, He L. An inexact programming approach for urban electric power systems management under random-interval-parameter uncertainty. ppl Math Model 2015;39(7):1757-68.
- [13] Li Z, Qiu F, Wang J. Data-driven real-time power dispatch for maximizing variable renewable generation. Appl Energy 2016;170:304–13. http://dx.doi.org/10.1016/
- j.apenergy.2016.02.125.

 Venkatesh B, Sadasivam G, Khan MA. A new optimal reactive power scheduling method for loss minimization and voltage stability margin maximization using successive multi-objective fuzzy lp technique. IEEE Trans Power Syst 2000:15(2):844-51.
- ong H, Lee B, Kwon S-H, Ajjarapu V. Reactive reserve-based contingency constrained optimal power flow (recopt) for enhancement of voltage stability margins. IEEE Trans Power Syst 2003;18(4):1538–46.
- Alsac O, Stott B. Optimal load flow with steady-state security. IEEE Trans Power Apparat Syst 1974(3):745–51.
- [17] Thomas JJ, Grijalva S, Flexible security-constrained optimal power flow, IEEE Trans
- Power Syst 2015;30(3):1195–202.

 [18] Condren J, Gedra TW. Expected-security-cost optimal power flow with small-signal stability constraints. IEEE Trans Power Syst 2006;21(4):1736–43.

 [19] Niknam T, Narimani M, Aghaei J, Tabatabaei S, Nayeripour M. Modified honey bee
- nating optimisation to solve dynamic optimal power flow considering gene constraints. IET Gener, Transm Distrib 2011;5(10):989–1002.
- [20] Iggland E. Wiget R. Chatzivasileiadis S. Anderson G. Multi-Area DC-OPF for HVAC and HVDC Grids. IEEE Trans Power Syst 2015;30(5):2450–9. http://dx.doi.org/10 1109/TPWRS.2014.2365724.
- [21] Gan L, Low SH. Convexification of AC optimal power flow. In: Power systems computation conference (PSCC); 2014. p. 1-11. http://dx.doi.org/10.1109/PSCC.
- [22] Farivar M, Low SH. Branch flow model: relaxations and convexification: Part I. IEEE Trans Power Syst 2013;28(3);2554-64, http://dx.doi.org/10.1109/TPWRS.2013
- O'Neill RP, Castillo A, Cain MB. The IV formulation and linear approximations of
- the AC optimal power flow problem. Tech rep. FERC; 2012.
 [24] Baradar M, Hesamzadeh MR, Ghandhari M. Second-order cone programming for ptimal power flow in 013;28(4):4282-91. ver flow in vsc-type ac-dc grids. IEEE Trans Power Sy
- Baradar M, Hesamzadeh MR. Ac power flow representation in conic format. IEEE [25]
- Trans Power Syst 2015;30(1):546-7.
 Bai X, Wei H, Fujisawa K, Wang Y. Semidefinite programming for optimal power flow problems. Int J Electr Power Energy Syst 2008;30(6):383–92.
- [27] Lavaei J, Low SH. Zero duality gap in optimal power flow problem. IEEE Trans Power Syst 2012;27(1):92–107.
 [28] Jubril A, Olaniyan O, Komolafe O, Ogunbona P. Economic-emission dispatch properties.
- blem: a semi-definite programming approach. Appl Energy 2014;134:446-5
- [29] Lesieutre BC, Molzahn DK, Borden AR, DeMarco CL. Examining the limits of the application of semidefinite programming to power flow problems. In: Communication, control, and computing (Allerton), 2011 49th annual Allerton conference on; 2011. p. 1492-9. http://dx.doi.org/10.1109/Allerton.2011
- [30] Lavaei J, Tse D, Zhang B. Geometry of power flows and optimization in distribution etworks. IEEE Trans Power Syst 2014;29(2):572-83.
- [31] Low S. Convex relaxation of optimal power flow, Part I: formulations and equiva-lence. IEEE Trans Control Network Syst 2014;1(1):15–27. http://dx.doi.org/10. 1109/TCNS.2014.2309732
- [32] Low S. Convex relaxation of optimal power flow, part II: exactness. IEEE Trans Control Network Syst 2014(2):177-89. http://dx.d
- [33] Conejo AJ, Aguado JA. Multi-area coordinated decentralized DC optimal power flow. IEEE Trans Power Syst 1998;13(4):1272-8. http://dx.doi.or

- [34] Geoffrion AM. Generalized Benders decomposition. J Optim Theory Appl 1972:10(4):237-60.
- Conejo AJ, Castillo E, Minguez R, Garcia-Bertrand R. Decomposition techniques in mathematical programming: engineering and science applications. Springer Science & Business Media: 2006.
- Quintana VH, Lopez R, Romano R, Valadez V. Constrained economic dispatch of multi-area systems using the Dantzig-Wolfe decomposition principle. IEEE Trans Power Apparat Syst 1981;PAS-100(4):2127-37. http://dx.doi.org/10.1109/TPAS.
- Erseghe T. Distributed optimal power flow using ADMM. IEEE Trans Power Syst
- 2014;29(5):2370–80. http://dx.doi.org/10.1109/TPWRS.2014.2306495.
 [38] Molzahn DK, Drfler F, Sandberg H, Low SH, Chakrabarti S, Baldick R, et al. A survey of distributed optimization and control algorithms for electric power systems. IEEE Trans Smart Grid 2017;PP(99):1. http://dx.doi.org/10.1109/TSG.2017.2720471.
- [39] Alguacil N. Conejo A.J. Multiperiod optimal power flow using Benders decomposin. IEEE Trans Power Syst 2000;15(1):196–201. http://dx.doi.org/10.1109,
- [40] Fu Y, Shahidehpour M, Li Z. Security-constrained unit commitment with AC constraints*. IEEE Trans Power Syst 2005;20(3):1538-50. http://dx.doi.org/10.1109/
- Binato S, Pereira MVF, Granville S. A new Benders decomposition approach to solve power transmission network design problems. IEEE Trans Power Syst 2001;16(2):235–40. http://dx.doi.org/10.1109/59.918292. Niknam T, Khodaei A, Fallahi F. A new decomposition approach for the thermal unit commitment problem. Appl Energy 2009;86(9):1667–74.
- [43] Wang Y, Wu L, Wang S. A fully-decentralized consensus-based ADMM approach for DC-OPF with demand response. IEEE Trans Smart Grid 2017;PP(99):1–11. http:// dx.doi.org/10.1109/TSG.2016.2532467.
- [44] Bazrafshan M. Gatsis N. Decentralized stochastic optimal power flow in radial networks with distributed generation. IEEE Trans Smart Grid 2017;8(2):787–801. http://dx.doi.org/10.1109/TSG.2016.2518644.
- [45] Loukarakis E. Bialek JW. Dent CJ. Investigation of maximum possible OPF problem decomposition degree for decentralized energy markets. IEEE Trans Power Syst 2015;30(5):2566–78. http://dx.doi.org/10.1109/TPWRS.2014.2365959.
- Lu W, Liu M, Lin S, Li L. Fully decentralized optimal power flow of multi-area interconnected power systems based on distributed interior point method. IEEE Trans Power Syst 2017;PP(99):1. http://dx.doi.org/10.1109/TPWRS.2017.
- [47] He C. Wu L. Liu T. Shahidehpour M. Robust co-optimization scheduling of elec-Nu I, Liu I, Shanidenpoin M. Robits Coopininasin Stretuning of recentricity and natural gas systems via admm. IEEE Trans Sustain Energy 2017;8(2):658–70. http://dx.doi.org/10.1109/TSTE.2016.2615104.

 Wen Y, Qu X, Li W, Liu X, Ye X. Synergistic operation of electricity and natural gas
- networks via admm. IEEE Trans Smart Grid 2017;PP(99):1. http://dx.doi.org/10.
- [49] Li Z, Shahidehpour M, Wu W, Zeng B, Zhang B, Zheng W. Decentralized multiarea robust generation unit and tie-line scheduling under wind power uncertainty. IEEE Trans Sustain Energy 2015;6(4):1377-88. http://dx.doi.org/10.1109/TSTE.2015.
- [50] Jabr RA, Singh R, Pal BC. Minimum loss network reconfiguration using mixed-integer convex programming. IEEE Trans Power Syst 2012;27(2):1106–15. http://dx.doi.org/10.1109/TPWRS.2011.2180406.
- Coffrin C, Hijazi HL, Hentenryck PV. The QC relaxation: a theoretical a tational study on optimal power flow. IEEE Trans Power Syst 2016;31(4):3008-18.
- http://dx.doi.org/10.1109/TPWRS.2015.2463111.
 [52] Fliscounakis S, Panciatici P, Capitanescu F, Wehenkel L. Contingency ranking with respect to overloads in very large power systems taking into account uncert preventive, and corrective actions. IEEE Trans Power Syst 2013;28(4):4909-17. http://dx.doi.org/10.1109/TPWRS.2013.2251015.
 Zimmerman RD, Murillo-Sánchez CE, Thomas RJ. Matpower: steady-state ope
- tions, planning, and analysis tools for power systems research and education. IEEE Trans Power Syst 2011:26(1):12-9.
- The mosek optimization software. < http://www.mosek.com >
- Stott B, Alsac O. Fast decoupled load flow. IEEE Trans Power Apparat Syst
- 1974;PAS-93(3):859-69. http://dx.doi.org/10.1109/TPAS.1974.2939985. Bussieck MR, Ferris MC, Meeraus A. Grid-enabled optimization with gams. INFORMS J Comput 2009;21(3):349-62.
- [57] The University of Washington Power Systems Test Case Archive. < http://www.ee.

For KTH Royal Institute of Technology DOCTORAL THESIS IN ELECTRICAL ENGINEERING TRITA-EECS-AVL-2018:10 www.kth.se

ISBN 978-91-7729-678-2